

SEMI-AUTOMATIC CLASSIFICATION OF VERY-HIGH-RESOLUTION
IMAGES FROM UAV FOR MAPPING WEED IN CASSAVA FIELDS



A Thesis Submitted in Partial Fulfillment of the Requirements for the
Degree of Doctor of Philosophy in Geoinformatics
Suranaree University of Technology
Academic Year 2022

การจำแนกแบบกึ่งอัตโนมัติจากภาพรายละเอียดสูงจากอากาศยานไร้คนขับ
สำหรับจำแนกวัชพืชในแปลงมันสำปะหลัง



นางสาวอภิญา บุญแรง

วิทยานิพนธ์นี้เป็นส่วนหนึ่งของการศึกษาตามหลักสูตรปริญญาวิทยาศาสตรดุษฎีบัณฑิต

สาขาวิชาภูมิสารสนเทศ

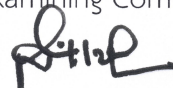
มหาวิทยาลัยเทคโนโลยีสุรนารี

ปีการศึกษา 2565

SEMI-AUTOMATIC CLASSIFICATION OF VERY-HIGH-RESOLUTION IMAGES
FROM UAV FOR MAPPING WEED IN CASSAVA FIELDS

Suranaree University of Technology has approved this thesis submitted in partial fulfillment of the requirements for the Degree of Doctor of Philosophy.

Thesis Examining Committee



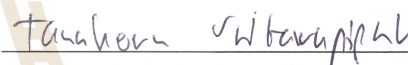
(Prof. Dr. Santi Maensiri)

Chairperson



(Asst. Prof. Dr. Pantip Piyatadsananon)

Member (Thesis Advisor)



(Dr. Tanakorn Sritarapipat)

Member (Thesis Co-advisor)



(Asst. Prof. Dr. Pipat Reungsang)

Member



(Dr. Siripon Kamontum)

Member



(Dr. Nobphadon Suksangpanya)

Member



(Prof. Dr. Santi Maensiri)

Dean of Institute of Science



(Assoc. Prof. Dr. Chatchai Jothityangkoon)

Vice Rector for Academic Affairs

and Quality Assurance

อภิญา บุญแรง : การจำแนกแบบกึ่งอัตโนมัติจากภาพรายละเอียดสูงจากอากาศยานไร้คนขับสำหรับจำแนกวัชพืชในแปลงมันสำปะหลัง (SEMI-AUTOMATIC CLASSIFICATION OF VERY-HIGH-RESOLUTION IMAGES FROM UAV FOR MAPPING WEED IN CASSAVA FIELDS) อาจารย์ที่ปรึกษา : ผู้ช่วยศาสตราจารย์ ดร.พันทิพย์ ปิยะทัศนานนท์, 178 หน้า.

คำสำคัญ: การจำแนกแบบกึ่งอัตโนมัติ / แผนที่วัชพืช / อากาศยานไร้คนขับ / มันสำปะหลัง / ภาพถ่ายรายละเอียดสูง

ภาพถ่ายรายละเอียดสูงจากอากาศยานไร้คนขับ (Unmanned Aerial Vehicle: UAV) มีการใช้เพื่อประเมินความอุดมสมบูรณ์ของพืชและสำรวจวัชพืชในการเกษตรแบบแม่นยำ การจำแนกประเภทของวัตถุในภาพเป็นขั้นตอนที่สำคัญหลังจากการสำรวจด้วย UAV โดยทั่วไปแล้วการจำแนกภาพถ่ายรายละเอียดสูงจาก UAV ใช้เวลาค่อนข้างมากและต้องอาศัยระบบประมวลผลที่มีประสิทธิภาพสูงซึ่งเป็นหนึ่งในอุปสรรคของการจำแนก ในขณะที่มีความต้องการใช้ภาพถ่ายรายละเอียดสูงกับการจำแนกหลายประเภท

การศึกษานี้มีวัตถุประสงค์เพื่อพัฒนาระบบการจำแนกแบบกึ่งอัตโนมัติจากภาพถ่ายรายละเอียดสูงจากอากาศยานไร้คนขับสำหรับจำแนกวัชพืชในแปลงมันสำปะหลัง โดยใช้หลักการการจำแนกแบบไม่มีผู้สอน (Unsupervised Learning) ด้วยวิธี K-means เพื่อจำแนกมันสำปะหลัง วัชพืช ดิน และต้นไม้ ในแปลงมันสำปะหลัง กระบวนการที่พัฒนาขึ้นประกอบด้วยเตรียมภาพโดยเลือกดัชนีที่คำนวณจากช่วงคลื่น RGB พารามิเตอร์ของ Mean-shift filtering และระยะระหว่างจุดศูนย์กลางจุดภาพบนพื้นดิน (Ground Sample Distance, GSD) ที่เหมาะสม รวมทั้งมีการสร้างกฎการจำแนกที่ได้จากแนวโน้มของคุณสมบัติเชิงสเปกตรัม (spectrum properties) ของแต่ละวัตถุแทนที่จะใช้ค่าสเปกตรัมโดยตรงซึ่งมีความแตกต่างกันในแต่ละพื้นที่ จากการทดสอบปรับตัวแปรต่าง ๆ และนำไปทดสอบกับภาพแปลงมันสำปะหลังที่ถ่ายในช่วงเวลาต่างกัน รวมทั้งการใช้เซ็นเซอร์ถ่ายภาพที่แตกต่างกัน ผลการทดสอบพบว่า การใช้ภาพที่มี GSD 5 ซม. ให้ผลการจำแนกที่ถูกต้อง (ร้อยละ 97) เทียบเท่ากับภาพความละเอียดสูง GSD 1.5 ซม. แต่ประมวลผลได้รวดเร็วกว่า ภาพที่เกิดจากช่วงคลื่นสีน้ำเงิน (B) ดัชนี Visible Atmospherically Resistant Index (VARI) และดัชนี Color Index (CI) ผ่านการฟิลเตอร์โดยใช้ตัวแปร spatial window radius (sp)=5 และ color window radius (sr)=10 สามารถแยกดินออกจากพืชได้ที่ที่สุด ในขณะที่ภาพที่เกิดจากดัชนี Excess Blue (ExB) Normalized Green-Red Difference Index (NGRDI) และ VARI ที่ฟิลเตอร์ครั้งแรกด้วยตัวแปร $sp=60$ $sr=40$ และฟิลเตอร์ครั้งที่สองด้วย $sp=20$ and $sr=40$ สามารถแยกต้นไม้ออกมาจาก

วัตถุประเภทอื่น ๆ ได้ดีที่สุด ส่วนมันสำปะหลังและวัชพืชแยกได้ดีที่สุดโดยใช้ ภาพที่เกิดจากช่วงคลื่น สีเขียว (G) ดัชนี Excess Red (ExR) และดัชนี Excess Green (ExG) ผ่านการฟิลเตอร์โดยใช้ตัวแปร $sp=10$ และ $sr=20$ ผลการจำแนกให้ความถูกต้องโดยรวม (Overall accuracy, OA) ที่ 0.97 และ สัมประสิทธิ์แคปปา (Kappa coefficient) 0.96 สำหรับภาพที่ไม่มีต้นไม้อื่น ส่วนภาพที่มีต้นไม้อื่นให้ค่า ความถูกต้องโดยรวม 0.82 และสัมประสิทธิ์แคปปา 0.74 การจำแนกโดยใช้กระบวนการที่พัฒนาขึ้น ให้ค่าความถูกต้องเทียบเท่ากับการจำแนกด้วยวิธีการ Random Forest (RF) ซึ่งใช้ชุดข้อมูลตัวอย่าง ในการเรียนรู้ การศึกษานี้ได้ทดสอบการใช้ภาพขนาดต่างกันในการจำแนก พบว่าการใช้ภาพขนาดเล็ก ลงสามารถเพิ่มความถูกต้องโดยรวมได้ 0.12 และสัมประสิทธิ์แคปปา 0.18 โดยเฉพาะภาพที่มีความหนาแน่นของวัชพืชแตกต่างกันมาก

การพัฒนากระบวนการจำแนกในการศึกษานี้สามารถลดเวลาในขั้นตอนการเตรียมภาพและ จำแนกภาพจากวิธีการปกติได้ เนื่องจากกระบวนการนี้ทำงานได้โดยไม่อาศัยข้อมูลตัวอย่าง และยัง สามารถใช้กับภาพแปลงมันสำปะหลังที่หลากหลายที่ถ่ายจาก UAV นอกจากนี้กระบวนการนี้ช่วยลด ขั้นตอนต่าง ๆ ในการเตรียมและจำแนกวัชพืชในแปลงได้



สาขาวิชาภูมิสารสนเทศ

ปีการศึกษา 2565

ลายมือชื่อนักศึกษา อริยญา บุญเรือง

ลายมือชื่ออาจารย์ที่ปรึกษา สุรินทร์ บุญเรือง

ลายมือชื่ออาจารย์ที่ปรึกษาร่วม สุรินทร์ บุญเรือง

APINYA BOONRANG : SEMI-AUTOMATIC CLASSIFICATION OF VERY-HIGH-RESOLUTION IMAGES FROM UAV FOR MAPPING WEED IN CASSAVA FIELDS.
THESIS ADVISOR : ASST. PROF. PANTIP PIYATADSANANON, Ph.D. 178 PP.

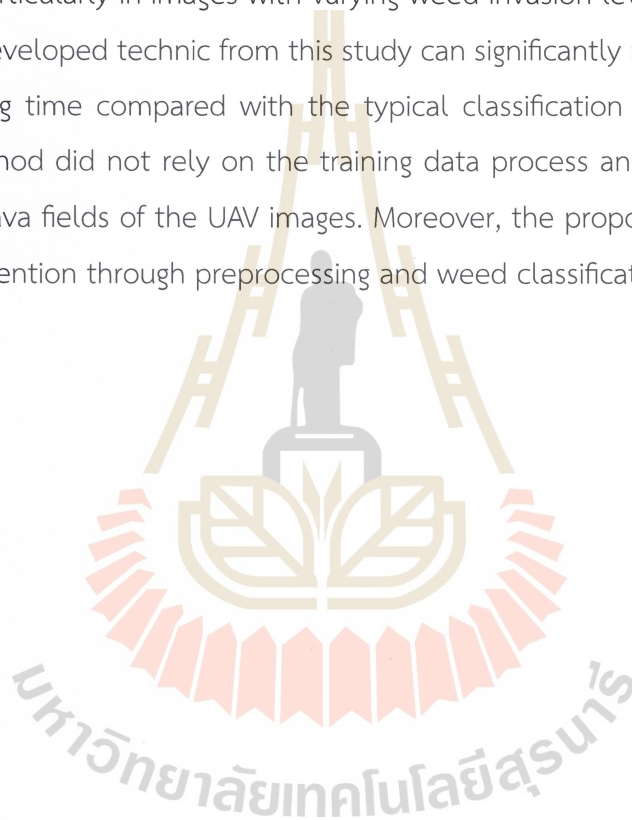
Keyword: SEMI-AUTOMATIC CLASSIFICATION / WEED MAPPING / UAV / CASSAVA / VERY-HIGH-RESOLUTION IMAGES

Very-high-resolution images from unmanned aerial vehicles (UAV) are utilized for crop health investigation and weed monitoring in precision agriculture. The classification process is a crucial procedure after surveying by the UAV. The classification process of very-high-resolution images derived from the UAV generally consumes time and computer capacity due to the great details of very-high-resolution pixels. Therefore, it could be a barrier to the classification process, while the UAV images are currently utilized in several classification tasks.

This study introduces a semi-automatic classification approach based on K-means unsupervised classification and labeling by the trend of spectral properties of each class. The process was specifically designed for classifying cassava, weed, soil, and tree objects in cassava fields taken from UAV optical sensor. The classification process minimizes manual intervention in generating classification maps by incorporating color indices based on RGB, mean-shift filtering parameters, and Ground Sample Distance (GSD). These factors are carefully examined to ensure the reliability and accuracy in classifying objects. The results show that using an image with a GSD of 5 cm presents the optimum result in terms of time-consuming and acceptable accuracy (97%) rather than using the finer GSD (1.5 cm). The combination of Blue (B), Visible Atmospherically Resistant Index (VARI), and Color Index (CI), with filtering parameters spatial window radius (sp)=5 and color window radius (sr)=10, showed the highest potential for discriminating soil from vegetation. The combination of Excess Blue (ExB), Normalized Green-Red Difference Index (NGRDI), and VARI, with filtering parameters in the first round, $sp=60$ and $sr=40$, in the second round $sp=20$ and $sr=40$, demonstrated the highest potential for distinguishing trees from other classes. Moreover, the combination of Green (G), Excess Red (ExR), and Excess Green (ExG), with

filtering parameters $sp=10$ and $sr=20$, exhibited the highest potential for separating cassava and weed from other classes. The classification maps achieved high overall accuracies (OA) of 0.97 and kappa coefficients of 0.96 for images without trees. For images with trees, the OA was 0.8217, and the kappa coefficient was 0.7445. Comparative analysis with sample sites demonstrated accuracy levels similar to supervised methods like RF classification. Implementing the split image process improved accuracy, with enhancements of 0.1195 for OA and 0.1786 for the kappa coefficient, particularly in images with varying weed invasion levels.

The developed technic from this study can significantly reduce the procedures and processing time compared with the typical classification method. Notably, the explored method did not rely on the training data process and could be applied to different cassava fields of the UAV images. Moreover, the proposed protocol reduced manual intervention through preprocessing and weed classification.



School of Geoinformatics
Academic Year 2022

Student's Signature Apinya Boonrong
Advisor's Signature Justice
Co-advisor's Signature Tanawan Sritavapitak

ACKNOWLEDGEMENTS

I am deeply grateful to the individuals who have played a significant role in my academic journey.

First and foremost, I would like to express my sincere thanks to my advisor, Asst. Prof. Dr. Pantip Piyatadsananon, and my co-advisor, Dr. Tanakorn Sritarapipat, for their invaluable patience and feedback during my study at the School of Geoinformatics, Institute of Science, Suranaree University of Technology.

I would also like to extend my sincere thanks to Prof. Dr. Santi Maensiri, Asst. Prof. Dr. Pipat Reungsang, Dr. Siripon Kamontam, and Dr. Nobphadon Suksangpanya for serving on my thesis committee and providing valuable feedback and suggestions that shaped my research. I am grateful to Assoc. Prof. Dr. Suwit Ongsomwang, Asst. Prof. Dr. Sanya Sarapirom, and Assoc. Dr. Songkot Dasananda for their guidance and suggestions.

Furthermore, I am grateful to my classmates, fellow students, and the staff of the School of Geoinformatics for their support and collaboration throughout my studies. My dear friends have also been a constant source of support and encouragement, which has been vital to my academic success.

I would like to express my deepest gratitude to my parents for their unwavering motivation and support throughout my study period.

Lastly, I would like to thank the Science Achievement Scholarship of Thailand (SAST) for their financial support during my bachelor's, master's, and Ph.D. studies.

Apinya Boonrang

CONTENTS

	Page
ABSTRACT IN THAI.....	I
ABSTRACT IN ENGLISH.....	III
ACKNOWLEDGEMENTS	V
CONTENTS	VI
LIST OF TABLES	IX
LIST OF FIGURES	XII
LIST OF ABBREVIATIONS	XVI
CHAPTER	
I INTRODUCTION.....	1
1.1 Background problems and significance of the study.....	1
1.2 Research objectives	6
1.3 Scope and limitations of study.....	6
1.3.1 Scope of study.....	6
1.3.2 Limitations of the study.....	7
1.4 Benefits of the study.....	7
1.4.1 Contribution to knowledge	7
1.4.2 Contribution to relevant stakeholders.....	8
1.5 State-of-the-art	9
1.6 Study area.....	13
II RELATED CONCEPTS AND LITERATURE REVIEWS.....	23
2.1 Cassava.....	23
2.1.1 Important of cassava	23
2.1.2 Growing cassava	26
2.1.3 Weed control.....	29
2.2 Spectral discrimination of vegetation	30

CONTENTS (Continued)

		Page
	2.3 Image segmentation	33
	2.4 Mean-shift filtering	37
	2.5 K-means clustering.....	39
	2.6 Previous studies of weed detection.....	42
III	RESEARCH METHODOLOGY	48
	3.1 Conceptual framework.....	48
	3.2 Data and materials.....	50
	3.2.1 Image acquisition	50
	3.2.2 Processing software.....	52
	3.3 Rerearch Procedures.....	52
	3.3.1 Developing classification	52
	3.3.2 Adjusting and validating classification	56
	3.3.3 Applying classification.....	59
IV	RESULTS AND DISCUSSION	61
	4.1 Finding in developing the classification process	61
	4.1.1 Input data.....	61
	4.1.2 Filtering	64
	4.1.3 Clustering.....	67
	4.1.4 Classification rules	69
	4.2 Results of adjusting and validating classification process.....	71
	4.2.1 Soil classification.....	71
	4.2.2 Tree classification	73
	4.2.3 Cassava and weed classification.....	74
	4.2.4 Classification in all classes.....	76
	4.3 Results of applying the proposed classification process	87
V	CONCLUSION AND SUGGESTIONS.....	97
	5.1 Conclusion	97
	5.2 Suggestions	101

CONTENTS (Continued)

	Page
REFERENCES	104
APPENDICES.....	116
Appendix A PROTOCOL FOR APPLYING PROPOSED CLASSIFICATION PROCESS.....	117
Appendix B RESULTS OF CLASSIFICATION FOR VARIOUS GSDs	121
Appendix C T-DISTRIBUTION TABLE OF CRITICAL VALUES.....	130
Appendix D RESULTS OF CLASSIFICATION FORM TREDITIONAL METHODS.....	132
Appendix E CLASSIFICATION RESULTS OF APPLYING PROPOSED CLASSIFICATION PROCESS TO STUDY AREAS	140
Appendix F WEED MAPS	165
CURRICULUM VITAE	178

LIST OF TABLES

Table		Page
1.1	Advantages and disadvantages of the classification approach	10
1.2	Process of traditional supervised classification, traditional unsupervised classification, and proposed classification process	12
1.3	Details of the study area	19
2.1	Pest management for cassava	28
2.2	Spectral indices based on RGB values to distinguish vegetation and non-vegetation	32
2.3	Advantages and disadvantages of the segmentation approach	35
3.1	Details of sensors	51
3.2	Acquisition details of the study area	51
3.3	Number of clusters in the K-means clustering process	55
3.4	Referent points of the testing site for the accuracy assessment process	57
3.5	Mean-shift parameters for the filtering process	59
3.6	Referent points for evaluating the classification results	60
4.1	Spectrum characteristics of objects after the clustering process	70
4.2	The rules set for the classification process	71
4.3	Selected soil classification condition of each GSD	72
4.4	Selected tree classification condition of each GSD	73
4.5	Selected cassava and weed classification condition of each GSD	75
4.6	Selected condition for classification	77
4.7	Overall accuracy, Kappa coefficient, and processing time of classification map	78
4.8	Producer's accuracy (PA) of classification map	80
4.9	User's accuracy (UA) of classification map	80
4.10	Result of statistical paired t-test between the result from GSD 1.5 cm and the other GSDs	83

LIST OF TABLES (Continued)

Table	Page
4.11 Input data and classification results of the RF, K-means classification, and the proposed classification process.....	85
4.12 The parameters of the proposed classification process.....	87
4.13 Overall accuracy (OA), kappa coefficient, and processing time of classification results.....	89
4.14 Producer's accuracy (PA) of the results in classification	91
4.15 User's accuracy (UA) of the results in classification	92
C1 Critical values (percentiles) for the t distribution.....	131
E1 Confusion matrix of classification result from process the entire area of plot 1	141
E2 Confusion matrix of classification result from process two pieces of plot 1	141
E3 Confusion matrix of classification result from process the entire area of plot 2.....	143
E4 Confusion matrix of classification result from process two pieces of plot 2.....	143
E5 Confusion matrix of classification result from process the entire area of plot 3.....	145
E6 Confusion matrix of classification result from process two pieces of plot 3.....	145
E7 Confusion matrix of classification result from process the entire area of plot 4.....	147
E8 Confusion matrix of classification result from process two pieces of plot 4.....	147
E9 Confusion matrix of classification result from process the entire area of plot 5.....	149
E10 Confusion matrix of classification result from process two pieces of plot 5.....	149

LIST OF TABLES (Continued)

Table		Page
E11	Confusion matrix of classification result from process the entire area of plot 6.....	151
E12	Confusion matrix of classification result from process two pieces of plot 6.....	151
E13	Confusion matrix of classification result from process the entire area of plot 7.....	153
E14	Confusion matrix of classification result from process two pieces of plot 7.....	153
E15	Confusion matrix of classification result from process the entire area of plot 8.....	155
E16	Confusion matrix of classification result from process two pieces of plot 8.....	155
E17	Confusion matrix of classification result from process the entire area of plot 9.....	157
E18	Confusion matrix of classification result from process two pieces of plot 9.....	157
E19	Confusion matrix of classification result from process the entire area of plot 10.....	159
E20	Confusion matrix of classification result from process two pieces of plot 10.....	159
E21	Confusion matrix of classification result from process the entire area of plot 11.....	161
E22	Confusion matrix of classification result from process two pieces of plot 11.....	161
E23	Confusion matrix of classification result from process the entire area of plot 12.....	163
E24	Confusion matrix of classification result from process two pieces of plot2.....	163

LIST OF FIGURES

Figure	Page
1.1 Thailand imported dangerous chemical substances for agriculture between 2016-2022	2
1.2 Flowchart of traditional supervised classification, traditional unsupervised classification, and proposed classification process.....	11
1.3 Cassava stems stored under trees.	14
1.4 Agriculture areas with trees from different provinces in Thailand	14
1.5 Locations, overview, and samples of cassava plot 1-5.....	16
1.6 Locations, overview, and samples of cassava plot 6-10.	17
1.7 Locations, overview, and samples of cassava plot 11-13.	18
1.8 Boxplot of canopy diameter of cassava in the study area.	20
1.9 Weeds invasion in study area.....	21
1.10 Boxplot of the the spectral value of cassava in the study area.....	22
2.1 Cassava harvested area of Thailand.....	24
2.2 Cassava production in Thailand.....	25
2.3 Cassava growth stages.....	26
2.4 Land preparation into ridges forms for cassava planting.....	27
2.5 Reflectance spectra of different types of green vegetation compared to a spectral signature for senescent leaves	31
2.6 Processes of K-means clustering.....	41
2.7 K-means clustering of the same dataset with $k=3$	42
3.1 Conceptual framework	49
3.2 Workflow of processes for developing the proposed classification process ...	53
3.3 Testing sites for adjusting and validating classification	57
4.1 Boxplot of the spectral value of classes	62

LIST OF FIGURES (Continued)

Figure	Page
4.2	63
Original RGB image (a) and results from clustering process from different indices combination: R-G-B (b), R-B-CI (c), G-ExB-VARI (d), ExB-NGRDI-VARI (e), and ExG-ExB-ExGR (f)	
4.3	65
Result of filtered R-G-B combination image (a) and ExG-ExGR-BI combination image (b) from various filtering parameters	
4.4	66
Effect of filtering on clustering result: UAV input image (a) and clustering result from unfiltered image (b), one-time filtering (c), and two-time filtering (d).....	
4.5	68
Clustering results from applying a different number of cluster (k): UAV input image (a) and (b) and the result of applying k=2 (c) and (d), and k=4 (e) and (f)	
4.6	69
Example of pixel value from clustering result: layer NGRDI from NGRDI-GLI-BI combination (a) and layer B from B-ExB-BI combination (b).....	
4.7	76
Results of soil classification and tree classification from GSD of 5 cm	
4.8	79
Overall accuracy (OA), Kappa coefficient, and processing time of classification map.....	
4.9	81
Producer's accuracy (PA) of classification results	
4.10	81
User's accuracy (UA) of classification results	
4.11	86
Overall accuracy of RF, K-means, and the proposed classification process	
4.12	86
Kappa coefficient of RF, K-means, and the proposed classification process ...	
4.13	88
Proposed classification process workflow with selected parameters.....	
4.14	90
Overall accuracy of classification results.	
4.15	90
Kappa coefficient of classification results.....	
4.16	93
Producer's accuracy of classification results from processing the entire area and two pieces	
4.17	94
User's accuracy of classification results from processing the entire area and two pieces	

LIST OF FIGURES (Continued)

Figure	Page
5.1	Classification process for processing the entire image and splitting image....102
A1	Example of UAV image and boundary shapefile for the proposed classification process118
A2	Visual interface of Classification.exe119
A3	Software interfaces during the processing.....120
A4	Examples of output from the proposed classification process120
B1	Classification results of test site 1122
B2	Classification results of test site 2123
B3	Classification results of test site 3124
B4	Classification results of test site 4125
B5	Classification results of test site 5126
B6	Classification results of test site 6127
B7	Classification results of test site 7128
B8	Classification results of test site 8129
D1	Classification results of test site 1133
D2	Classification results of test site 2134
D3	Classification results of test site 3135
D4	Classification results of test site 4136
D5	Classification results of test site 5137
D6	Classification results of test site 7138
D7	Classification results of test site 8139
E1	Classification results of plot 1142
E2	Classification results of plot 2144
E3	Classification results of plot 3146
E4	Classification results of plot 4148
E5	Classification results of plot 5150
E6	Classification results of plot 6152
E7	Classification results of plot 7154

LIST OF FIGURES (Continued)

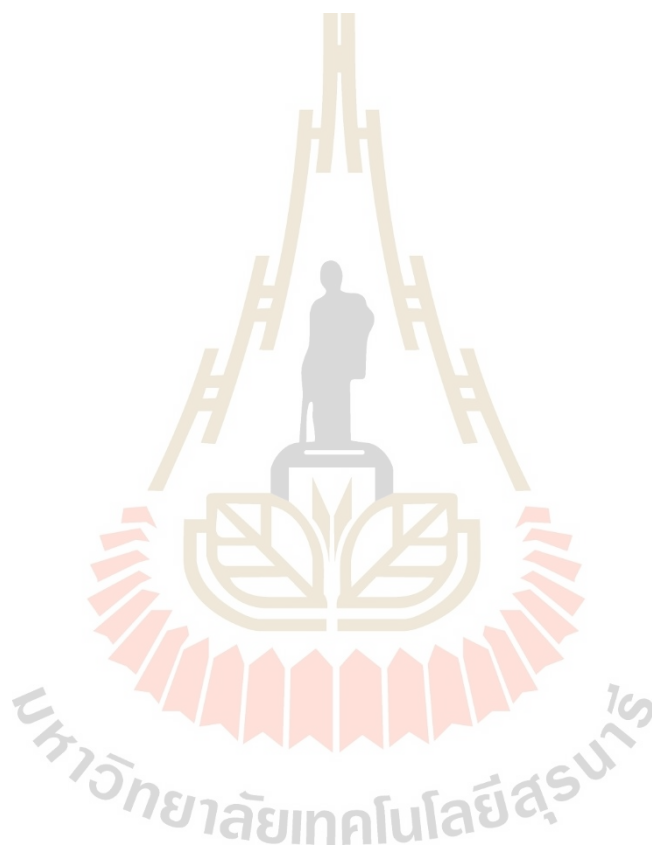
Figure	Page
E8	Classification results of plot 8156
E9	Classification results of plot 9158
E10	Classification results of plot 10.....160
E11	Classification results of plot 11.....162
E12	Classification results of plot 12.....164
F1	Weed map of plot 1.....166
F2	Weed map of plot 2.....167
F3	Weed map of plot 3.....168
F4	Weed map of plot 4.....169
F5	Weed map of plot 5.....170
F6	Weed map of plot 6.....171
F7	Weed map of plot 7.....172
F8	Weed map of plot 8.....173
F9	Weed map of plot 9.....174
F10	Weed map of plot 10.....175
F11	Weed map of plot 11.....176
F12	Weed map of plot 12.....177

LIST OF ABBREVIATIONS

B	Blue
BI	Brightness Index
CI	Color Index
DN	Digital Number
ExB	Excess Blue
ExG	Excess Green
ExGR	Excess Green minus Excess Red
ExR	Excess Red
FOV	Field of View
G	Green
GLI	Green Leaf Index
GSD	Ground Sample Distance
k	number of clusters
NGRDI	Normalized Green Red Difference Index
NDVI	Normalized Difference Vegetation Index
NIR	Near Infrared
OA	Overall Accuracy
OBIA	Object-Based Image Analysis
PA	Producer's Accuracy
R	Red
RF	Random Forest
RGB	Red, Green, and Blue
S.D.	Standard Deviation
sp	Spatial window radius
sr	Color window radius
SVM	Support Vector Machine
UA	User's Accuracy

LIST OF ABBREVIATIONS (Continued)

UAVs	Unmanned Aerial Vehicles
VARI	Visual Atmospheric Resistance Index



CHAPTER I

INTRODUCTION

1.1 Background problems and significance of the study

Agriculture is one of the essential activities in human society, especially in Thailand. In 2019, 46.54% of the country's total land area was used for agricultural purposes (Office of Agricultural Economics, 2019). The expected world population will reach over 9 billion in 2050 (FAO, 2009). Due to the increase in the global population, the demand for food production correspondingly increased by 35-56% (van Dijk, Morley, Rau, and Saghai, 2021). Thus, farmers need to increase their yields to serve the increasing demand. However, many causes hinder the increase of crop productivity, such as pests, pathogens, and weeds (Fried, Chauvel, Reynaud, and Sache, 2017).

Weed invasion is one of the significant problems for crop health and productivity. Weeds compete with crops for nutrients, sunlight, moisture, and space. Loss of agricultural productivity due to weed infestation is the main problem of agricultural production (Oerke, 2006). In Thai agricultural production, yield loss from weed competition was 20% for rice (Chiranan, Anan, and Arunee, 2014), 22-43% for corn (Lueang-a-pamong, 1998), and 20-80% for cassava (Jeamjamnanja, Phuddacharoen, Palsa-nguan, Rojanaridpiched, and Saengkaewsuk, 1984; Onochie, 1975).

Cassava is one of the most important economic crops in Thailand. Thailand is the third-largest cassava producer and the largest exporter of cassava products globally (FAOSTAT Statistical Database, 2022). Cassava is a drought-tolerant crop that can be grown in dried soils and adapted well to various cultivating conditions (Howeler, Litaladio, and Thomas, 2013). Although cassava is simple to grow, weeds and diseases dominantly affect the productivity of cassava yield (Wydra and Verdier, 2002). The period from germination to four months after planting is vital for cassava because its root system is young and weak. Weed control is usually done 2-3 times post-emergent

in this period. However, the weed will stop invading the cassava's canopy expansion and tuber development.

Weed control is crucial for increasing crop production, including many approaches to limiting invasion. Herbicides are widely used to control weed invasion in conventional agriculture practices. Typically, farmers spray herbicide over the whole field, even in less weed distribution or non-weed areas. Overusing herbicides is a major concern in increasing cost, contaminated environment, and human health (Marin-Morales, Ventura-Camargo, and Hoshina, 2013).

According to the importing report from the Office of Agricultural Economics of Thailand (2023), herbicides were the highest volume and most costly from 2016 to 2022 (Figure 1.1). More than 50% of all imported chemical substances were herbicides, valued at around 10,000 million Baths per year. Consequently, there were 49,000-61,000 cases per year of pesticide intoxication, most of which were caused by herbicides (Tawatsin, 2015).

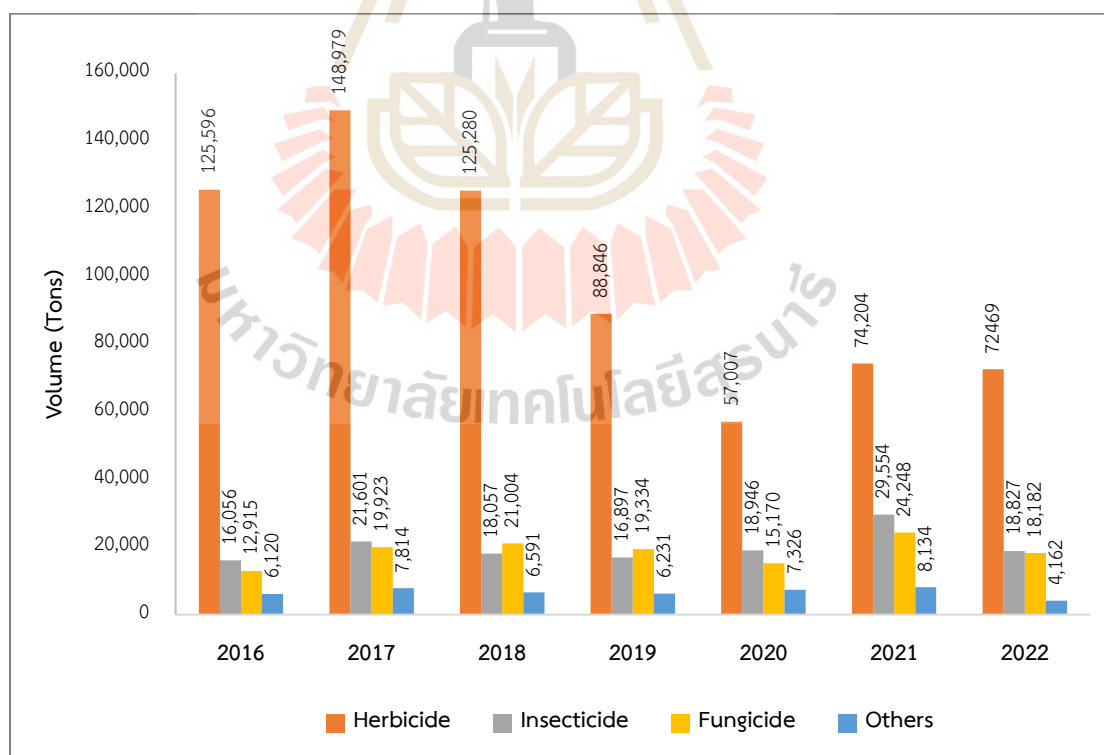


Figure 1.1 Thailand imported dangerous chemical substances for agriculture between 2016-2022.

To reduce the number of herbicides used in the fields, applying the herbicides only to the invasion area would reduce up to 40% of herbicides (Miller, 2003). However, accurate weed location is challenging and crucial for planning strategies to control weeds in the field.

High-resolution images captured by Unmanned Aerial Vehicles (UAVs) are widely used in precision agriculture to monitor and map weeds in the fields. The UAVs offer great possibilities to acquire spatial data with high spatial resolutions in the range of centimeters which is fast, easy, and flexible to work in the field. The data from true color images from the UAVs can generate a map for presenting the growth state of their crops. Also, their color indices can be used for distinguishing the type and spatial distribution of weeds in the field. (Gao et al., 2018; Gašparović, Zrinjski, Barković, and Radočaj, 2020; Lottes, Khanna, Pfeifer, Siegwart, and Stachniss, 2017; Peña, Torres-Sánchez, de Castro, Kelly, and López-Granados, 2013).

The mosaic images from the UAV are generated from several images taken at different times, which may cause inconsistencies in light conditions within the image. Moreover, the images taken from UAVs contained high resolution. An object in a high-resolution image has a wide range of reflectance values. The heterogeneity in an object causes different results in the segmentation and classification process (Huang, Li, and Chen, 2018). Typically, very high-resolution UAV images must be done with image segmentation before the feature extraction and classification process (Tsouros, Bibi, and Sarigiannidis, 2019).

Segmentation is a process for separating data into homogeneous regions by finding a similar pattern. The subgroups called image segments reduced the complexity of the image data. Various approaches to segment images include threshold, edge, region, and cluster-based. Filtering is a technique of image enhancement techniques to reduce the heterogeneity of an object and diminish illumination problems (Pajares, Ruz, and de la Cruz, 2005). Mean shift is a filtering technique that reduces an object's heterogeneity and can produce a smoother image by removing noise pixels or small objects. Moreover, this technique provides the result with segmentation property through filtering (Morales, Torres, and Sossa, 2011; Rodríguez, Suarez, and Sossa, 2011).

Image classification is an essential process for identifying weeds and crops in fields. There are two main approaches, supervised and unsupervised classification. The supervised approach categorizes data based on the user's training. The advantages of this approach are summarized as follows: (1) the final classes can control and set to a specific purpose and specific region from the known identification, (2) the classification model is fitted to a specific area, (3) the final map did not face the matching spectral categories problem, and (4) the classification error can be correct by the training process (James B. Campbell and Wynne, 2011). There is a variety of supervised classification approaches applied for discriminating weeds in a crop field, for example, random forest (RF) (Gao et al., 2018), support vector machine (SVM) (Hall et al., 2018; Ishida et al., 2018), and deep learning (Huasheng Huang et al., 2018; Louargant et al., 2018; Pantazi et al., 2017). The potential of these approaches is based on training data that relies on the user's knowledge and experience. The training data could carefully collect quality and quantity aspects to produce an accurate classifier (Foody and Mathur, 2004; Ge, Bai, Wang, and Cao, 2012). Other limitations of this approach were that training data did not respond to the natural classes based on their spectral properties, and therefore the classifier model may not classify in other data spaces (James B. Campbell and Wynne, 2011). Also, the manual training data can be time-consuming, and the analyst should have good experience in the study area.

In contrast, the unsupervised classification approach does not require training data, but the region's knowledge is still required. Generally, when the user specifies the number of groups or clusters, the algorithm defines subgroups or clusters from the homogeneous or pattern of data then the user will label the class to the cluster data later. The advantages of this approach are that it does not require training data, minimizes the opportunity for human error in conducting classes, and this approach can recognize small or unique classes (James B. Campbell and Wynne, 2011). The limitation of this technique is that result classes may not correspond with interest classes, and spectral properties of classes change over time (James B. Campbell and Wynne, 2011). There are many methods of unsupervised classification approach, for example, K-means clustering, fuzzy C-means clustering, Self-Organizing Map (SOM), and Gaussian Mixture Model.

K-means clustering is a simple and valuable unsupervised classification method. To perform the K-means clustering, the user has to specify the number of clusters (k) which is an important step. With the prior fixed number, K-means clustering can process automatically, so this method is widely applied in automatic detection. K-means clustering is usually applied together with another classifier in classification analysis. For example, K-means was used as a preprocessing to segment weed or plant areas from the image before classifying by SVM (Saha, 2019; Zhang, Guo, and Wang, 2019), and K-means was used for clustering weed invasion levels in oat fields after classified by SVM (Gašparović et al., 2020). This method has some limitations: more clusters, more challenging to define the class name, and the result of clusters depending on the spectral properties, which change over time and region (James B. Campbell and Wynne, 2011).

Nowadays, cameras or sensors are increasingly applied to agriculture. UAVs offer great possibilities to acquire data in the field, which are fast and easy at a lower price than in the past. Various companies provide services and solutions for agriculture, for example, crop health monitoring, weed invasion, fertilization, and pesticide spraying. There are numerous advantages and opportunities of remote sensing in precision agriculture and weed management, but there are some limits to user knowledge. Weed mapping is a crucial process for weed management. This process requires classification technic and knowledge of the user. As mentioned earlier, the classification process requests training data (supervised classification) or knowledge for defining number of clusters (unsupervised classification), which are limited to the researcher and specialists. Semi-automatic mapping is essential to distribute the advantages of UAVs and weed-controlling management to various users (Bansod, Singh, Thakur, and Singhal, 2017; LÓPez-Granados, 2011).

1.2 Research objectives

This study aims to develop a semi-automatic classification process for classifying objects in cassava fields. The proposed classification process combines various preprocessing and classification techniques aimed at creating a streamlined and efficient workflow. The research objectives are as follows:

- (1) To develop processes of a semi-automatic classification process;
- (2) To investigate indices, mean-shift filtering parameters (spatial radius and color radius), and GSD for improving classification accuracy;
- (3) To examine the developed method with the varieties of cassava fields in Nakhon Ratchasima province.

1.3 Scope and limitations of study

1.3.1 Scope of study

The following is the scope of the study:

(1) The preprocessing and classification process of the proposed classification process involved using UAV imagery specifically taken in cassava fields. The cassava field images consist of three or four categories: 1) cassava, 2) weed, 3) soil, and 4) tree.

(2) Images of cassava plots planted in Nakhon Ratchasima Province, recognized as the region with the highest cassava cultivation in Thailand were utilized in this study.

(3) The cassava field images were taken approximately 3-4 months after the planting stage. During this time, weeds heavily invade the field; therefore, it is crucial to implement weed control measures before the cassava canopies fully cover the field.

(4) The preprocessing, classification, and accuracy assessment processes were implemented using Python.

(5) The images tested in this study cover an area ranging from 3,092.98 to 70,671.1 square meters, equivalent to 1.93 to 44.17 rai.

(6) UAV flight conditions were followed by Thai Remotely Piloted Aircraft (RPA) Regulations, including flying areas do not close to manned aircraft, persons, vehicles, instructions, or buildings at a distance less than 30 meters horizontally, not flying in restricted areas, and altitude of UAV flying was limited at 90 meters.

1.3.2 Limitations of the study

The following are the limitations of the study:

(1) The proposed classification process focuses specially on common objects in cassava fields, cassava, weed, soil, and trees. Classification parameters and rules are exclusively defined for these specific categories.

(2) The proposed classification process works well with cassava field images taken within the 3-4 month range. Accordingly, the images captured outside this timeframe may include young cassava plants that are too small to be accurately detected. Additionally, cassava plants older than 3-4 months tend to have larger and interconnected canopies, which can reduce the accuracy of the classification.

(3) UAV Images captured under cloudy or significantly varying lighting conditions can lead to reduced efficiency in image classification.

(4) The images of cassava fields exhibit significant variations in weed invasion levels, which can potentially lead to a decrease in classification accuracy.

1.4 Benefits of the study

1.4.1 Contribution to knowledge

The study explored significant findings associated with the objectives of the research that presents a decent contribution to knowledge, which are:

(1) An appropriate process of a semi-automatic classification of objects in cassava fields of the sensitive variations of the UAV images. This process shows a simplified method for the classification technique using UAV images. It reduces the repeating process and time from training objects in the supervised classification. The explored finding can be a typical guideline for the UAV image classification to distinguish objects in other conditions.

(2) The study found indices suitable for identifying objects on the UAV image for a specific classification purpose. Also, the parameters examined in this research provide knowledge of the condition to set appropriate parameters for UAV image classification processes. It would say that it presents a structured process for examining the indices regarding similar objects in the UAV image classification. It presents a set of parameters, window sizes of the filtering process for extraction objects, spectral properties of objects, and rules of classifying objects acquired in the UAV image classification.

(3) This study explored the protocol for developing a classification process for UAV images, particularly suitable for identifying weeds in cassava fields in Nakhon Ratchasima province. The processes and parameters were tested in 12 cassava fields with plenty of data and variations. Traditional cassava cultivation presents similarities in objects of the cassava fields, which consist of cassava, weeds, soil, and perhaps trees. The developed protocol presents higher accuracy than common techniques like K-means and Random Forest classification. Considering the benefit of short-time processing, it also discriminates weeds from cassava precisely. This explored protocol can be applied to the cassava fields in Nakhon Ratchasima province, the most productive area in Thailand, and other fields with similar objects existing in the fields.

Regarding the knowledge contribution, the identified weed areas in the cassava field may be helpful for further classifying the specific weed species in the cassava field. The findings of this study initially shed light on the development of classifying objects with very detailed data on UAV images.

1.4.2 Contribution to relevant stakeholders

The results of this study contribute to the relevant stakeholders, government officers, and the private sector, as described in the following details.

(1) Government officers, such as GIS experts in the Department of Agriculture, may consider the explored weed maps of the study area to pilot and educate farmers about weed control in only the highly invasive weed areas. This protocol can be done repeatedly to monitor the invasive patterns of weeds in cassava fields using UAV images at different times. The identified weed areas in cassava fields can be delivered to the

farmers to control the weed invasion in those specific areas. This proactive effort will support the government policy to limit imported herbicides to Thailand. Therefore, the farmers will obtain an alternative way to control weeds in their fields and save the budget for spraying herbicides in the entire field. Eventually, customers of cassava product lines will not suffer from high toxin accumulation according to this activity.

(2) Private sectors, such as agricultural drone companies, may study the protocol of this research, which is able to create an extension of their service business in servicing the weed control in only highly invasive places in cassava fields. They probably monitor the invasive patterns of weeds in serviced cassava fields using the protocol of the explored semi-automatic classification, which can be done quickly and easily.

1.5 State-of-the-art

Very high-resolution images captured by UAVs are widely used in precision agriculture for weed monitoring and mapping. However, the process of capturing multiple images to create a map can introduce variations in lighting conditions. Additionally, the high resolution of UAV images leads to objects with a wide range of reflectance values, causing heterogeneity in the image analysis process.

Image classification is a crucial step in identifying weeds and crops in the field. For very high-resolution images, classification involves several processes, including preprocessing, feature extraction, classification, and validation. Segmentation and filtering techniques are used to simplify the data and improve image quality by dividing the image into homogeneous regions. Features extracted from the image, such as specific indices for objects or classes, play a vital role in the classification process. There are two main approaches of the classification process: supervised and unsupervised classification. In supervised classification, the user provides training to categorize the data, while unsupervised classification does not require training but relies on knowledge of the region. The classification model can produce accurate results for a specific area based on training or spectral characteristics of the image.

Customizing the model to specific requirements is important. Table 1.1 summarizes the advantages and disadvantages of these classification approaches.

Table 1.1 Advantages and disadvantages of the classification approach.

Approach	Advantages	Disadvantages
Supervised classification	<ul style="list-style-type: none"> • It can control and set to a specific purpose and specific region • Fitted to a specific area • The final map does not face the match the spectral categories problem • Classification errors can be corrected by the training process 	<ul style="list-style-type: none"> • The potential accurate results rely on training data that based on the user's knowledge and experience • Training data collect carefully in terms of quality and quantity aspects • Training data did not respond to the natural classes based on their spectral properties; thus, the classifier model may not classify in other data spaces
Unsupervised classification	<ul style="list-style-type: none"> • Not required training data • Minimizing the opportunity for human error in conducting classes • Recognizing small or unique classes 	<ul style="list-style-type: none"> • Require specifies the number of groups or clusters • Require region's knowledge • Result classes may not correspond with interest classes • Spectral properties of classes change over time

The developed classification process in this study, so called the proposed classification process, is a collection of preprocessing and classification techniques integrated to create a semi-automatic workflow. Various factors including indices, filtering parameters, and ground sample distance (GSD), are considered to ensure the

classification's reliability. The proposed classification process minimizes manual intervention in generating classification maps, distinguishing it from traditional supervised and unsupervised methods. Furthermore, the proposed process incorporates filtering and feature extraction steps, making it more user-friendly. Figure 1.2 and Table 1.2 provide a comparison between the conventional classification approach and the proposed classification process.

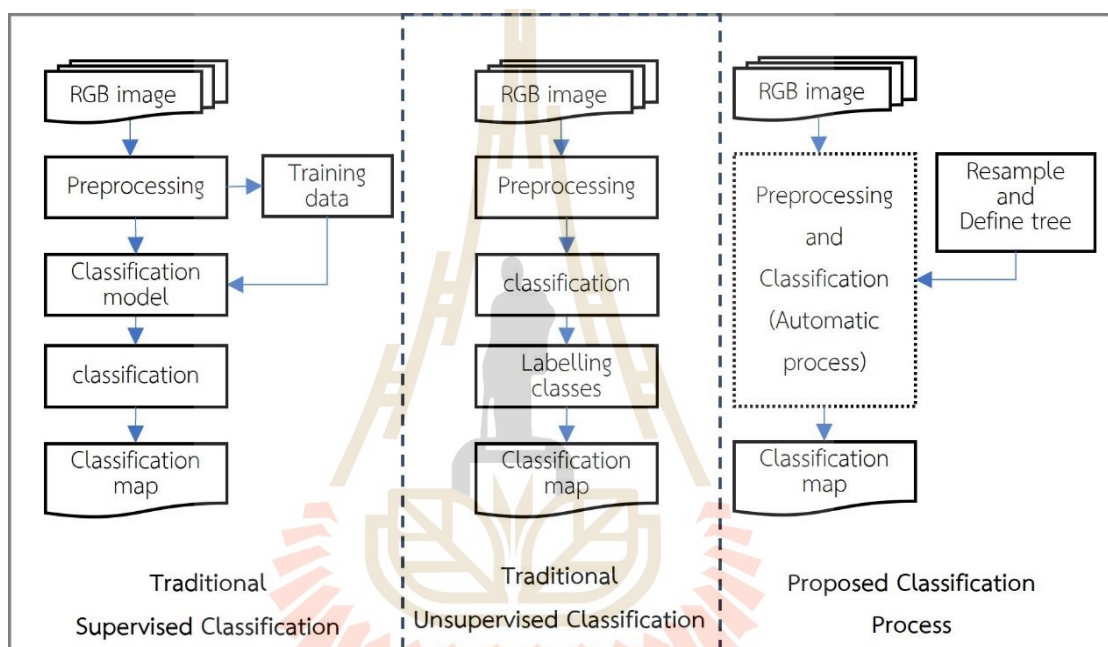


Figure 1.2 Flowchart of traditional supervised classification, traditional unsupervised classification, and proposed classification process.

Table 1.2 Process of traditional supervised classification, traditional unsupervised classification, and proposed classification process.

Process	Traditional Supervised Classification	Traditional Unsupervised classification	Proposed Classification Process
Preprocessing			
- Resample	Manual	Manual	Manual
- Define tree in image (with/without tree)	-	-	Manual
- Fill missing data	Manual	Manual	Automatic
- Filtering	Manual	Manual	Automatic
- Image segmentation	Manual	Manual	-
- Feature extraction and selection (Indices)	Manual	Manual	Automatic
Classification			
- Model building and training	Manual	-	-
- Classification: select classifier and define parameters	Manual	Manual	Automatic
- Labelling classes	-	Manual	Automatic

The study identified the optimal features, parameters, and conditions required for accurate classification in this context through extensive experimentation. The proposed classification process was then applied to analyze various cassava field images, considering various conditions. The classification maps of twelve cassava plots exhibited the highest overall accuracies (OA) at 0.97 and the highest kappa coefficients at 0.96. The experiment conducted at the seven sample sites (selected from the twelve cassava plots) revealed that the proposed classification process achieved a level of accuracy that is comparable to supervised methods such as RF classification. However, RF classification requires users to manually select the sample set for training, features for classification, segmentation parameters, and RF classification parameters for each area. In contrast, the proposed classification process simplifies the user's role

by only requiring the definition of whether an image contains a tree or not, with the remaining processes being automated. This new classification process for objects in cassava fields using very-high-resolution images from UAVs provides accurate results while reducing the manual effort required from the user. These advantages make the proposed classification process a promising approach for achieving efficient classification in the domain of cassava fields.

1.6 Study area

The study areas are cassava fields located in Mueang district, Nakhon Ratchasima province, Northeastern region of Thailand. Nakhon Ratchasima is renowned for having the highest cassava harvested area and production in the country.

Generally, the cultivation area of field crops or economic crops is often prepared in open areas, but some areas still have a tree in the field for some purposes. In the study of Vityakon and Prachaiyo (1992), it was found that the presence of trees in the plantation area was caused by the farmers in the past who changed the forest area to agricultural areas. Some of the trees were left at the edge of the plot or in the plot because it was a large tree or a tree that affected beliefs or presented of anthill (according to Thai belief, that is a place of holy things). The trees in the fields are used as food, fuel, animal feed, and a place for rest while farmers work in the fields. For cassava planting, the shade of the trees was used for placing cassava stems for 2-3 months from harvesting to the new planting season, as seen in Figure 1.3. The trees in the fields are still present in current agriculture in Thailand. Figure 1.4 shows agricultural areas with trees from different provinces in Thailand.



Source: Polthane (2018)

Figure 1.3 Cassava stems stored under trees.



Figure 1.4 Agriculture areas with trees from different provinces in Thailand.

The study areas were selected to display the plantation culture in Thailand. The selected area includes twelve cassava plantation plots (plots 1-12), as shown in Figures 1.5-1.7. Each plot consists of three main components, including cassavas, weeds, and soil, and some plots contain trees inside and outside the cultivation area. The planting patterns of the study area varied; the growing condition, including soil type and water system. Plots 4, 5, and 11 were planted with a drip irrigation system. Each plot presented varied weed invasion levels and cassava and tree canopy sizes. Moreover, the light illumination of each image was dissimilar because of the different captured times.



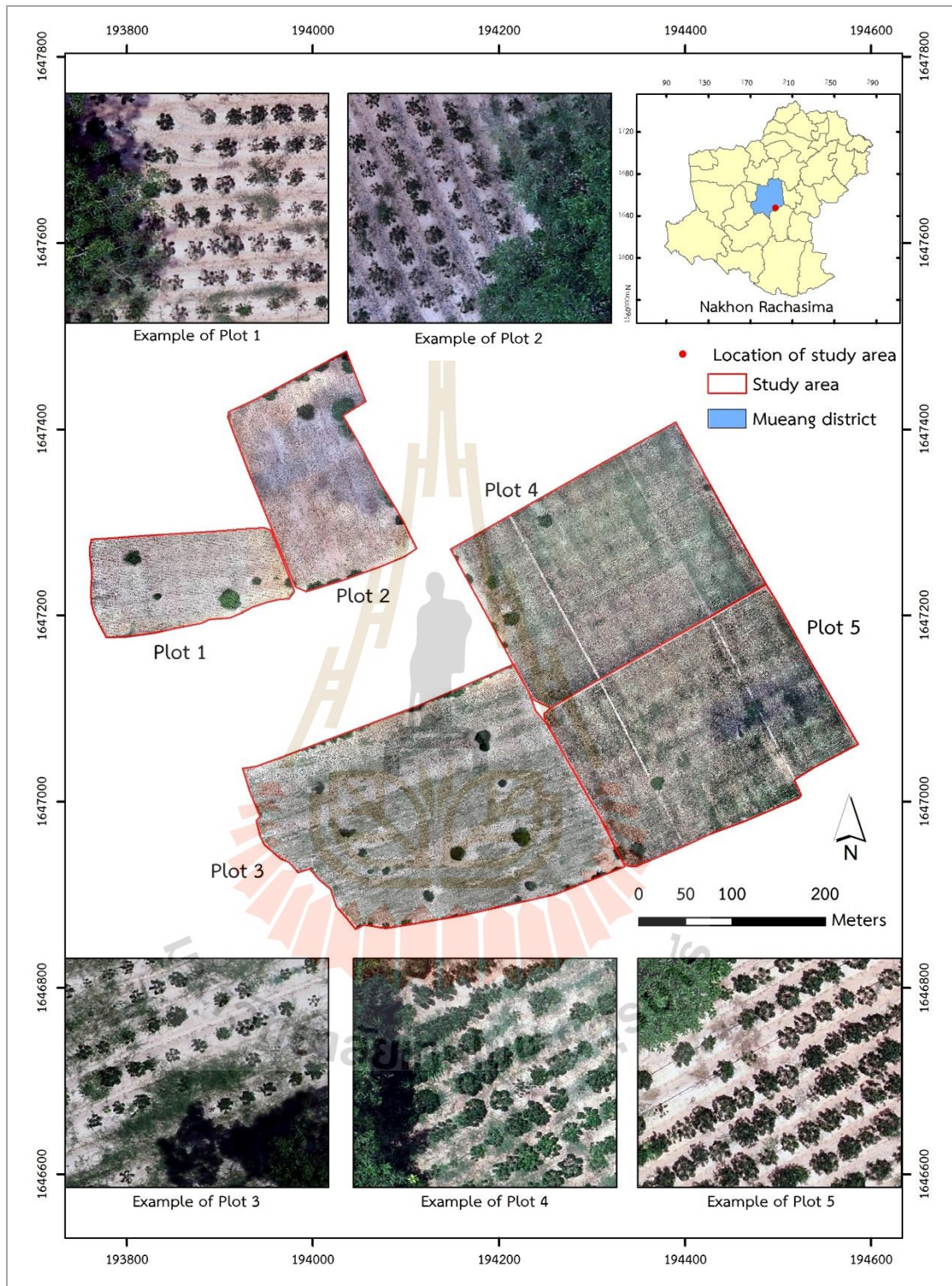


Figure 1.5 Locations, overview, and samples of cassava plot 1-5.

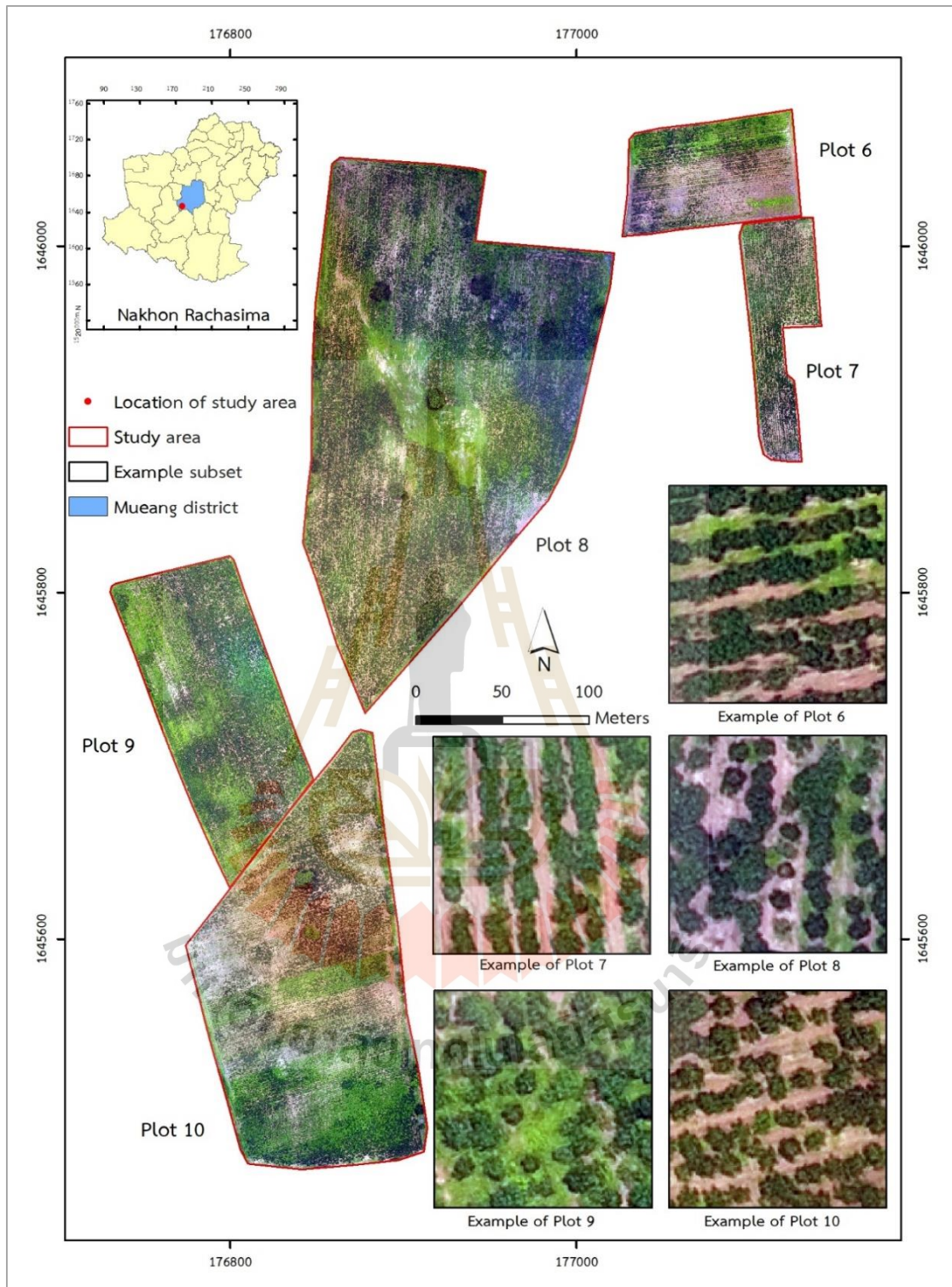


Figure 1.6 Locations, overview, and samples of cassava plot 6-10.

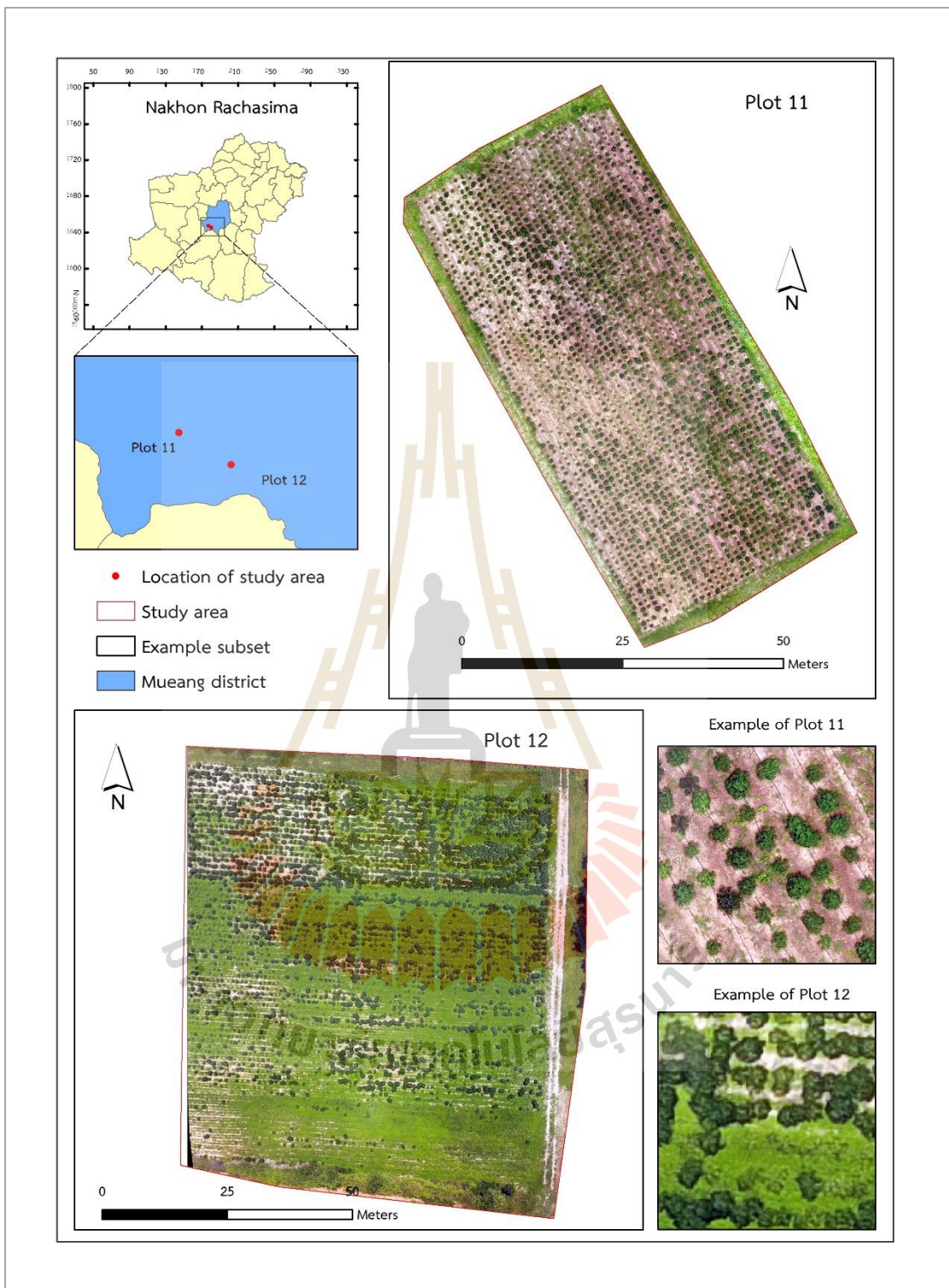


Figure 1.7 Locations, overview, and samples of cassava plot 11-12.

The study areas were captured from two different sensors that contain different properties. The original GSD of the images was between 1.21-5.00 cm due to the flight altitude and sensor. The cassava canopy's average diameter and standard deviation (S.D.) were measured from the original image by randomly selecting 100 samples for each plot. The average cassava diameter varied between 52-88 centimeters, representing the difference in cassava size in the study area. The details of the study area are shown in Table 1.3.

Table 1.3 Details of the study area.

Plot	Area (sq.m.)	Area (rai)	Contain Tree	Average cassava diameter (cm)	S.D. (cm)
1	19,826.8	12.39	✓	57.42	08.25
2	27,816.8	17.39	✓	52.11	09.09
3	70,671.1	44.17	✓	52.14	09.25
4	56,636.6	35.40	✓	71.28	09.05
5	55,741.4	34.84	✓	70.36	08.37
6	5,918.68	3.70	✗	76.22	15.31
7	4,271.5	2.67	✗	75.80	13.27
8	36,776.5	22.99	✓	86.38	14.92
9	11,657.5	7.29	✓	83.38	15.91
10	22,928.2	14.33	✓	74.88	12.78
11	3,092.98	1.93	✗	65.26	11.56
12	5,884.63	3.68	✗	87.83	15.04

The Cassava canopy size of the study area was plotted as a boxplot, as shown in Figure 1.8, to demonstrate the spread and skewness of the diameter data. Data from each plot were arranged and grouped into five elements to draw the box: minimum, maximum, median, first quartile, and third quartile. The line in the box represented

the median of the data for each plot, the lower and upper area from the median line presented the first and third quartile of the data, extended line from the box (whisker) illustrated the minimum and maximum data within 1.5 box height from the box, and dots beyond the whiskers present the outlier of the data. Cassava sizes in the study areas were between 52-88 centimeters. The study area shows the various canopy sizes of cassava, both within and between plots.

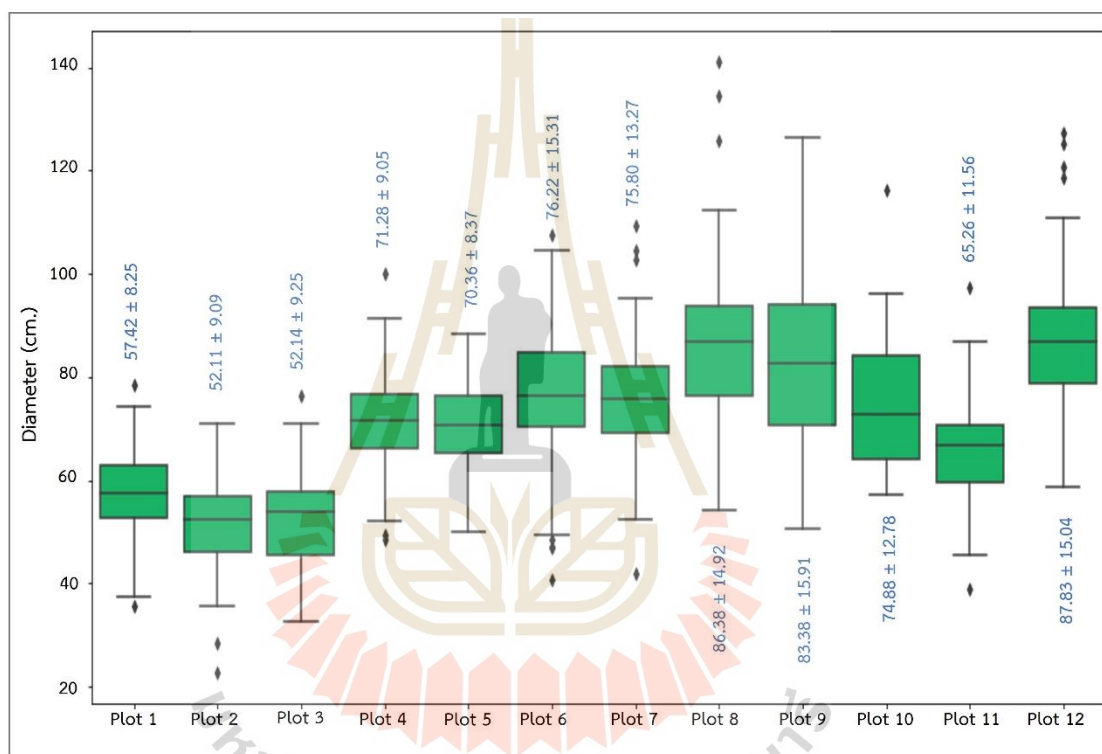


Figure 1.8 Boxplot of canopy diameter of cassava in the study area.

The cassavas were infested with weeds, and the trees covered part of the cassava and weed in the field. There are many types of weeds in the study area. Examples of images of weeds are shown in Figure 1.9. Weeds were presented as a single and patches around the cassavas. Cassavas and weeds are in different colors, textures, and leaves shades.



Figure 1.9 Weeds invasion in study area.

Figure 1.10 presents the spectral values of cassava, weed, soil, and the tree in the study area. The red, green, and blue bands normalized from 0-255 and extracted to a polygon created based on virtual interpretation from the original image. Spectral values of each class were collected from pixels within the polygon and then averaged to represent the sample value. The boxplot of classes in the study area's red, green, and blue bands shows the high variation of digital number (DN) value in the class. Vegetation with green color in the study area shows lower value in red, green, and blue than non-vegetation components. Although the plot is a neighboring area, the value of all classes contained in each plot had different ranges within the class, representing the study area's diversity.

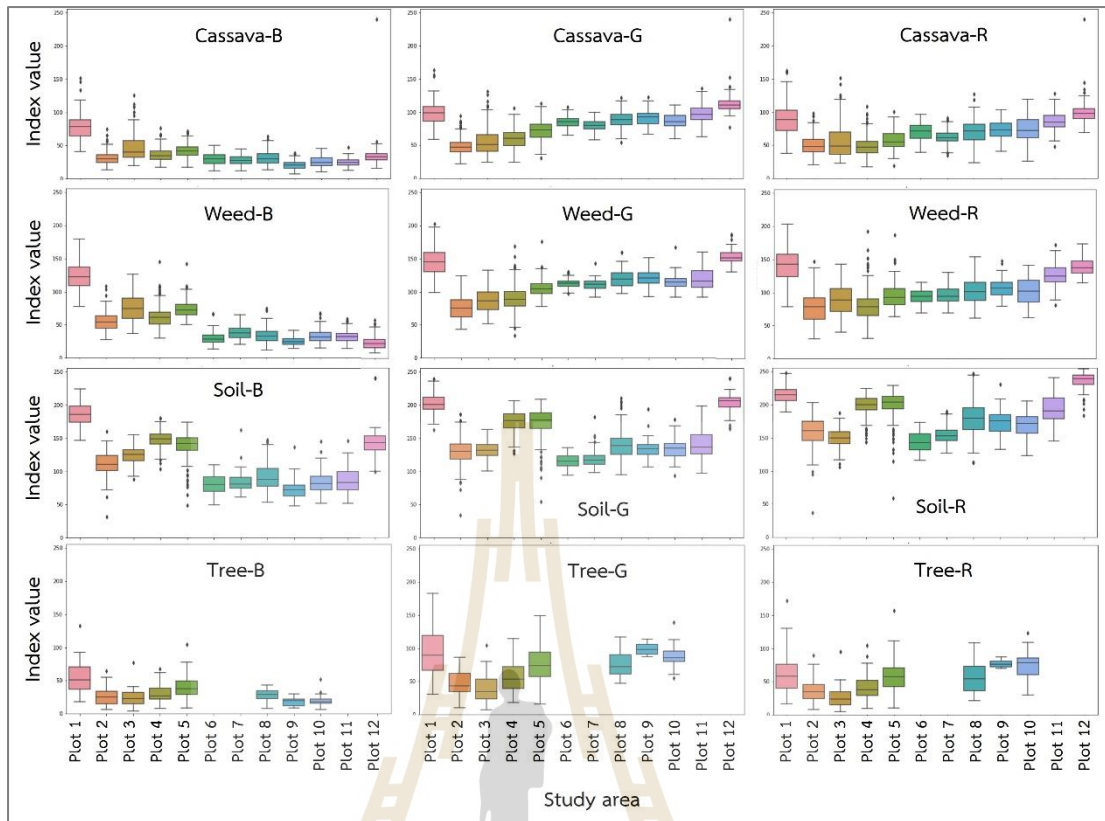


Figure 1.10 Boxplot of the spectral value of cassava in the study area.

CHAPTER II

RELATED CONCEPTS AND LITERATURE REVIEWS

This section uses UAV images to explain concepts and theories for detecting weeds in crop fields. First, the importance of cassava and the processes for growing cassava were summarized in the topic of cassava. Details of RGB data and their indices are described in the spectral discrimination of vegetation because these are crucial components for weed discrimination. Finally, critical theories for developing the classifier were summarized, including image segmentation, mean-shift filtering, and K-means clustering.

2.1 Cassava

2.1.1 Important of cassava

Cassava or tapioca (*Manihot esculenta Crantz*) is one of the most important economic crops in Thailand. Products of cassava are fresh root, starch, chip, and pellets. Most of them are raw materials in food, pharmaceutical, animal feed, sweeteners, textiles, monosodium glutamate (MSG), and ethanol. Thailand is the third-largest cassava producer and the world's largest exporter of cassava products (FAOSTAT Statistical Database, 2022). Approximately 8 million tons of cassava were exported in 2018, valued at around 74 billion bahts (Arthey, Srisompun, and Zimmer, 2018; Office of Agricultural Economics, 2021).

In Thai agriculture, cassava has increased in the harvested area since the 1970s (Figure 2.1), covering more than 1.7 million hectares in 2021 (FAOSTAT Statistical Database, 2022; OAE, 2022). Figure 2.2 presents Thailand's cassava production of 2020 at the provincial level, with most of the cassava produced in the Northeastern region. The five provinces that produced the highest cassava production included Nakhon Ratchasima (4.6 million tons), Kamphaeng Phet (2.3 million tons), Chaiyaphum (1.8 million tons), Kanchanaburi (1.6 million tons), and Ubon Ratchathani

(1.5 million tons). Cassavas are called insurance crops because the farmer can harvest and sell them at any time, not only during the period as sugarcane (Polthanee, 2018). Thus, cassavas are an essential source of cash income for farmers.

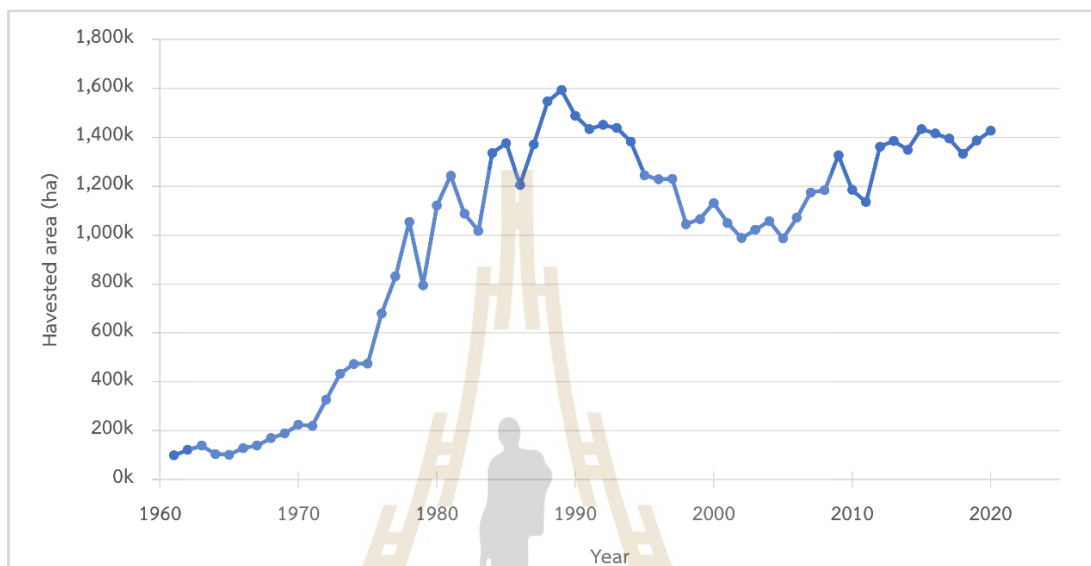


Figure 2.1 Cassava harvested area of Thailand.



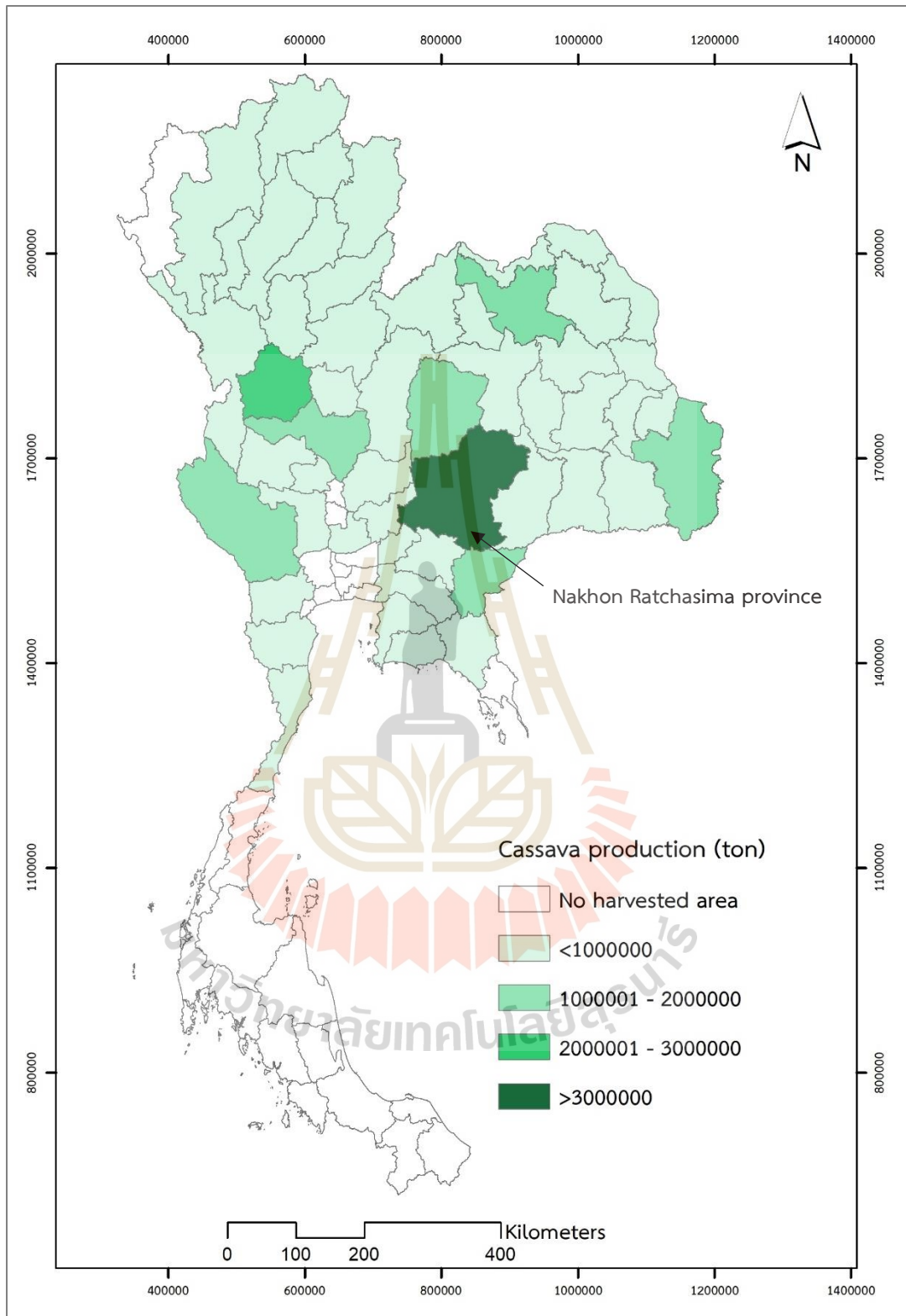
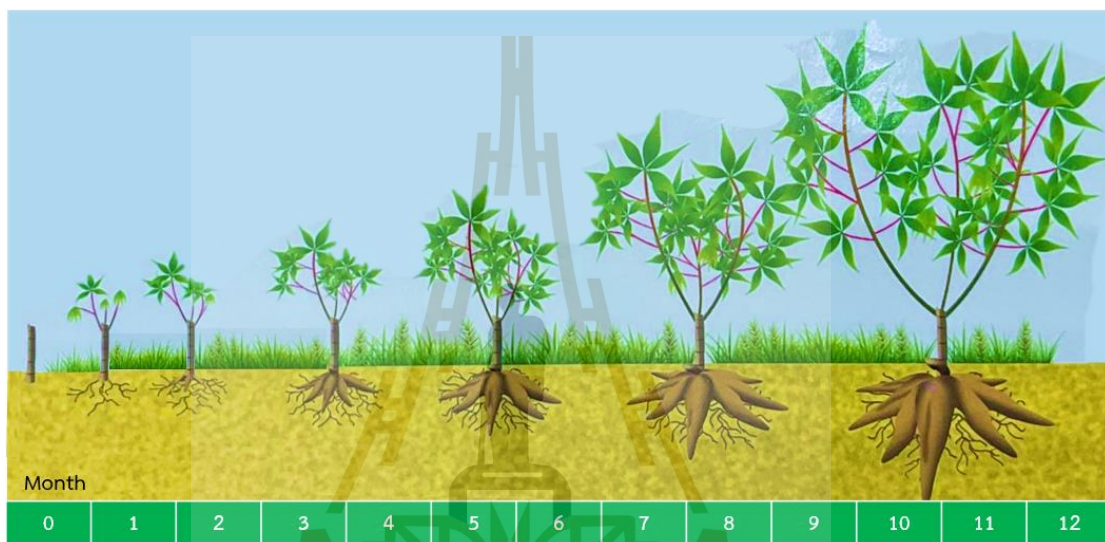


Figure 2.2 Cassava production in Thailand.

2.1.2 Growing cassava

Cassava is a drought-tolerant crop grown in dried soils and adapted well to various cultivating conditions (Howeler et al., 2013). Although cassava is simple to grow, weeds and diseases have dominantly affected the productivity of cassava yield (Wydra and Verdier, 2002). Cassava requires a long growing period; growth states are shown in Figure 2.3.



Source: Plant protection research and development office (2016).

Figure 2.3 Cassava growth stages.

Typically, Thai farmers plant cassava before the rainy season (March-April) or after the rainy season (November-December). The processes of cassava planting include cassava variety preparation, land preparation, pest control, and harvesting. Details of the processes are as follows:

(1) Cassava varieties and preparing

There are three groups of cassava planting in Thailand: sweet type (for direct consumption), bitter type (for processing), and ornamental type. Most cassavas planted in Thailand are bitter, have high starch content, and are usually used as raw industrial materials. The cassava species included Rayong 1, Rayong 3, Rayong 5, Rayong 7, Rayong 9, Rayong 11, Rayong 60, Rayong 72, Rayong 90, Kasetart 50, Huay Bong 60, Huay Bong 80, Sriracha 1 and others (OAE, 2022).

Cassava is planted with stems cut about 20-35 centimeters from the middle of a healthy and free of diseases and pathogens cassava. Farmers always soak the stems in pesticides before planting to eliminate diseases and pathogens.

(2) Land preparing

Cassava requires a loose texture and well-drained soil to facilitate the growth of roots and clearing from weeds to prevent competition with young crops in its initial state. The land should dry for at least two weeks and till again to control weeds. The land should form into ridges (Figure 2.4) with a space of 0.8-1 meter and a height of 30 centimeters. Cassava stems are usually planted at a distance of 0.8-1 meter between and within a row.



Source: Department of Agriculture (2001).

Figure 2.4 Land preparation into ridges forms for cassava planting.

(3) Pest management

Cassavas are weak and require well-managed in the first four months after planting or until the cassava canopy is closed. Pest management is done according to the age range, as shown in Table 2.1.

Table 2.1 Pest management for cassava.

Age (month)	Pest	Management
0	Mealy bug and Scale insect	Soak stems in pesticides
	Stem bright disease	Soak stems in fungicide
	Weeds	Apply pre-emergent weed control
1	Witches' broom and bright stem disease	Remove stem and burn outside the fields
	Red mite	Apply insecticide
2-3	Mealy bug	Control by insects (parasitic wasps or green lacewing) or apply insecticide
	Anthracnose, root rot, and root-knot disease	Apply fungicide
	Weeds	Apply post-emergent herbicide or remove them with human labor
4	Anthracnose, root rot, and root-knot disease	Apply fungicide
	Witches' broom disease	Remove the disease stem and burn outside the fields, and apply fungicides to the rest of the crops
	Weeds	Apply post-emergent herbicide or remove them with human labor

(4) Harvesting

Cassava roots were harvested 8-14 months after being planted, and around 70 percent of cassavas in Thailand were harvested at 10-12 months (OAE, 2022). Cassavas were harvested by cutting the stem above the ground at least 30 centimeters and digging the roots out by hand or machine. Due to the growing conditions, average cassava yields are 21-23 tons per hectare (Arthey et al., 2018).

2.1.3 Weed control

Weeds are a barrier to growing crops, which causes the loss of quality and quantity of crops. Not only snatching up the essential nutrients of crops, but weeds are also a habitat of pests, including aphids, mealybugs, scarlet mites, and phytoplasma, the causative agent of cassava bush disease (Plant protection research and development office, 2016). Because cassavas are slowly grown in the initial period, weeds have a high opportunity to compete with the young cassavas. An extreme invasion of weeds can cease the growth and reduce up to 80% of cassava yields (Jeamjamnanja et al., 1984).

Controlling weeds is an essential process in cassava growing. The appropriate time for controlling weeds is in the early period before the canopy closes, at 3, 8, and 12 weeks after planting (Ekanayake, Osiru, and Porto, 1997). For the first 3-4 months, cassava leaves, stems, roots, and tubers are produced. Several tubers developed in this period; thus, this was crucial for cassava. However, cassava cannot compete well with weeds in this period because the root system is young and weak. Weed competition, especially the fast-growing weeds, is obstructed for canopy and tubers development. After planting for four months, the tuber size is developed, the cassava canopy grows and connects to the neighbors, the canopy will shade, and most weeds cannot compete with cassava.

Common approaches for controlling weeds in crops are physical control (removal by mowing, mulching, tilling, burning, grazing, or by hand), cultural practices (tillage, irrigation), and chemical control (use of chemical substances). Herbicides, chemical substances used for weed control, are often used to control weed in a large field or when lacking labor. Weed controlling costs one-third of the total cost of cassava growing (Plant protection research and development office, 2016), which is trending to increase due to the increasing price of herbicides (McGeeney, 2022).

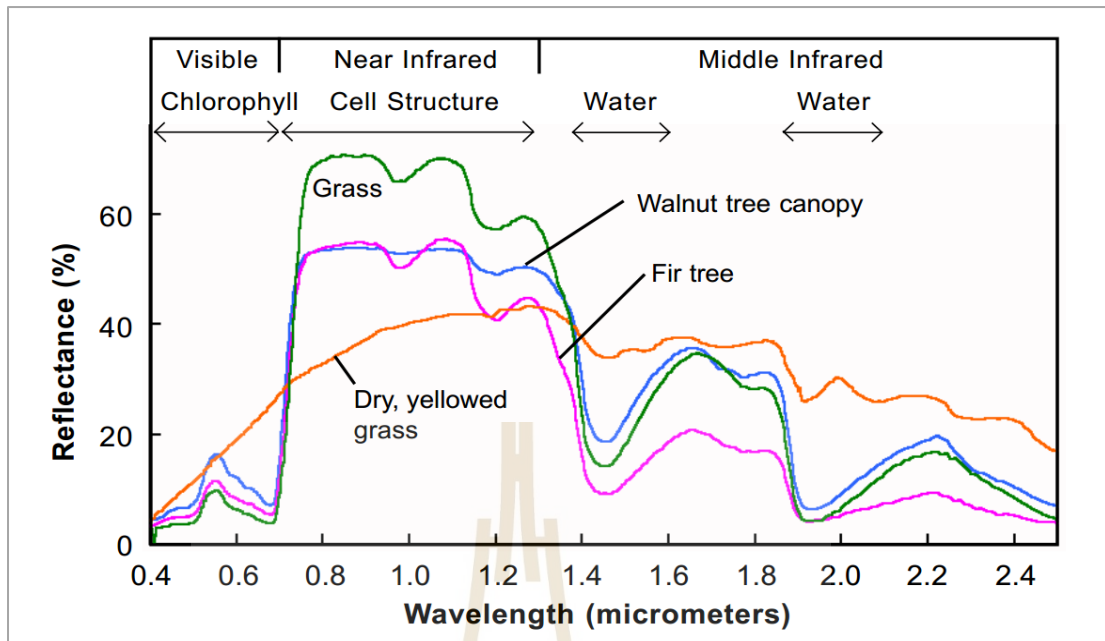
Herbicides for weed control in crops are applied by spray equipment using human labor, which has some limitations, including difficulty accessing the complex area with the terrain and managing the number of herbicides, and the effect of herbicides on human health has been a concern. Recently, UAV spray technology has been developed to serve agricultural purposes, including pesticide and herbicide

applications. Regarding the combined advantages of UAV spraying and weed identification systems, herbicide control becomes more cost-effective and safer for farmers' health.

2.2 Spectral discrimination of vegetation

The relation of electromagnetic radiation with plants varies with the radiation wavelength. Each vegetation type has a signature spectral pattern that can identify its species. Also, the same plant leaves will exhibit significant differences in how they reflect light depending on health and vigor (Woolley, 1971). The amount of radiation reflected from plants is inversely related to radiation absorbed by plant pigments and varies with the wavelength of incident radiation (Mulla, 2013). The reflectance of vegetation in various spectrum wavelengths is shown in Figure 2.5.

The study of vegetation is mainly based on near infrared (NIR) wavelength because it has a strong reflectance, as seen in Figure 2.5, which can clearly show the differences in plants. However, a sensor for collecting the NIR data was more costly and more difficult to mount to UAVs because it is not available with optical sensors. Moreover, the NIR-based images were difficult to verify the anomaly of vegetation without comparing it to natural color (G. E. Meyer and Neto, 2008). According to the visible spectral, the reflectance of plants is shared the same pattern but is different in percent of reflectance due to the different colors and shades of leaves (Gates, Keegan, Schleiter, and Weidner, 1965), which refer to plant species and health of the plant. These properties make the optical sensors able to separate objects also plant types. The studies of Bah, Hafiane, and Canals (2018); Gao et al. (2018); Gašparović et al. (2020); Huasheng Huang et al. (2018); Lottes et al. (2017); Subeesh et al. (2022); Woebbecke, Meyer, Barga, and Mortensen (1995) showed that the low-cost RGB sensor was applied for weed identification.



Source: Smith (2012).

Figure 2.5 Reflectance spectra of different types of green vegetation compared to a spectral signature for senescent leaves.

RGB-color images with red (R), green (G), and blue (B) channels have been used to detect information in plants such as stress, disease, and type (Chaudhary, Chaudhari, and Godara, 2012; Hall et al., 2018; Lameski, Zdravevski, Trajkovik, and Kulakov, 2017; Zakaluk, Sri Ranjan, and Ranjan, 2008). The data provided from UAV images are DN values, while the signature of objects is presented by reflectance spectra value. The DN data can represent the trend of the reflectance value. Thus, the indices calculated from the DN data also provided qualities of the object's spectral signature (Candiago, Remondino, De Giglio, Dubbini, and Gattelli, 2015).

The index is a spectral transformation of two or more bands designed to enhance the contribution of vegetation properties. Indices have been widely used for evaluating vegetation cover, growth dynamics, and biomass (Jinru and Su, 2017). Using color indices in crop and weed detection has various advantages. For example, the indices highlighted green color from the images, less sensitive in light conditions and can extract information which challenging to distinguish and compare by humans (G. E. Meyer and Neto, 2008).

The UAV image quality is susceptible to illumination; rapid changes in weather conditions may cause non-smooth light in the images. Several studies in weed detection using UAV images have developed the processes of image processing techniques to solve illumination problems. Illumination issues play an essential role in the classification process. Color indices have been proven to reduce illumination problems in normal light conditions (Hamuda, Glavin, and Jones, 2016). However, the indices vary depending on crop types and intense light conditions (Hamuda et al., 2016). The widely used RGB-based indices showing plant and soil properties are shown in Table 2.2.

Table 2.2 Spectral indices based on RGB values to distinguish vegetation and non-vegetation.

Index	Equation	Dominant	Reference
Excess Red (ExR)	$1.4 \times r - g$	red spectrum extraction	G. Meyer, Hindman, and Laksmi (1999)
Excess Green (ExG)	$2g - r - b$	green spectrum extraction	Woebbecke et al. (1995).
Excess Blue (ExB)	$1.4 \times b - g$	blue spectrum extraction	Guijarro et al. (2011)
Excess Green minus Excess Red (ExGR)	$ExG - ExR$	highlight vegetation	G. E. Meyer and Neto (2008)
Normalized Green Red Difference Index (NGRDI)	$\frac{G - R}{G + R}$	vegetation discrimination	Tucker (1979)
Green Leaf Index (GLI)	$\frac{2G - R - B}{2G + R + B}$	vegetation discrimination	Louhaichi, Borman, and Johnson (2001)
Visual Atmospheric Resistance Index (VARI)	$\frac{G - R}{G + R - B}$	vegetation discrimination	Gitelson, Kaufman, Stark, and Rundquist (2002)

Table 2.2 Spectral indices based on RGB values to distinguish vegetation and non-vegetation (Continued).

Index	Equation	Dominant	Reference
Brightness Index (BI)	$\sqrt{\frac{G^2 + R^2}{2}}$	soil discrimination	Mathieu, Pouget, Cervelle, and Escadafal (1998)
Color Index (CI)	$\frac{R - G}{R + G}$	soil discrimination	Escadafal and Huete (1991)

where:

R, G, B is digital number of red, green, and blue channels (0-255)

$$r = \frac{R^*}{R^*+G^*+B^*}, g = \frac{G^*}{R^*+G^*+B^*}, b = \frac{B^*}{R^*+G^*+B^*}$$

$$R^* = \frac{R}{255}, G^* = \frac{G}{255}, B^* = \frac{B}{255}$$

2.3 Image segmentation

Image segmentation is a process for segmenting or grouping the objects in the images. Segmentation is an essential process for image processing applications, which is applied in many fields, such as medicine, object recognition, and agriculture. In the agricultural field, the segmentation process is mainly used to segment plants from the background (soil and sky) and segment plant types (crop and weed). Segmentation is an important process in image analysis since the segmentation results impact the analysis's quality and performance in automatic processing (Morales et al., 2011).

There are various ways to categorize image segmentation approaches, for example, thresholding, edge-based, region-based, clustering, watershed, Partial Differential Equation (PDE), Artificial Neural Network (ANN), and neural network. The main approaches were summarized as follows:

(1) Edge Based

Segmentation based on edge detection is a method for locating the boundary of objects. The edges or boundaries were identified from the rapid change of intensity or pixel brightness value, then connected to form closed object boundaries. The edge location was detected by following one of these criteria (Kaur and Kaur, 2014; Narkhede, 2013):

- 1) the first derivative of intensity is larger than the threshold, or
- 2) the second derivative of intensity is zero crossing.

This approach was sensitive to noise. Thus, it requires an image enhancement process to reduce or remove noise (Kuruville, Sukumaran, Sankar, and Joy, 2016; Narkhede, 2013). There are many techniques for detecting edges, for example, Sobel, Laplacian, Canny, and Laplacian of Gaussian detection.

(2) Threshold-based

Image segmentation based on thresholding is the simplest method for segmentation. The threshold values are calculated from a binary image, which can be manually defined or automatically calculated from the image. The threshold value is the criteria for separating pixels of an image into the region or separating objects from the background. This approach is suitable for segmenting the light object on a shaded background but is sensitive to light illumination (Kuruville et al., 2016).

(3) Region-based

Segmentation based on region is a process of partitioning an image into a region. Regions are used to represent the whole object or some part of the object in the image (Kuruville et al., 2016). The region-based segmentation used value similarity (which contains grey value differences and variance) and spatial proximity (which contains Euclidean distance and compactness of a region) for partitioning pixels (Narkhede, 2013). This approach also requires the thresholding technique. There are two main types of region-based segmentation: region growing and splitting and merging. Some researchers grouped the watershed method and clustering method in the region-based segmentation approach because these methods produced

segmentation based on the similarity of pixel data (Raja, Abdul KhadiRr, and Ahamed, 2009).

(4) Cluster-based

Image segmentation based on clustering is a method for grouping objects using similarity properties. Pixels with similar characteristics were grouped together to form clusters. There are two main types of clusters: hard clustering and soft clustering. A pixel belongs to only one cluster in the hard, complex clustering type. An example of a hard clustering type is K-means clustering. While soft clustering is more flexible, a pixel is partitioned into a cluster; thus, one pixel can belong to more than one cluster. Fuzzy C-means is an example of a soft clustering type.

Segmentation is an essential process for digital image processing, especially high-resolution images. This process aims to remove the complexities of the image and or enhance or edit the image's appearance. However, implementing each method is suitable for different images and purposes of use. There are some advantages and disadvantages of each segmentation approach summarized in Table 2.3.

Table 2.3 Advantages and disadvantages of the segmentation approach.

Approaches	Advantages	Disadvantages
Edge-based	<ul style="list-style-type: none"> • Results are similar to the human perspective • Suit for image with good contrast between objects 	<ul style="list-style-type: none"> • Not suited for images with ill-defined edges or many edges • Sensitive to noise • Difficult to produce close curve boundary
Threshold-based	<ul style="list-style-type: none"> • Fast processing • Noncomplex for computational • Not require prior information 	<ul style="list-style-type: none"> • Sensitive to noise • Depending on histogram peaks • Not suited for images with unapparent peak (broad or flat)

Table 2.3 Advantages and disadvantages of the segmentation approach (Continued).

Approaches	Advantages	Disadvantages
Region-based	<ul style="list-style-type: none"> • Suit for image with good contrast between objects • Work well with the homogeneous region • Consider spatial information • Provide region continuity result 	<ul style="list-style-type: none"> • Require more time and memory for computational • Not suited for images with noise
Cluster-based	<ul style="list-style-type: none"> • Fast processing for a small number of clusters • Eliminate noise • Can process automatically 	<ul style="list-style-type: none"> • Difficult for the high-value clusters

These segmentation approaches are based on an iterative technic with stop criteria limitations. The stop criteria require much memory or involve threshold parameters that are difficult to optimize (Tian, Hsiao-Chun, and Huang, 2014). Mean-shift filtering is a non-parametric method. This method uses entropy as a stop criterion for the iterative process. The entropy of the region or group was reduced in an iterative process until it reached a stable value (convergence) when the image became homogeneous. The study of Rodríguez et al. (2011) proved that the results from mean-shift filtering were similar to results obtained by segmentation; the image presented natural aspects and still preserved details of the original images. Dorin Comaniciu and Meer (2002) and Grenier, Revol-Muller, and Gimenez (2006) also state that mean-shift filtering gives products close to products from clustering-based segmentation. Thus, segmentation can be obtained directly through filtering (Morales et al., 2011; Rodríguez et al., 2011).

2.4 Mean shift filtering

Mean shift is a non-parametric iterative algorithm developed by Fukunaga and Hostetler (Fukunaga and Hostetler, 1975) and has been widely used for filtering and clustering analysis in computer vision and image processing. The mean shift shows a high potential for edge preservation in filtering and segmentation processes (D. Comaniciu and Meer, 1999). The mean-shift method considers the image's geometric and photometric during the process (Song, Gu, Cao, and Viberg, 2006). The theory of the mean-shift algorithm and mean-shift filtering summarized by Li (2012) are described below.

The mean-shift algorithm can be considered a gradient ascent on the density function. This problem can be written as:

$$\nabla \hat{f}(x) = 0 \quad (1)$$

Using a non-parametric kernel-based probability density function estimation to solve the problem in equation (1), the quantity $m(x)$ is called the mean-shift vector as the following:

$$m(x) = x^{[t+1]} - x^{[t]} = \frac{\sum_{i=1}^n g(d^2(x^{[t]}, x_i, H)) \cdot x_i}{\sum_{i=1}^n g(d^2(x^{[t]}, x_i, H))} - x^{[t]} \quad (2)$$

Where t is the iteration variable, d is Mahalanobis distance, $x^{[0]}$ is set to a given x_i , and $g(\cdot)$ is a weight function deriving from the kernel function.

The procedures of mean-shift filtering are described as follows. Let $x = (x_s, x_r)$ be vector and bandwidth matrix H composed of $[H_s, H_r]$. Where subscript s and p represent spatial and range (pixel value) of vector and bandwidth matrix. The bandwidth matrix can be defined as

$$H = \begin{bmatrix} H_s & 0 \\ 0 & H_r \end{bmatrix} = \begin{bmatrix} h_s^2 \cdot I^p & 0 \\ 0 & h_r^2 \cdot I^q \end{bmatrix} \quad (3)$$

where h_s is the scalar value of spatial bandwidth, h_r is the scalar value of range bandwidth, I is the identity matrix, p is the number of spatial dimensions, and q is the

number of range dimensions of an image. For the three-layer image, p and q are 2 and 3, respectively.

The kernel in one-dimensional is expressed as:

$$K(x) = [x_s, x_r] = \frac{c}{(h_s)^p \cdot (h_r)^q} K\left(\left\|\frac{x_s}{h_s}\right\|^2\right) \cdot K\left(\left\|\frac{x_r}{h_r}\right\|^2\right) \quad (4)$$

A color image that includes three feature space components is taken to illustrate the procedures of mean-shift filtering. Let $\{x_i\}_{i=1,2,\dots,n}$ and $\{z_i\}_{i=1,2,\dots,n}$ be the original and the filtered image points in the d -dimensional feature space, respectively. The mean-shift filtering algorithm can be summarized as:

- (1) Initialize $x^{[0]}$ to a given x_i ,
- (2) Initialize a bandwidth matrix $H = \begin{bmatrix} h_s^2 & 0 & 0 & 0 & 0 \\ 0 & h_s^2 & 0 & 0 & 0 \\ 0 & 0 & h_r^2 & 0 & 0 \\ 0 & 0 & 0 & h_r^2 & 0 \\ 0 & 0 & 0 & 0 & h_r^2 \end{bmatrix}$,
- (3) Compute $x^{[t+1]}$ the following equation (2) until convergence,
- (4) Assign to z_i the spatial position of x_i and the range value of $x^{[t+1]}$, so $z_i = ((x_i)_s, (x^{[t+1]})_r)$,
- (5) Iterate the above steps for each point x_i of the image.

The method operates by defining the window (kernel) from geometric (spatial radius) and photometric (color or pixel value). The pixels in the window were neighbors. The window slides in the image and analyzes the neighborhood's mean, then shifts the target pixel with the mean value. These processes will iterate until the mean value is not changed or convergence, which corresponds to the object of interest. The resulting image is smoothed, and the noise is reduced. Mean shift filtering is highly adaptive to object shape and size, which makes it an extensive method for detecting and tracking in computer vision applications (Khattak, Raja, Anjum, and Qasim, 2015). The kernel size only controls the mean-shift and requires less manual intervention than other algorithms (Zhou, Wang, and Schaefer, 2011). Moreover, this method is computationally efficient, fast processing, and robust to variations of object shape (Dorin Comaniciu and Meer, 2002; Xiang, 2009).

While the mean-shift method has several advantages, limitations should be considered. The convergence to the local than the global maximum, especially in images with multiple objects. The performance of the mean-shift method was impacted by the parameter (bandwidth), which is based on the size and contrast of objects (Morales et al., 2011). However, the size of the mean-shift kernel is essential. However, there is no method for selecting the optimum kernel size (Collins, 2003). Finding an optimal kernel size of mean-shift filtering to the interest object is challenging.

2.5 K-means clustering

Clustering is a technique for finding subgroups or clusters in the dataset based on the homogeneous character of the dataset without training or supervision. K-means clustering is one of the most popular unsupervised classifications. K-means clustering is an approach for partitioning data into clusters. The K-means clustering algorithm requires the user to specify the desired number of clusters (k). It then assigns each observation in the dataset to one of the k clusters. The objective of K-means clustering is to minimize the summation of within-cluster variation.

Gareth, Daniela, Trevor, and Robert (2015) summarized the principle of K-means clustering as follows. The within-cluster variation $W(C_k)$ is estimated from the different observation data and a mean value of the cluster, the calculation starts from:

$$\underset{C_1, \dots, C_k}{\text{minimize}} \left\{ \sum_{k=1}^K W(C_k) \right\} \quad (5)$$

where C_k contains the indices of the observation data in each cluster. The sum of within-cluster variation could be as small as possible. The square Euclidean distance was the method for finding the minimized value of equation (5), defined as

$$W(C_k) = \frac{1}{|C_k|} \sum_{i, i' \in C_k} \sum_{j=1}^p (x_{ij} - x_{i'j})^2, \quad (6)$$

where $|C_k|$ is the number of observation data in cluster k and p is the number of features of observation data. Then replace the Euclidean function with the mean for feature i in the cluster C_k as expressed in (7), and the within-cluster variation function becomes (8)

$$\bar{x}_{kj} = \frac{1}{|C_k|} \sum_{i \in C_k} x_{ij} \quad (7)$$

$$\frac{1}{|C_k|} \sum_{i, i' \in C_k} \sum_{j=1}^p (x_{ij} - x_{i'j})^2 = 2 \sum_{i \in C_k} \sum_{j=1}^p (x_{ij} - \bar{x}_{kj})^2 \quad (8)$$

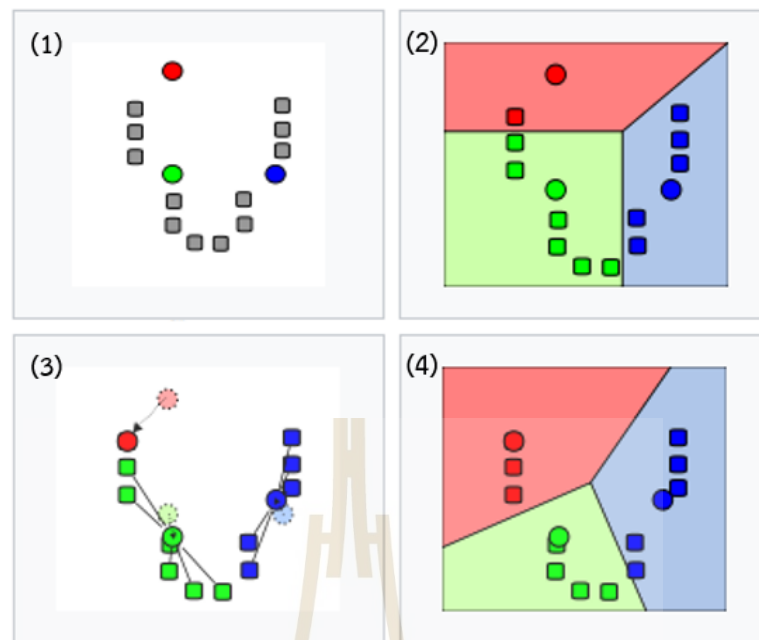
K-means clustering aims to minimize the summation of within-cluster variation in equation (6). The processes for solving the problem are described as follows:

(1) Define the number of clusters (k), then random k numbers as an initial cluster centroid. Figure 2.6 (1) represents the process of clustering data with $k=3$; red, green, and blue points are the random initial centroids for each cluster.

(2) Defined Voronoi diagram from the partition of the distance between cluster centroids and created boundary around the centroids. Regions of each centroid are presented in color corresponding to the color of the centroid, as shown in Figure 2.6 (2). Assign the observation data to the closest centroid; the data within the same region are clustered.

(3) Compute the new cluster centroid for each cluster. The cluster's centroid is a new mean value of the observation in the cluster of p features. The new centroids moved to a new position, as presented in Figure 2.6 (3).

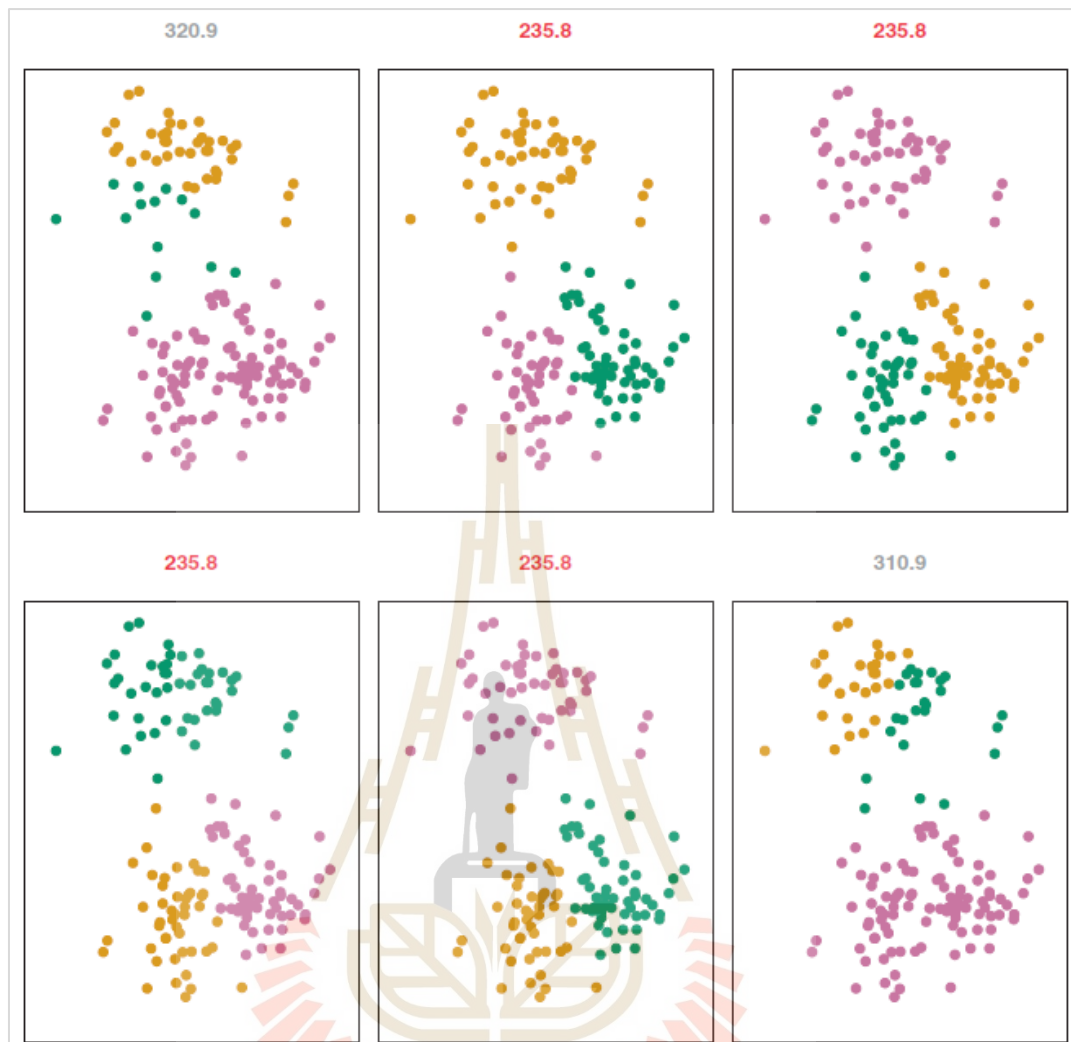
(4) Repeat processes (2) and (3) until the cluster centroid does not change, resulting in the final clustering process presented in Figure 2.6 (4).



Source: Weston.pace (2007)

Figure 2.6 Processes of K-means clustering.

Even with the process's simplicity and fewer tuning parameters, K-means clustering has some problems. The random initialization trap is the main problem for this method. The random value for the initial centroid is essential to find the optimum centroid, but it can be a local optimum. Figure 2.7 shows an example of the random initialization trap. The three clusters' results were presented in different colors, sizes, and members of each cluster were different due to the initial centroid. The within-cluster variation value was calculated based on the centroid and member of the cluster. These plots in Figure 2.7 showed that the final cluster with the within-cluster variation value of the same dataset processing multiple times produced different clusters with distinct within-cluster variation values. Thus, processing multiple times with different random initial centroids is necessary. Then select the best solution with the smallest within-cluster variation value to solve the problem.



Source: Gareth et al. (2015)

Figure 2.7 K-means clustering of the same dataset with $k=3$. Each plot shows the clustering result using a different set of initial centroids, and the number above the plot is the within-cluster variation.

2.6 Previous studies of weed detection

This section provides a review of weed classification using UAV images, summarizing the studies conducted by other researchers in this field. It highlights the input features, processes, and results employed in these studies. Moreover, the gaps of the previous are discussed.

Peña, Torres-Sánchez, de Castro, Kelly, and López-Granados (2013) developed the process for mapping weed in Early-Season Maize Fields. An automated object-based image analysis (OBIA) procedure was developed using a six-band multispectral camera (visible and near-infrared range) on a series of UAV images to generate a weed map for a maize field. The procedure consists of three phases: 1) classifying crop rows using a dynamic and auto-adaptive classification approach, 2) distinguishing between crops and weeds based on Normalized Difference Vegetation Index (NDVI) threshold and crop rows, and 3) generating a weed infestation map in a grid structure. The estimation of weed coverage through image analysis yielded promising results, with R-squared value of 0.89 and a root mean square error of 0.02. A map categorizing weed coverage into three categories was produced, achieving an overall accuracy of 86%. In the experimental field, 23% of the area was weed-free, and 47% had low weed coverage (<5% weeds), indicating significant potential for reducing herbicide application or other weed-related operations. Nevertheless, the classification of vegetation and background through the use of NDVI number is subject to variation depending on the specific image and geographical area.

The study of Pérez-Ortiz et al. (2015) introduces a weed mapping system in sunflower crop that utilizes vegetation indices derived from RGB and NIR sensors, as well as crop rows, with various classification methods including K-means, Repeated K-means, K-nearest neighbor, linear SVM, kernel SVM, and semi-supervised SVM. The semi-supervised method is developed based on SVM classification and incorporates both labeled and unlabeled data. The results demonstrate that the semi-supervised method achieves the highest performance, and the inclusion of NIR data contributes to improved classification accuracy. However, the semi-supervised classification requires training data, even if the study mentions using a smaller amount of data.

The study of P. Lottes, R. Khanna, J. Pfeifer, R. Siegwart, and C. Stachniss (2017) focuses on developing a classification system for identifying weeds in sugar beet fields. The system incorporates an index to differentiate vegetation from the background and utilizes crop rows in the classification process. The classifier is based on RF

classification. The testing involved three different sensors: two RGB sensors and one RGB+NIR sensor. The system effectively identifies sugar beets and weed species in images of sugar beet farms, benefiting from crop rows and spatial relationships. It performs well even in challenging conditions such as overlapping plants and can detect weeds within the rows. Furthermore, the inclusion of an additional NIR channel improves vegetation detection and classification performance. The study utilizes very high-resolution images, ranging from 0.2 to 5 mm/pixel, captured at low altitudes (2-15 m). These images contain a significant amount of data and require substantial processing time. This method also requires threshold of index for separate background and training data for training RF classification model, which should be done manually.

The study of Gao et al. (2018) focuses on developing a classification process for mapping weeds in early growth state maize fields from RGB images. The method utilizes pixel-based identification of crop rows and detects inter-row weeds, which are automatically labeled and used as training data for RF classification. The segmented image is then inputted into the RF classification to classify intra-row weeds. The process incorporates various geometry features such as length-to-width ratio and asymmetry, obtained through the OBIA technique. The overall accuracy (0.945) and Kappa value (0.912) metrics demonstrate that the RF classifier exhibits strong generalization ability. The OBIA approach was employed for segmentation and feature generation, resulting in high-quality inputs for image classification. However, users are required to manually set parameters, select specific information, and perform the processing steps. The input image has a high resolution of 1.78 mm/pixel, which requires significant time for acquisition and analysis.

De Castro et al. (2018) developed an automatic RF-OBIA algorithm for early weed mapping between and within crop rows using UAV imagery. In this study, an automatic classifier based on RF and OBIA approach was developed and tested in the early stages of sunflower and cotton cultivation. The image underwent segmentation, Digital Surface Model (DSM) extraction, and shadow removal. Vegetation was differentiated from the soil using the NIR/G ratio, which was automatically calculated.

Crop rows were detected by analyzing the length-to-width ratio of the targets after merging. Weeds outside the crop rows were identified based on their location, while weeds within the crop rows were detected using RF classification. The RF model was trained using a predefined dataset of classes, and object features obtained from the segmentation were used for classification. The combination of UAV imagery and RF-OBIA showcased in this study enables accurate weed mapping, both between and within crop rows, with a high weed detection accuracy of 87.9%. The images were captured with a high overlap of 93% to facilitate 3D reconstruction of the crops and obtain crop height information. However, this approach is time-consuming due to the extended duration required for flying the UAV and the subsequent mosaic process. The input features for classification are derived from segmented objects, requiring users to manually set parameters, select specific information, and perform processing steps.

Louargant et al. (2017) evaluated hierarchical self-organising maps for weed mapping using UAV multispectral imagery. This study introduces hierarchical map classifiers for mapping the spatial distribution of *S. marianum* weed. The classifiers utilize features derived from a combination of spectral information from multispectral images and textural information. Three hierarchical map classifiers, namely Supervised Kohonen Network (SKN), Counter-propagation Artificial Neural Network (CP-ANN) and XY-Fusion network (XY-F) were employed to classify the data into *S. marianum* and other plants. The results demonstrate that the CP-ANN classification map achieved the highest accuracy, reaching 98.87%. Nevertheless, the input image resolution of 0.5 m is not suitable for detecting small patches of weeds.

Gašparović et al. (2020) developed an automatic method for weed mapping in oat fields based on UAV imagery. In this study, four classification algorithms were used to create weed maps: manual RF (using pixel-based RF and object-based methods) and automatic RF (using pixel-based and object-based methods). These algorithms applied for weeds and bare soil extraction. The automatic methods used the top 0.1% of NGRDI values for weeds and BI values for bare soil as training data sets. The K-means algorithm was then applied to estimate the presence of weeds and bare soil in areas

without weeds or soil. The automatic object-based classification method achieved the highest accuracy, with an overall accuracy of 89.0% for subset A and 87.1% for subset B. The automatic classification methods were well-developed, using at least 0.25% of the scene size as the training dataset to ensure optimal performance of the random forest classification algorithm in all expected scenarios. The automatic training approach in this study, selecting 0.1% of the index, may be affected by color variation and noise. The presence of white flowers of weed interferes with the BI index, as mentioned by the authors.

Khan et al. (2021) developed a semi-supervised framework for UAV based crop/weed classification. In this study, the development of an optimized semi-supervised learning approach is proposed, offering a method for crop and weed classification at early growth stage. The proposed algorithm based on Generative Adversarial Network (GAN), the framework consists of a generator that provides extra training data for the discriminator, which distinguishes weeds and crops using a small number of image labels. The proposed system was evaluated on the RGB images of pea and strawberry plots. Nonetheless, the inclusion of training data remains essential, even if the study mentions utilizing a smaller dataset. The outcomes of this approach involve sub-images that are categorized as either weed or crop, rather than providing precise pixel coordinates for weed locations.

Su et al. (2022) analyzed spectral and developed process for mapping of blackgrass weed by leveraging machine learning and UAV multispectral imagery. In this study, spectral indices based on multispectral data were generated. The RF classifier with Bayesian hyperparameter optimization was employed to classify blackgrass weed in wheat fields. The results demonstrated high accuracy, especially when using the triangular greenness index (TGI) composed of Green-NIR. The feature selection process reduced the number of features while yielding better results compared to using all the produced features. Additionally, incorporating spatial information from the Guided Filter enhanced the classification outcome by improving results and reducing noise.

However, the classification based on RF requires training data for training classification model.

Previous research has shown that weed mapping in crop fields is crucial for decision-making and management. Researchers are actively exploring new methods for weed detection and trying to find suitable parameters for classification. These efforts indicate a shift towards semi-automatic or fully automatic weed detection processes. However, most weed mapping methods rely on supervised classification, requiring training data. Thresholding methods, on the other hand, depend on variable indices affected by factors like area, time, and lighting conditions, making it difficult to determine optimal values. This research aims to develop a semi-automatic classification process tailored for classifying objects in cassava fields. It combines various preprocessing and classification techniques to establish an efficient workflow.



CHAPTER III

RESEARCH METHODOLOGY

This chapter presents details of the research methodology, including (1) conceptual framework, (2) data and materials, and (3) research procedures. The specific details are as follows.

3.1 Conceptual framework

The conceptual framework of this research is designed to address the research objectives outlined in section 1.2. The research framework consists of three main steps, as depicted in Figure 3.1. Firstly, the development of classification processes, which includes preprocessing and classification, referred to as the proposed classification process, is in line with objective (1). Adjusting and validating the proposed classification process across various test sites to identify the appropriate parameter settings correspond to objective (2). Lastly, applying the adjusted proposed classification process to the study area aligns with objective (3).

The first part of the conceptual framework focuses on developing a classification process for objects in cassava fields. The preprocessing stage includes feature extraction, filtering, and clustering. After preprocessing, rule-based classification methods are applied to produce a classification map. The chosen preprocessing and classification methods prioritize simplicity and semi-automatic processing to reduce the chance of human errors.

The second part involves adjusting and validating the proposed classification process to identify suitable parameters for classifying cassava field images. Various parameters, such as indices, filtering parameters, and GSD, were tested in selected testing sites within the study area. Suitable parameters were selected based on the classification results and statistical test accuracy. The chosen parameter set was then implemented in the proposed classification process.

Lastly, the proposed classification process with adjusted parameters was implemented across all study areas. Furthermore, the input images were divided into various sizes to assess the effectiveness of the proposed classification process in terms of accuracy and processing time.

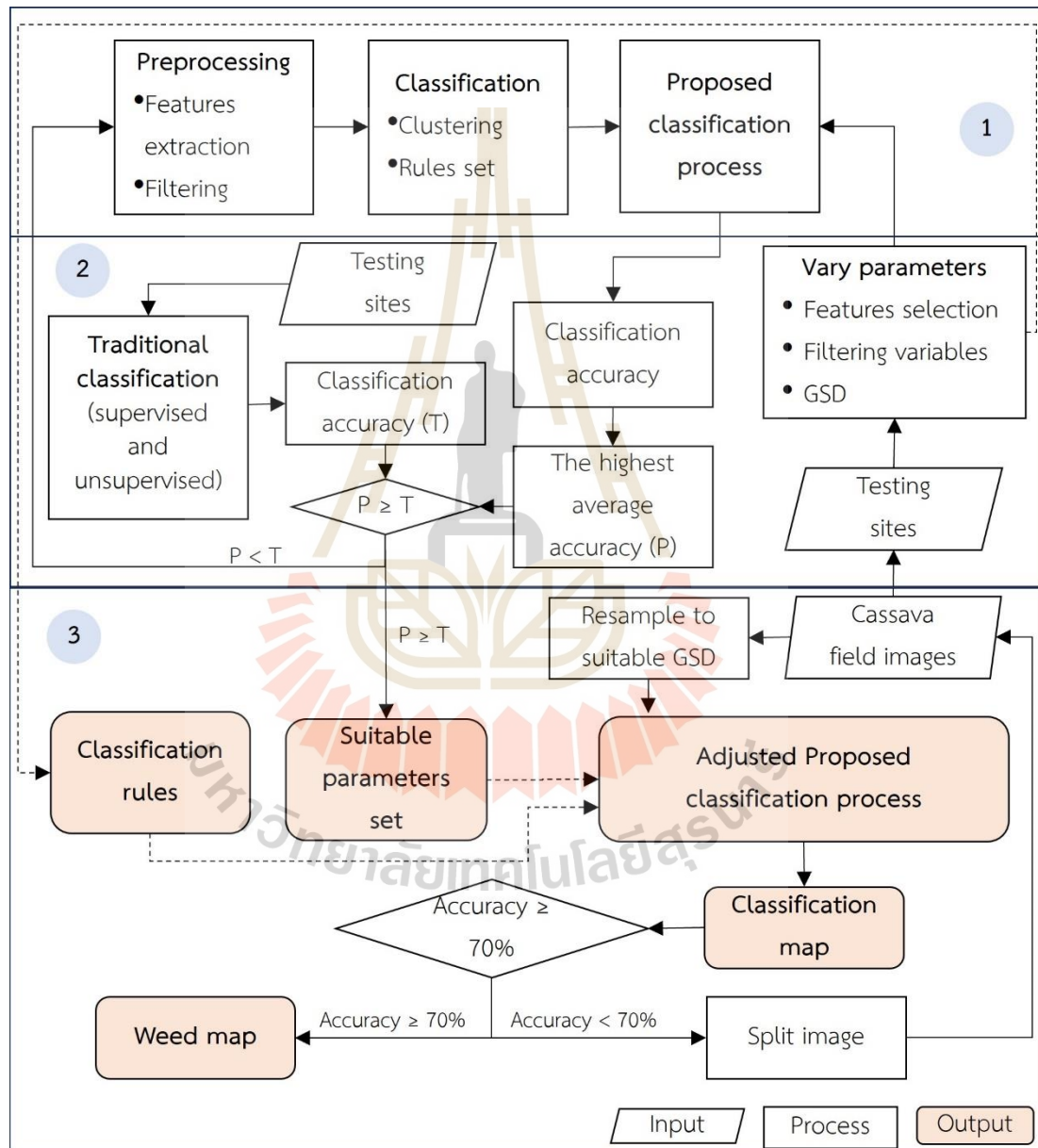


Figure 3.1 Conceptual framework.

3.2 Data and materials

3.2.1 Image acquisition

Images were acquired in 2018-2021 with two different sensors, as shown in Table 3.1. Images of study plots 1-5 were taken by a built-in optical sensor (sensor model FC6310) in DJI Phantom 4 Pro quadcopter. The sensor provides twenty million pixels with a 1-inch CMOS sensor, the focal length is 8.8 mm, the field of view (FOV) of 84°, and the image size is 5472x3648 pixels. Images of study plots 6-12 were captured using a DJI Phantom 4 built-in optical sensor (sensor model FC330). The UAV's sensor is a 1/2.3-inch CMOS sensor with effective pixels of 12.4 million pixels, a focal length of 3.6 mm, an FOV of 3.6 mm, a FOV of 94°, and an image size of 4000x3000 pixels. Table 3.1 shows the details of the sensors used in this study. The sensor FC6310 and FC330 capture photos in the visible light spectrum in red, green, and blue (RGB). The coordinates of photos acquired from GPS/GLONASS satellite positioning systems, the navigation system of both UAV platforms. Images of each plot were taken from the separated flight; thus, the light conditions differed. The UAV images were processed and mosaiced by Pix4Dmapper software. The DN values were normalized from 0 to 255 on each red, green, and blue layer and stored in 8 bits with GeoTiff format.

The study areas were captured from two different sensors, as mentioned above. The original GSD of the images was between 1.21-5.00 cm due to the flight altitude and sensor. The acquisition details of the study area are shown in Table 3.2.

Table 3.1 Details of sensors.

Model	FC6310	FC330
Sensor	1-inch CMOS	1/2.3-inch CMOS
Effective pixels (Million)	20	12.4
Focal length (mm)	8.8	3.6
field of view (FOV) (°)	84	94
Sensor width (mm)	13.2	6.17
Sensor height (mm)	8	4.55
Image width (pixel)	5472	4000
Image height (pixel)	3648	3000

Table 3.2 Acquisition details of the study area.

Plot	Sensor	Taken date	Taken Time	Original GSD (cm)
1	FC6310	4/28/2018	11:00	1.413
2	FC6310	4/28/2018	11:25	1.267
3	FC6310	4/28/2018	12:40	1.398
4	FC6310	4/28/2018	12:20	1.291
5	FC6310	4/28/2018	12:00	1.369
6	FC330	5/21/2021	11:20	5.00
7	FC330	5/21/2021	11:20	5.00
8	FC330	5/21/2021	11:20	5.00
9	FC330	5/21/2021	11:20	5.00
10	FC330	5/21/2021	11:20	5.00
11	FC330	9/5/2018	12:01	1.21
12	FC330	7/5/2021	12:03	4.414

3.2.2 Processing software

The procedure of this experiment, which includes calculating indices, filtering data, clustering, labeling, and assessing accuracy, was implemented using the Python language. The experimentation was conducted on a system with Microsoft Windows 10, a 64-bit operating system equipped with 64.0 GB of Random Access Memory (RAM), and powered by a 3.60 GHz Core i9-9900KF CPU processor.

3.3 Research Procedures

The research procedure consists of three main parts: (1) development of classification processes, (2) adjustment and validation of the proposed classification process, and (3) application of the adjusted proposed classification process to the study areas. Each part is described in detail below.

3.3.1 Developing classification

The workflow diagrams in Figure 3.2 illustrate the processes involved in developing the classification. This part of the research addresses the first objective. The classification was performed using unsupervised classification techniques. The UAV images were classified into three or four classes, which may include cassava, weed, soil, and/or tree, depending on the components present in the input image.

Previous research demonstrates the positive impact of mean-shift filtering on classification accuracy, particularly when considering the size and pixel values of objects (Boonrang, Sritarapat, and Piyatadsananon, 2021). Hence, in this study, the input images and mean-shift algorithm parameters were fine-tuned individually to identify the most suitable input image and parameters for each class.

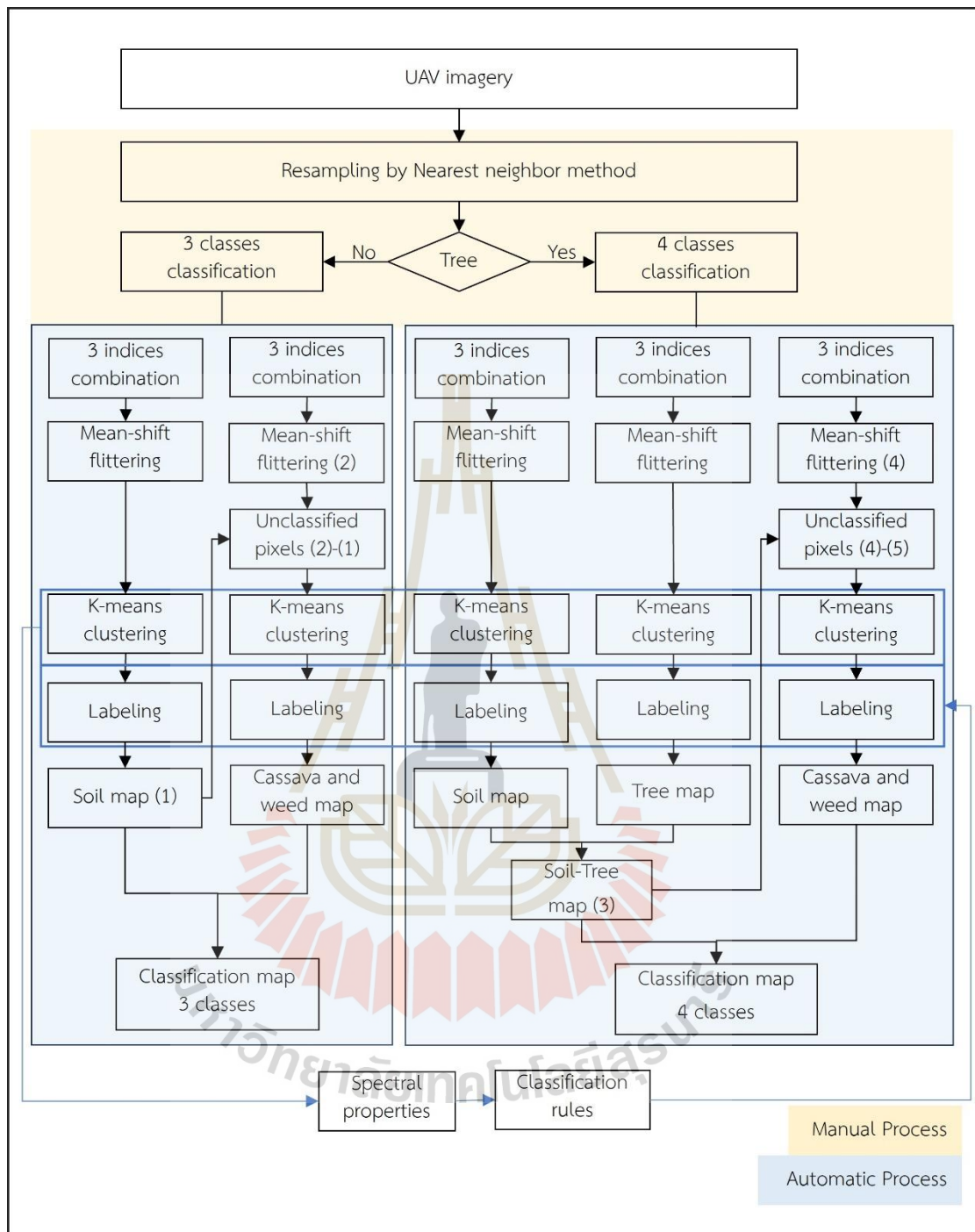


Figure 3.2 Workflow of processes for developing the proposed classification process.

The development of the classification involves four main processes, which are described below.

(1) Input producing

The R, G, and B layers of the UAV image were used as input for calculating various indices, such as ExR, ExG, ExB, ExGR, NGRDI, GLI, VARI, BI, and CI, using the equations provided in Table 2.2. These RGB and indices data were then combined to create a three-layer input image for future processes.

(2) Filtering

The three-layer input images were filtered by mean-shift filtering method. User needs to set two main parameters, namely the spatial window radius (sp) and the color window radius (sr). The algorithm iteratively performs mean shift calculations on the input image pixels, considering the following conditions:

$$(x, y): X - sp \leq x \leq X + sp, Y - sp \leq y \leq Y + sp, \quad (9)$$

$$\|(R, G, B) - (r, g, b)\| \leq sr \quad (10)$$

where (R, G, B) and (r, g, b) represent the color vectors at the pixel locations (X, Y) and (x, y) , respectively. The mean-shift algorithm computes the average spatial value (X', Y') and the average color vector (R', G', B') to serve as the neighborhood center for the next iteration. It is worth noting that the algorithm is independent of the color space used, allowing for the utilization of any three-component color space.

(3) Clustering

The filtered images were classified using the K-means algorithm, a clustering approach implemented in the scikit-learn library (Pedregosa et al., 2011). The K-means clustering algorithm utilizes the K-means++ method, which improves the selection of initial centroids by considering the maximum distance from the nearest centroid to address the random initialization trap problem (Arthur and Vassilvitskii, 2006). This enhancement increases the likelihood of selecting new centroids from different clusters.

The number of clusters was determined based on the expected cluster results, as outlined in Table 3.3. For soil classification, the expected clusters were soil, vegetation, and background. In tree classification, the anticipated clusters were trees, non-trees, and backgrounds. In cassava and weed classification, soil and tree pixels were removed from the image, and the remaining pixels were used in the proposed classification. The expected cassava and weed classification clusters included cassava, weed, soil and tree pixels, and background.

Table 3.3 Number of clusters in the K-means clustering process.

Class	Number of clusters	Expected cluster result
Soil	3	Soil, vegetation, and background
Tree	3	Tree, not tree, and background
Cassava and weed	4	Cassava, Weed, pixel of soil and tree, and background

(4) Labeling

The K-means clustering process partitions pixels into distinct cluster numbers, with each cluster having unique spectral values. These clusters are expected to represent pixels belonging to the same type or class, enabling the use of cluster values to assign cluster names. Instead of relying on spectral values, the classification rules are designed based on the trends observed in the spectral values of the classes. This approach recognizes that different images may exhibit varying spectral values and emphasizes using spectral value patterns for classification purposes.

3.3.2 Adjusting and validating classification

This section aims to enhance the performance of the developed classification process by adjusting the parameters in the algorithm. The classifier is applied to various testing areas to assess its accuracy, kappa coefficient, and statistical significance. For the testing, study sites are selected from the study area and include four classes (cassavas, weeds, soil, and trees) as well as areas with three classes (cassavas, weeds, and soil). Eight study sites from different plots are chosen to test the performance of the proposed classifier's algorithms and fine-tune the parameters before applying them to the entire study area. Each study site covers an area of 40 x 50 square meters, as depicted in Figure 3.3.

The overall accuracy and the kappa coefficient are used. Reference points are generated through visual interpretation of the UAV images prior to the classification process. These validation points are randomly selected and distributed throughout the study area. The number of validation points for each class is presented in Table 3.4.

Furthermore, the performance of the developed classification process is compared with that of traditional classification methods. Specifically, the Random Forest (RF) method, which represents supervised classification, and the K-means clustering method, which represents unsupervised classification, are used for comparison. Prior to classification, the test sites are segmented using eCognition software. For the RF method, a classification model is generated using three layers and different variables of the RF classifier. The best-performing model is selected, and the image is then classified accordingly. It is important to note that this model creation process is conducted for each individual area. In the case of the K-means clustering method, the same set of inputs as the RF method is used, and the resulting clusters are visually labeled based on the majority of cluster data. The overall accuracy, kappa coefficient, producer's accuracy, and user's accuracy obtained from the developed classification process are compared with those obtained from the RF and K-means clustering methods.

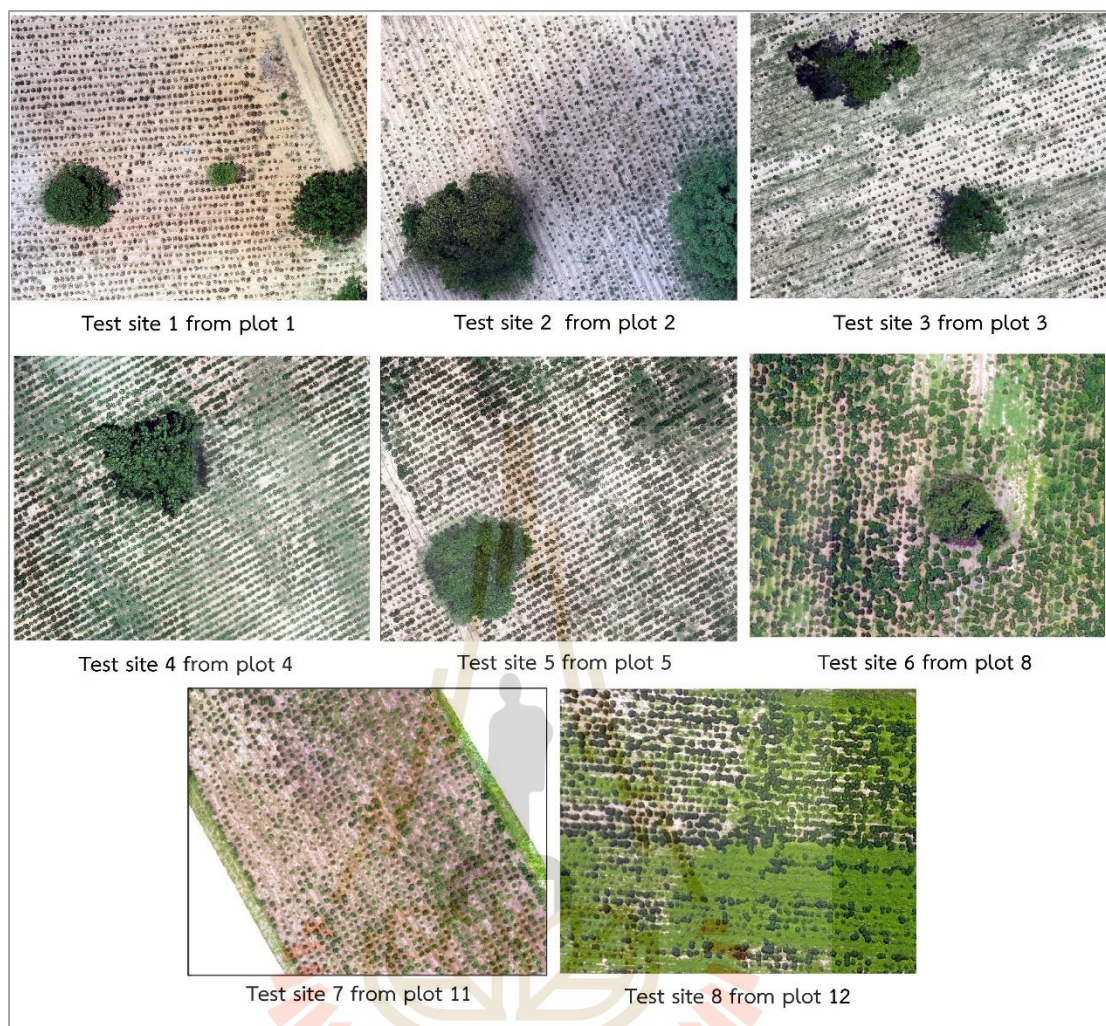


Figure 3.3 Testing sites for adjusting and validating classification.

Table 3.4 Referent points of the testing site for the accuracy assessment process.

Study site	1	2	3	4	5	6	7	8
Cassava	100	100	100	100	100	100	100	100
Weed	100	100	100	100	100	100	100	100
Soil	100	100	100	100	100	100	100	100
Tree	65	65	75	30	35	20	-	-
Total	365	365	375	330	335	320	300	300

The study sites were tested to search for suitable 3-layer combination input, filtering parameters, and GSD for the proposed classification process. Details of varying input data, filtering parameters, and GSD of input image are described as follows.

(1) Input data

The input data is generated in three layers based on the specifications of the mean-shift filtering method. This involved assigning one index to each of the three layers, such as BI-BI-BI, and using three different indices, such as R-G-B, R-G-ExG, and ExG-ExGR-GLI. There are 232 combination images, each of which serves as input for the filtering process.

(2) Filtering parameters

The input images were enhanced using mean-shift filtering under various conditions, with the parameters of the filtering process determined based on the size of the object of interest. The sizes of the sp (spatial radius) and sr (color radius) parameters of the filtering window vary depending on the target object's characteristics, which can vary in size and color compared to the image. For soil classification, the sp and sr values ranged from 20 to 80 and 5 to 25, respectively. As for tree classification, the combination images were subjected to two rounds of mean-shift filtering, each with a different set of parameters. In the first filtering round, which targets trees consisting of multiple pixels, sp and sr values were extended to 20-100 and 5-50, respectively. The second round of filtering helped eliminate small pixels around the trees, with sp and sr values set at 20-60 and 40-50, respectively. The sp and sr parameters were set to 20-80 and 10-25 for cassava and weed classification, respectively. Table 3.5 displays the parameters used in the filtering process.

Table 3.5 Mean-shift parameters for the filtering process.

Class/ Parameter	Soil	Tree 1 st filtering	Tree 2 nd filtering	Cassava and weed
<i>sp</i>	20, 40, 60, 80	20, 40, 60, 80, 100	20,40,60	5, 10, 15, 20, 25
<i>sr</i>	5, 10, 15, 20, 25	5, 10, 15, 20, 25, 30, 35, 40, 45, 50	40,50	10, 15, 20, 25

(3) GSD of the input image

Very high-resolution images captured by UAVs, which have centimeter-level precision, contain a substantial amount of information represented by a large number of pixels. Consequently, processing such images can be time-consuming. The UAV input images were resized using the nearest neighbor method from their original GSD range of 1.2-5.0 cm to GSDs of 1.5, 5, 10, 20, 30, 40, and 50 cm. The purpose of testing different GSD sizes for the input images was to identify the most suitable GSD for classification in the cassava field.

3.3.3 Applying classification

The proposed classification process used optimal parameters from section 3.3.2. The study area was resampled to an appropriate GSD from section 3.3.2 and classified using the adjusted process. This adjusted classification process will be applied to the study area, which consists of 12 cassava plots. The robustness and limitations of the developed classification method will be revealed by examining the various components and physical properties of the study plots.

As the developed image classification relies on the K-means clustering method, the input data values influence the classification results. A discriminant test was conducted to evaluate the effect of input data values on the performance of the developed classification method. It involved comparing the results obtained from using the entire image data with those obtained after splitting the image into two pieces.

The classification results' accuracy from study plots was measured using referent points generated from the original GSD images by visual interpretation. These points are randomly selected and distributed in the study plots. The ratio of referent points to the area is 27-70 points per area (rai). Details of referent points are shown in Table 3.6.

Table 3.6 Referent points for evaluating the classification results.

Plot	Referent point					Area (sq.m.)	Area (rai)	Ratio (point/rai)
	Cassava	Weed	Soil	Tree	Total			
1	167	116	197	49	529	19,826.8	12.39	43
2	171	138	236	55	600	27,816.8	17.39	35
3	345	345	402	80	1,172	70,671.1	44.17	27
4	448	448	448	-	1,344	56,636.6	35.40	38
5	364	364	364	-	1,092	55,741.4	34.84	31
6	81	64	55	-	200	5,918.7	3.70	54
7	40	40	40	-	120	4,271.5	2.67	45
8	231	231	231	-	693	36,776.5	22.99	30
9	130	100	63	-	293	11,657.5	7.29	40
10	149	143	143	-	435	22,928.2	14.33	30
11	45	45	45	-	135	3,093.0	1.93	70
12	50	50	50	-	150	5,884.6	3.68	41

CHAPTER IV

RESULTS AND DISCUSSION

This chapter presents the results and findings of the study, which were obtained by following the research procedures and objectives. The results report encompasses three main sections: (1) findings in the development of the classification process, (2) results of adjusting and validating the classification process, and (3) results of applying the adjusted proposed classification process in the study areas. The following sections provide detailed descriptions of each set of results.

4.1 Finding in developing the classification process

The classification development in this research comprises four main processes: input selection, mean-shift filtering, clustering, and labeling. These processes were tested numerous times to determine the most appropriate steps, and the results obtained throughout the development are summarized as follows.

4.1.1 Input data

The R, G, and B layers of the UAV image were processed and normalized within the range of 0-255. Boxplots were created to represent the spectral values of sample classes from R, G, B, and indices, indicating each class's spectral values range. Figure 4.1 shows spectral overlap between classes and within classes for all indices, making it challenging to separate classes using a single index. The original data from the blue, green, and red channels exhibit a wider range of values than their respective indices.

A total of 232 different combination images were generated by combining three different R, G, B, and indices combinations for each class's classification process. These combined images were then used in the filtering and clustering processes. The results obtained from the same filtering parameters and cluster number in clustering process were examined to assess the potential of the combined images.

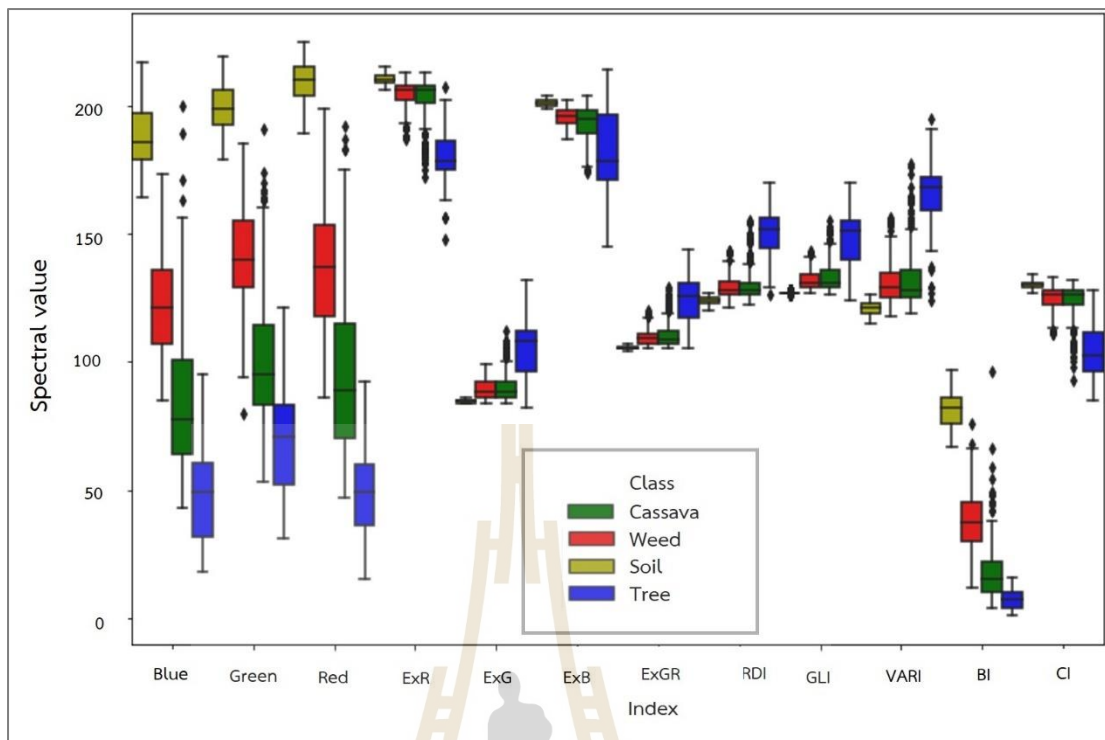


Figure 4.1 Boxplot of the spectral value of classes.

The results of different combination images using filtering parameters $sp=20$ and $sr=20$ and number of clusters 3 (the result shows two clusters because the other cluster is background data) are shown in Figure 4.2. Among the combinations, the clustering results from R-G-B (Figure 4.2(b)), R-B-CI (Figure 4.2(c)), and G-ExB-VARI (Figure 4.2(d)) demonstrate effective separation between vegetation and soil. On the other hand, the combination of ExB-NGRDI-VARI (Figure 4.2(e)) and ExG-ExB-ExGR (Figure 4.2(f)) can identify trees and some small groups of vegetation in the image.

Based on these results, it is evident that the choice of parameter values has distinct effects on different indices. The image comprises red, green, or blue layers with a wide spectrum value range. When a small sp value is used during the filtering process, it becomes difficult to distinguish individual plants. However, in the case of the composite image derived from the 3-index, which has a narrower range, employing the same value makes it possible to identify a tree pixel. These findings indicate that the choice of image combination has an impact on the clustering results.

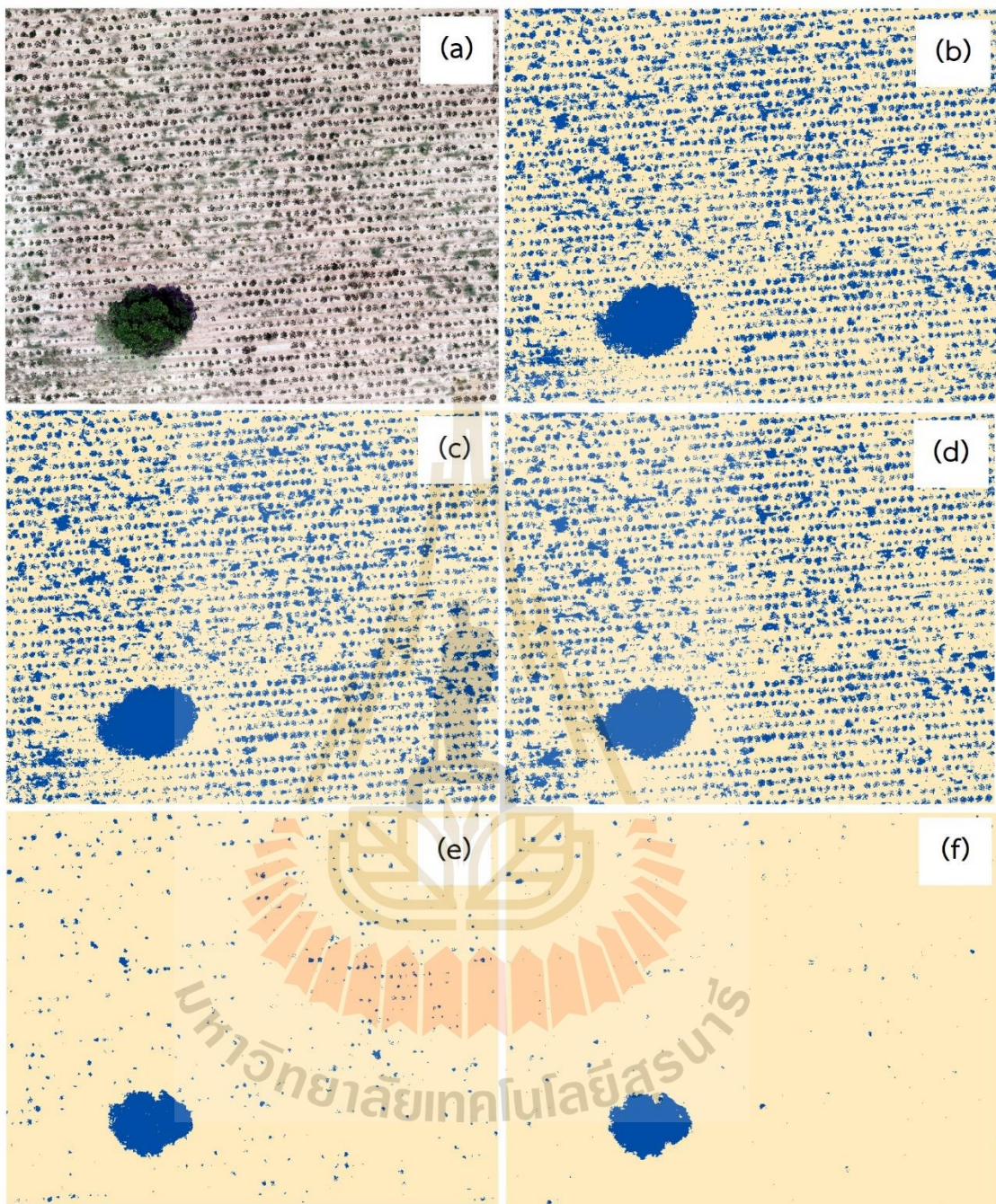


Figure 4.2 Original RGB image (a) and results from clustering process from different indices combination: R-G-B (b), R-B-CI (c), G-ExB-VARI (d), ExB-NGRDI-VARI (e), and ExG-ExB-ExGR (f).

4.1.2 Filtering

In the classification preprocessing, a mean-shift filtering algorithm was employed to eliminate intensity and illumination variations, and the non-entity heterogeneity within objects. The bandwidth selection, which includes spatial window radius (sp) and color window radius (sr), plays a crucial role in this algorithm. The filtering results using different mean-shift parameters are shown in Figure 4.3. For the R-G-B combination images (Figure 4.3(a)), changes in the parameters had a minimal effect. However, the ExG-ExGR-BI combination image (Figure 4.3(b)) exhibited noticeable changes with increased sr values, resulting in higher smoothness and the removal of small objects.

The impact of the mean shift filtering process on the input image varied depending on the parameters and the combination used. While the R-G-B combination image showed slight changes with increased sr values due to its broad spectral range, the ExG-ExGR-BI combination image underwent rapid changes due to its smaller spectral range, as observed in the boxplot in Figure 4.1.

It is important to note that the filtering process may lead to the loss of certain information, including noise and outlier data. To evaluate this, the NGRDI-GLI-BI combination was tested under three conditions: (1) unfiltered image, (2) filtering once with $sp=80$ and $sr=30$, and (3) filtering twice with $sp=80$, $sr=30$, and $sp=30$, $sr=30$, respectively, followed by clustering the images into three groups. The impact of the mean shift filtering process is clearly visible in Figure 4.4, where objects were removed in the filtered images compared to the unfiltered image (Figure 4.4(a)). Furthermore, applying the filtering process twice helped eliminate small objects around the tree, as shown in Figure 4.4(d).

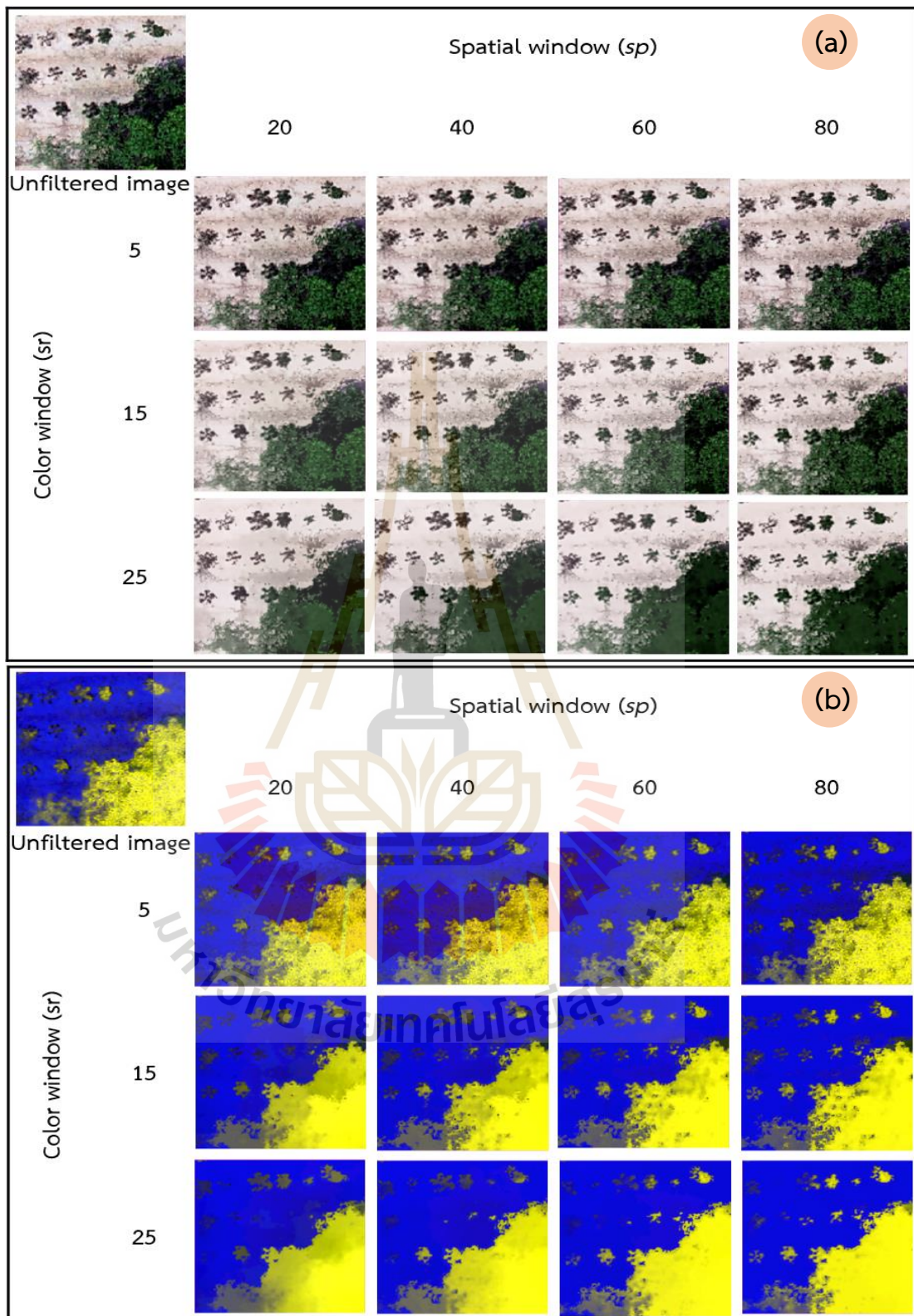


Figure 4.3 Result of filtered R-G-B combination image (a) and ExG-ExGR-BI combination image (b) from various filtering parameters.

The selection of filtering parameters significantly impacts the clustering results, as demonstrated in Figure 4.4. The tree class can be effectively identified by using appropriate parameters. Due to objects with different sizes within each class. The filtering parameters were tailored individually for each specific class. This approach treated the size of sp and sr as distinct class characteristics. As a result, filtering the images with suitable parameters can enhance the quality of clusters and improve the overall classification outcome.



Figure 4.4 Effect of filtering on clustering results: UAV input image (a) and clustering results from unfiltered image (b), one-time filtering (c), and two-time filtering (d).

4.1.3 Clustering

The results from the filtering process were applied in the clustering process to distinguish subgroups, which can label classes in the following process. The K-means clustering algorithm was employed to cluster the filtered images.

Figure 4.5 provides the results of the clustering process, which applied various k values on different images. Different colors represent the clusters in the resulting image. The results indicate that using $k=2$ effectively separates vegetation and soil. However, when $k=4$ was applied, the clustering outcome was highly influenced by lighting conditions, resulting in mixed clusters of cassava, weed, and tree. Employing a high number of clusters in the process generated diverse groups with distinct values, making it challenging to assign class names to the clusters.

The results of the clustering process highlight that the outcomes of the clusters are influenced by the lighting conditions present within each image, which may vary across different images. Moreover, employing a higher number of clusters further complicates the task of assigning appropriate class names to the clusters.

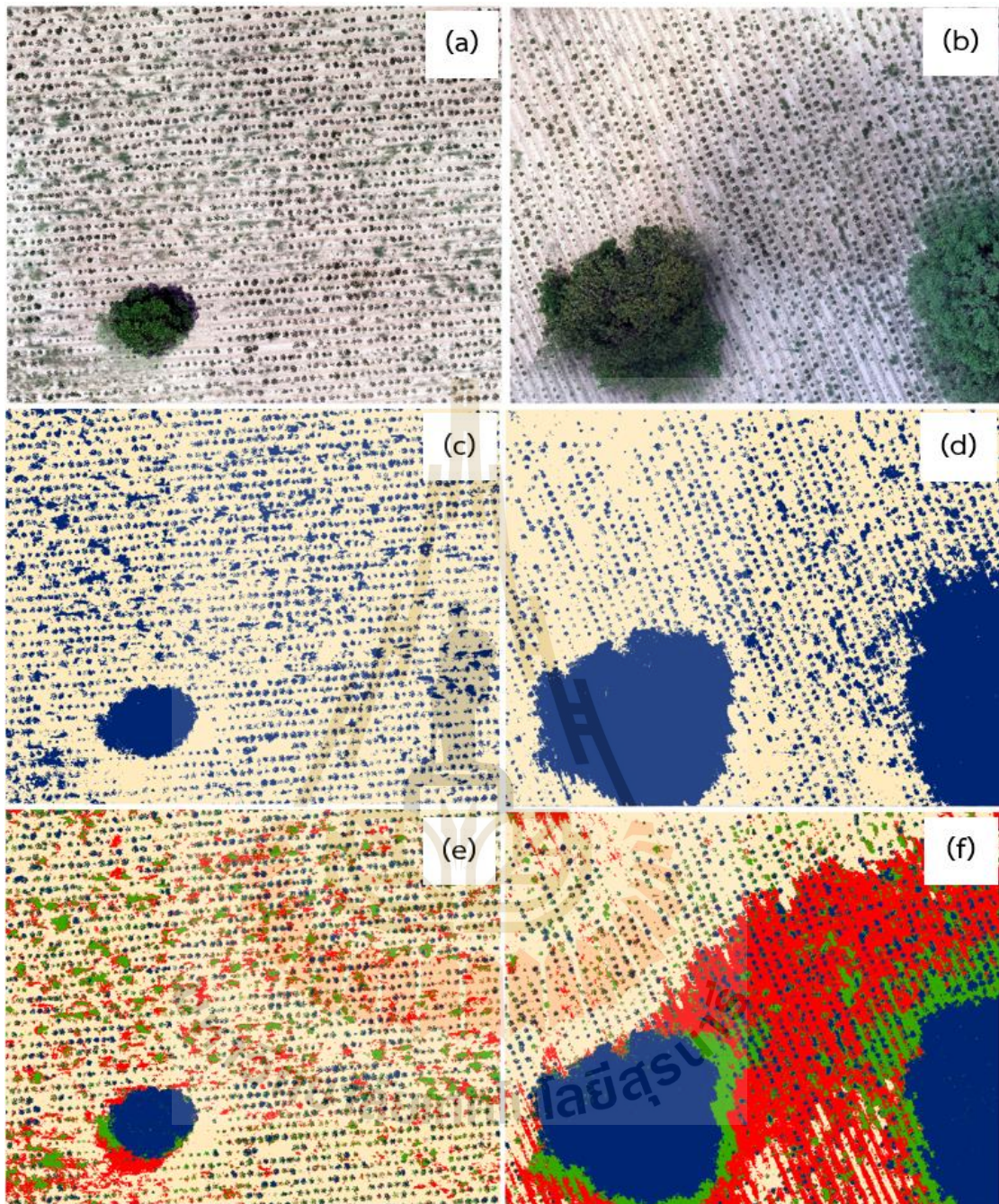


Figure 4.5 Clustering results from applying a different number of cluster (k): UAV input image (a) and (b) and the result of applying $k=2$ (c) and (d), and $k=4$ (e) and (f).

4.1.4 Classification rules

The clustering results provided specific values for each cluster, which served as thresholds for classifying classes. However, variations in illumination and light conditions across different images affected the pixel values. The trend of spectral values for each class was utilized instead to label classes accurately. Classification rules were established based on the properties of each class. This approach allowed for an automatic process that was not dependent on varying numbers or light conditions.

The combination of indices was filtered with different parameters and then clustered to separate pixels in the image into distinct classes. An example of the clustering result can be seen in Figure 4.6, where different indices combinations produced two clusters with distinct pixel values. The values of these clusters were collected from various indices combinations and presented as trends (low and high) in Table 4.1.

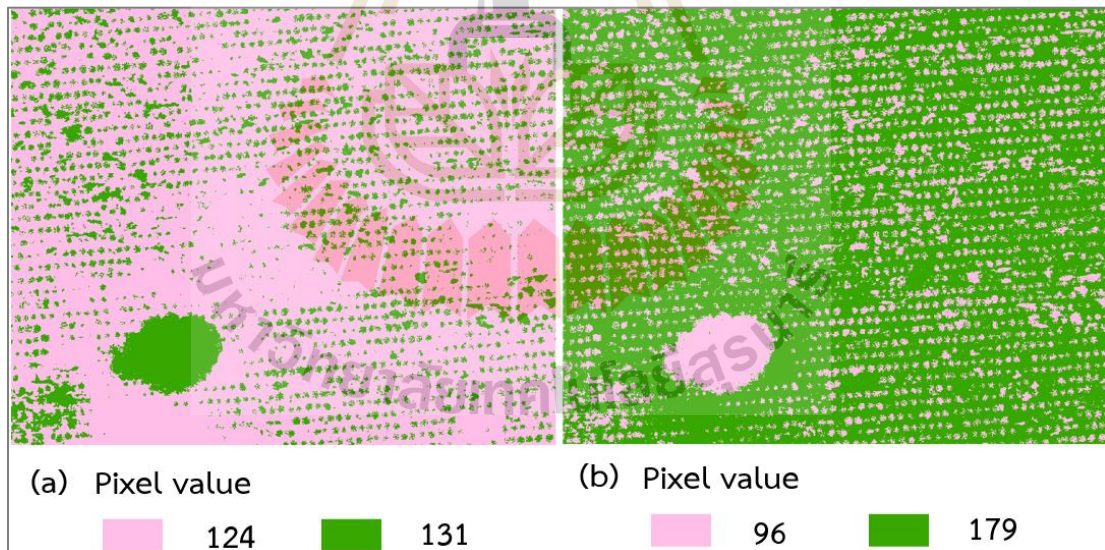


Figure 4.6 Example of pixel value from clustering result: layer NGRDI from NGRDI-GLI-BI combination (a) and layer B from B-ExB-BI combination (b).

Table 4.1 Spectrum characteristics of objects after the clustering process.

Index	Clustering for soil	Clustering for tree	Clustering for cassava and weed	
			Cassava	Weed
R	high	low	low	high
G	high	low	low	high
B	high	low	low	high
ExR	high	low	low	high
ExG	low	high	high	low
ExB	high	low	low	high
ExGR	low	high	high	low
NGRDI	low	high	high	low
GLI	low	high	high	low
VARI	low	high	high	low
BI	high	low	low	high
CI	high	low	low	high

Table 4.1 categorizes the indices into two groups based on their spectral values. The first group, consisting of R, G, B, ExR, ExB, BI, and CI, exhibit high spectral values for soil and weed while demonstrating low values for trees and cassava. On the other hand, the second group, comprising ExG, ExGR, NGRDI, GLI, and VARI, displays opposite characteristics compared to the first group. Consequently, classification rules were established separately for each class, considering their specific properties and input indices. These classification rules are presented as simple if-else statements in Table 4.2, considering the spectral characteristics outlined in Table 4.1.

Table 4.2 The rules set for the classification process.

Index	Soil	Tree	cassava and weed
R, G, B, ExR, ExB, BI, CI	If the pixel value is high Then the class is Soil	If the pixel value is low Then the class is Tree	If the pixel value is low Then the class is Cassava If the pixel value is high Then the class is Weed
ExG, ExGR, NGRDI, GLI, VARI	If the pixel value is low Then the class is Vegetation	If the pixel value is high Then the class is Not the tree	If the pixel value is high Then the class is Cassava If the pixel value is low Then the class is Weed

4.2 Results of adjusting and validating classification process

This section presents the results of implementing the developed classification process across various study sites. The classification process includes preprocessing and classification steps, and the protocol for the proposed classification process is provided in Appendix A. Different parameters and ground sample distances (GSDs) were tested, and the obtained results are documented and discussed in the following section.

4.2.1 Soil classification

The filtered images of various combinations were clustered into three clusters. These clusters were further classified into two classes, with the third cluster representing "no data". The result of this process presents pixels of soil and vegetation mixed with cassava, weed, and trees. Different conditions were tested across all study sites to optimize the classification performance, and the overall accuracy and kappa

coefficient were measured. Each classification condition's average and standard deviation (S.D.) were calculated. Table 4.3 shows the condition that produces the highest kappa coefficient of each GSD, which is selected for future steps.

Table 4.3 Selected soil classification condition of each GSD.

GSD (cm)	Combination	Mean-shift parameter		Kappa coefficient	
		<i>sp</i>	<i>sr</i>	Average	S.D.
1.5	ExB-BI-CI	5	15	0.9419	0.0305
5	B-VARI-CI	5	10	0.9513	0.0358
10	R-B-CI	10	5	0.9346	0.0738
20	B-VARI-CI	20	5	0.8940	0.0629
30	R-B-CI	15	5	0.8282	0.1008
40	R-ExG-CI	20	5	0.7450	0.1336
50	R-B-CI	20	5	0.6651	0.1304

Among the different GSDs tested, the soil map generated using GSD 5 cm exhibited the highest average kappa coefficient with a small standard deviation (S.D.). This was followed by the results obtained from images with GSD 1.5 cm, 10 cm, 20 cm, 30 cm, 40 cm, and 50 cm, respectively. The accuracy of soil classification decreased with increasing GSD from 5 cm to 50 cm.

Based on the selected parameters for each GSD, it was observed that different values of *sp* yielded high accuracy for soil classification. This observation supports the notion that the soil class does not have a precise shape, making it challenging to determine the optimal *sp* value. On the other hand, using a small value of *sr* resulted in high accuracy. This is because the indices combined in the input have a smaller spectral range, enabling the differentiation of vegetation from the soil.

Among the indices used, the Color Index (CI) consistently showed favorable results for soil classification. It is sensitive to variations in soil color and

composition, making it capable of distinguishing soil from other elements in an image (Escadafal and Huete, 1991). It measures the color difference between an image's red and green components, allowing for the quantification of color variations specific to soil and vegetation. One of the advantages of the CI index is its relatively lower sensitivity to vegetation cover. Therefore, the CI index is a valuable choice, especially for distinguishing between soil and vegetation.

4.2.2 Tree classification

Combination images for tree classification were filtered in two rounds using different mean-shift parameter sets. The filtered images were then clustered into three groups using K-means clustering, labeled as trees, not trees, and background. Like the soil classification process, the average kappa coefficients and S.D. were calculated for each parameter set across all study sites. Table 4.4 presents the conditions that yielded the highest kappa coefficient for each GSD, which were chosen for further steps.

Table 4.4 Selected tree classification condition of each GSD.

GSD (cm)	Combination	Mean-shift parameter				Kappa coefficient	
		<i>sp1</i>	<i>sr1</i>	<i>sp2</i>	<i>sr2</i>	Average	S.D.
1.5	ExG-ExB-GLI	40	40	40	60	0.8371	0.1594
5	ExB-NGRDI-VARI	60	20	20	40	0.8744	0.0750
10	VARI-VARI-VARI	40	20	20	40	0.8653	0.0865
20	VARI-VARI-VARI	20	20	20	40	0.8681	0.1158
30	VARI-VARI-VARI	20	20	20	40	0.8373	0.0948
40	ExG-ExB-CI	40	20	20	40	0.6849	0.1002
50	ExR-ExB-CI	20	20	20	50	0.4879	0.2027

The results of tree classification showed that images with a GSD of 5 cm achieved the highest accuracy, followed by GSDs of 20, 10, 30, 1.5, 40, and 50 cm, respectively. The results in Table 4.4 show that the large values of sp and sr get high accuracy in tree classification, suggesting that the size of the filtering window should align with the size of the object. Since tree canopies are larger sp value can effectively smooth the tree pixels. Additionally, the spectral range of trees is wider compared to other classes within the same index, making a higher sr value useful for smoothing tree pixels.

The VARI index had a beneficial effect on tree classification. It is specifically designed for vegetation analysis to reduce the influence of atmospheric conditions and variations in illumination on reflectance measurements. The VARI index is computed by dividing the difference between the green and red bands by dividing it by the sum of the red, green, and blue bands. Vegetation typically exhibits higher reflectance in the green band and lower reflectance in the red band due to chlorophyll's absorption of red light. By quantifying the difference in reflectance between these two bands and normalizing it, the VARI index enhances the sensitivity to vegetation, enabling more accurate discrimination between vegetation and other land cover types.

The condition that produced the highest average kappa coefficient for each GSD was selected and combined with the soil classification results to generate a mask layer for the classification of cassava and weed. However, the proposed classification process did not perform well in test site 6. Therefore, manual classification was employed to generate the tree map for future processes.

4.2.3 Cassava and weed classification

The combination images for cassava and weed classification were filtered, then removed pixels of soil and tree. The remaining pixels were then clustered into four groups using K-means clustering. The clusters were labeled as cassava, and weed, no data, and background. Similar to soil and tree classification, the average kappa accuracies and standard deviations were calculated for each parameter set

across all study sites. Table 4.5 displays the conditions that yielded the highest kappa values for each GSD, which were selected for further analysis.

The highest kappa value was observed for the GSD of 1.5 cm, followed by GSDs of 5, 10, 20, 30, 40, and 50 cm, respectively. As the GSD increased, the accuracy of cassava and weed classification decreased.

Table 4.5 Selected cassava and weed classification condition of each GSD.

GSD (cm)	Combination	Mean-shift parameter		Kappa coefficient	
		<i>sp</i>	<i>sr</i>	Average	S.D.
1.5	G-ExR-GLI	15	25	0.8317	0.1007
5	G-ExR-ExG	10	20	0.8226	0.1045
10	G-VARI-CI	15	10	0.7771	0.1378
20	G-ExR-ExG	20	10	0.7441	0.1290
30	G-B-ExR	25	10	0.6483	0.1501
40	G-ExG-ExGR	5	5	0.5858	0.1649
50	R-G-ExGR	20	10	0.5084	0.1739

The selected filtering window size parameters, *sp*, and *sr*, played a significant role in capturing the properties of cassava. The *sp* parameter, chosen specifically for the GSD of 5 cm with a spatial window of 10 pixels, corresponded to the average size of cassava canopies, ranging from 52 to 88 centimeters. This result indicated that the *sp* parameter was related to the size of the focus object. In contrast, the *sr* parameter responded to the spectral values of cassava in the indices.

Green and Excess Red (ExR) help discriminate cassava and weed. The green band reflects the amount of green light absorbed and reflected by plants. Different plant species may have distinct green reflectance patterns due to leaf structure, density, and pigmentation variations. By considering the reflectance in the green band, it becomes possible to capture these differences and discriminate

between different types of plants. On the other hand, the ExR index measures the excess amount of red light reflected by plants compared to their reflectance in the green band. This index is particularly useful in distinguishing plant species that exhibit varying absorption properties of chlorophylls a and b in their leaves (Virtanen, Constantinidou, and Tyystjärvi, 2022).

4.2.4 Classification in all classes

The selected soil, tree, cassava, and weed maps were arranged in a specific order. The class labeling order began with trees, followed by soil, cassava, and weed. The tree class was placed as the top layer due to the smooth values observed within the class, as illustrated in Figure 4.7. The chosen conditions for each GSD are presented in Table 4.6.



Result from soil classification Result from tree classification

Figure 4.7 Results of soil classification and tree classification from GSD of 5 cm.

Table 4.6 Selected condition for classification.

GSD (cm)	Class	Input	Mean-shift parameter			
			<i>sp1</i>	<i>sr1</i>	<i>sp2</i>	<i>sr2</i>
1.5	Tree	ExG-ExB-GLI	40	40	40	60
	Soil	ExB-BI-CI	5	15	-	-
	Cassava-weed	G-ExR-GLI	15	25	-	-
5	Tree	ExB-NGRDI-VARI	60	20	20	40
	Soil	B-VAR-CI	5	10	-	-
	Cassava-weed	G-ExR-ExG	10	20	-	-
10	Tree	VARI-VARI-VARI	40	20	20	40
	Soil	R-B-CI	10	5	-	-
	Cassava-weed	G-VARI-CI	15	10	-	-
20	Tree	VARI-VARI-VARI	20	20	20	40
	Soil	B-VARI-CI	20	5	-	-
	Cassava-weed	G-ExR-ExG	20	10	-	-
30	Tree	VARI-VARI-VARI	20	20	20	40
	Soil	R-B-CI	15	5	-	-
	Cassava-weed	G-B-ExR	25	10	-	-
40	Tree	ExG-ExB-CI	40	20	20	40
	Soil	R-ExG-CI	20	5	-	-
	Cassava-weed	G-ExG-ExGR	5	5	-	-
50	Tree	ExR-ExB-CI	20	20	20	50
	Soil	R-B-CI	20	5	-	-
	Cassava-weed	R-G-ExGR	20	10	-	-

The classification accuracies and kappa coefficients were calculated for different GSDs, revealing varying levels of accuracy. The OA ranged from 0.6430 to 0.8628, while the kappa coefficients ranged from 0.5178 to 0.8226, as shown in Table 4.7. A bar chart in Figure 4.8 illustrates the trend of decreasing accuracy and increasing S.D. with higher GSD values. The processing time for classification significantly decreases when working with high GSD images, as it relates to the number of pixels in the image. The highest classification accuracy was achieved with an OA of 0.9628 and a kappa coefficient of 0.8226 using an input image GSD of 5 cm. The OA and kappa coefficient from the 5 cm GSD were similar to those obtained with a 1.5 cm GSD, but there was a notable difference in processing time.

Table 4.7 Overall accuracy, Kappa coefficient, and processing time of classification map.

GSD (cm)	Overall accuracy		Kappa coefficient		Processing time (minute)	
	Average	S.D.	Average	S.D.	Average	S.D.
1.5	0.8624	0.0714	0.8128	0.1018	12.7858	3.8646
5	0.8628	0.0722	0.8226	0.0834	1.1970	0.4797
10	0.8411	0.0832	0.7876	0.1153	0.3189	0.0756
20	0.8445	0.1003	0.7843	0.1349	0.1981	0.0199
30	0.7682	0.0978	0.6761	0.1351	0.2287	0.0166
40	0.7140	0.1158	0.6038	0.1572	0.1951	0.0163
50	0.6430	0.1393	0.5178	0.1723	0.1948	0.0162

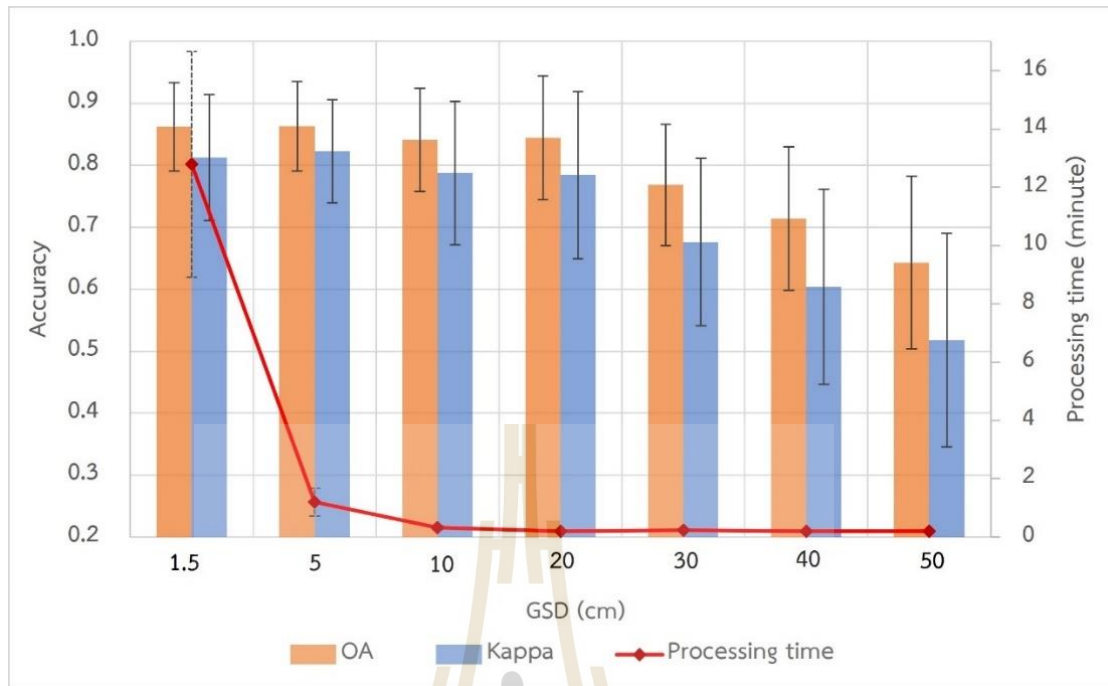


Figure 4.8 Overall accuracy (OA), Kappa coefficient, and processing time of classification map.

The Producer's Accuracy (PA) and User's Accuracy (UA) values for each class (cassava, weed, soil, and tree) are reported for different GSDs, as shown in Tables 4.8 and 4.9 and Figures 4.9 and 4.10. The PA values range from 0.6951 to 0.8331 for cassava, 0.6332 to 0.8857 for weed, 0.7434 to 0.9439 for soil, and 0.5397 to 0.9812 for trees. The UA values range from 0.5663 to 0.9150 for cassava, 0.5338 to 0.7813 for weed, 0.7000 to 0.9888 for soil, and 0.8239 to 0.9508 for tree.

The PA values represent the accuracy of correctly identifying pixels or samples belonging to a specific class, while the UA values represent correctly classifying pixels or samples as a specific class. The variation in PA and UA values across different GSDs suggests that the classification performance can be influenced by the level of detail captured in the images. As the GSD increases, meaning larger pixel sizes and lower spatial resolution, the classification accuracy may decrease due to the reduced ability to distinguish fine details and features within the image. Conversely, smaller GSDs with higher spatial resolution may result in higher accuracy as more detailed information is available for classification.

Table 4.8 Producer's accuracy (PA) of classification map.

GSD (cm)	Cassava		Weed		Soil		Tree	
	Average	S.D.	Average	S.D.	Average	S.D.	Average	S.D.
1.5	0.8331	0.1532	0.8857	0.0868	0.9000	0.1062	0.9812	0.0364
5	0.8220	0.1353	0.8592	0.0830	0.9439	0.0473	0.9703	0.0494
10	0.7881	0.1583	0.8017	0.1608	0.9541	0.0538	0.9467	0.0655
20	0.7921	0.1636	0.7612	0.0948	0.8871	0.0725	0.9723	0.0348
30	0.7146	0.1651	0.6814	0.1356	0.8550	0.1064	0.9717	0.0379
40	0.7183	0.1642	0.6410	0.1516	0.7905	0.1241	0.7610	0.1978
50	0.6951	0.1651	0.6322	0.1215	0.7438	0.1200	0.5397	0.2737

Table 4.9 User's accuracy (UA) of classification map.

GSD (cm)	Cassava		Weed		Soil		Tree	
	Average	S.D.	Average	S.D.	Average	S.D.	Average	S.D.
1.5	0.9150	0.0639	0.7438	0.1919	0.9888	0.0136	0.8258	0.2103
5	0.8900	0.0355	0.7813	0.1877	0.9888	0.0136	0.8692	0.1349
10	0.8538	0.0655	0.7325	0.2187	0.9588	0.0930	0.8806	0.1480
20	0.7700	0.0773	0.7400	0.1916	0.9738	0.0256	0.8605	0.1598
30	0.6925	0.0871	0.6750	0.2210	0.9225	0.0742	0.8239	0.1570
40	0.6200	0.1242	0.6388	0.2101	0.8325	0.1371	0.8467	0.1578
50	0.5663	0.1888	0.5338	0.2168	0.7000	0.1452	0.9508	0.0801

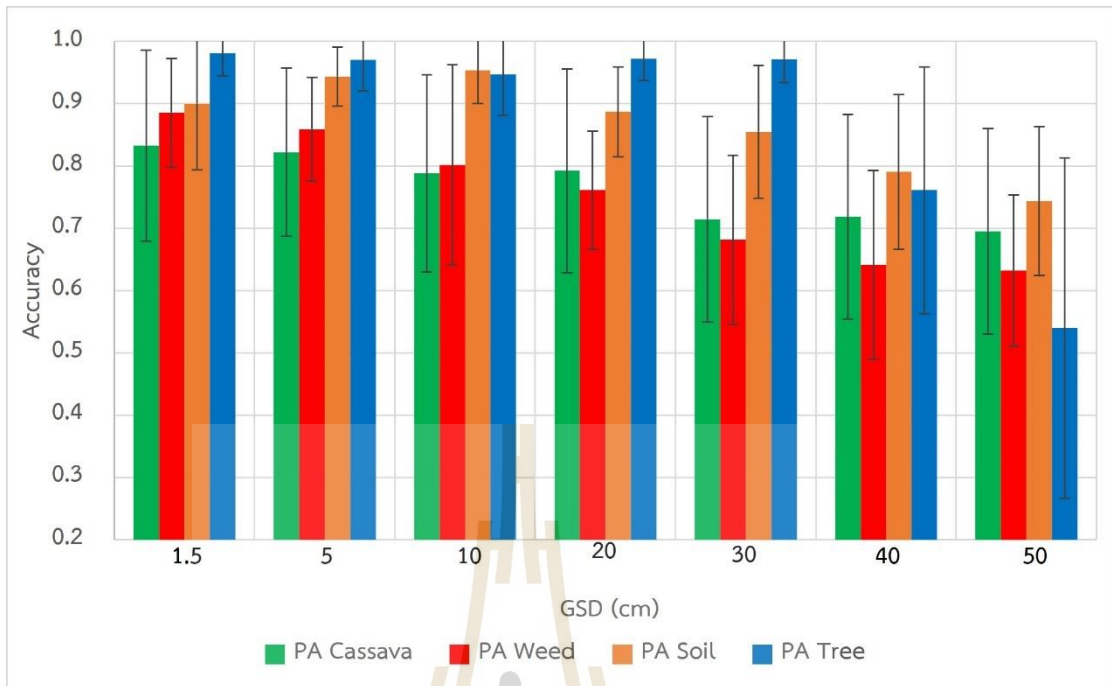


Figure 4.9 Producer's accuracy (PA) of classification results.

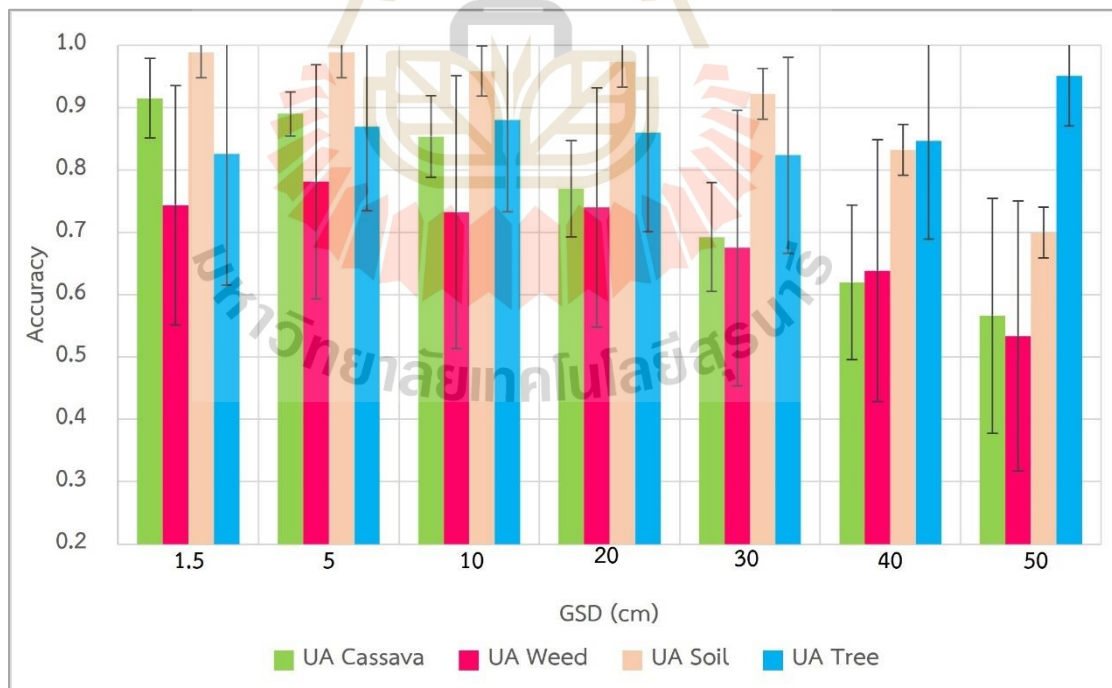


Figure 4.10 User's accuracy (UA) of classification results.

The combined classification maps of the study site with different GSDs were arranged in a specific order, starting with the tree class, followed by soil, cassava, and weed, respectively. The classification results for each class and GSD are presented in appendix B. The classification maps indicate that the filtering process has a drawback at the edges of the image, particularly with higher GSD values. It occurs because the sliding window or kernel-based techniques used in filtering do not have a complete neighborhood for the pixels at the image boundaries. Consequently, incomplete filtering occurs, resulting in the potential loss of information (Bankhead, 2022).

A paired-sample t-test was performed to compare the average accuracies of the two groups. The t-test aimed to assess the differences in classification results between GSD 1.5 cm and other GSDs. The classification accuracies for each GSD, including OA, Kappa coefficient, PA, and UA for cassava, weed, soil, and tree, and the processing time for eight areas were evaluated. The results of the paired-sample t-test, comparing the results from GSD 1.5 with the other GSDs (5, 10, 20, 30, 40, and 50 cm), are presented in Table 4.10. A one-tailed t-test was conducted to compare the classification accuracies between GSD 1.5 cm and other GSDs. The null hypothesis assumed no statistically significant difference between the results. The significance level was set at 0.05, critical values for the t distribution shown in Appendix C.

The findings presented in Table 4.10 demonstrate a significant difference in classification accuracies between GSD 1.5 cm and GSD 20, 30, 40, and 50 cm. However, there is no significant difference in classification accuracies between GSD 1.5 cm and GSD 5 cm or 10 cm. Additionally, the processing time of GSD 5-50 cm significantly differs from the processing time of GSD 1.5 cm. GSD 5 cm and 10 cm exhibit high classification performance and shorter processing time, with slightly better results observed for GSD 5 cm. As a result, GSD 5 cm is selected for future processes.

Table 4.10 Result of statistical paired t-test between the result from GSD 1.5 cm and the other GSDs.

Tested value	t-value					
	GSD (cm)					
	5	10	20	30	40	50
OA	-0.6084	0.8521	1.3789	2.1017*	2.1997*	2.2269*
Kappa	0.6499	0.8620	1.4364	2.1980*	2.2741*	2.2999*
PA cassava	0.4883	1.4929	1.2726	2.1226*	2.0903*	2.2104*
PA weed	1.2129	1.6986	2.1310*	2.3421*	2.3524*	2.4023*
PA soil	-1.0950	-1.8150	0.3679	1.0680	1.8148	2.0469*
PA tree	0.6075	1.0024	0.6553	0.4627	1.7266	1.9171*
UA cassava	1.1087	1.6680	2.1174*	2.2398*	2.3486*	2.2370*
UA weed	-0.6897	0.2226	0.1085	1.4654	1.9350*	2.0202*
UA soil	0.0000	0.7906	0.9716	1.6303	1.9390*	2.2891*
UA tree	-0.8358	-0.7425	-0.4440	0.0276	-0.3985	-1.4849
Processing time	2.5480*	2.5419*	2.5437*	2.5430*	2.5435*	2.5435*

$t_{(0.05,7)} = 1.895$

* t-test shows a significant (p -value<0.05) difference between GSD 1.5 cm and comparison GSD.

The chosen input images, mean-shift parameters, number of clusters, and classification rules utilized in the proposed classification process demonstrated a consistently high average accuracy across study sites 1-8. This provides evidence of the strong performance and robustness of the proposed classification process when applied in diverse areas. The cassava and weed classification error mainly occurred near the tree, the shadow area. The GSD of the input image plays a crucial role in the classification results, the higher the GSD shows the lower the classification accuracy. However, applying the fine GSD in classification takes more processing time.

In order to assess the classification performance, the traditional classification methods were evaluated. The process involves combining three indices at a GSD of 5 cm and segmenting them using eCognition software. These segmented indices are then used as input for the classification process, with RF method representing the supervised approach and K-means representing the unsupervised approach. The classification was tested in seven test sites, specifically sites 1-5 and 7-8. The training data was collected from each site and used to generate separate RF classification models that were applied individually to each study site. In the case of K-means clustering, the clusters were labeled through visual interpretation, and the class assignment was based on the majority of pixels within each cluster.

Table 4.11 shows the input and classification results obtained through these methods. The RF and K-means classification methods achieved their highest accuracy when applied with different inputs. The results indicate the importance of developing customized classification models for each specific area. The OA and kappa coefficients of seven test sites are presented in Figures 4.11-4.12. Classification results of the traditional methods present in Appendix D.

The average classification accuracies were compared using a one-tailed paired t-test at a significance level 0.05. The test was conducted on a sample with 6 degrees of freedom, examining the differences in accuracy between RF, K-means classification, and the proposed classification process. The results showed a statistically significant difference between the K-means and proposed classification results. However, no significant difference was observed between the RF and proposed classification results. These findings indicate that the proposed classification process achieved accuracy comparable to the supervised classification and outperformed the unsupervised classification—additionally, the proposed process required less manual intervention and user-provided data.

Table 4.11 Input data and classification results of the RF, K-means classification, and the proposed classification process.

Test site	Input for RF and K-means classification	RF		K-means		Proposed classification	
		OA	Kappa	OA	Kappa	OA	Kappa
1	G-GLI-VARI	0.8082	0.7402	0.7753	0.6958	0.8356	0.7771
2	R-B-NGRDI	0.7589	0.6759	0.4192	0.2471	0.7616	0.6786
3	R-G-ExGR	0.8687	0.8185	0.6448	0.5235	0.8896	0.8467
4	G-BI-CI	0.8720	0.8281	0.4960	0.3425	0.8533	0.8027
5	ExR-ExB-BI	0.8848	0.8404	0.4545	0.2823	0.9000	0.8609
7	R-ExG-ExGR	0.9300	0.8950	0.8200	0.7300	0.9469	0.8750
8	R-B-ExB	0.9933	0.9900	0.8900	0.8350	0.9733	0.9600
Average		0.8737	0.8269	0.6428	0.5223	0.8801	0.8411
S.D.		0.0765	0.1015	0.1902	0.2369	0.0711	0.0900
t-value		0.3034	0.6979	2.5273*	2.3923*	-	-
$t_{(0.05,6)} = 1.943$							

* *t*-test shows a significant (p -value < 0.05) difference between result from proposed classification process and traditional classification process.

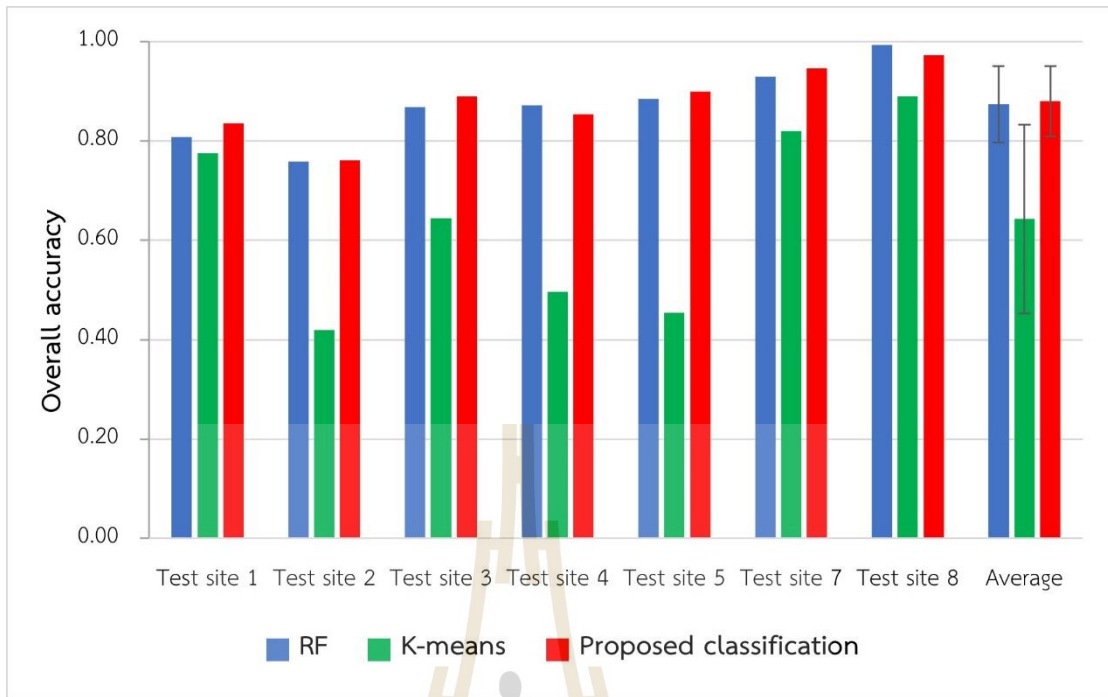


Figure 4.11 Overall accuracy of RF, K-means, and the proposed classification process.

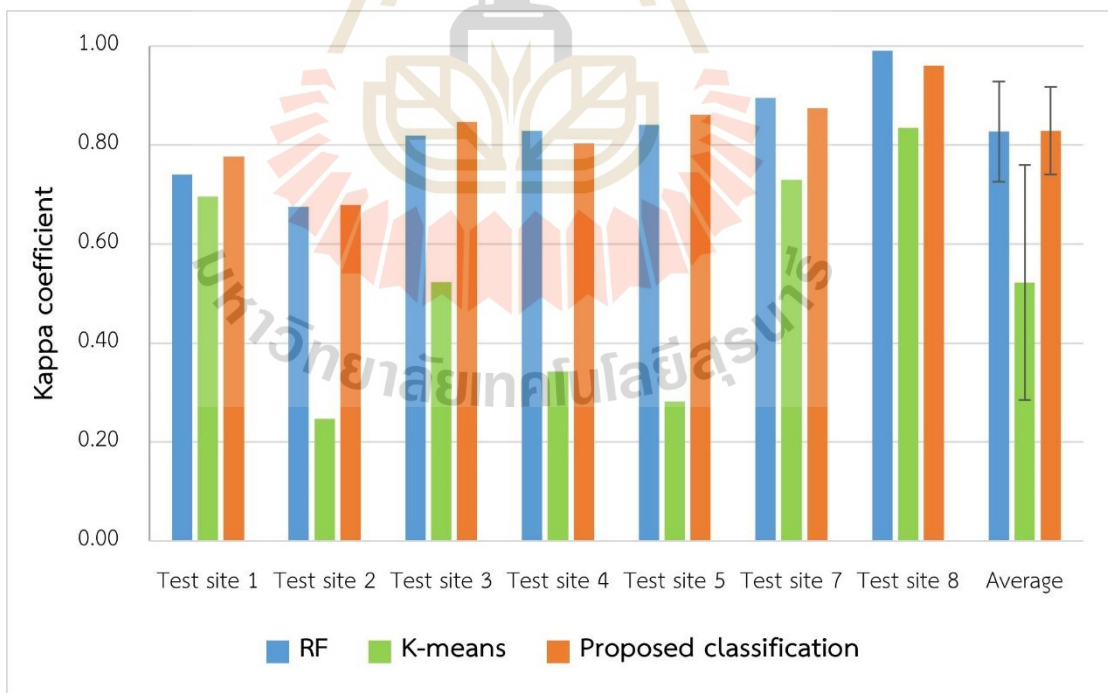


Figure 4.12 Kappa coefficient of RF, K-means, and the proposed classification process.

4.3 Results of Applying the proposed classification process

The proposed classification process was refined by adjusting the optimal parameters identified in the previous step, as documented in Table 4.12. The classification procedure, utilizing the selected parameters, is illustrated in Figure 4.13. The classification process begins with resampling the image to a GSD of 5cm using nearest neighbor method. Then, each class is classified individually, starting with soil classification followed by tree classification. The soil and tree classification results are combined and applied in the cassava and weed classification step. The outputs from soil, tree, cassava, and weed classification are integrated to generate a classification map, from which the weed can be extracted to create a weed map for other related applications.

Table 4.12 The parameters of the proposed classification process.

	Process	Parameter
	Image GSD (cm)	5
Soil classification	Input	B-VARI-CI
	Filtering	$sp = 5, sr = 10$
	Clustering	$k = 3$
Tree classification	Input	ExB-NGRDI-VARI
	Filtering (first filtering)	$sp = 60, sr = 20$
	Filtering (second filtering)	$sp = 20, sr = 40$
	Clustering	$k = 3$
Cassava and weed classification	Input	G-ExR-ExG
	Filtering	$sp = 10, sr = 20$
	Clustering	$k = 4$

The proposed classification process was implemented to classify 12 cassava plots, with the option to classify either three or four classes. The images were divided into two sections to compare the processing results between analyzing and processing

the entire area separately. The classification accuracies for the obtained results can be found in Table 4.13. Figures 4.14-4.15 present, and charts depicting the obtained OA and kappa coefficients.

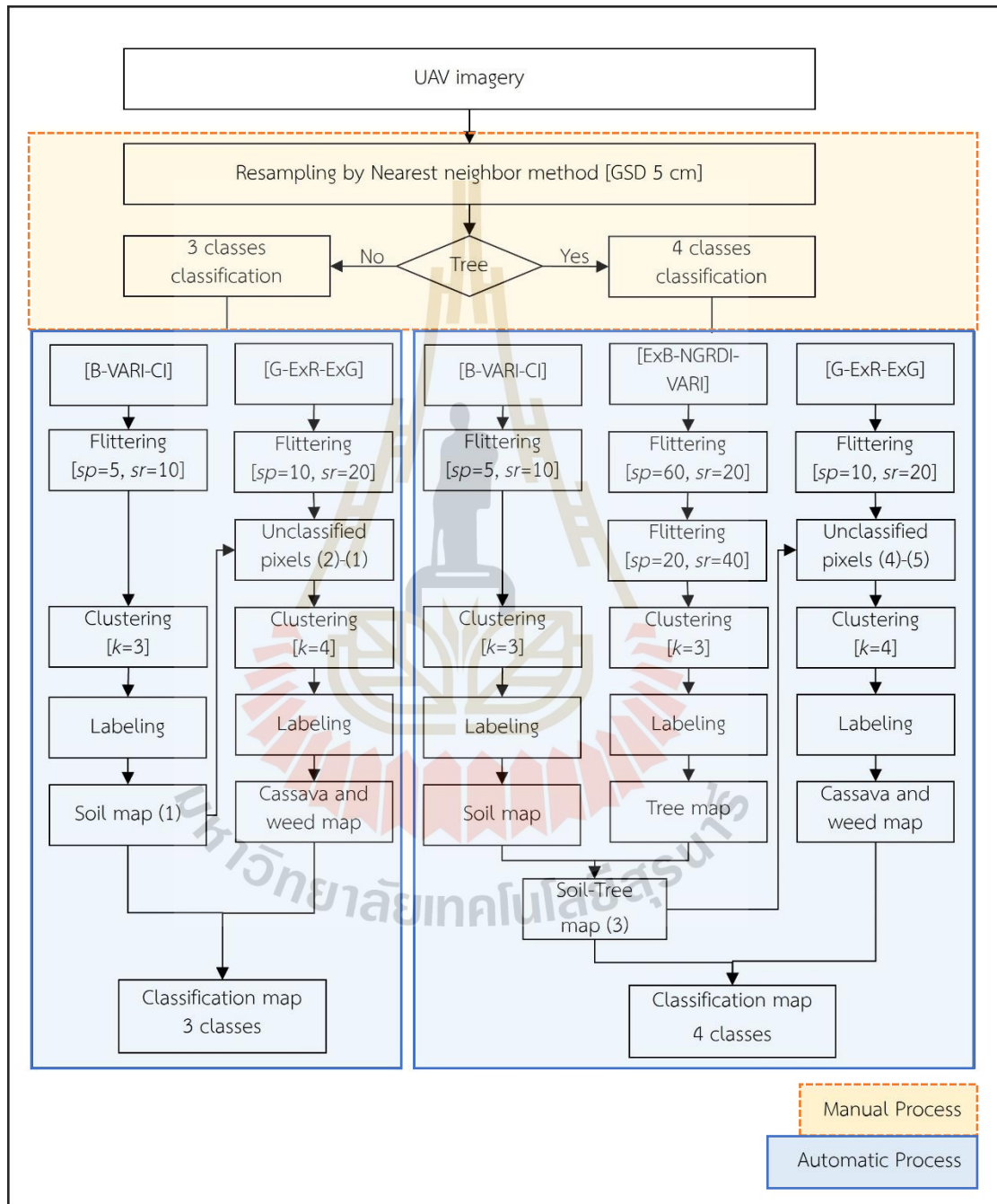


Figure 4.13 Proposed classification process workflow with selected parameters.

The proposed classification process for classifying four classes (for images containing trees) was successfully applied to plots 1, 2, and 3 but encountered difficulties with plots 4, 5, 8, 9, and 10. In these plots, the average canopy diameter of cassava was larger, and the cassava canopies were connected, making it challenge to separate the trees from the cassava. The trees were removed from the images to generate classification maps for these plots, and the remaining pixels were classified into three classes (cassava, weed, and soil).

The OA of the classification maps ranged from 0.6161 to 0.9867, while the kappa coefficients ranged from 0.4262 to 0.9800. Most classification maps achieved OA and kappa coefficients above 0.7 and 0.6, respectively. The OA, kappa coefficient, and processing time for the entire area and processing with two pieces of the input image was found to be quite similar in accuracies and processing time.

Table 4.13 Overall accuracy (OA), kappa coefficient, and processing time of classification results.

Plot	Area (rai)	Process the entire area			Process two pieces		
		OA	Kappa	time (min)	OA	Kappa	time (min)
1	12.39	0.7467	0.6344	5.15	0.7448	0.6313	5.01
2	17.39	0.7950	0.7025	8.21	0.7817	0.6824	8.15
3	44.17	0.8217	0.7445	18.32	0.8148	0.7347	19.23
4	35.4	0.8981	0.8471	10.02	0.8936	0.8404	9.27
5	34.84	0.8443	0.7665	10.11	0.8416	0.7624	10.00
6	3.70	0.6350	0.4570	1.08	0.6300	0.4494	2.02
7	2.67	0.8417	0.7625	1.02	0.8417	0.7625	1.12
8	22.99	0.8038	0.7056	5.48	0.8975	0.8463	9.15
9	7.29	0.8840	0.8215	2.12	0.8737	0.8056	2.19
10	14.33	0.6161	0.4262	3.44	0.7356	0.6048	3.59
11	1.93	0.8963	0.8444	1.04	0.9037	0.8556	1.12
12	3.68	0.9867	0.9800	1.02	0.9867	0.9800	1.39

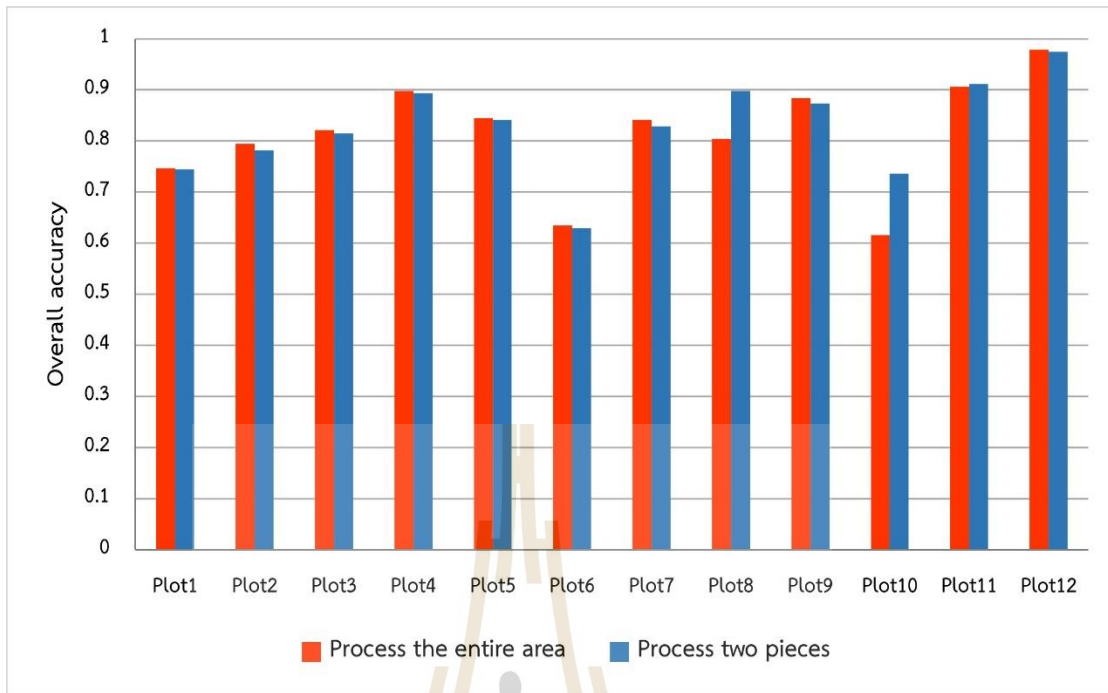


Figure 4.14 Overall accuracy of classification results.

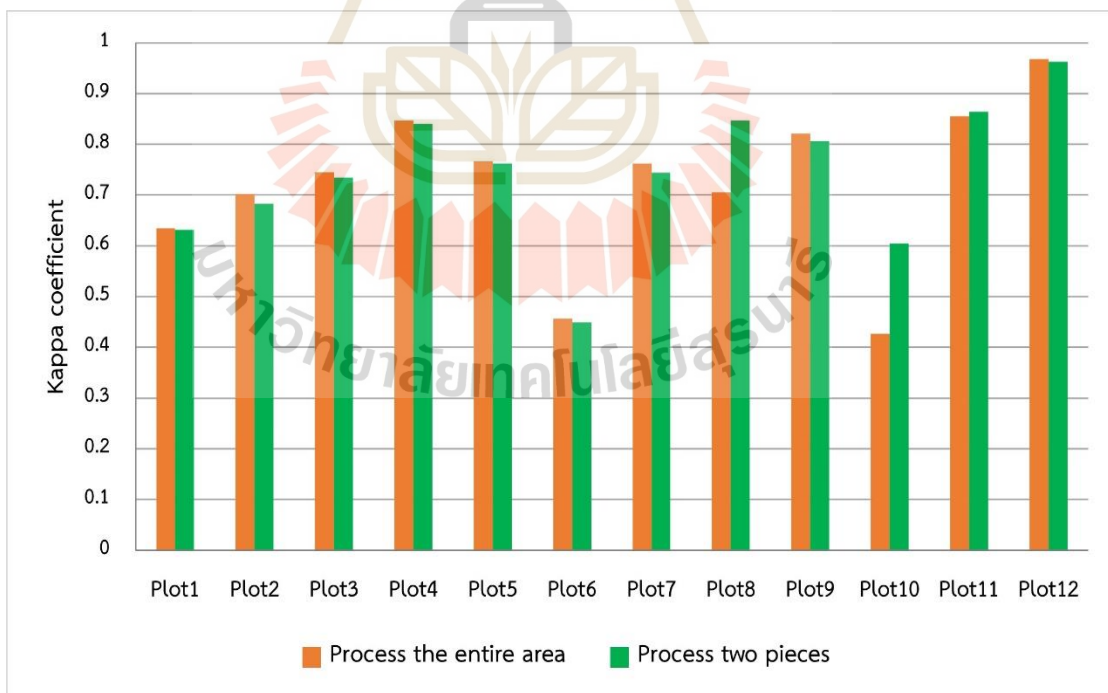


Figure 4.15 Kappa coefficient of classification results.

Producer's accuracy (PA) and user's accuracy (UA) were calculated to classify images into four classes: cassava, weed, soil, and tree. The PA and UA data are presented in Tables 4.14-4.15. The classifier was tested on 12 cassava plots. Reference points evaluated on the classification maps, and the number of points in each class is presented in Table 3.6. The PA of class cassava was in the range of 0.3356-0.9600, class weed was in the range of 0.5245-1.0000, class soil was in the range of 0.9915-1.0000, and class tree was in the range of 0.8182-0.8776 for classification results from the entire area and two pieces process. In comparison, the UA was in the range of 0.5435-1.0000 for class cassava, 0.4412-0.9804 for class weed, 0.7076-0.9804 for class soil, and 0.9714-1.0000 for class tree. Charts of producer's and user's accuracies are in Figures 4.15-4.16.

Table 4.14 Producer's accuracy (PA) of the results in classification.

Plot	Process the entire area				Process two pieces			
	Cassava	Weed	Soil	Tree	Cassava	Weed	Soil	Tree
1	0.5449	0.5603	0.9949	0.8776	0.5389	0.5603	1.0000	0.8571
2	0.6784	0.6087	0.9831	0.8182	0.6199	0.6087	0.9915	0.8182
3	0.8377	0.5942	0.9975	0.8500	0.8290	0.5768	1.0000	0.8500
4	0.8571	0.8415	0.9955	-	0.8571	0.8281	0.9955	-
5	0.8324	0.7005	1.0000	-	0.8187	0.7060	1.0000	-
6	0.3704	0.6563	1.0000	-	0.3704	0.6406	1.0000	-
7	0.7500	0.7750	1.0000	-	0.8000	0.7250	1.0000	-
8	0.5844	0.8268	1.0000	-	0.8398	0.8528	1.0000	-
9	0.8154	0.9000	1.0000	-	0.8077	0.8800	1.0000	-
10	0.3356	0.5245	1.0000	-	0.5168	0.6993	1.0000	-
11	0.8444	0.8444	1.0000	-	0.8667	0.8444	1.0000	-
12	0.9600	1.0000	1.0000	-	0.9600	1.0000	1.0000	-

Table 4.15 User's accuracy (UA) of the results in classification.

Plot	Process the entire area				Process two pieces			
	Cassava	Weed	Soil	Tree	Cassava	Weed	Soil	Tree
1	0.9192	0.5909	0.7076	1.0000	0.9184	0.5909	0.7061	1.0000
2	0.7682	0.7119	0.8140	0.9783	0.7571	0.7059	0.7932	0.9783
3	0.8281	0.8300	0.7909	0.9855	0.8195	0.8257	0.7852	0.9714
4	0.9771	0.8549	0.8745	-	0.9771	0.8588	0.8593	-
5	0.7932	0.8252	0.9077	-	0.7926	0.8107	0.9123	-
6	0.6122	0.4516	0.9483	-	0.6000	0.4505	0.9322	-
7	0.8108	0.7561	0.9524	-	0.7805	0.7838	0.9524	-
8	0.8333	0.6702	0.9390	-	0.9065	0.8455	0.9390	-
9	0.9636	0.7895	0.9130	-	0.9459	0.7788	0.9130	-
10	0.5435	0.4412	0.8266	-	0.7778	0.5952	0.8512	-
11	0.9268	0.8444	0.9184	-	0.9286	0.8636	0.9184	-
12	1.0000	0.9804	0.9804	-	1.0000	0.9804	0.9804	-

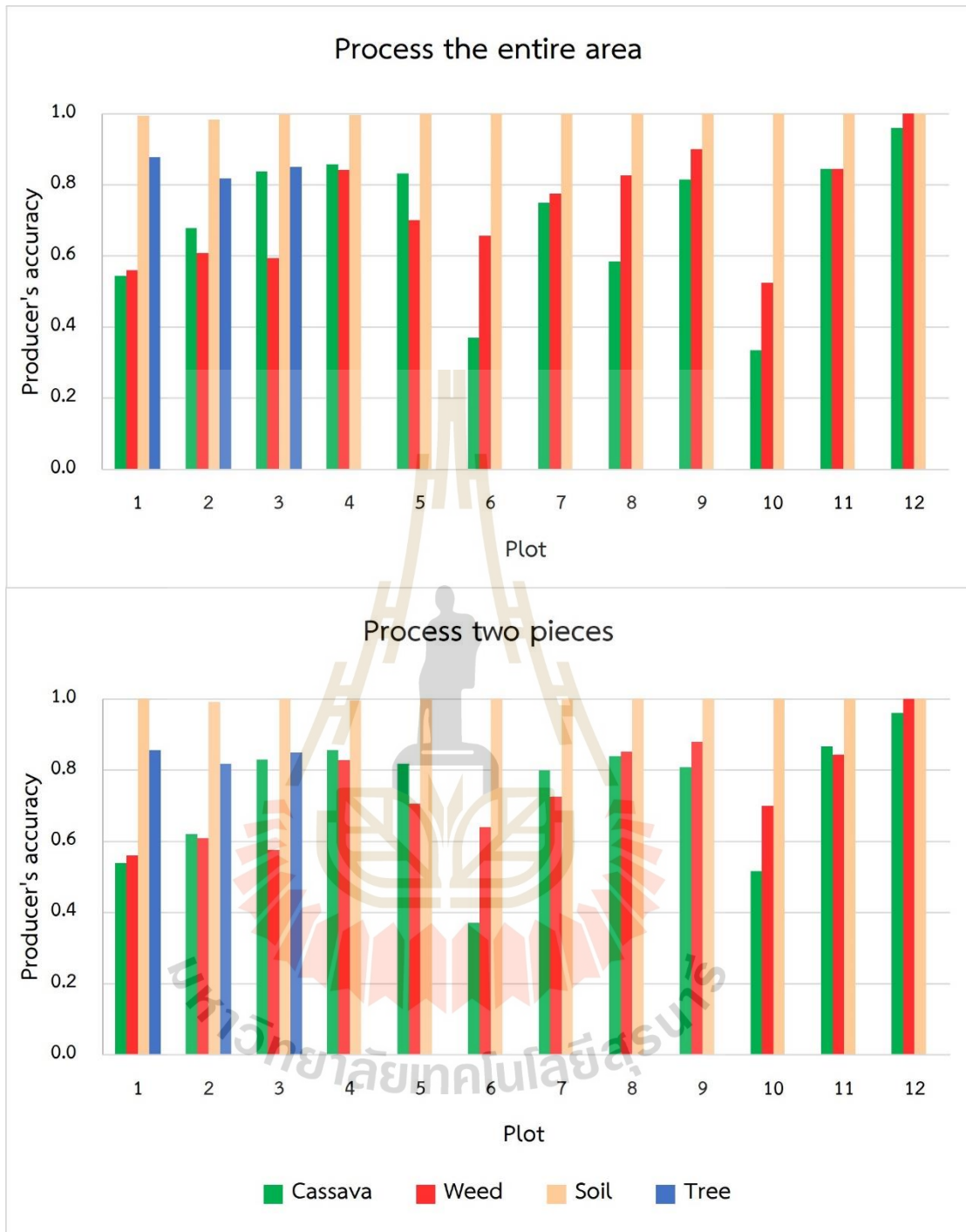


Figure 4.16 Producer's accuracy of classification results from processing the entire area and two pieces.

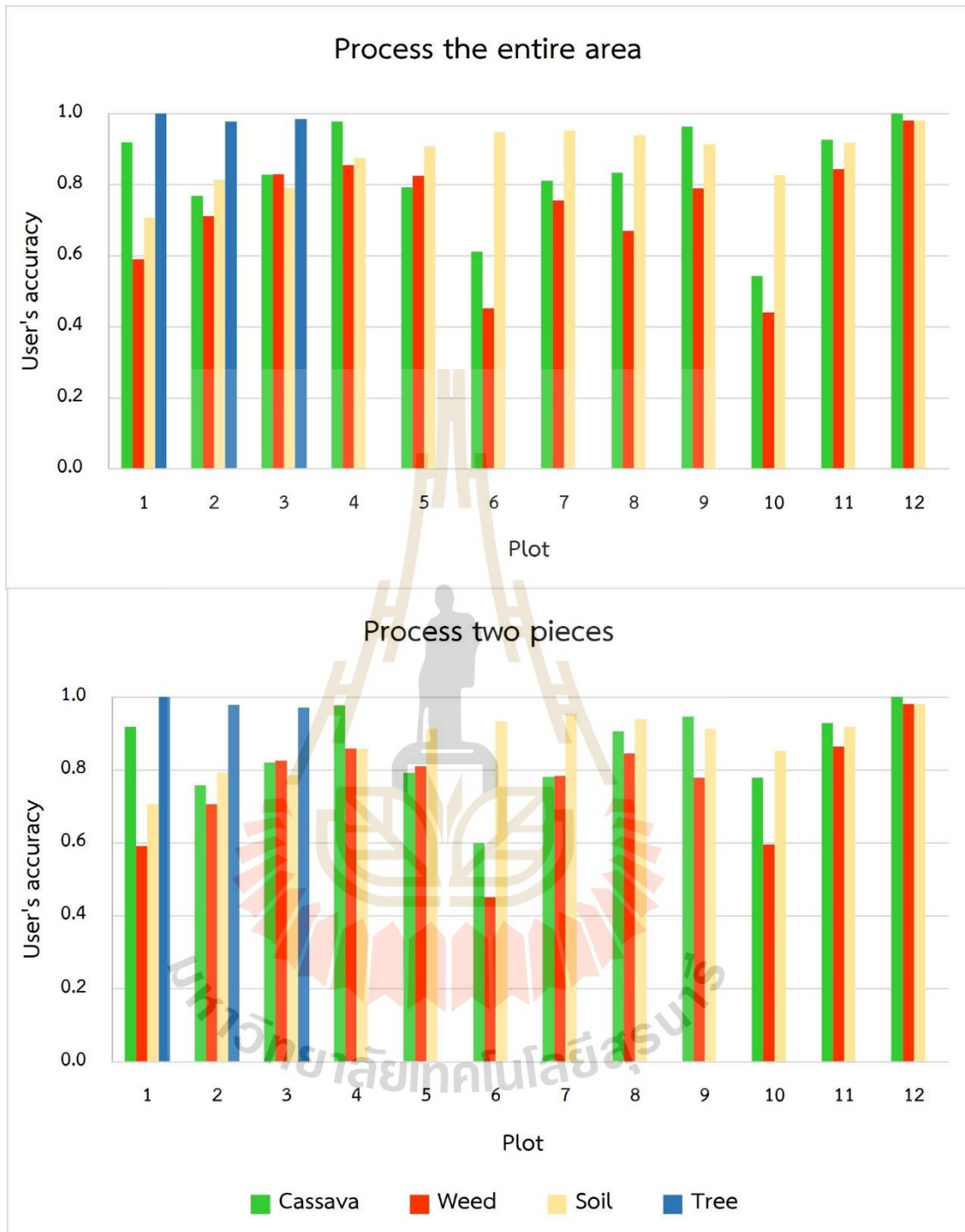


Figure 4.17 User's accuracy of classification results from processing the entire area and two pieces.

The results demonstrate that the proposed classification process exhibited strong performance in accurately identifying soil and trees. However, it showed lower to moderate accuracy in identifying cassava and weed. Plots 6 and 8 displayed less accurate classification results, with kappa coefficients below 0.7. These plots showed significant variations in weed invasion levels, as shown in Figure 1.5. Moreover, there was a wide range of differences in the diameter of the cassava canopy within these plots, as illustrated in Figure 1.7.

The input images were processed using two approaches: processing the entire area and splitting the input image into two separate pieces. Subsequently, the proposed classification process was applied to both sets. Table 4.12 presents the classification accuracies for both sets, while Appendix E displays confusion matrix and classification maps for plots 1-12 for processing by both approaches.

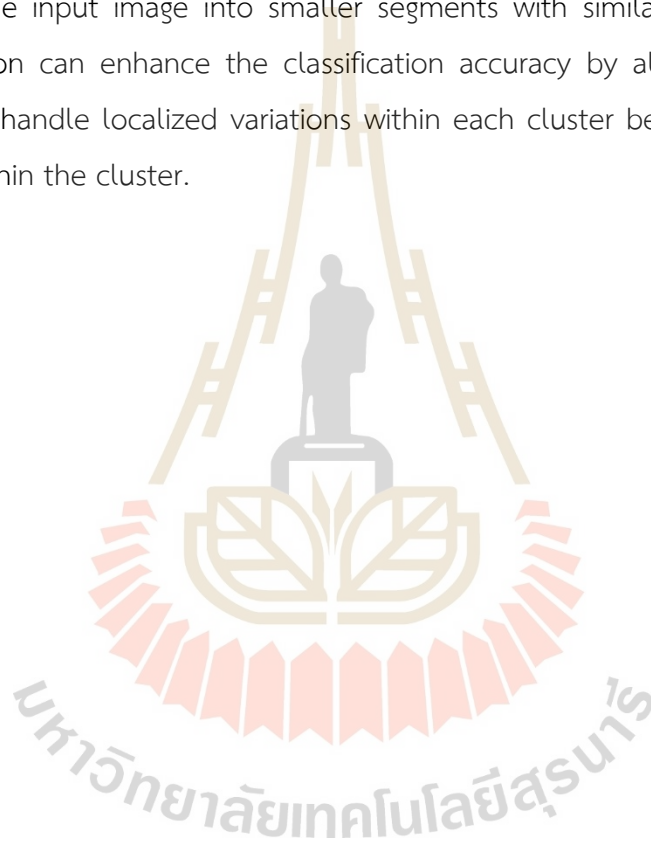
The classification results for the two different image sizes yielded similar accuracy. However, there were notable differences in the results for plot 8 and plot 10 (Appendix E, Figure E8 and E10). These cassava plots have non-smooth lighting conditions in the image, which has a noticeable impact on the classification outcomes when processed the entire area. Splitting the images into two sections resulted in increased accuracy compared to processing the entire area as a single entity. By employing a clustering algorithm that utilizes input data to generate a Voronoi partition for grouping purposes, the process of splitting the input image led to the formation of smaller and distinct input groups. Consequently, the diverse input data generated disparate clusters. By partitioning the input data into smaller groups, the clustering algorithm can efficiently handle localized data, ultimately leading to enhanced classification performance.

The maps demonstrate that classification using different image sizes generates highly similar results. However, certain maps exhibit non-smoothness in the classification of objects, as observed in plot 10 (Appendix E, Figure E10). It contributes to the classification process relying on clustering and variations in the input data can lead to the formation of different clusters.

The weed present in the plot can be extracted from the classification map, which can be utilized in future applications for weed management. The weed map can

be found in Appendix F. Figures F1 to F12 illustrate the weed maps for plots 1 to 12, showcasing the best classification accuracy achieved between processing the entire area and splitting it into two pieces.

The study results suggest that the proposed classification process may not work well in areas with varying cassava canopy sizes, diverse weed invasion levels, and lighting conditions. These factors can negatively impact classification accuracy, resulting in less desirable outcomes. However, a potential solution to these challenges is splitting the input image into smaller segments with similar physical properties. The separation can enhance the classification accuracy by allowing the clustering algorithm to handle localized variations within each cluster better handle localized variations within the cluster.



CHAPTER V

CONCLUSION AND SUGGESTIONS

This chapter presents the summary of the findings and results of the study. This study was undertaken to design a semi-automatic classification process for classifying objects in cassava fields from very high-resolution UAV images. The summary of results includes the finding in developing the classification process, the results of adjusting and validating the classification process, and the result of applying the adjusted proposed classification process in the study areas. Moreover, this chapter provided suggestions for the study for future work. Details are described as follows.

5.1 Conclusion

In this experiment, various RGB and RGB-based indices were applied as input for the classification image. The images were taken from UAV which contained very-high spectral resolution and various color values; the image needs to be enhanced to reduce the heterogeneity and noise for other processes. The selected method for enhancing images was mean-shift filtering. The three layers from RGB and indices were combined to produce a three-layer image that matched the requirement of the mean-shift filtering algorithm. According to the classification results, different classes reached high accuracy when applying different combination images. Therefore, the combination of indices was evaluated as a significant feature of the classification process.

In the process of adjusting parameters, various indices demonstrated their performance in separating classes. The Color Index (CI) emerged as a reliable index for soil classification, effectively differentiating soil from other elements in an image due to its sensitivity to soil color and composition (Escadafal and Huete, 1991). Notably, the CI index is less influenced by vegetation cover, making it valuable for distinguishing between soil and vegetation.

For tree classification, the VARI index proves to be a valuable tool. It accounts for atmospheric conditions and illumination variations, which can impact reflectance measurements. By enhancing sensitivity to vegetation, the VARI index improves discrimination among different types of vegetation and other land cover categories.

The Green and Excess Red (ExR) indices play a crucial role in differentiating cassava and weed. The green band reflects the green light absorbed and reflected by plants, enabling discrimination based on leaf structure, density, and pigmentation. The ExR index measures the excess red light reflected by plants compared to their reflectance in the green band, aiding in distinguishing plant species with varying chlorophyll absorption properties (Virtanen et al., 2022).

The application of mean-shift filtering aimed to improve image quality by adjusting parameters to find an appropriate set. The adjusting and validating classification process results demonstrated that using suitable parameters allowed for the quick and accurate detection of interesting objects. The filtering process effectively detected differences in spectral value and size, underscoring the importance of selecting optimal parameter values to achieve the best results.

In soil classification, the optimal values for sp and sr were determined to be 5 and 10, respectively. The use of various sp values resulted in high accuracy, indicating the soil class's lack of a well-defined shape, making it difficult to determine the exact sp value. Conversely, employing a small sr value yielded high accuracy allowing for better differentiation between vegetation and soil by considering the narrower spectral range of the combined indices used.

In tree classification, higher accuracy was achieved using larger values of sp and sr in the filtering process. For the first filter, a sp value of 60 and a sr value of 20 were found to be optimal, while for the second filter, a sp value of 20 and a sr value of 40 yielded good results. These findings suggest that the size of the filtering window should correspond to the size of the tree canopy. Given that tree canopies are typically larger, using a larger sp value effectively smoothed the tree pixels. Additionally, trees exhibit

a wider spectral range than other classes within the same index, making a higher sr value advantageous for smoothing tree pixels.

The selected filtering window size parameters for cassava and weed classification were $sp=10$ and $sr=20$. The sp parameter was specifically chosen based on a GSD of 5 cm and a spatial window of 10 pixels, aligning with the average size of cassava canopies ranging from 52 to 88 centimeters. This finding indicates that the sp parameter is related to the size of the targeted object. Additionally, the sr parameter was responsive to the spectral values of cassava in the indices, further enhancing the accuracy of the classification.

K-means clustering was utilized for classifying different classes, demonstrating its potential in extracting and separating these classes. The number of clusters (k) played a crucial role in controlling the clustering outcome, making it essential to adjust this parameter correctly. This study designs cluster results consisting of four clusters: cassava, weed, soil, and tree. However, achieving accurate classification for all classes in a single attempt was challenging, necessitating separate or hierarchical processes. For soil classification, $k=3$ was used to separate soil, vegetation, and background data. In tree classification, $k=3$ was employed to cluster tree, non-tree, and background. Lastly, cassava and weed classification utilized $k=4$ to classify cassava, weed, pixels of soil and tree, and background data. The cluster results were influenced by the number of clusters and the properties of input data, as evident from the variations observed in the classification outputs with different input and image sizes, even within the same area.

The spectral properties of the clusters varied, with the centroid of each cluster being influenced by the input data. Different combinations of indices resulted in distinct centroid values even within the same class. The spectral value trends were flexibly applied to label the classes to accommodate different input images and study sites with varying DN values due to light conditions. For labeling the soil class in image of GSD 5 cm, the trend of the cluster's spectral value centroid in index B was utilized, where the cluster with high values was labeled as soil and the rest as vegetation.

The spectral value centroid in the ExB index was used in tree classification, with low values labeled as tree and the remaining as non-tree. As for labeling cassava and weed, the G index was employed, where cassava exhibited low G values and weed showed high G values.

The results obtained from adjusting and validating the classification process highlight the importance of using different parameters for classifying objects in the fields. Objects in the fields have distinct sizes and spectral properties, necessitating specific parameters for accurate identification and analysis. Additionally, the accuracy of the classification results is influenced by the image's Ground Sample Distance (GSD). The image with finer GSDs tends to yield higher accuracy but requires more processing time. In contrast, a GSD of 5 cm demonstrates a comparable classification accuracy to that of a GSD of 1.5 cm, as evidenced by high values in OA and kappa coefficient, with a significance level of 0.05 determined by a t-test. Additionally, it significantly reduces processing time. Hence, employing an image with a GSD of 5 cm ensures both accuracy and time efficiency.

The performance of traditional classification methods: RF and K-means, were compared to the results obtained from the proposed classification process. The results from the proposed classification process showed significantly higher accuracy than the K-means method, as determined by a t-test at a significance level of 0.05. In contrast, the proposed classification process yielded high accuracy comparable results to RF. Furthermore, the proposed process demonstrated a reduced requirement for manual intervention and user-provided data.

The proposed classification process was evaluated in 12 distinct cassava plots, employing two approaches: processing the entire area and splitting the image into two pieces. For most plots, both approaches produced comparable levels of accuracy. In the four-class classification, the highest accuracy achieved was 0.8217 for OA and 0.7445 for the kappa coefficient. For the three-class classification, the accuracy reached 0.9867 for OA and 0.9800 for the kappa coefficient. On the other hand, employing the split image process led to improved accuracy. Specifically, in specific plots,

the implementation of this approach resulted in a notable increase in accuracy, with improvements of 0.1195 for OA and 0.1786 for the kappa coefficient.

The study's findings reveal that the proposed classification process successfully identified soil and trees. However, it demonstrated lower to moderate accuracy in identifying cassava and weed. The study suggests that the classification process may encounter difficulties in areas with varying canopy sizes, diverse weed invasion, and lighting conditions. Splitting the input image into smaller segments can improve accuracy by handling local differences. However, it's important to consider that the results can still be affected by lighting conditions and the level of weed invasion in the image.

This study demonstrates that using color indices, mean-shift filtering, K-means clustering, and rules can effectively classify and generate weed maps in cassava fields. One advantage of this approach is its ability to detect different vegetation species using images captured by various RGB sensors. Additionally, the classification method does not rely on training data, allowing it to be applied to different areas of cassava images. The parameters in the proposed classification process were carefully chosen to suit the classification objectives in cassava fields. Furthermore, the proposed classification process encompasses preprocessing and weed classification, reducing the need for extensive manual intervention. Lastly, the method operates in a semi-automatic manner, making it suitable for applications in precision agriculture.

5.2 Suggestions

(1) Cloud cover during UAV flights can affect image illumination, potentially leading to misclassification in the results, as seen in plot 8. It is recommended to avoid capturing images in cloudy conditions. To improve classification accuracy, it is advisable to capture images around noon to minimize the impact of shadows.

(2) The analysis of the classification results demonstrates that plots with varying levels of weed invasion in cassava substantially impact classification accuracy.

Splitting the image into smaller sizes can enhance the classification results. Further testing is recommended to assess the effect of varying the size of the spliced images.

(3) The process of applying the proposed classification process to the image is shown in Figure 5.1. When the accuracy of classification results is lower than 0.7 or 70%, the image should split before classification.

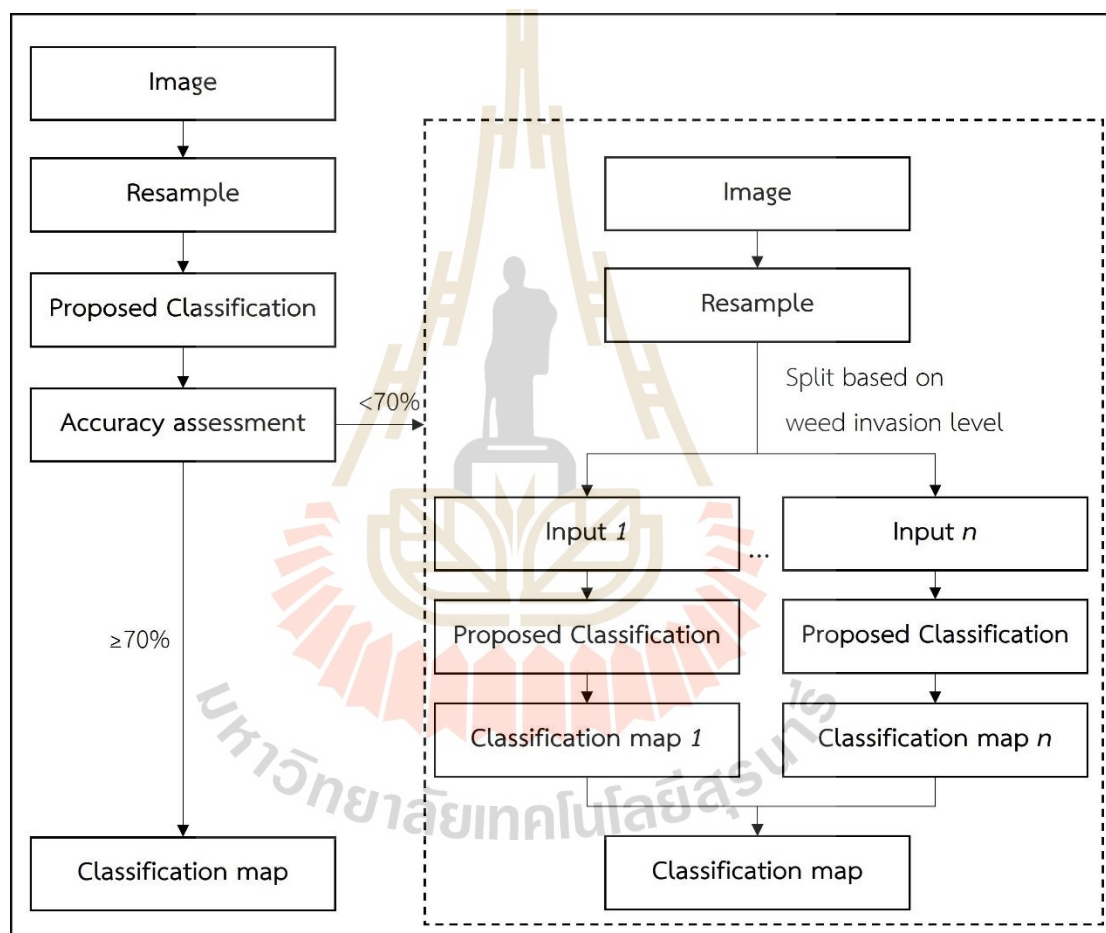


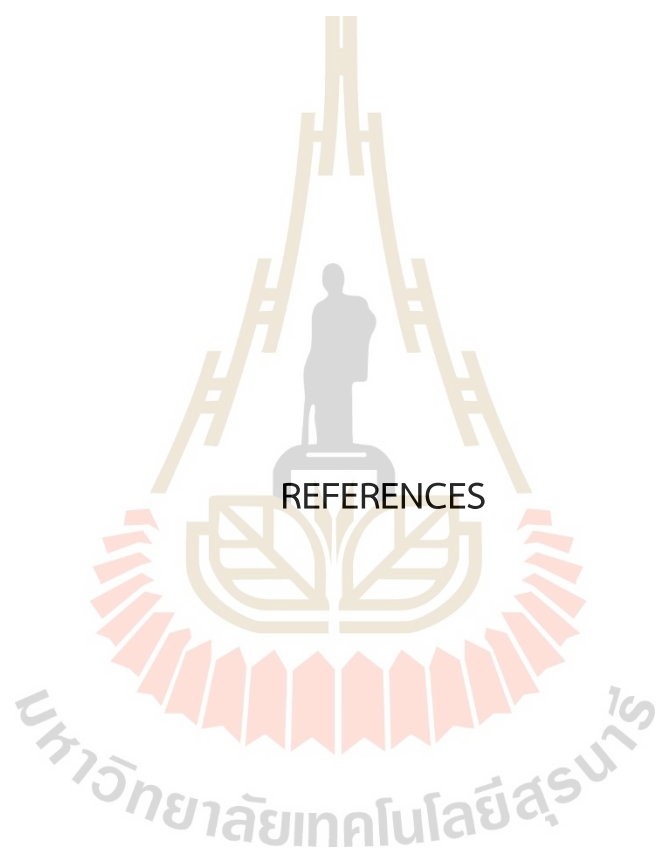
Figure 5.1 Classification process for processing the entire image and splitting image.

(4) Since the classification map can be integrated with other agriculture applications, such as spraying systems, which require accurate position. Therefore, the georeferencing process is needed. The ground control points (GCPs) should be applied during the image acquisition process.

(5) Although the coordination of weed patches can be identified and transferred to applicable with the drone service, personal accessibility is essential to weed management in the cassava fields. A guiding map with row numbers representing the cassava row is necessary for this activity. Counting the row automatically with coding in Python would be possible by setting the rule to define the first canopy in cassava rows. Therefore, codes of row numbering on cassava maps are recommended for future work. This suggestion will be helpful to smart farmers who would like to access the weed patches to control the invasion areas.

(6) The proposed classification processes can also be applied to high-resolution satellite images for the semi-automatic classification of objects. By adapting the proposed processes to high-resolution satellite data, it becomes possible to get the advantages of remote sensing technology and extend the application of the classification method to a wider range of scenarios.

(7) For future studies, the automatic classification process can be enhanced by splitting the proposed classification process into two programs. One program can focus on classifying images of cassava plots that contain trees, while the other program can be dedicated to classifying images of cassava plots that do not contain trees. These enhancements can reduce the need for manually defining trees during the classification process.



REFERENCES

REFERENCES

- Arthey, T., Srisompun, O., and Zimmer, Y. (2018). Report to FAO Cassava Production and Processing in Thailand.
- Arthur, D., and Vassilvitskii, S. (2006). k-means++: The advantages of careful seeding.
- Bah, M. D., Hafiane, A., and Canals, R. (2018). Deep Learning with Unsupervised Data Labeling for Weed Detection in Line Crops in UAV Images. *Remote Sensing*, 10(11), 1690.
- Bankhead, P. (2022). Filters. In Introduction to Bioimage Analysis. Retrieved from <https://bioimagebook.github.io/chapters/2-processing/4-filters/filters.html>.
- Bansod, B., Singh, R., Thakur, R., and Singhal, G. (2017). A comparison between satellite based and drone based remote sensing technology to achieve sustainable development: A review. *Journal of Agriculture and Environment for International Development*, 111, 383-407. doi:10.12895/jaeid.20172.690.
- Boonrang, A., Sritarapipat, T., and Piyatadsananon, P. (2021, November). Applicable Mean-Shift Filtering Parameters for Mapping Weed in Cassava Fields based on UAV Images. Proceeding of the 42nd Asian Conference on Remote Sensing (ACRS2021), Can Tho University, Can Tho city, Vietnam. Retrieved from https://a-a-r-s.org/proceeding/ACRS2021/2%20Algorithm%20and%20Image%20Processing/ACRS21_146.pdf.
- Candiago, S., Remondino, F., De Giglio, M., Dubbini, M., and Gattelli, M. (2015). Evaluating Multispectral Images and Vegetation Indices for Precision Farming Applications from UAV Images. *Remote Sensing*, 7(4). doi:10.3390/rs70404026.
- Chaudhary, P., Chaudhari, A., and Godara, S. (2012). Color Transform Based Approach for Disease Spot Detection on Plant Leaf. *International Journal of Computer Science and Telecommunications*, 3, 65-71.
- Chiranan, P., Anan, P., and Arunee, P. (2014). Effects of planting methods and weed control measures on growth and yield of dry-direct seeded rice under rainfed conditions. *Khon Kaen agriculture Journal*, 42, 411-416.

- Collins, R. T. (2003). Mean-shift blob tracking through scale space. Proceedings of the 2003 IEEE Computer Society Conference on Computer Vision and Pattern Recognition. Madison, WI, USA. doi: 10.1109/CVPR.2003.1211475.
- Comaniciu, D., and Meer, P. (1999, September). Mean shift analysis and applications. Proceedings of the Seventh IEEE International Conference on Computer Vision, Kerkyra, Greece, 1999, 1197-1203 vol.2, doi: 10.1109/ICCV.1999.790416.
- Comaniciu, D., and Meer, P. (2002). Mean shift: A robust approach toward feature space analysis. *IEEE Transactions on pattern analysis and machine intelligence*, 24(5), 603-619.
- De Castro, A. I., Torres-Sánchez, J., Peña, J. M., Jiménez-Brenes, F. M., Csillik, O., and López-Granados, F. (2018). An Automatic Random Forest-OBIA Algorithm for Early Weed Mapping between and within Crop Rows Using UAV Imagery. *Remote Sensing*, 10(2). doi:10.3390/rs10020285.
- Ekanayake, I., Osiru, D., and Porto, M. (1997). Agronomy of cassava: IITA research guide, No. 60. International Institute of Tropical Agriculture (IITA), Ibadan, Nigeria.
- Escadafal, R., and Huete, A. (1991). Improvement in remote sensing of low vegetation cover in arid regions by correcting vegetation indices for soil 'noise'. *Comptes Rendus - Academie des Sciences, Serie II*, 312(11), 1385-1391.
- FAO. (2009). How to Feed the World in 2050 (High-Level Expert Forum, 2009). Retrieved from https://www.fao.org/fileadmin/templates/wsfs/docs/Issues_papers/HLEF_2050_Global_Agriculture.pdf.
- FAOSTAT Statistical Database. (2022). Crops and livestock products. Retrieved 20/12/2022, from [Rome]: FAO.
- Foody, G. M., and Mathur, A. (2004). Toward intelligent training of supervised image classifications: directing training data acquisition for SVM classification. *Remote Sensing of Environment*, 93(1), 107-117. <https://doi.org/10.1016/j.rse.2004.06.017>.
- Fried, G., Chauvel, B., Reynaud, P., and Sache, I. (2017). Decreases in Crop Production by Non-native Weeds, Pests, and Pathogens. In M. Vilà and P. E. Hulme (Eds.),

- Impact of Biological Invasions on Ecosystem Services*, 12, 83-101. Springer, Cham. https://doi.org/10.1007/978-3-319-45121-3_6.
- Fukunaga, K., and Hostetler, L. (1975). The estimation of the gradient of a density function, with applications in pattern recognition. *IEEE Transactions on Information Theory*, 21(1), 32-40. doi:10.1109/TIT.1975.1055330.
- Gao, J., Liao, W., Nuytens, D., Lootens, P., Vangeyte, J., Pižurica, A., . . . Pieters, J. G. (2018). Fusion of pixel and object-based features for weed mapping using unmanned aerial vehicle imagery. *International Journal of Applied Earth Observation and Geoinformation*, 67, 43-53. <https://doi.org/10.1016/j.jag.2017.12.012>.
- Gareth, J., Daniela, W., Trevor, H., and Robert, T. (2015). An introduction to statistical learning: with applications in R: Springer.
- Gašparović, M., Zrinjski, M., Barković, Đ., and Radočaj, D. (2020). An automatic method for weed mapping in oat fields based on UAV imagery. *Computers and Electronics in Agriculture*, 173, 105385. <https://doi.org/10.1016/j.compag.2020.105385>.
- Gates, D. M., Keegan, H. J., Schleiter, J. C., and Weidner, V. R. (1965). *Spectral Properties of Plants*. *Applied Optics*, 4(1), 11-20. doi:10.1364/AO.4.000011.
- Ge, Y., Bai, H., Wang, J., and Cao, F. (2012). Assessing the quality of training data in the supervised classification of remotely sensed imagery: a correlation analysis. *Journal of Spatial Science*, 57(2), 135-152. doi:10.1080/14498596.2012.733616.
- Gitelson, A. A., Kaufman, Y. J., Stark, R., and Rundquist, D. (2002). Novel algorithms for remote estimation of vegetation fraction. *Remote Sensing of Environment*, 80(1), 76-87. [https://doi.org/10.1016/S0034-4257\(01\)00289-9](https://doi.org/10.1016/S0034-4257(01)00289-9).
- Grenier, T., Revol-Muller, C., and Gimenez, G. (2006, October). Hybrid approach for multiparametric mean shift filtering. Proceedings of the 2006 International Conference on Image Processing. Atlanta, GA, USA, 2006. 1541-1544, doi: 10.1109/ICIP.2006.312644.

- Guijarro, M., Pajares, G., Riomoros, I., Herrera, P. J., Burgos-Artizzu, X. P., and Ribeiro, A. (2011). Automatic segmentation of relevant textures in agricultural images. *Computers and Electronics in Agriculture*, 75(1), 75-83. doi: 10.1016/j.compag.2010.09.013.
- Hall, O., Dahlin, S., Marstorp, H., Archila Bustos, M. F., Öborn, I., and Jirström, M. (2018). Classification of Maize in Complex Smallholder Farming Systems Using UAV Imagery. *Drones*, 2(3), 22. <https://doi.org/10.3390/drones2030022>.
- Hamuda, E., Glavin, M., and Jones, E. (2016). A survey of image processing techniques for plant extraction and segmentation in the field. *Computers and Electronics in Agriculture*, 125, 184-199. <https://doi.org/10.1016/j.compag.2016.04.024>.
- Howeler, R., Lutaladio, N., and Thomas, G. (2013). *Save and Grow: Cassava. A guide to sustainable production intensification*. Rome, Italy: FAO.
- Huang, H., Deng, J., Lan, Y., Yang, A., Deng, X., and Zhang, L. (2018). A fully convolutional network for weed mapping of unmanned aerial vehicle (UAV) imagery. *PLOS ONE*, 13(4), e0196302. doi:10.1371/journal.pone.0196302.
- Huang, H., Li, X., and Chen, C. (2018). Individual Tree Crown Detection and Delineation From Very-High-Resolution UAV Images Based on Bias Field and Marker-Controlled Watershed Segmentation Algorithms. *IEEE Journal of Selected Topics in Applied Earth Observations and Remote Sensing*, 11(7), 2253-2262. doi:10.1109/JSTARS.2018.2830410.
- Ishida, T., Kurihara, J., Viray, F. A., Namuco, S. B., Paringit, E. C., Perez, G. J., . . . Marciano, J. J. (2018). A novel approach for vegetation classification using UAV-based hyperspectral imaging. *Computers and Electronics in Agriculture*, 144, 80-85. <https://doi.org/10.1016/j.compag.2017.11.027>.
- James B. Campbell, and Wynne, R. H. (2011). *Introduction to Remote Sensing: Fifth Edition*. New York: The Guilford Press.
- Jeamjamnanja, J., Phuddacharoen, S., Pulsa-nguan, P., Rojanaridpiched, C., and Saengkaewsuk, W. (1984). Timing of weed control in cassava. 2(3), 144-147.

- Jinru, X., and Su, B. (2017). Significant Remote Sensing Vegetation Indices: A Review of Developments and Applications. *Journal of Sensors*, 2017, 1353691. <https://doi.org/10.1155/2017/1353691>.
- Kaur, D., and Kaur, Y. (2014). Various image segmentation techniques: a review. *International Journal of Computer Science and Mobile Computing*, 3(5), 809-814.
- Khan, S., Tufail, M., Khan, M. T., Khan, Z. A., Iqbal, J., and Alam, M. (2021). A novel semi-supervised framework for UAV based crop/weed classification. *PLOS ONE*, 16(5), e0251008. doi:10.1371/journal.pone.0251008.
- Khattak, A., Raja, G., Anjum, N., and Qasim, M. (2015, December). Integration of Mean-Shift and Particle Filter: A Survey. Proceedings of the 2014 12th International Conference on Frontiers of Information Technology, Islamabad, Pakistan, 2014, 286-291. doi:10.1109/FIT.2014.60.
- Kuruvilla, J., Sukumaran, D., Sankar, A., and Joy, S. P. (2016, March). A review on image processing and image segmentation. Proceedings of the 2016 International Conference on Data Mining and Advanced Computing (SAPIENCE), Ernakulam, India, 2016, 198-203, doi: 10.1109/SAPIENCE.2016.7684170.
- Lameski, P., Zdravevski, E., Trajkovik, V., and Kulakov, A. (2017). Weed Detection Dataset with RGB Images Taken Under Variable Light Conditions. *Communications in Computer and Information Science*, 778, 112-119. https://doi.org/10.1007/978-3-319-67597-8_11.
- Li, T. (2012). Contributions to Mean Shift filtering and segmentation: Application to MRI ischemic data. INSA de Lyon.
- LÓPez-Granados, F. (2011). Weed detection for site-specific weed management: mapping and real-time approaches. *Weed Research*, 51(1), 1-11. <https://doi.org/10.1111/j.1365-3180.2010.00829.x>.
- Lottes, P., Khanna, R., Pfeifer, J., Siegwart, R., and Stachniss, C. (2017, 29 May-3 June 2017). UAV-based crop and weed classification for smart farming. Proceeding of

- the 2017 IEEE International Conference on Robotics and Automation (ICRA). Singapore, 2017, 3024-3031. doi: 10.1109/ICRA.2017.7989347.
- Louargant, M., Villette, S., Jones, G., Vigneau, N., Paoli, J. N., and Gée, C. (2017). Weed detection by UAV: simulation of the impact of spectral mixing in multispectral images. *Precision Agriculture*, 18, 1-20. doi:10.1007/s11119-017-9528-3.
- Louargant, M., Jones, G., Faroux, R., Paoli, J.-N., Maillot, T., Gée, C., and Villette, S. (2018). Unsupervised Classification Algorithm for Early Weed Detection in Row-Crops by Combining Spatial and Spectral Information. *Remote Sensing*, 10(5), 761.
- Louhaichi, M., Borman, M. M., and Johnson, D. E. (2001). Spatially Located Platform and Aerial Photography for Documentation of Grazing Impacts on Wheat. *Geocarto International*, 16(1), 65-70. doi:10.1080/10106040108542184.
- Lueang-a-papong, P. (1998). Effect of Certain Weed Managements on Yield of Corn (*Zea mays*). *Journal of Agriculture*, 14(2), 134-141. Retrieved from <https://li01.tci-thaijo.org/index.php/joacmu/article/download/247303/169167>.
- Marin-Morales, M. A., Ventura-Camargo, B. d. C., and Hoshina, M. M. (2013). Toxicity of Herbicides: Impact on Aquatic and Soil Biota and Human Health. InTech. doi: 10.5772/55851.
- Mathieu, R., Pouget, M., Cervelle, B., and Escadafal, R. (1998). Relationships between Satellite-Based Radiometric Indices Simulated Using Laboratory Reflectance Data and Typic Soil Color of an Arid Environment. *Remote Sensing of Environment*, 66(1), 17-28. [https://doi.org/10.1016/S0034-4257\(98\)00030-3](https://doi.org/10.1016/S0034-4257(98)00030-3).
- McGeeney, R. (2022). 'This is a year to survive': High input costs, weed pressure top concerns for growers gearing up for 2022. Retrieved from <https://www.uaex.uada.edu/media-resources/news/2022/01-28-2022-ark-hazen-herbicides.aspx>.
- Meyer, G., Hindman, T., and Laksmi, K. (1999, January). Machine vision detection parameters for plant species identification. Proceeding of the Precision Agriculture and Biological Quality. <https://doi.org/10.1117/12.336896>.

- Meyer, G. E., and Neto, J. C. (2008). Verification of color vegetation indices for automated crop imaging applications. *Computers and Electronics in Agriculture*, 63(2), 282-293. <https://doi.org/10.1016/j.compag.2008.03.009>.
- Miller, P. C. (2003). Patch spraying: future role of electronics in limiting pesticide use. *Pest Manag Sci*, 59(5), 566-574. doi:10.1002/ps.653.
- Morales, R., Torres, E., and Sossa, H. (2011). Image segmentation based on an iterative computation of the mean shift filtering for different values of window sizes. *International Journal of Imaging and Robotics*, 6(A11), 1-19.
- Mulla, D. J. (2013). Twenty five years of remote sensing in precision agriculture: Key advances and remaining knowledge gaps. *Biosystems Engineering*, 114(4), 358-371. <https://doi.org/10.1016/j.biosystemseng.2012.08.009>.
- Narkhede, H. (2013). Review of image segmentation techniques. *International Journal of Science and Modern Engineering*, 1(8), 54-61.
- OAE. (2022). Data of Agriculture production (in Thai). Retrieved from www.oae.go.th.
- Oerke, E. C. (2006). Crop losses to pests. *The Journal of Agricultural Science*, 144(1), 31-43. doi:10.1017/S0021859605005708.
- Office of Agricultural Economics. (2019). Agricultural Utilized Areas by Province, Year 2019 (In Thai). Retrieved from <https://www.oae.go.th/assets/portals/1/files/socio/LandUtilization2562.pdf>.
- Office of Agricultural Economics. (2021). Export-import of agricultural products (In Thai). Retrieved from <http://mis-app.oae.go.th/>.
- Office of Agricultural Economics. (2023, 16 February 2023). Quantity and Value of Imported Pesticides in 2018 - 2022 (In Thai). Retrieved from <https://www.oae.go.th/view/1/ปัจจัยการผลิต/TH-TH#>.
- Onochie, B. E. (1975). Critical Periods for Weed Control in Cassava in Nigeria. *PANS Pest Articles & News Summaries*, 21(1), 54-57. doi:10.1080/09670877509411488.
- Pajares, G., Ruz, J. J., and de la Cruz, J. M. (2005). Performance Analysis of Homomorphic Systems for Image Change Detection. In: Marques, J.S., Pérez de la Blanca, N., Pina, P. (eds) Pattern Recognition and Image Analysis. Lecture Notes in

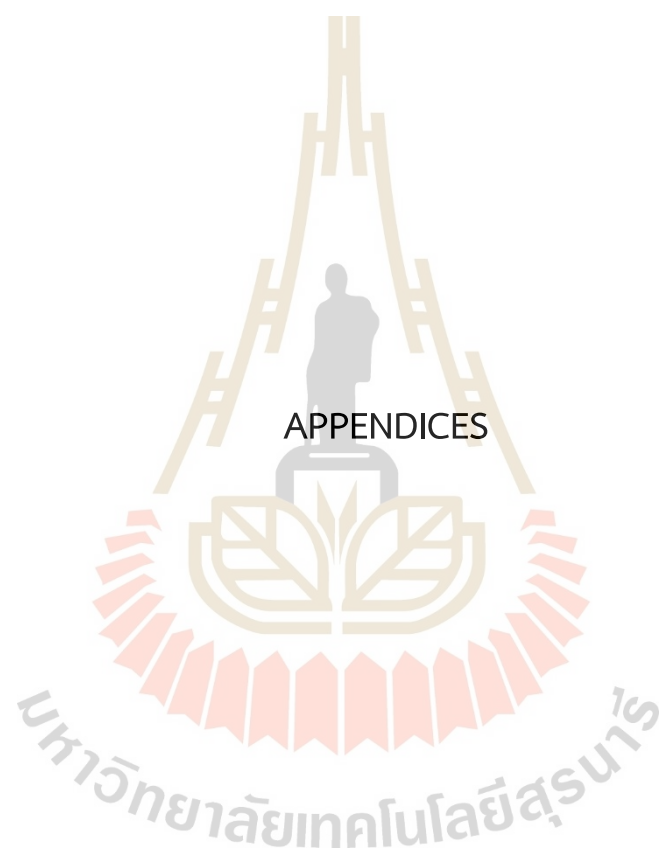
- Computer Science, 3522. Springer, Berlin, Heidelberg. https://doi.org/10.1007/11492429_68.
- Pantazi, X. E., Tamouridou, A. A., Alexandridis, T. K., Lagopodi, A. L., Kashefi, J., and Moshou, D. (2017). Evaluation of hierarchical self-organising maps for weed mapping using UAS multispectral imagery. *Computers and Electronics in Agriculture*, 139, 224-230. <https://doi.org/10.1016/j.compag.2017.05.026>.
- Pedregosa, F., Varoquaux, G., Gramfort, A., Michel, V., Thirion, B., Grisel, O., . . . Dubourg, V. (2011). Scikit-learn: Machine learning in Python. *the Journal of machine Learning research*, 12, 2825-2830. Retrieved from <https://scikit-learn.org/stable/modules/generated/sklearn.cluster.KMeans.html>.
- Peña, J. M., Torres-Sánchez, J., de Castro, A. I., Kelly, M., and López-Granados, F. (2013). Weed Mapping in Early-Season Maize Fields Using Object-Based Analysis of Unmanned Aerial Vehicle (UAV) Images. *PLOS ONE*, 8(10), e77151. doi:10.1371/journal.pone.0077151.
- Plant protection research and development office. (2016). Integrated Pest Management Guide for Cassava (In Thai). Bangkok, Thailand.
- Polthanee, A. (2018). Cassava as an insurance crop in a changing climate: The changing role and potential applications of cassava for smallholder farmers in Northeastern Thailand. *Forest and Society*, 2, 121. doi:10.24259/fs.v2i2.4275.
- Raja, S. K., Abdul KhadiRr, A. S., and Ahamed, S. R. (2009). Moving Toward Region-based Image Segmentation Techniques: A Study. *Journal of Theoretical & Applied Information Technology*, 5(1), 81-87. Retrieved from https://www.researchgate.net/profile/Kasmir-S-v/publication/255610876_MOVING_TOWARD_REGION-BASED_IMAGE_SEGMENTATION_TECHNIQUES_A_STUDY/links/59157ae40f7e9b70f49c7a17/MOVING-TOWARD-REGION-BASED-IMAGE-SEGMENTATION-TECHNIQUES-A-STUDY.pdf.
- Rodríguez, R., Suarez, A. G., and Sossa, J. H. (2011). A segmentation algorithm based on an iterative computation of the mean shift filtering. *Journal of Intelligent & Robotic Systems*, 63(3), 447-463.

- Saha, D. (2019). Development of Enhanced Weed Detection System with Adaptive Thresholding, K-Means and Support Vector Machine. Electronic Theses and Dissertations. 3374. <https://openprairie.sdstate.edu/etd/3374>.
- Smith, R. B. (2012). Hyperspectral Imaging. Plant Spectra. Retrieved from <https://microimages.com/documentation/Tutorials/hyprspec.pdf>.
- Song, N., Gu, L., Cao, Z., and Viberg, M. (2006). Enhanced spatial-range mean shift color image segmentation by using convergence frequency and position. Proceeding of the 2006 14th European Signal Processing Conference, Florence, Italy, 2006, 1-5.
- Su, J., Yi, D., Coombes, M., Liu, C., Zhai, X., McDonald-Maier, K., and Chen, W.-H. (2022). Spectral analysis and mapping of blackgrass weed by leveraging machine learning and UAV multispectral imagery. *Computers and Electronics in Agriculture*, 192, 106621. <https://doi.org/10.1016/j.compag.2021.106621>.
- Subeesh, A., Bhole, S., Singh, K., Chandel, N. S., Rajwade, Y. A., Rao, K. V. R., . . . Jat, D. (2022). Deep convolutional neural network models for weed detection in polyhouse grown bell peppers. *Artificial Intelligence in Agriculture*. 6, 47-54. <https://doi.org/10.1016/j.aiia.2022.01.002>.
- Tawatsin, A. (2015). Pesticides used in Thailand and toxic effects to human health. *Medical Research Archives*. (3). Retrieved from <https://esmed.org/MRA/mra/article/view/176>.
- Tian, X., Hsiao-Chun, W., and Huang, S. C. H. (2014). A new stopping criterion for fast low-density parity-check decoders. *IEEE Communications Letters*, 18(10), 1679-1682. doi: 10.1109/LCOMM.2014.2349988.
- Tsouros, D. C., Bibi, S., and Sarigiannidis, P. G. (2019). A Review on UAV-Based Applications for Precision Agriculture. *Information*, 10(11), 349. Retrieved from <https://www.mdpi.com/2078-2489/10/11/349>.
- Tucker, C. J. (1979). Red and photographic infrared linear combinations for monitoring vegetation. *Remote Sensing of Environment*, 8(2), 127-150. [https://doi.org/10.1016/0034-4257\(79\)90013-0](https://doi.org/10.1016/0034-4257(79)90013-0).

- van Dijk, M., Morley, T., Rau, M. L., and Saghai, Y. (2021). A meta-analysis of projected global food demand and population at risk of hunger for the period 2010–2050. *Nature Food*, 2(7), 494-501. doi:10.1038/s43016-021-00322-9.
- Virtanen, O., Constantinidou, E., and Tyystjärvi, E. (2022). Chlorophyll does not reflect green light – how to correct a misconception. *Journal of Biological Education*, 56(5), 552-559. doi:10.1080/00219266.2020.1858930.
- Vityakon, P., and Prachaiyo, B. (1992, March). The role of trees in the rice paddies of the Northeast in the sustainability of the rain-fed agro-ecology and development as a resource for the community (In Thai). Proceeding of the 9th Thailand National Farming Systems Seminar, Phuket Merlin Hotel, Phuket, Thailand.
- Weston.pace. (2007). k-means clustering. Retrieved from https://en.wikipedia.org/wiki/K-means_clustering.
- Woebbecke, D., Meyer, G., Bargaen, K., and Mortensen, D. (1995). Color Indices for Weed Identification Under Various Soil, Residue, and Lighting Conditions. *Transactions of the ASAE*, 38, 259-269. doi:10.13031/2013.27838.
- Woolley, J. T. (1971). Reflectance and Transmittance of Light by Leaves. *Plant Physiology*, 47(5), 656-662. doi:10.1104/pp.47.5.656.
- Wydra, K., and Verdier, V. (2002). Occurrence of cassava diseases in relation to environmental, agronomic and plant characteristics. *Agriculture, Ecosystems & Environment*, 93(1), 211-226. [https://doi.org/10.1016/S0167-8809\(01\)00349-8](https://doi.org/10.1016/S0167-8809(01)00349-8).
- Xiang, G. (2009, 17-19 Oct. 2009). Real-Time Follow-Up Tracking Fast Moving Object with an Active Camera. Proceeding of the 2009 2nd International Congress on Image and Signal Processing. Tianjin, China. doi: 10.1109/CISP.2009.5303457.
- Zakaluk, R., Sri Ranjan, R., And, S., and Ranjan. (2008). Predicting the leaf water potential of potato plants using RGB reflectance. Canadian Biosystems Engineering / Le Genie des biosystems au Canada, 50. Retrieved from <https://library.csbe-scgab.ca/docs/journal/50/c0712.pdf>.

- Zhang, S., Guo, J., and Wang, Z. (2019). Combing K-means Clustering and Local Weighted Maximum Discriminant Projections for Weed Species Recognition. *Frontiers in Computer Science*, 1. doi:10.3389/fcomp.2019.00004.
- Zhou, H., Wang, X., and Schaefer, G. (2011). Mean Shift and Its Application in Image Segmentation. In H. Kwaśnicka and L. C. Jain (Eds.), *Innovations in Intelligent Image Analysis*. Berlin, Heidelberg: Springer Berlin Heidelberg.





The logo of Sakon Nakhon Rajabhat University is centered on the page. It features a stylized golden structure resembling a traditional Thai roof or a tiered stupa, with a silhouette of a person standing on a platform in the center. Below this structure is a golden emblem of an open book. The entire logo is surrounded by a decorative border of red and orange triangular shapes. At the bottom of the logo, the university's name is written in Thai script: มหาวิทยาลัยเทคโนโลยีสุรนารี.

APPENDIX A

PROTOCOL FOR APPLYING PROPOSED CLASSIFICATION PROCESS

Protocol for applying the proposed classification process:

This protocol processes the entire image of a cassava field, including cassava, weeds, soil, and trees. It generates a classification map specifically for cassava aged 3-4 months.

1. Data Preparation:

1.1 Resize images to a Ground Sample Distance (GSD) of 5 cm using the nearest neighbor method.

1.2 Normalize pixel values of the UAV image to a range of 0-255 for the red, green, and blue layers. Store the images in 8-bit GeoTIFF format.

1.3 Create a boundary shapefile to define the area for classification.

Figure A1 shows example of input for the proposed classification process, the input consist of UAV image, which is in the .tif format, and the shapefile boundary, which is in the .shp format.



Figure A1 Example of UAV image and boundary shapefile for the proposed classification process.

2. Classification Process:

- 2.1 Create two folders to store the input and output files.
- 2.2 Place the UAV image and the shapefile boundary into the input folder.
- 2.3 To run the "Classification.exe" file, you can follow these steps:
 - 1) Locate the "Classification.exe" file on your computer.
 - 2) Execute the "Classification.exe" file by double-clicking on it. After launching, the command line window will appear, displaying in Figure A2.

launching, the command line window will appear, displaying in Figure A2.

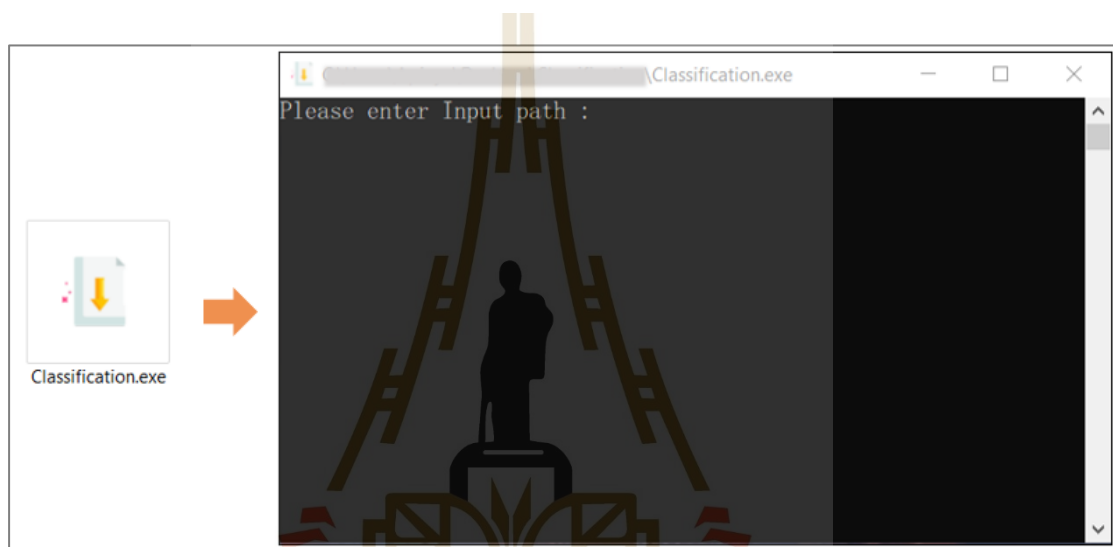


Figure A2 Visual interface of Classification.exe.

- 2.4 In the command line window, enter the path location of the input folder and the output folder in step 2.1. Press the "Enter" key to move on to the next step.
- 2.5 Specify the classification system information as follows:
 - 1) For images that contain trees, assign 1.
 - 2) For images that do not contain trees, assign 0.
- 2.6 Press the "Enter" key, the software interface will be displayed as shown in Figure A3. The results of the classification process will consist of the classification map and the weed map.

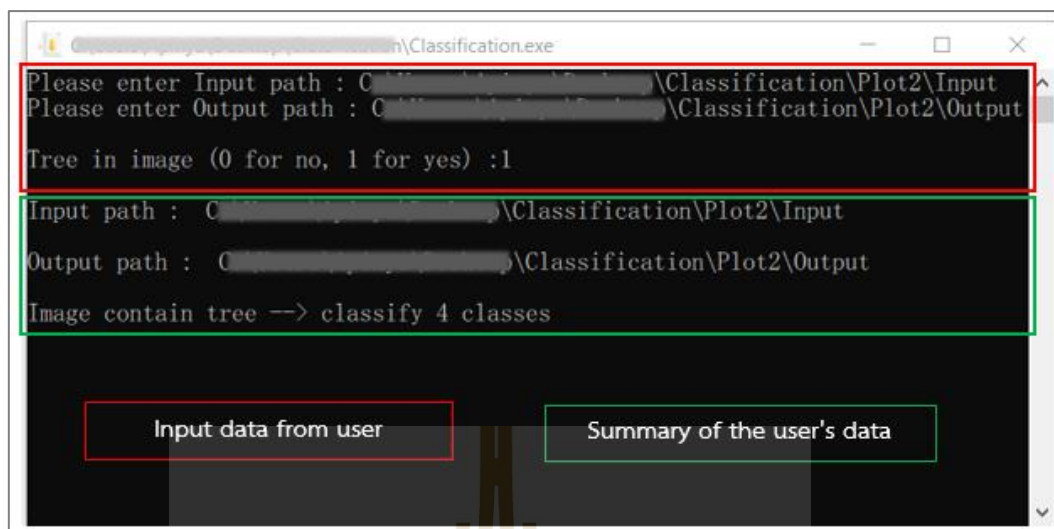


Figure A3 Software interfaces during the processing.

The example of output results from the classification using Classification.exe present in Figure A4. The classification map consists of three classes labeled as class number 1-3 in the three-class classification. In the four-class classification, it contains four classes labeled as number 1-4. These numbers have specific meanings: class 1 represents cassava, class 2 represents weed, class 3 represents soil, and class 4 represents trees.

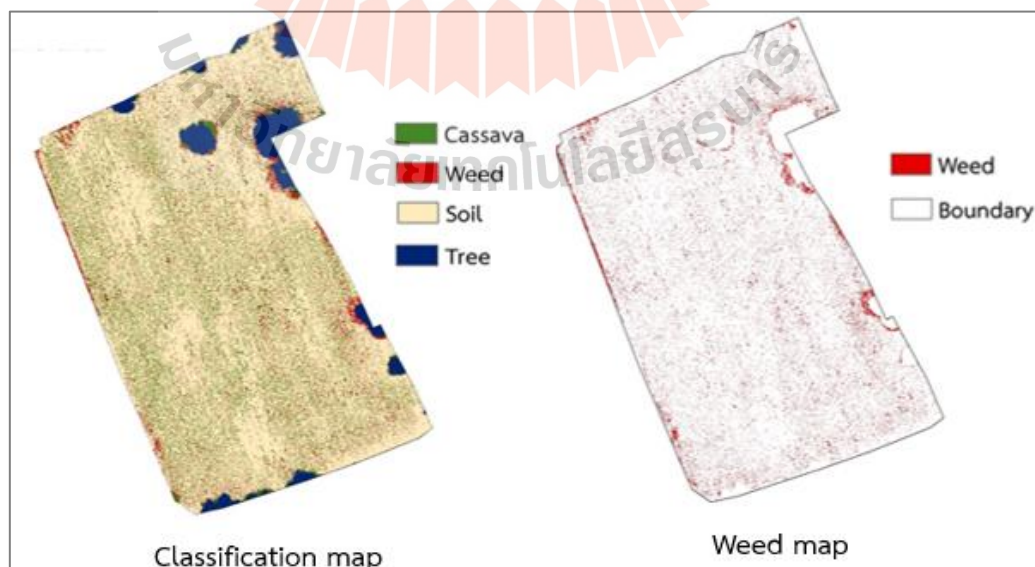
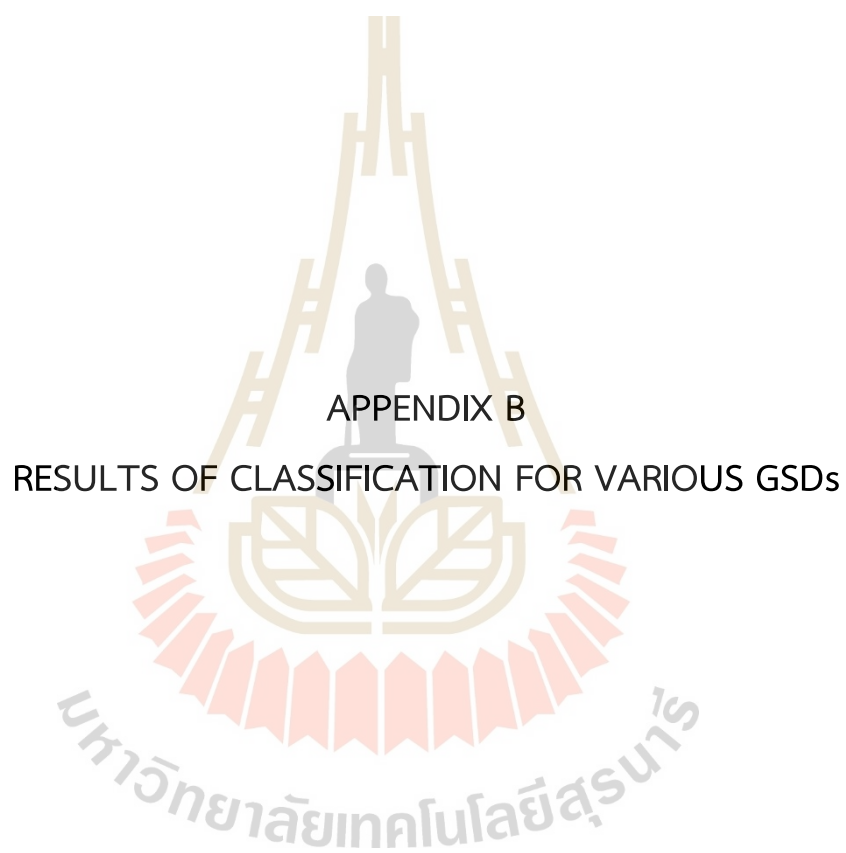


Figure A4 Examples of output from the proposed classification process.



APPENDIX B

RESULTS OF CLASSIFICATION FOR VARIOUS GSDs

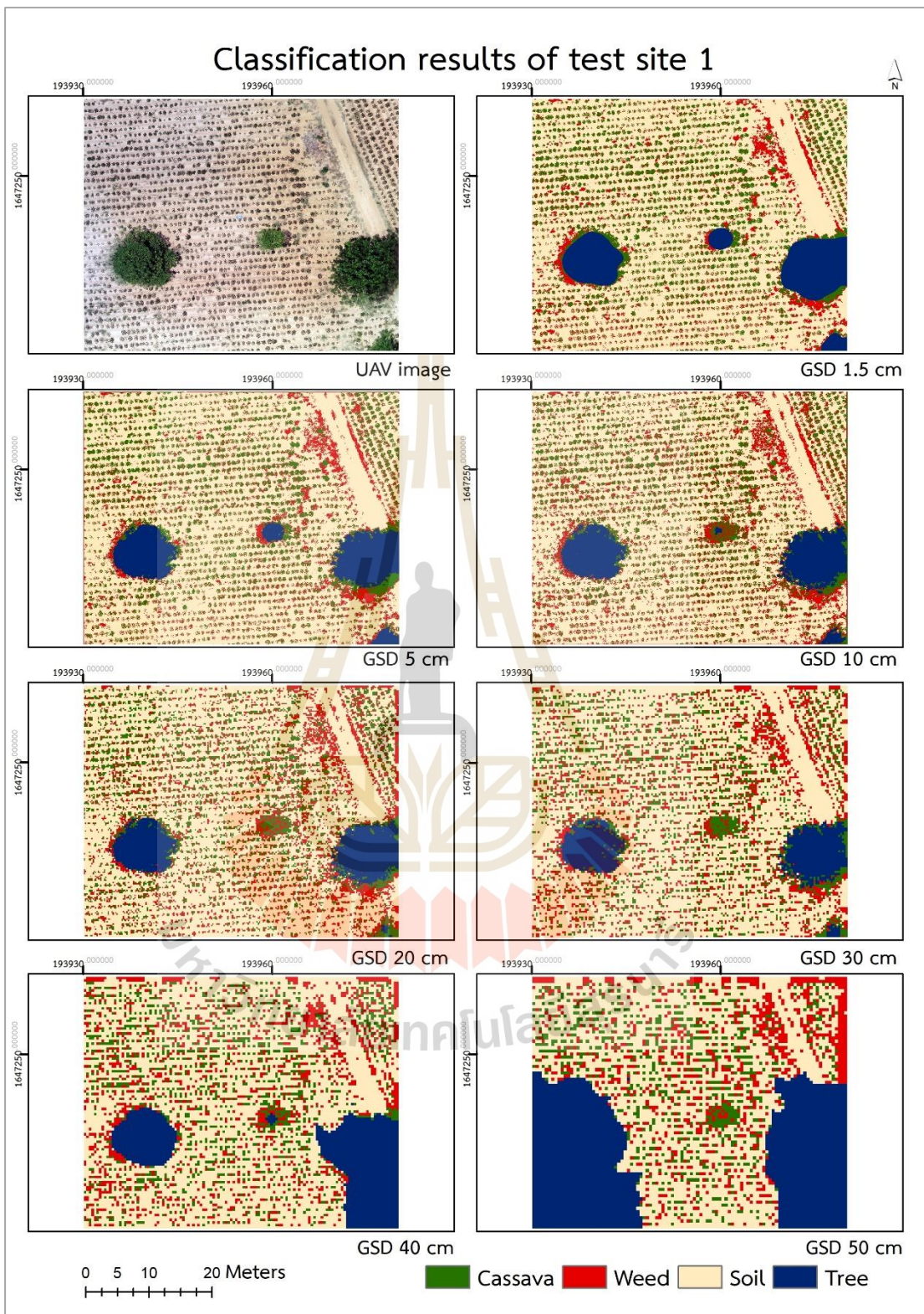


Figure B1 Classification results of test site 1.

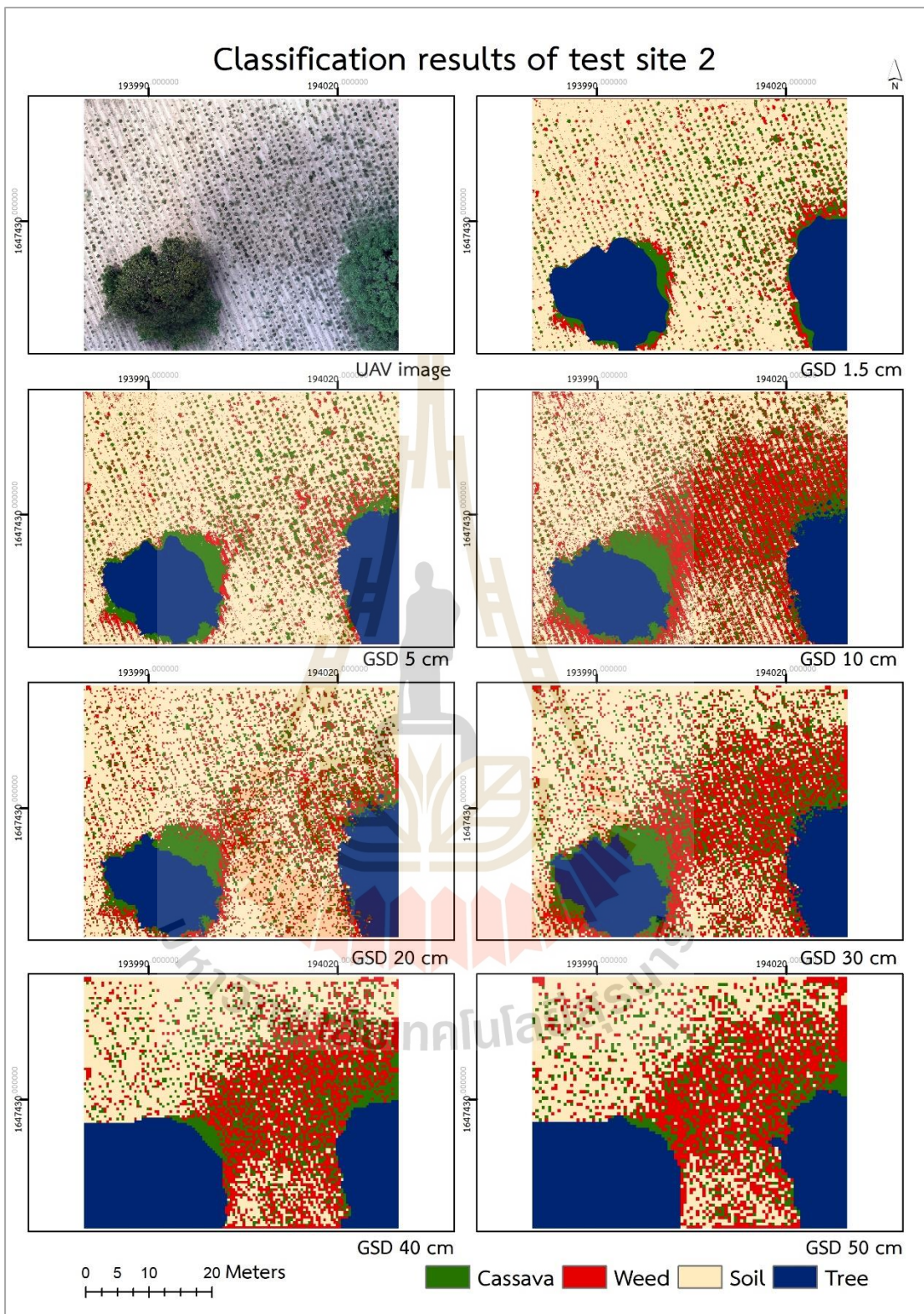


Figure B2 Classification results of test site 2.

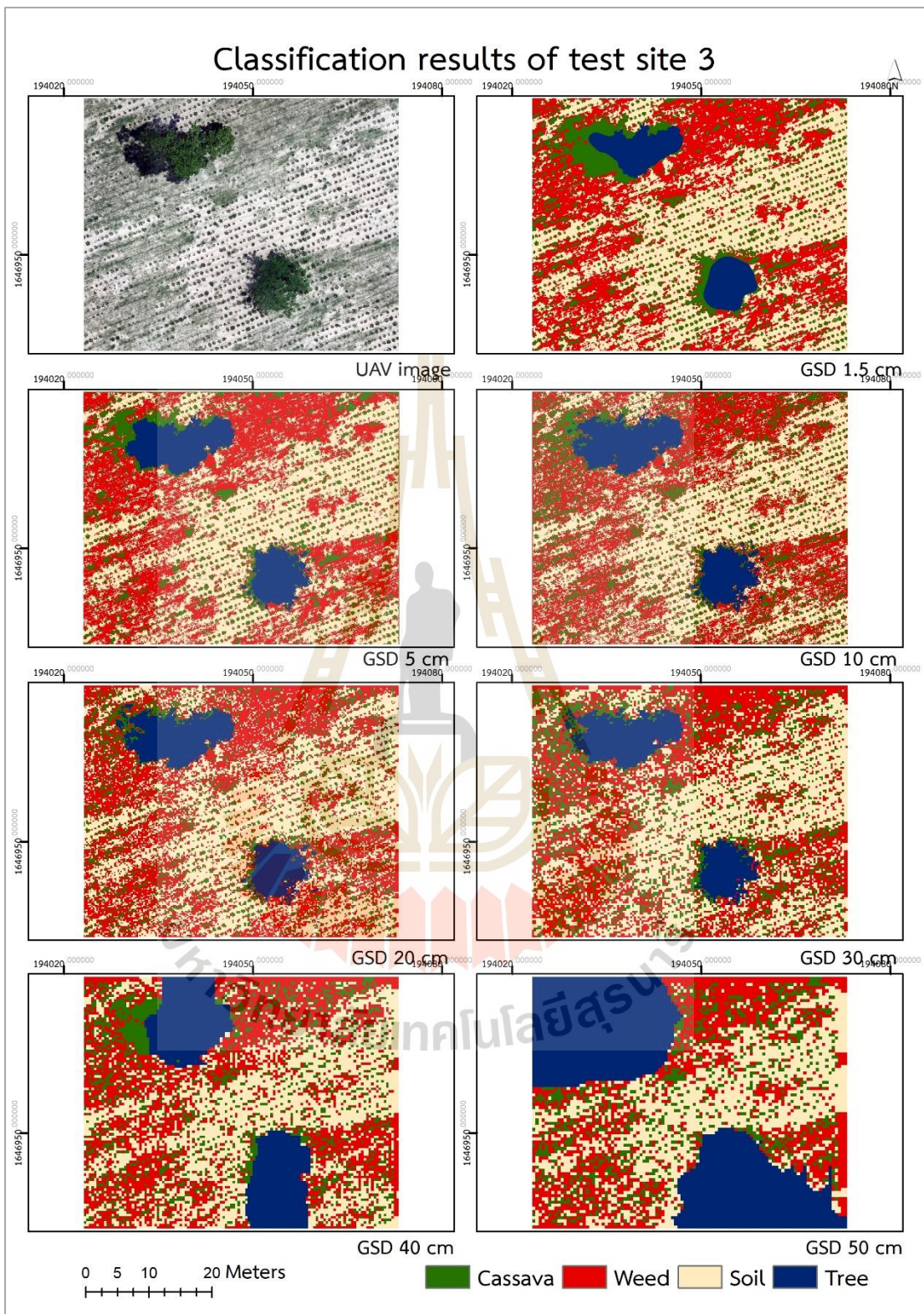


Figure B3 Classification results of test site 3.

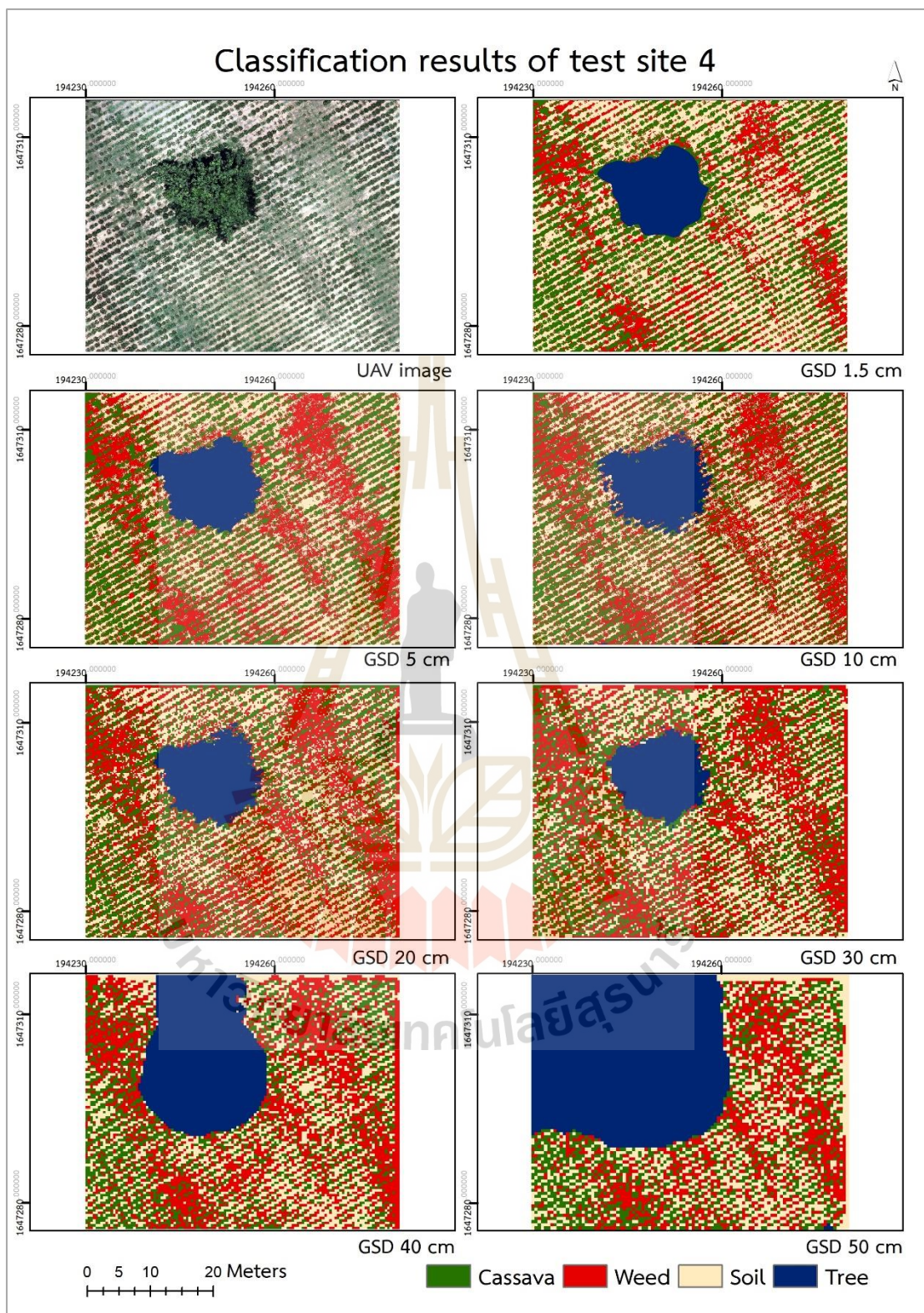


Figure B4 Classification results of test site 4.

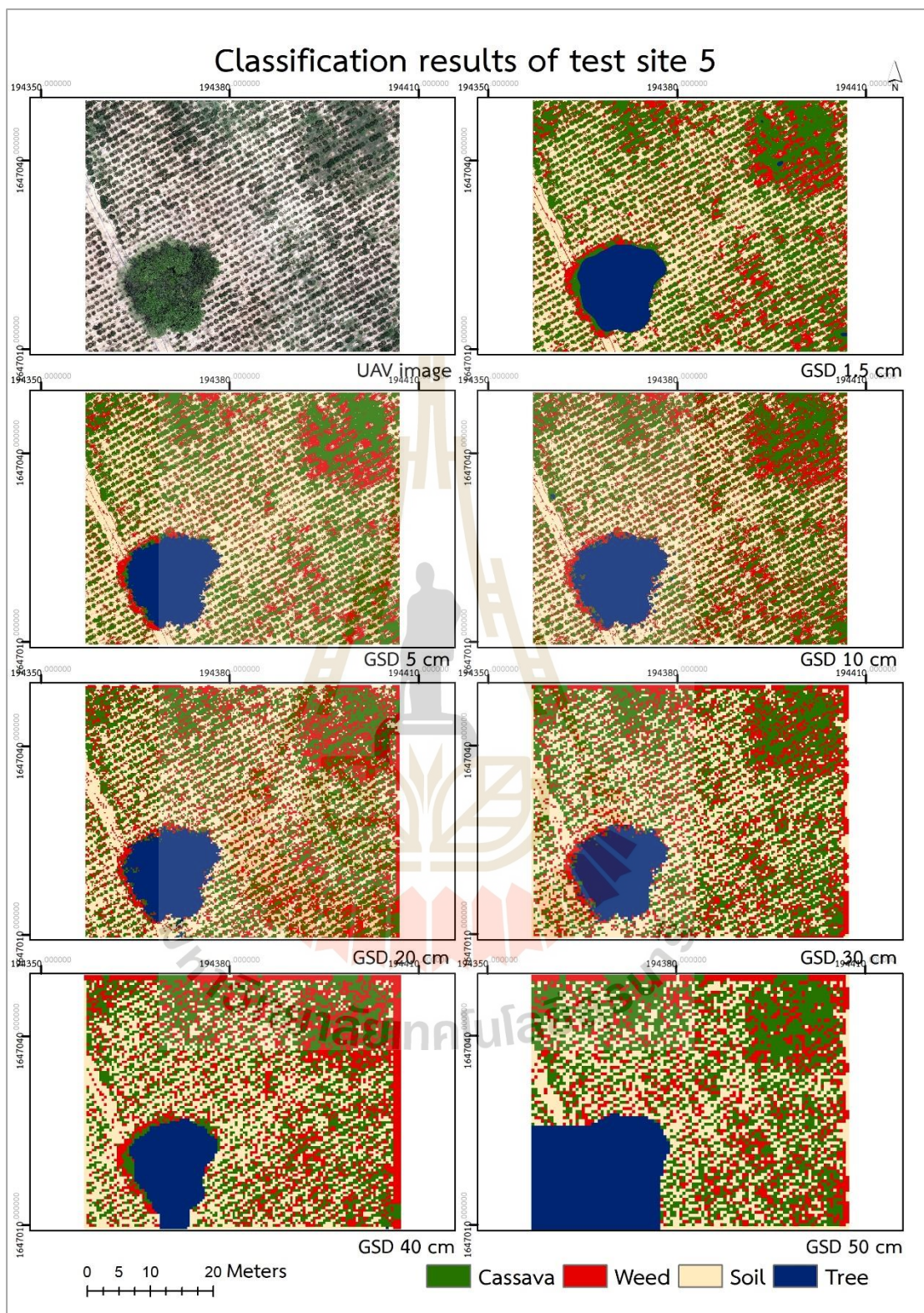


Figure B5 Classification results of test site 5.

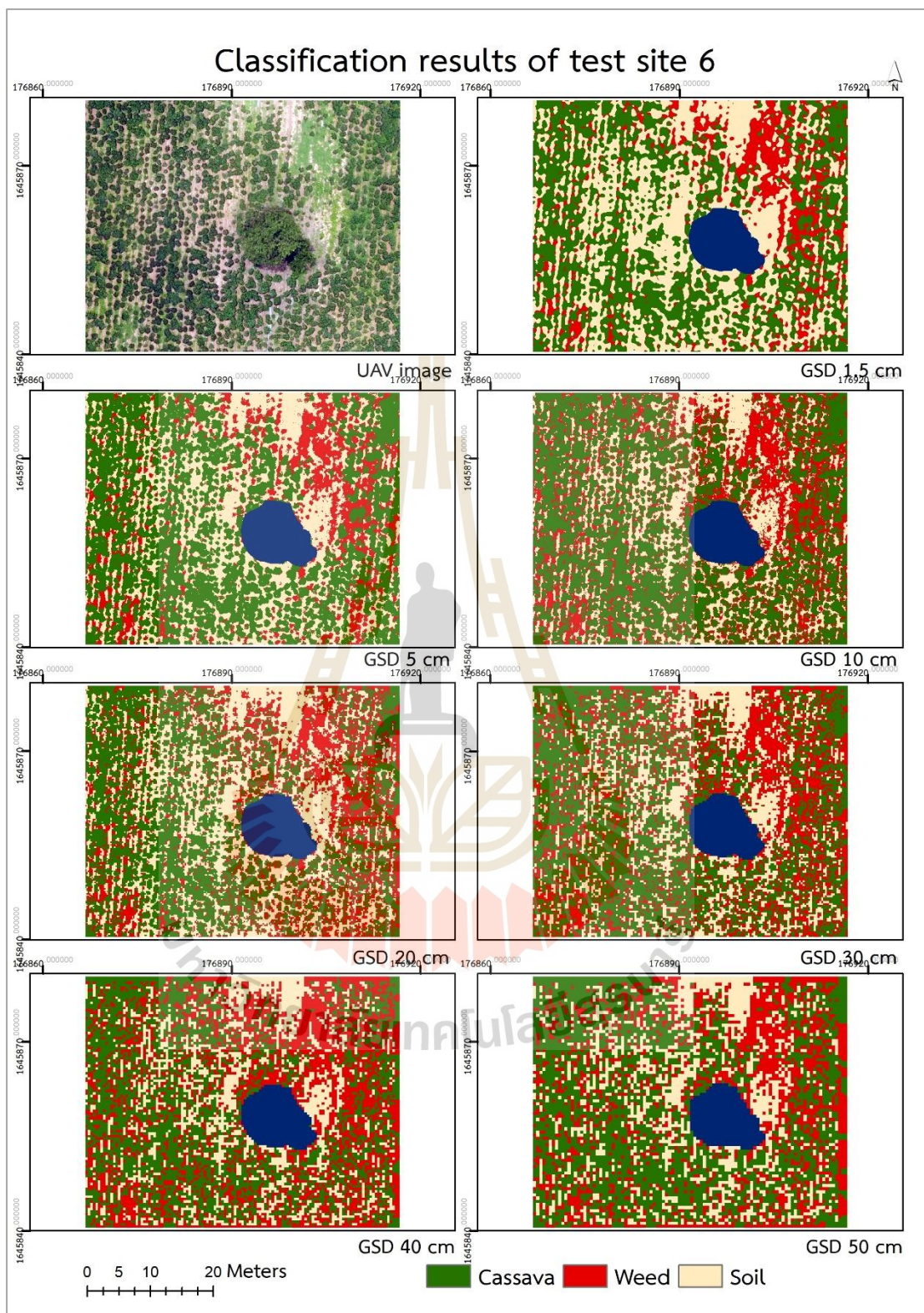


Figure B6 Classification results of test site 6.

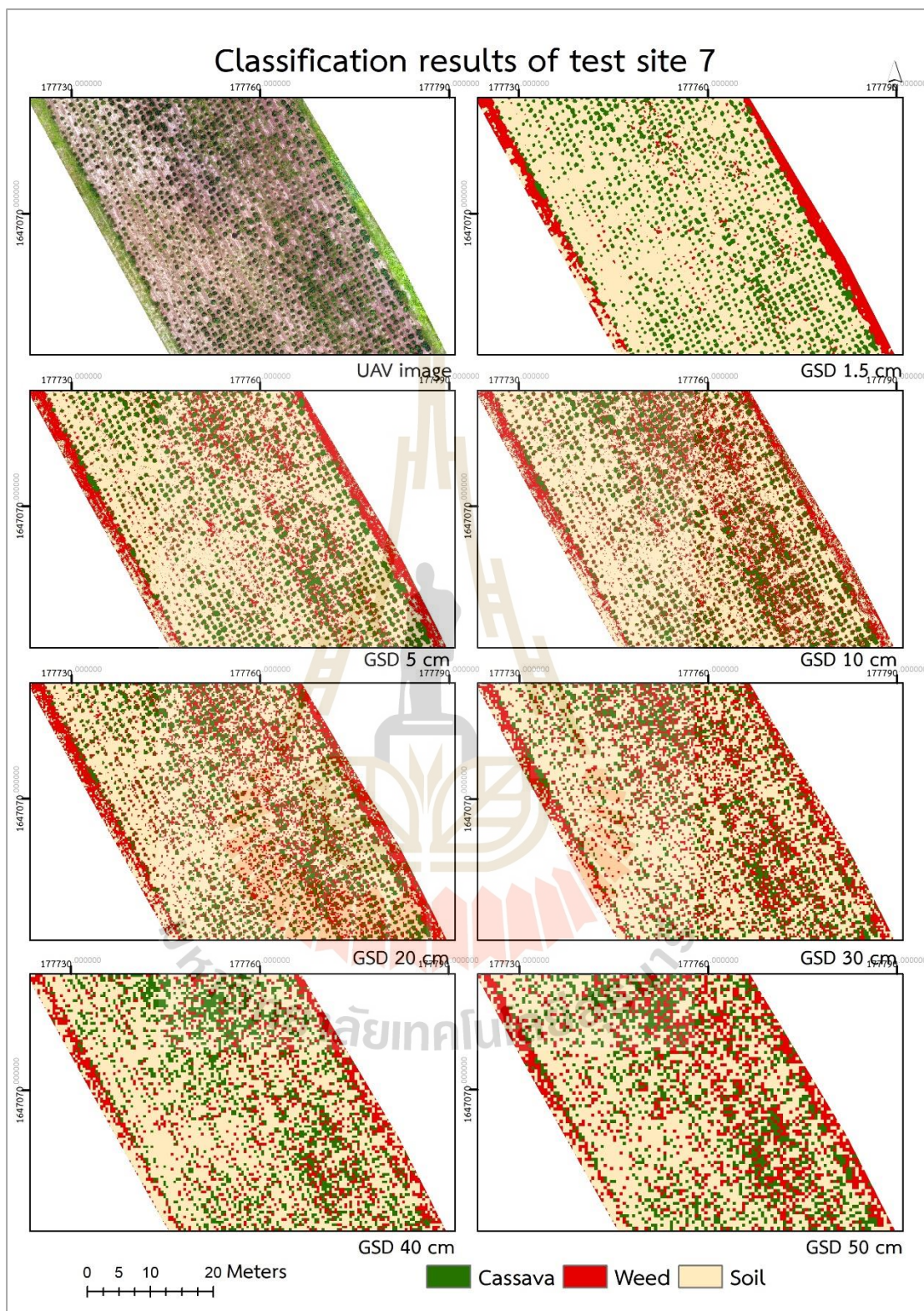


Figure B7 Classification results of test site 7.

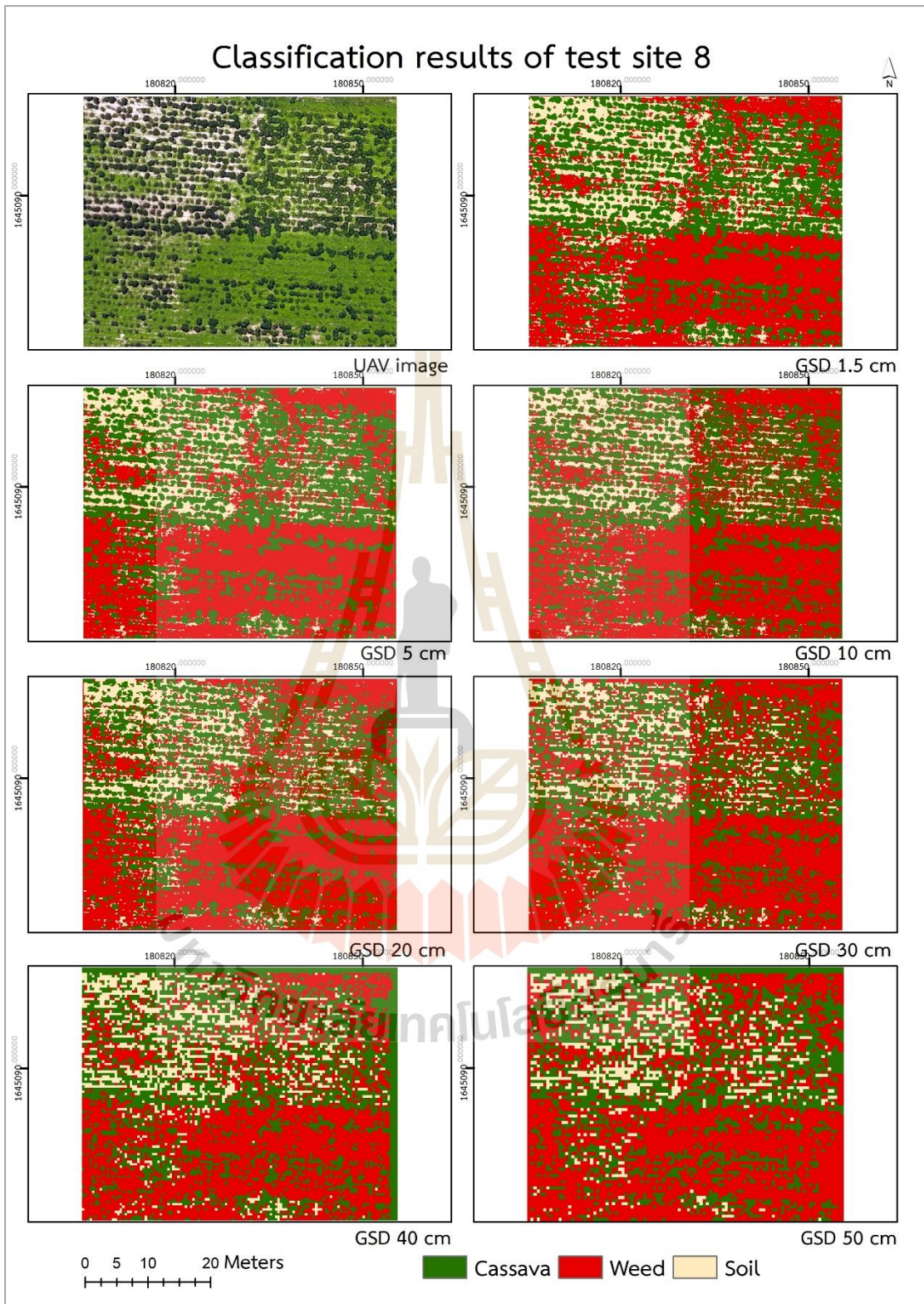
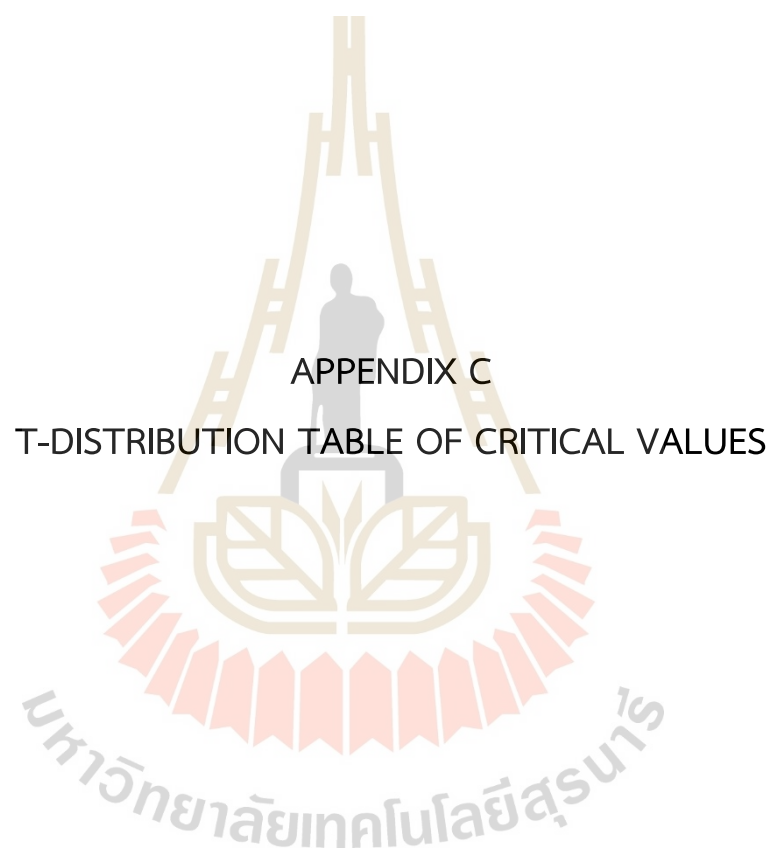


Figure B8 Classification results of test site 8

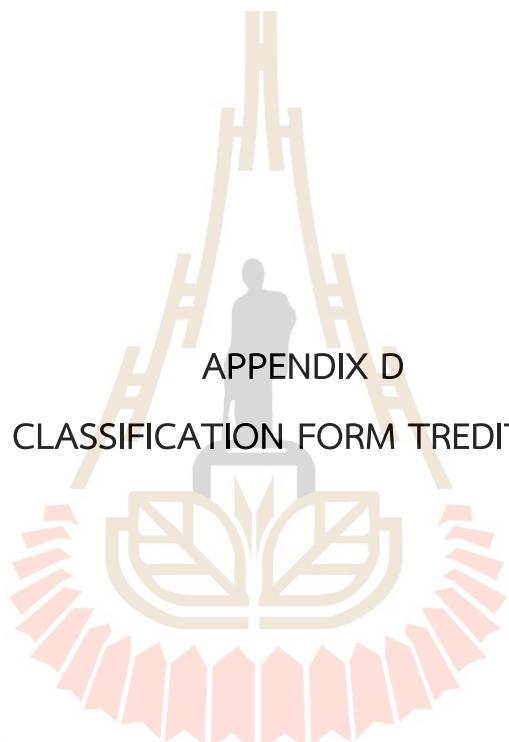


APPENDIX C

T-DISTRIBUTION TABLE OF CRITICAL VALUES

Table C1 Critical values (percentiles) for the t distribution.

One-tailed α	0.10	0.05	0.025	0.01	0.005	0.0005
Two-tailed α	0.20	0.10	0.05	0.02	0.01	0.001
df						
1	3.078	6.314	12.71	31.82	63.66	636.62
2	1.886	2.920	4.303	6.965	9.925	31.599
3	1.638	2.353	3.182	4.541	5.841	12.924
4	1.533	2.132	2.776	3.747	4.604	8.610
5	1.476	2.015	2.571	3.365	4.032	6.869
6	1.440	1.943	2.447	3.143	3.707	5.959
7	1.415	1.895	2.365	2.998	3.499	5.408
8	1.397	1.860	2.306	2.896	3.355	5.041
9	1.383	1.833	2.262	2.821	3.250	4.781
10	1.372	1.812	2.228	2.764	3.169	4.587
11	1.363	1.796	2.201	2.718	3.106	4.437
12	1.356	1.782	2.179	2.681	3.055	4.318
13	1.350	1.771	2.160	2.650	3.012	4.221
14	1.345	1.761	2.145	2.624	2.977	4.140
15	1.341	1.753	2.131	2.602	2.947	4.073



APPENDIX D
RESULTS OF CLASSIFICATION FORM TREDITIONAL METHODS

มหาวิทยาลัยเทคโนโลยีสุรนารี

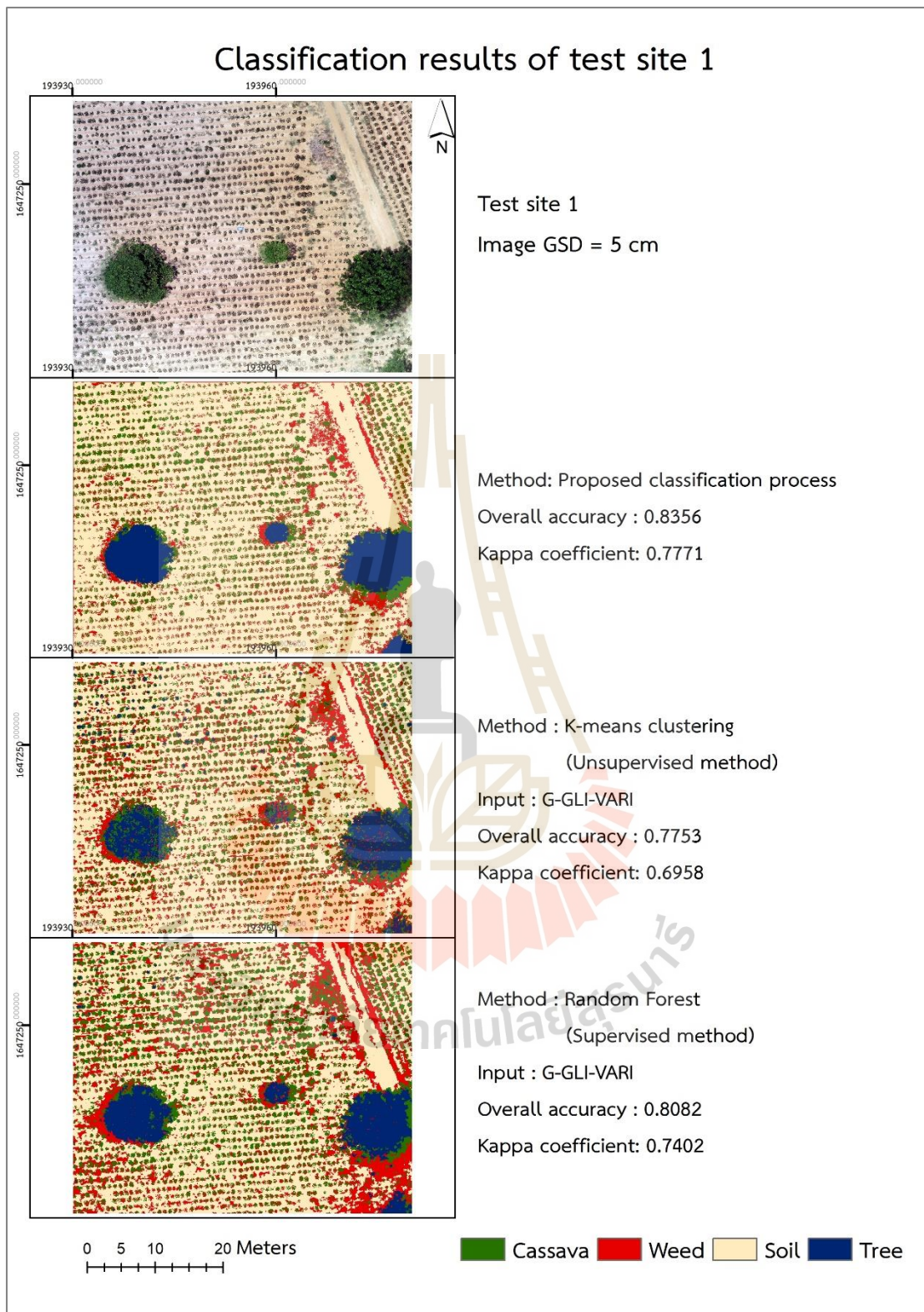


Figure D1 Classification results of test site 1.

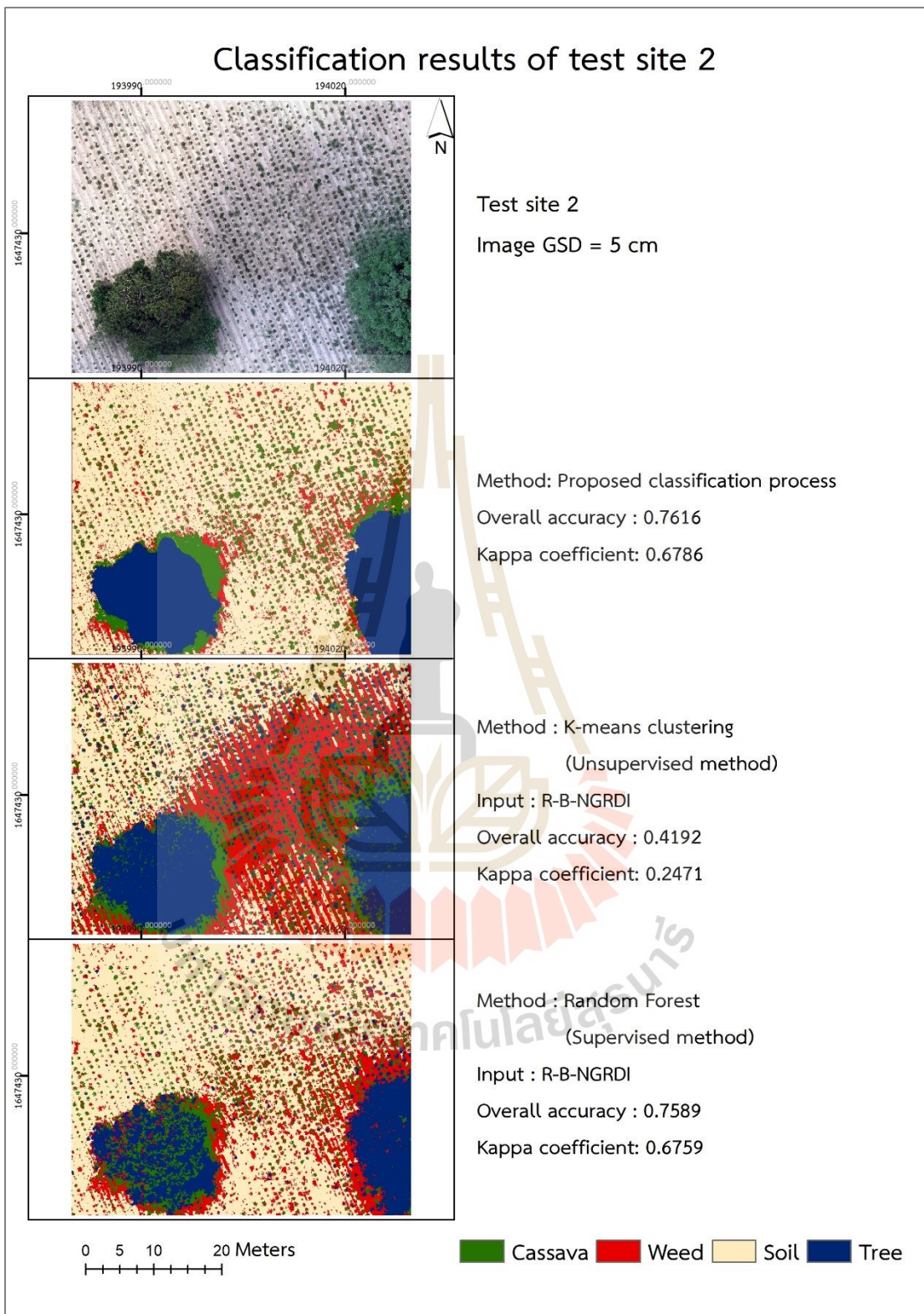


Figure D2 Classification results of test site 2.

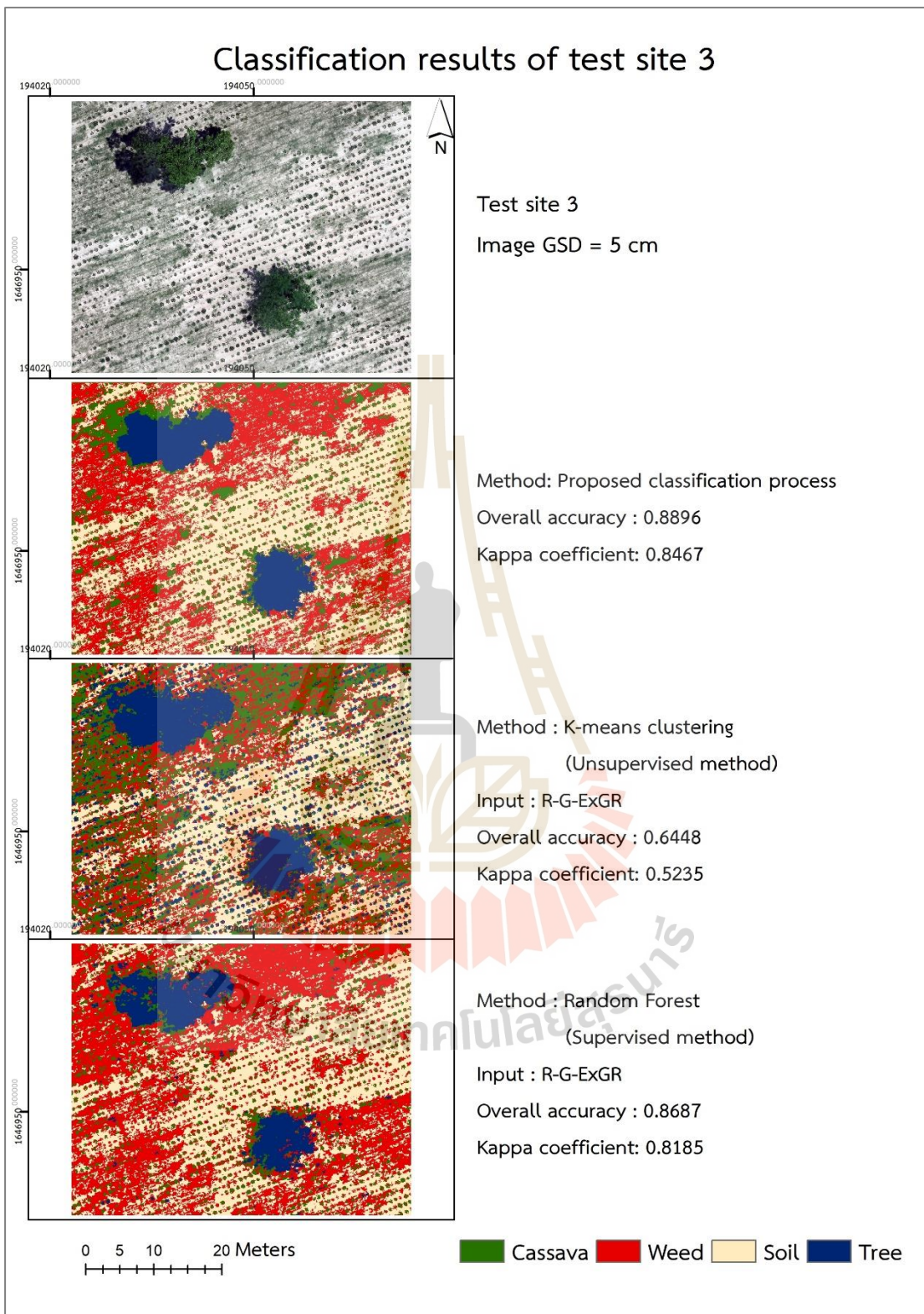


Figure D3 Classification results of test site 3.

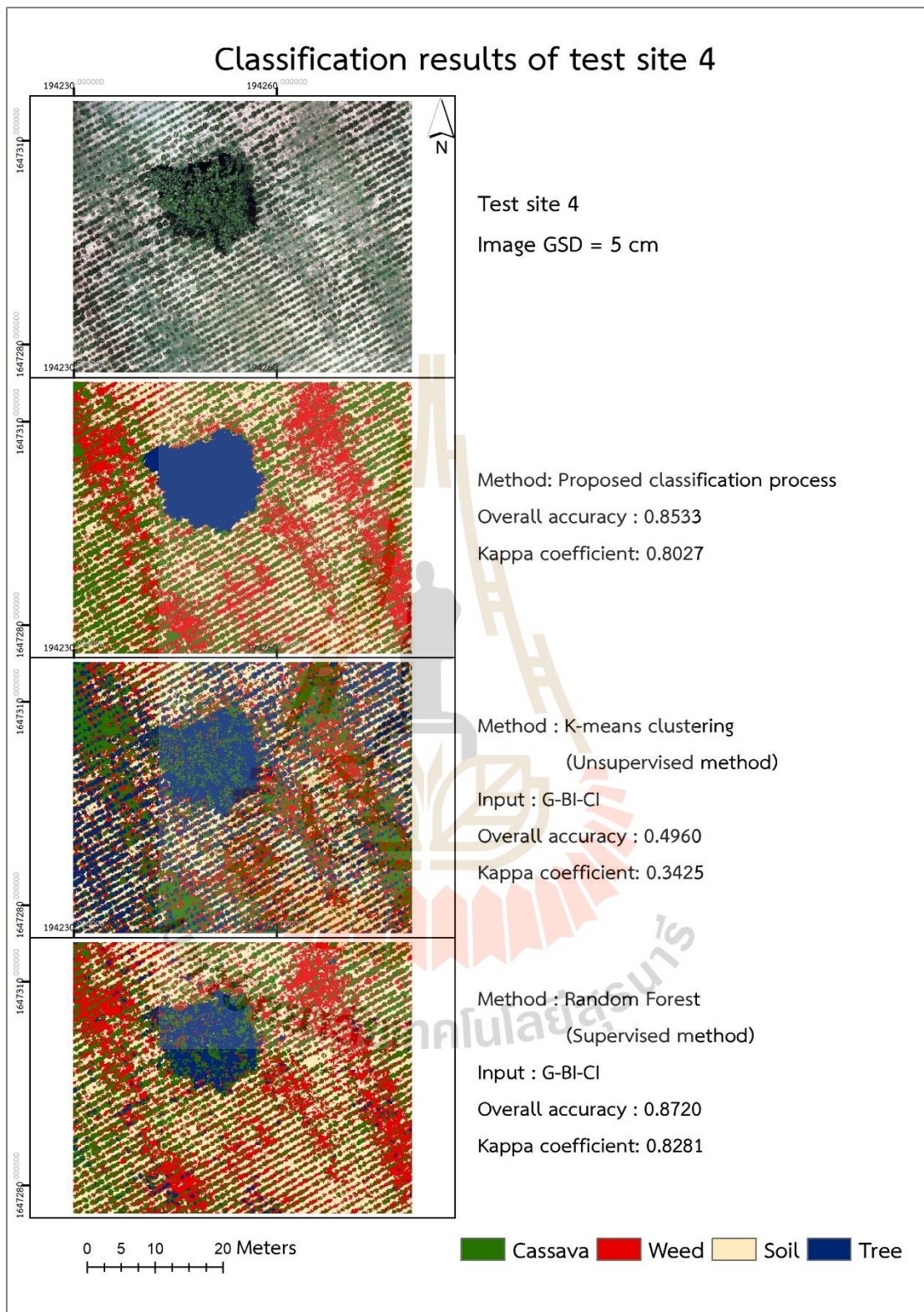


Figure D4 Classification results of test site 4.

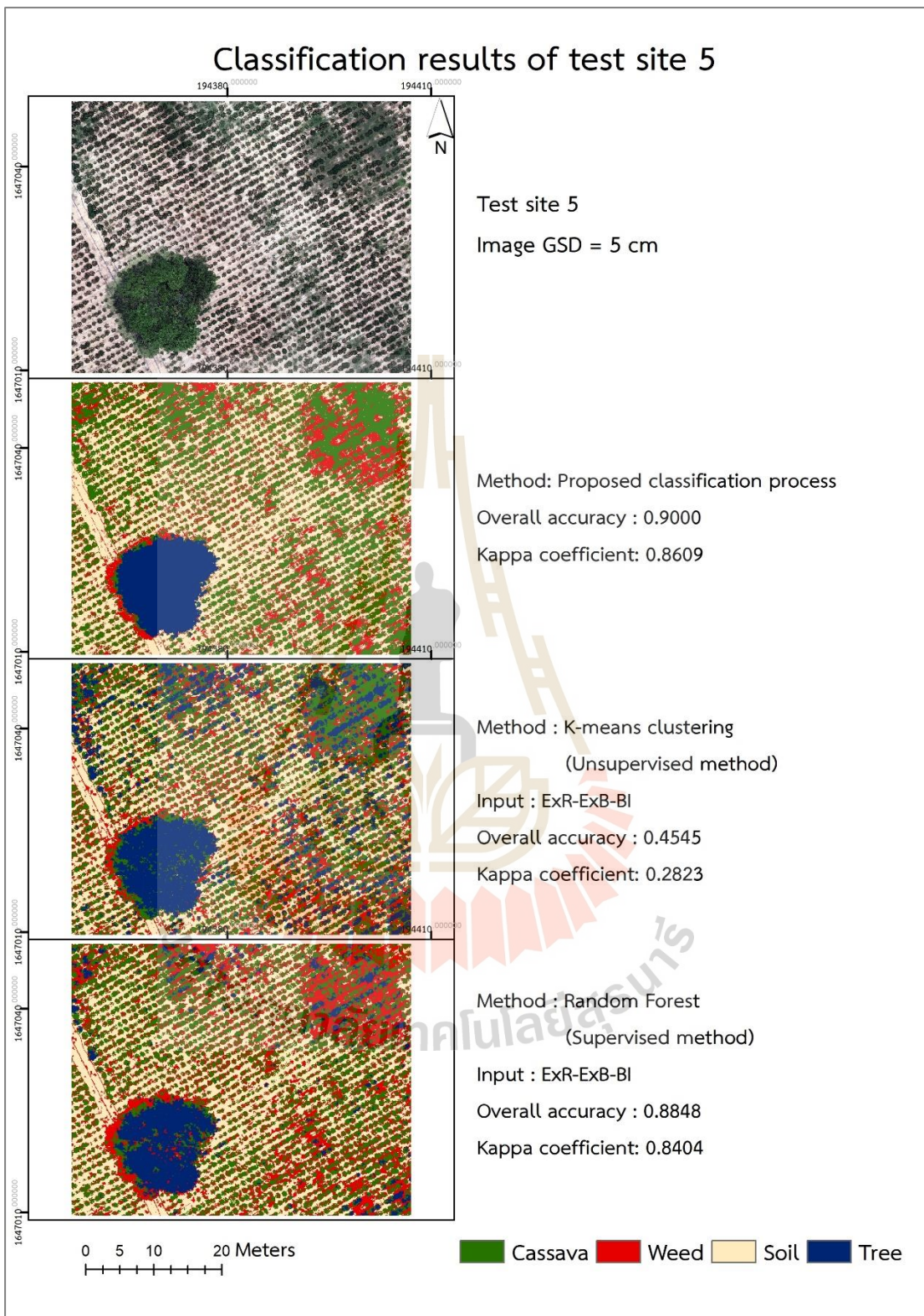


Figure D5 Classification results of test site 5.

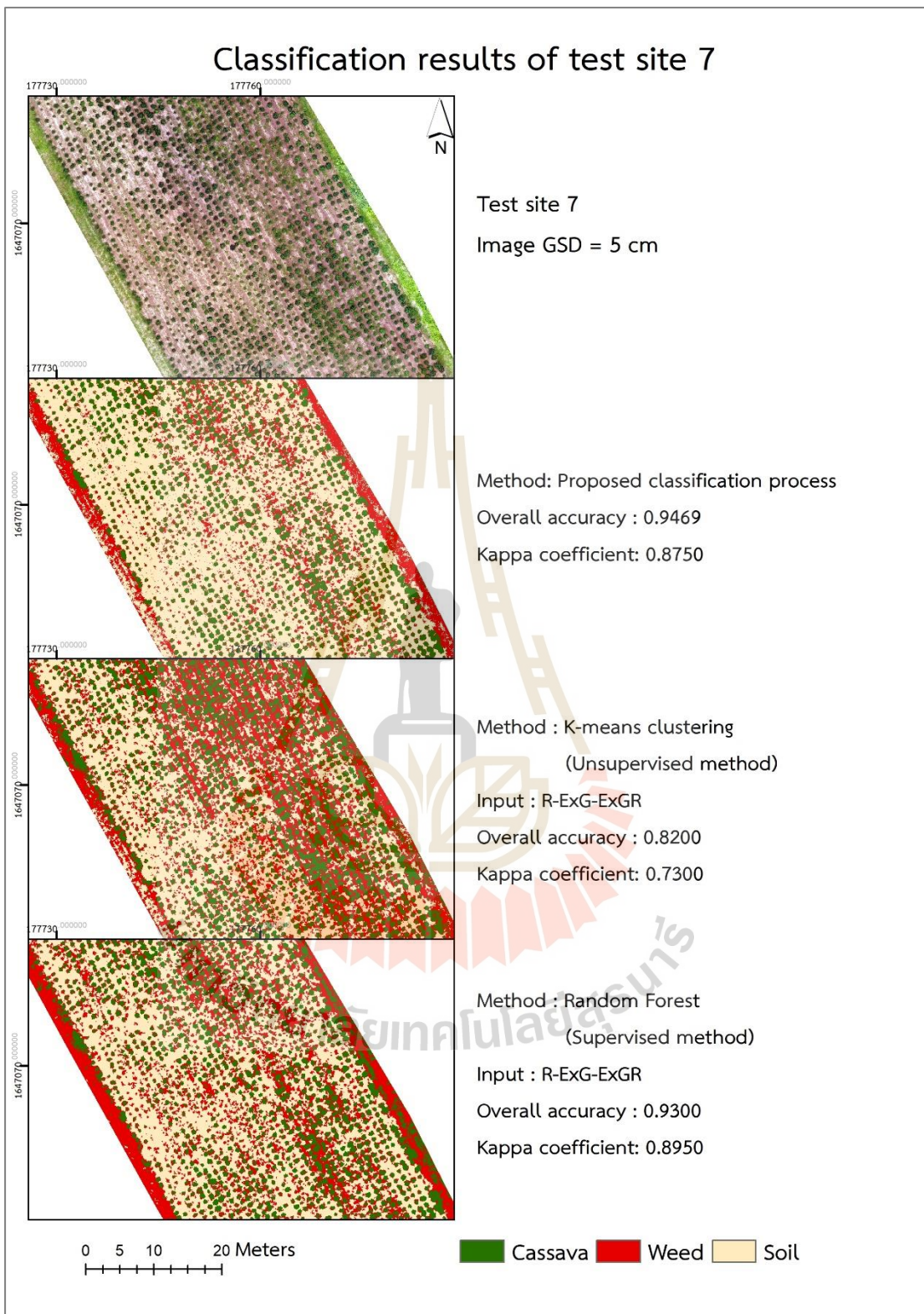


Figure D6 Classification results of test site 7.

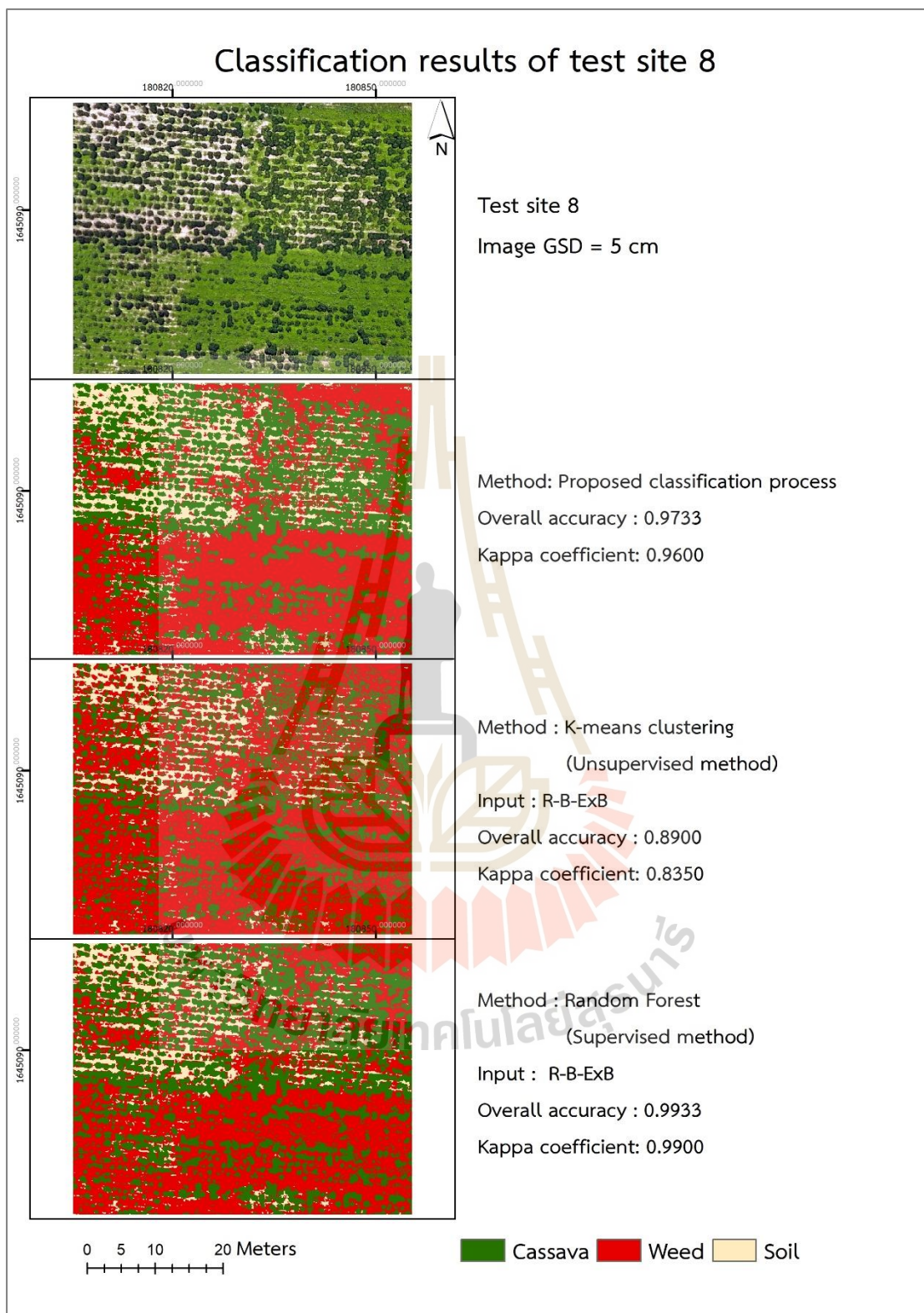


Figure D7 Classification results of test site 8

APPENDIX E
CLASSIFICATION RESULTS OF APPLYING PROPOSED
CLASSIFICATION PROCESS TO STUDY AREAS

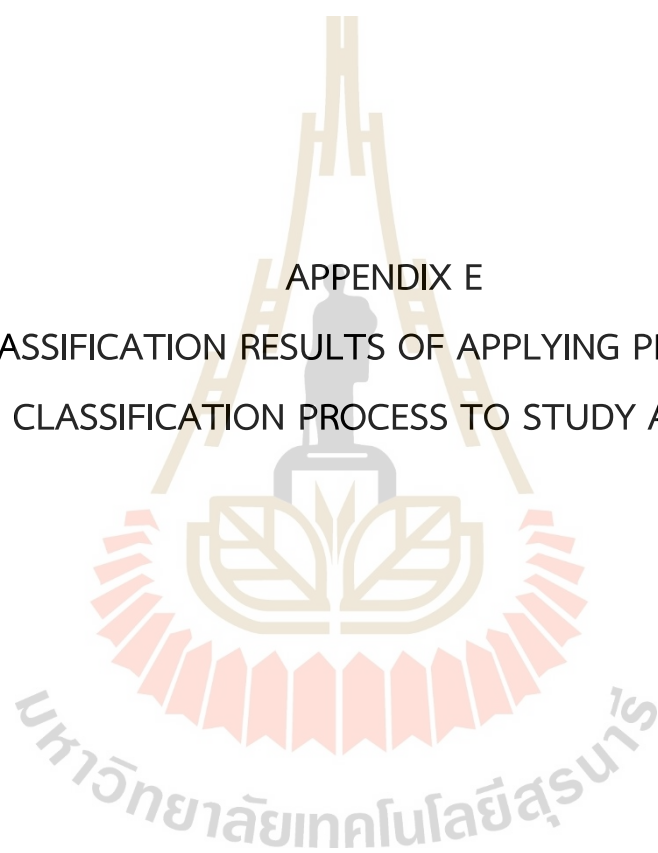


Table E1 Confusion matrix of classification result from process the entire area of plot 1.

Class		Reference				Total
		Cassava	Weed	Soil	Tree	
Classification	Cassava	91	5	0	3	99
	Weed	41	65	1	3	110
	Soil	35	46	196	0	277
	Tree	0	0	0	43	43
Total		167	116	197	49	529
PA		0.5449	0.5603	0.9949	0.8776	
UA		0.9192	0.5909	0.7076	1.0000	
OA		0.7467				
Kappa coefficient		0.6344				

Table E2 Confusion matrix of classification result from process two pieces of plot 1.

Class		Reference				Total
		Cassava	Weed	Soil	Tree	
Classification	Cassava	90	5	0	3	98
	Weed	41	65	0	4	110
	Soil	36	46	197	0	279
	Tree	0	0	0	42	42
Total		167	116	197	49	529
PA		0.5389	0.5603	1.0000	0.8571	
UA		0.9184	0.5909	0.7061	1.0000	
OA		0.7448				
Kappa		0.6313				

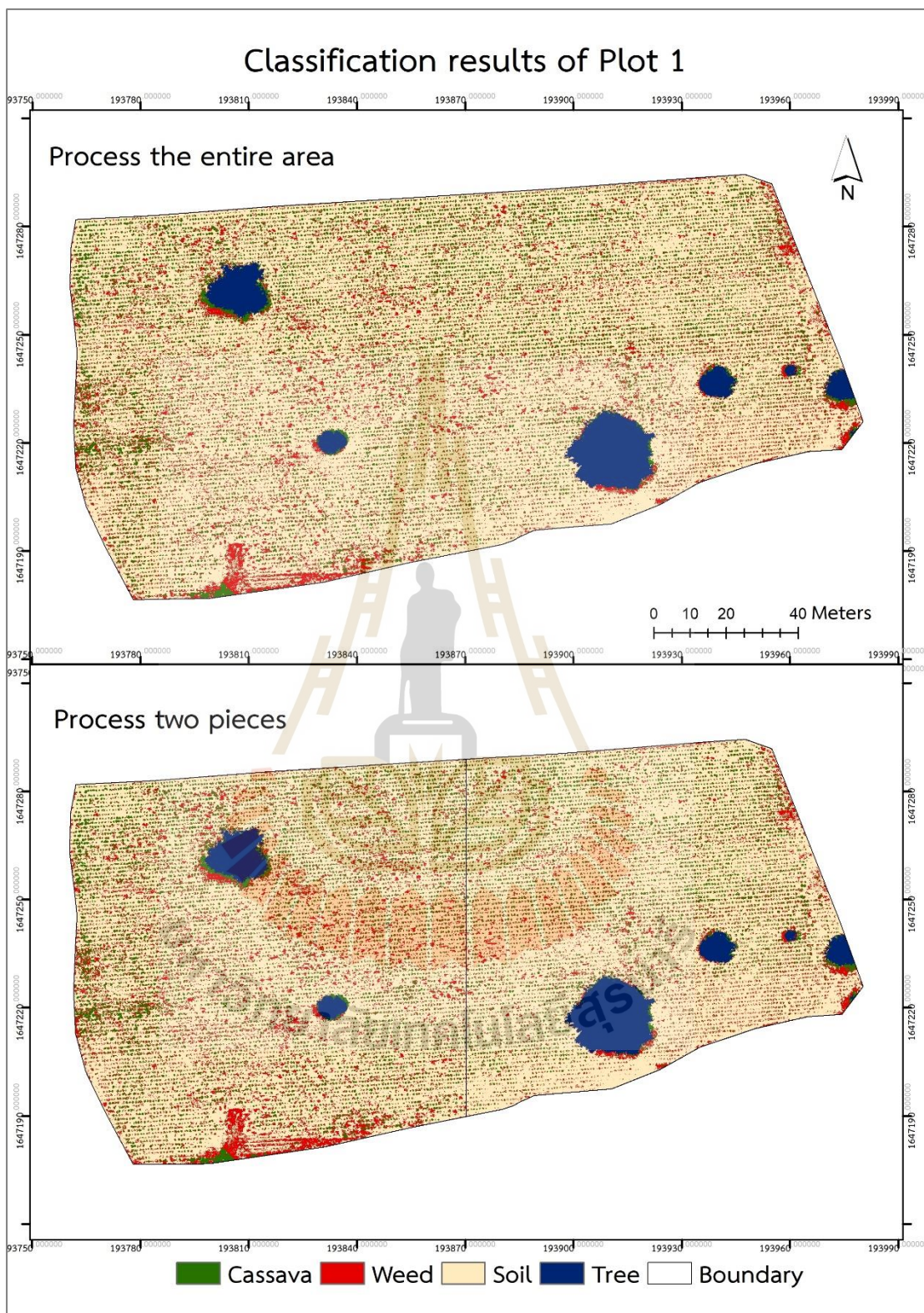


Figure E1 Classification results of plot 1.

Table E3 Confusion matrix of classification result from process the entire area of plot 2.

Class		Reference				Total
		Cassava	Weed	Soil	Tree	
Classification	Cassava	116	27	1	7	151
	Weed	28	84	3	3	118
	Soil	27	26	232	0	285
	Tree	0	1	0	45	46
Total		171	138	236	55	600
PA		0.6784	0.6087	0.9831	0.8182	
UA		0.7682	0.7119	0.8140	0.9783	
OA		0.7950				
Kappa		0.7025				

Table E4 Confusion matrix of classification result from process two pieces of plot 2.

Class		Reference				Total
		Cassava	Weed	Soil	Tree	
Classification	Cassava	106	27	0	7	140
	Weed	30	84	2	3	119
	Soil	35	26	234	0	295
	Tree	0	1	0	45	46
Total		171	138	236	55	600
PA		0.6199	0.6087	0.9915	0.8182	
UA		0.7571	0.7059	0.7932	0.9783	
OA		0.7817				
Kappa		0.6824				

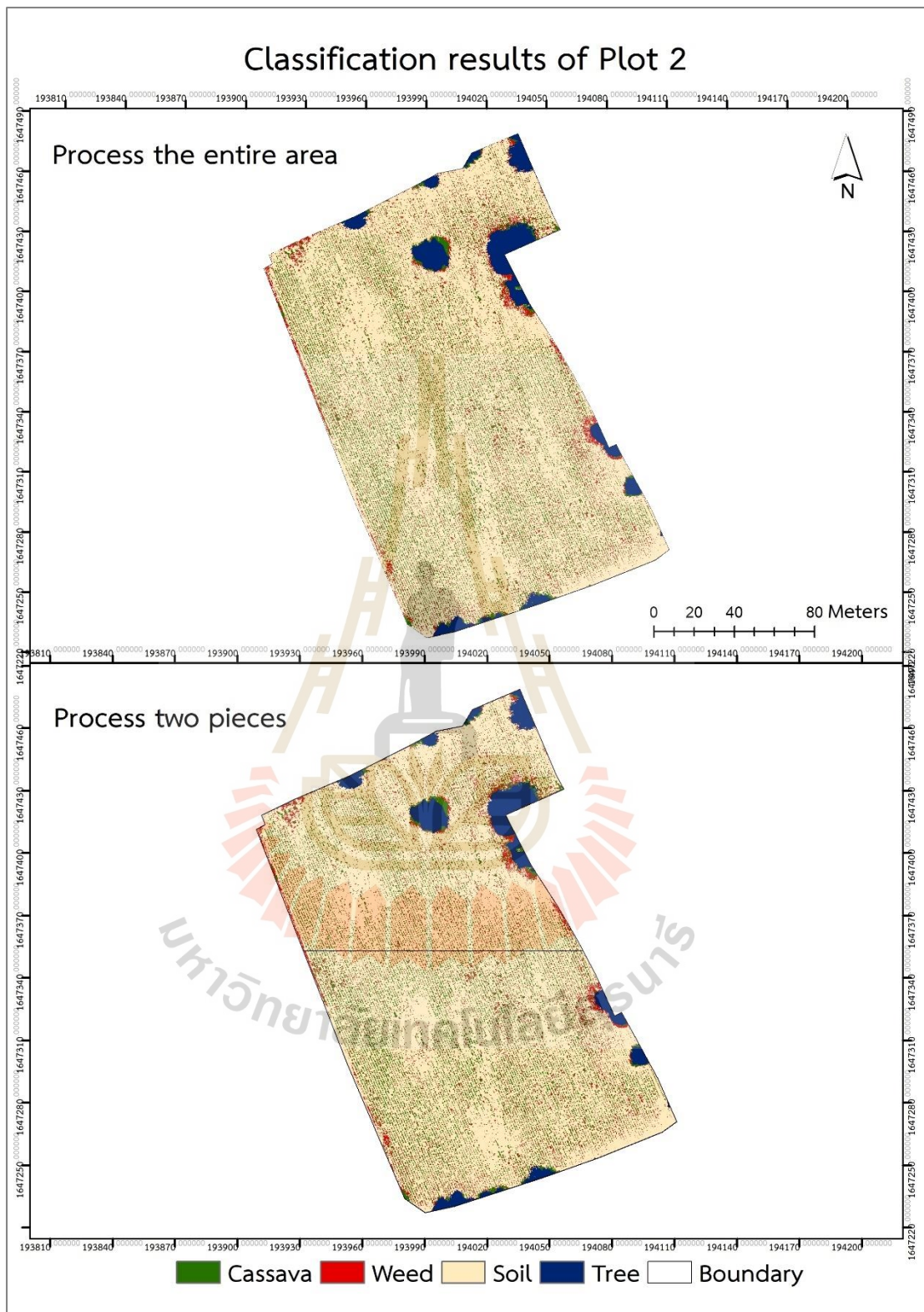


Figure E2 Classification results of plot 2.

Table E5 Confusion matrix of classification result from process the entire area of plot 3.

Class		Reference				Total
		Cassava	Weed	Soil	Tree	
Classification	Cassava	289	49	0	11	349
	Weed	41	205	1	0	247
	Soil	15	90	401	1	507
	Tree	0	1	0	68	69
Total		345	345	402	80	1172
PA		0.8377	0.5942	0.9975	0.8500	
UA		0.8281	0.8300	0.7909	0.9855	
OA		0.8217				
Kappa		0.7445				

Table E6 Confusion matrix of classification result from process two pieces of plot 3.

Class		Reference				Total
		Cassava	Weed	Soil	Tree	
Classification	Cassava	286	52	0	11	349
	Weed	42	199	0	0	241
	Soil	16	93	402	1	512
	Tree	1	1	0	68	70
Total		345	345	402	80	1172
PA		0.8290	0.5768	1.0000	0.8500	
UA		0.8195	0.8257	0.7852	0.9714	
OA		0.8148				
Kappa		0.7347				

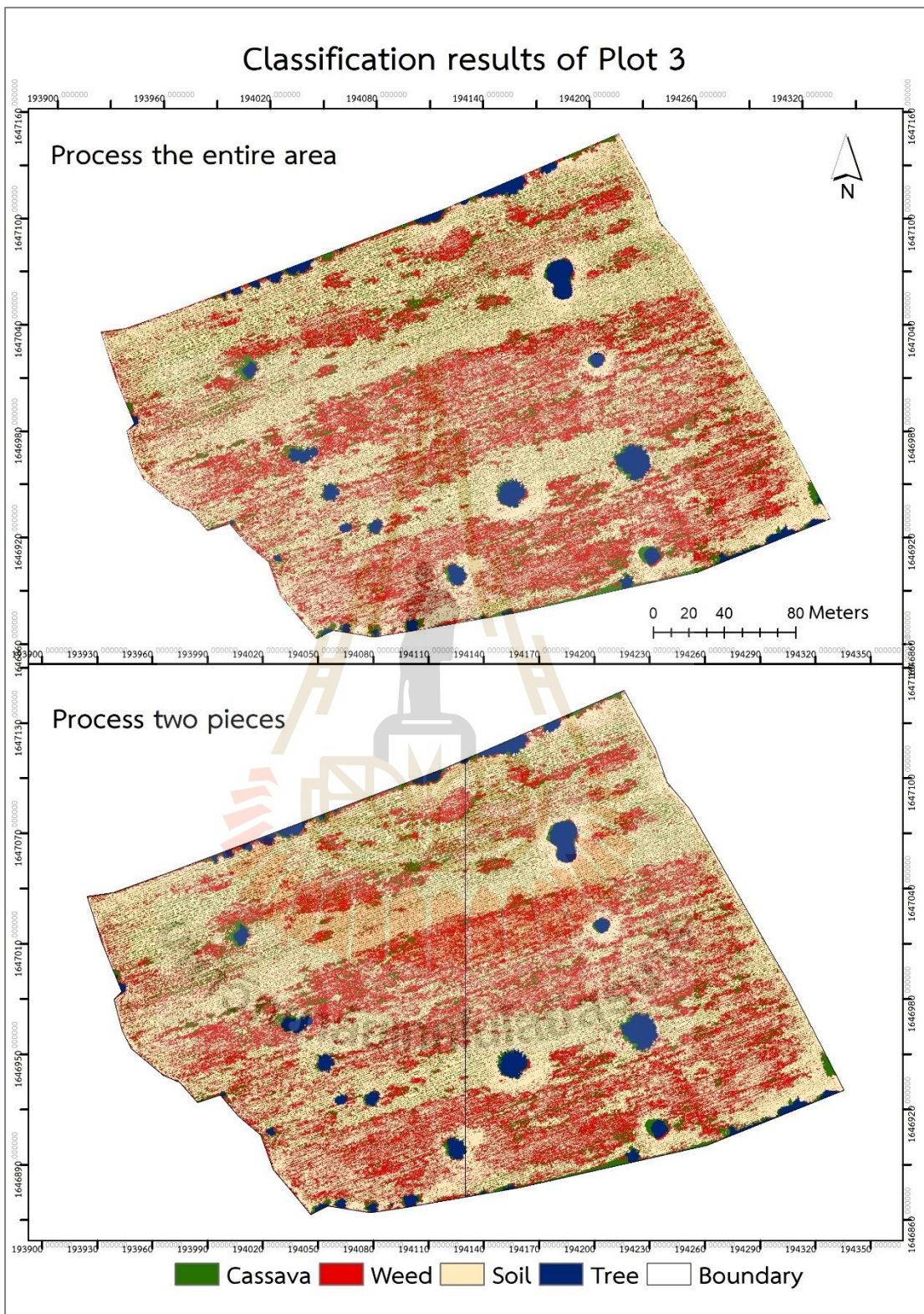


Figure E3 Classification results of plot 3.

Table E7 Confusion matrix of classification result from process the entire area of plot 4.

Class		Reference			Total
		Cassava	Weed	Soil	
Classification	Cassava	384	9	0	393
	Weed	62	377	2	441
	Soil	2	62	446	510
Total		448	448	448	1344
PA		0.8571	0.8415	0.9955	
UA		0.9771	0.8549	0.8745	
OA		0.8981			
Kappa		0.8471			

Table E8 Confusion matrix of classification result from process two pieces of plot 4.

Class		Reference			Total
		Cassava	Weed	Soil	
Classification	Cassava	384	9	0	393
	Weed	59	371	2	432
	Soil	5	68	446	519
Total		448	448	448	1344
PA		0.8571	0.8281	0.9955	
UA		0.9771	0.8588	0.8593	
OA		0.8936			
Kappa		0.8404			

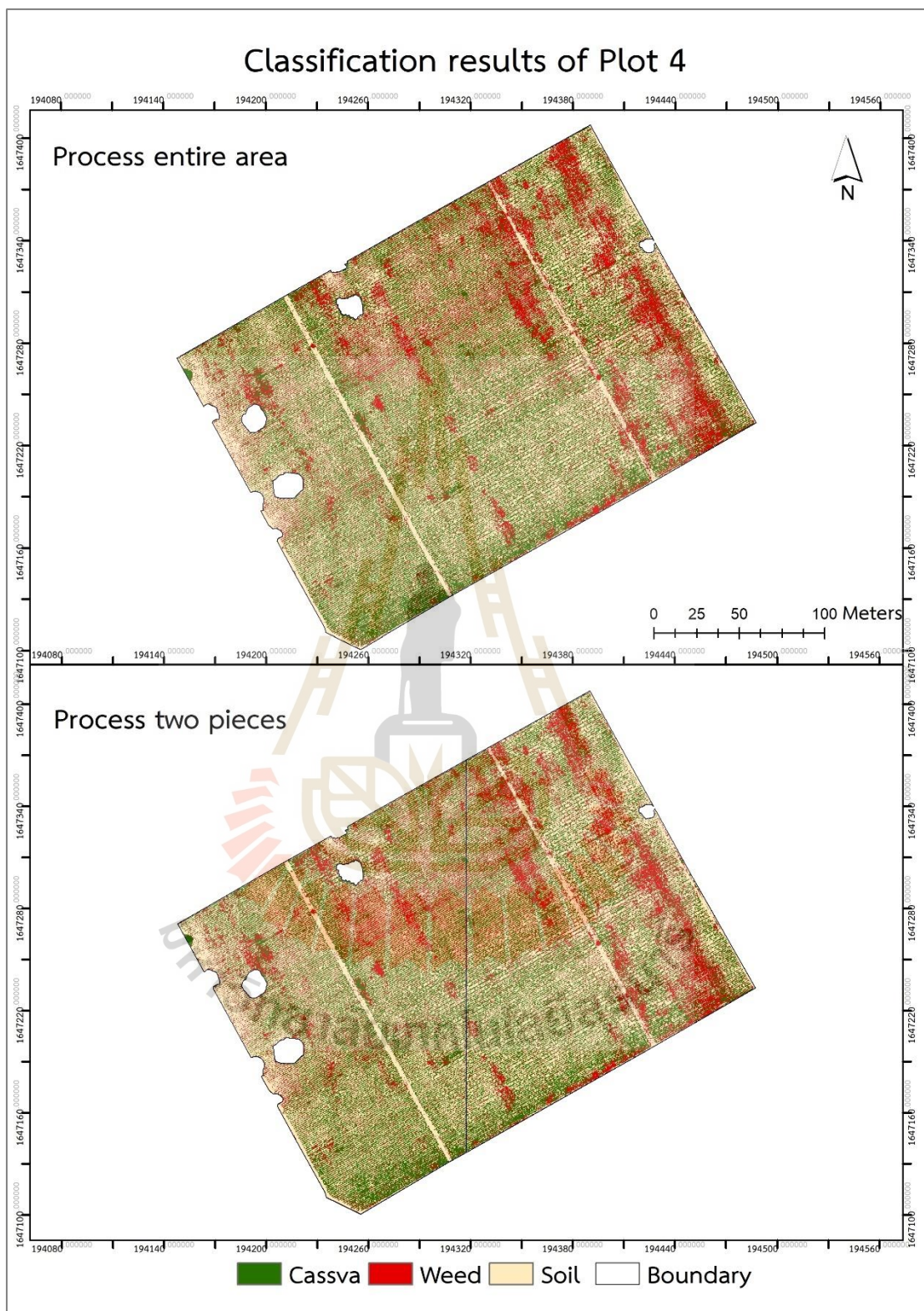


Figure E4 Classification results of plot 4.

Table E9 Confusion matrix of classification result from process the entire area of plot 5.

Class		Reference			Total
		Cassava	Weed	Soil	
Classification	Cassava	303	79	0	382
	Weed	54	255	0	309
	Soil	7	30	364	401
Total		364	364	364	1092
PA		0.8324	0.7005	1.0000	
UA		0.7932	0.8252	0.9077	
OA		0.8443			
Kappa		0.7665			

Table E10 Confusion matrix of classification result from process two pieces of plot 5.

Class		Reference			Total
		Cassava	Weed	Soil	
Classification	Cassava	298	78	0	376
	Weed	60	257	0	317
	Soil	6	29	364	399
Total		364	364	364	1092
PA		0.8187	0.7060	1.0000	
UA		0.7926	0.8107	0.9123	
OA		0.8416			
Kappa		0.7624			

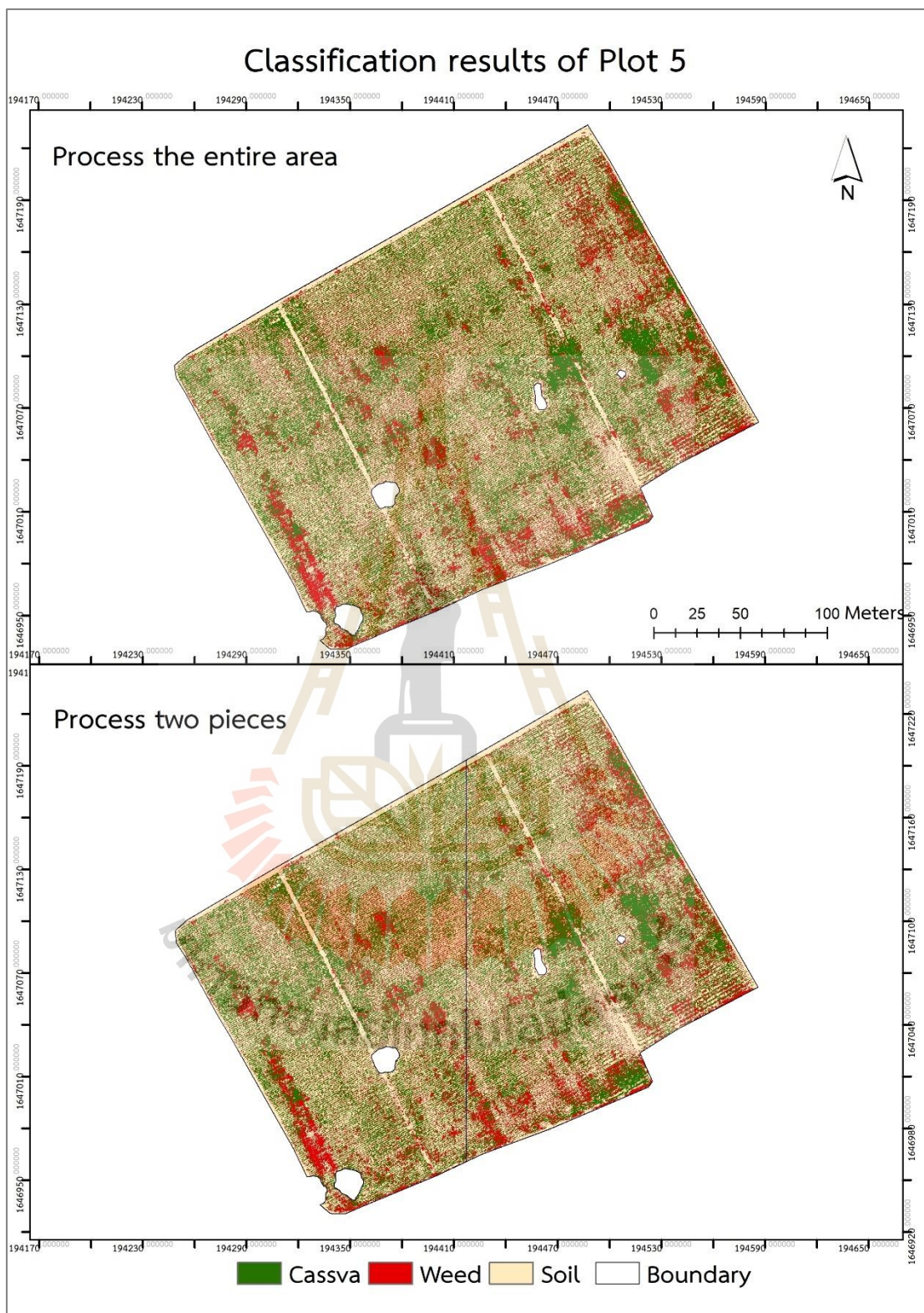


Figure E5 Classification results of plot 5.

Table E11 Confusion matrix of classification result from process the entire area of plot 6.

Class		Reference			Total
		Cassava	Weed	Soil	
Classification	Cassava	30	19	0	49
	Weed	51	42	0	93
	Soil	0	3	55	58
Total		81	64	55	200
PA		0.3704	0.6563	1.0000	
UA		0.6122	0.4516	0.9483	
OA		0.6350			
Kappa		0.4570			

Table E12 Confusion matrix of classification result from process two pieces of plot 6.

Class		Reference			Total
		Cassava	Weed	Soil	
Classification	Cassava	30	20	0	50
	Weed	50	41	0	91
	Soil	1	3	55	59
Total		81	64	55	200
PA		0.3704	0.6406	1.0000	
UA		0.6000	0.4505	0.9322	
OA		0.6300			
Kappa		0.4494			

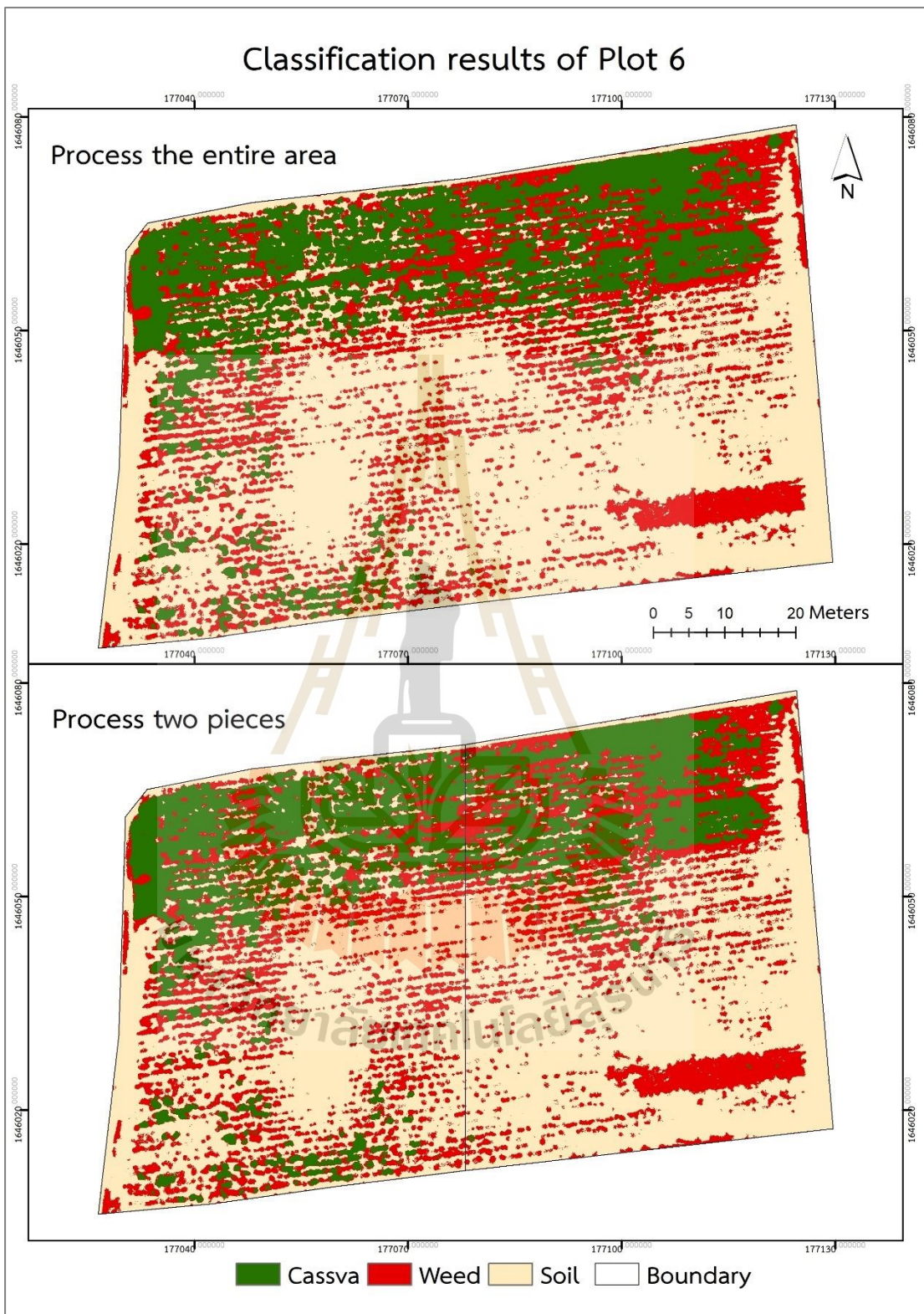


Figure E6 Classification results of plot 6.

Table E13 Confusion matrix of classification result from process the entire area of plot 7.

Class		Reference			Total
		Cassava	Weed	Soil	
Classification	Cassava	30	7	0	37
	Weed	10	31	0	41
	Soil	0	2	40	42
Total		40	40	40	120
PA		0.7500	0.7750	1.0000	
UA		0.8108	0.7561	0.9524	
OA		0.8417			
Kappa		0.7625			

Table E14 Confusion matrix of classification result from process two pieces of plot 7.

Class		Reference			Total
		Cassava	Weed	Soil	
Classification	Cassava	32	9	0	41
	Weed	8	29	0	37
	Soil	0	2	40	42
Total		40	40	40	120
PA		0.8000	0.7250	1.0000	
UA		0.7805	0.7838	0.9524	
OA		0.8417			
Kappa		0.7625			

Table E15 Confusion matrix of classification result from process the entire area of plot 8.

Class		Reference			Total
		Cassava	Weed	Soil	
Classification	Cassava	135	27	0	162
	Weed	94	191	0	285
	Soil	2	13	231	246
Total		231	231	231	693
PA		0.5844	0.8268	1.0000	
UA		0.8333	0.6702	0.9390	
OA		0.8038			
Kappa		0.7056			

Table E16 Confusion matrix of classification result from process two pieces of plot 8.

Class		Reference			Total
		Cassava	Weed	Soil	
Classification	Cassava	194	20	0	214
	Weed	36	197	0	233
	Soil	1	14	231	246
Total		231	231	231	693
PA		0.8398	0.8528	1.0000	
UA		0.9065	0.8455	0.9390	
OA		0.8975			
Kappa		0.8463			

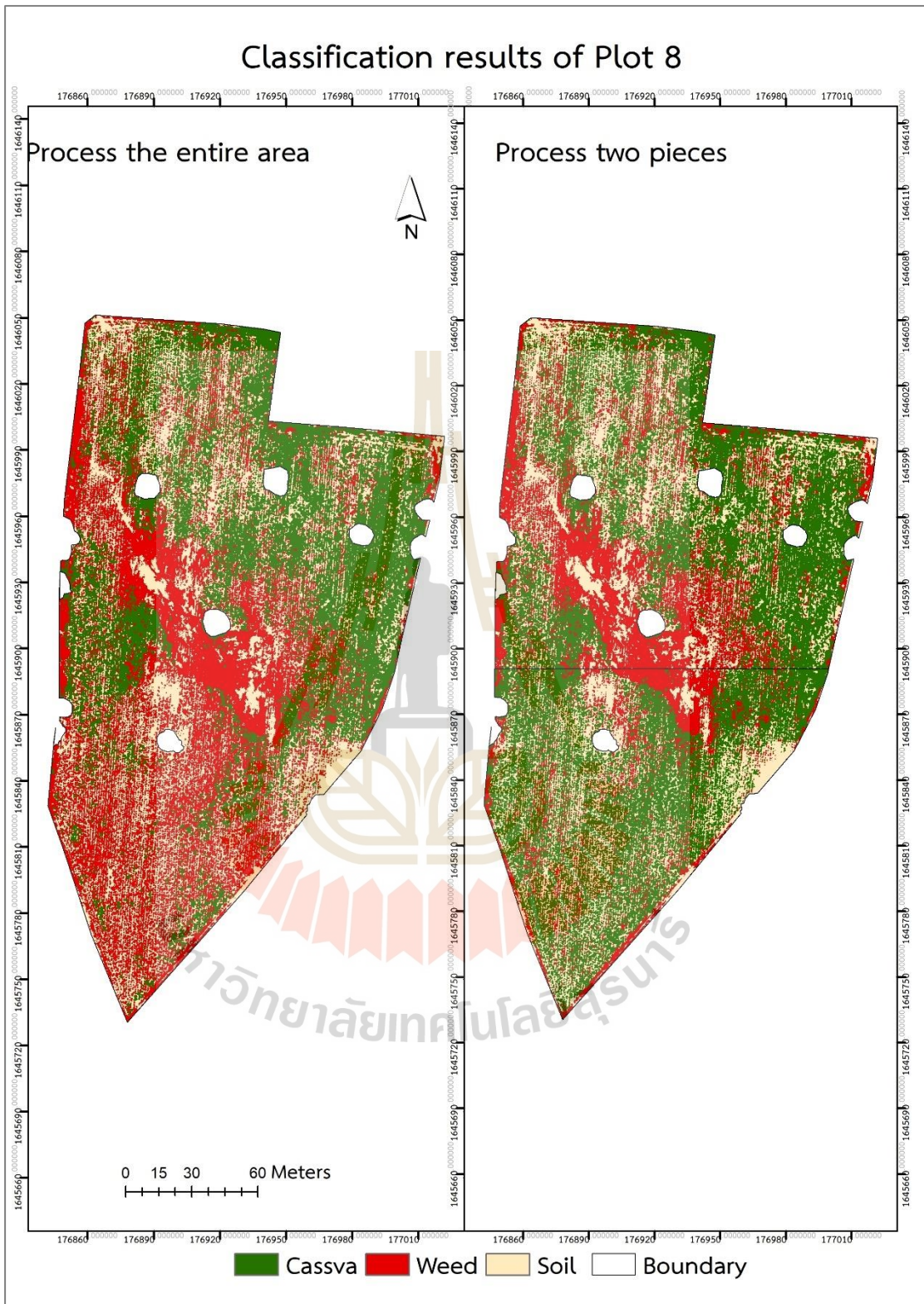


Figure E8 Classification results of plot 8.

Table E17 Confusion matrix of classification result from process the entire area of plot 9.

Class		Reference			Total
		Cassava	Weed	Soil	
Classification	Cassava	106	4	0	110
	Weed	24	90	0	114
	Soil	0	6	63	69
Total		130	100	63	293
PA		0.8154	0.9000	1.0000	
UA		0.9636	0.7895	0.9130	
OA		0.8840			
Kappa		0.8215			

Table E18 Confusion matrix of classification result from process two pieces of plot 9.

Class		Reference			Total
		Cassava	Weed	Soil	
Classification	Cassava	105	6	0	111
	Weed	25	88	0	113
	Soil	0	6	63	69
Total		231	231	231	693
PA		0.8077	0.8800	1.0000	
UA		0.9459	0.7788	0.9130	
OA		0.8737			
Kappa		0.8056			

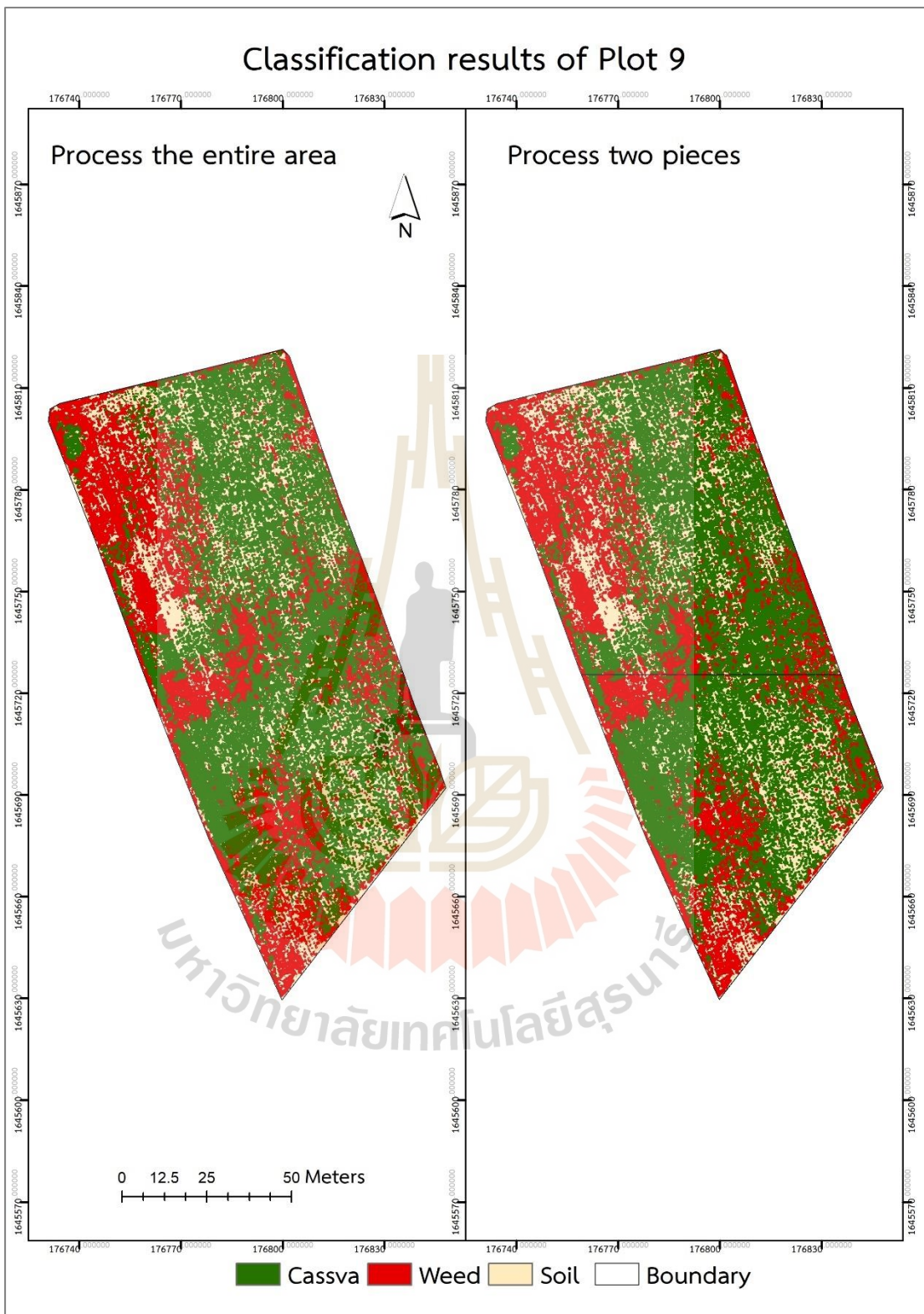


Figure E9 Classification results of plot 9.

Table E19 Confusion matrix of classification result from process the entire area of plot 10.

Class		Reference			Total
		Cassava	Weed	Soil	
Classification	Cassava	50	42	0	92
	Weed	95	75	0	170
	Soil	4	26	143	173
Total		149	143	143	435
PA		0.3356	0.5245	1.0000	
UA		0.5435	0.4412	0.8266	
OA		0.6161			
Kappa		0.4256			

Table E20 Confusion matrix of classification result from process two pieces of plot 10.

Class		Reference			Total
		Cassava	Weed	Soil	
Classification	Cassava	77	22	0	99
	Weed	68	100	0	168
	Soil	4	21	143	168
Total		149	143	143	435
PA		0.5168	0.6993	1.0000	
UA		0.7778	0.5952	0.8512	
OA		0.7356			
Kappa		0.6043			

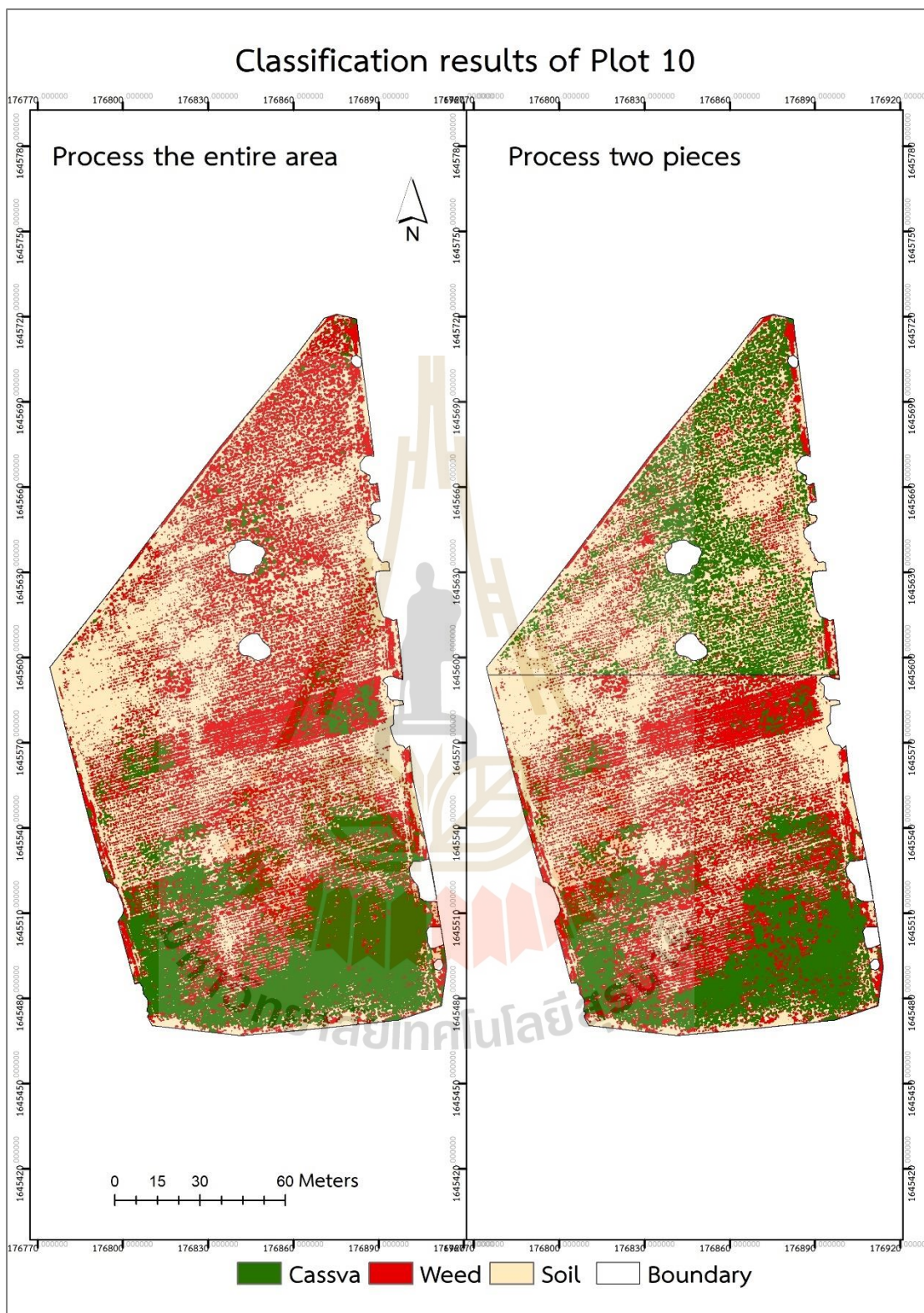


Figure E10 Classification results of plot 10.

Table E21 Confusion matrix of classification result from process the entire area of plot 11.

Class		Reference			Total
		Cassava	Weed	Soil	
Classification	Cassava	38	3	0	41
	Weed	7	38	0	45
	Soil	0	4	45	49
Total		45	45	45	135
PA		0.8444	0.8444	1.0000	
UA		0.9268	0.8444	0.9184	
OA		0.8963			
Kappa		0.8444			

Table E22 Confusion matrix of classification result from process two pieces of plot 11.

Class		Reference			Total
		Cassava	Weed	Soil	
Classification	Cassava	39	3	0	42
	Weed	6	38	0	44
	Soil	0	4	45	49
Total		45	45	45	135
PA		0.8667	0.8444	1.0000	
UA		0.9286	0.8636	0.9184	
OA		0.9037			
Kappa		0.8556			

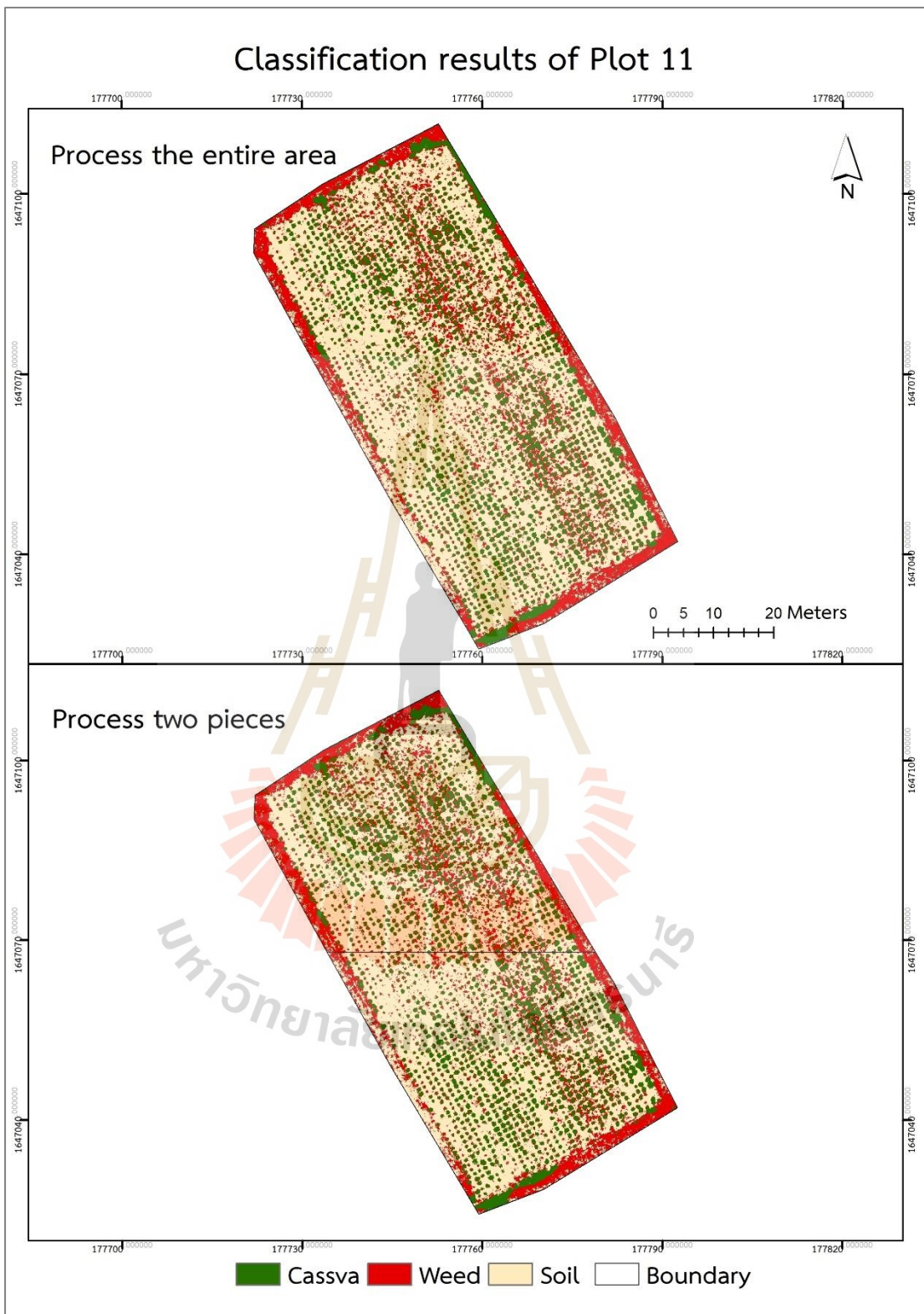


Figure E11 Classification results of plot 11.

Table E23 Confusion matrix of classification result from process the entire area of plot 12.

Class		Reference			Total
		Cassava	Weed	Soil	
Classification	Cassava	48	0	0	48
	Weed	1	50	0	51
	Soil	1	0	50	51
Total		50	50	50	150
PA		0.9600	1.0000	1.0000	
UA		1.0000	0.9804	0.9804	
OA		0.9867			
Kappa		0.9800			

Table E24 Confusion matrix of classification result from process two pieces of plot 12.

Class		Reference			Total
		Cassava	Weed	Soil	
Classification	Cassava	48	0	0	48
	Weed	1	50	0	51
	Soil	1	0	50	51
Total		50	50	50	150
PA		0.9600	1.0000	1.0000	
UA		1.0000	0.9804	0.9804	
OA		0.9867			
Kappa		0.9800			

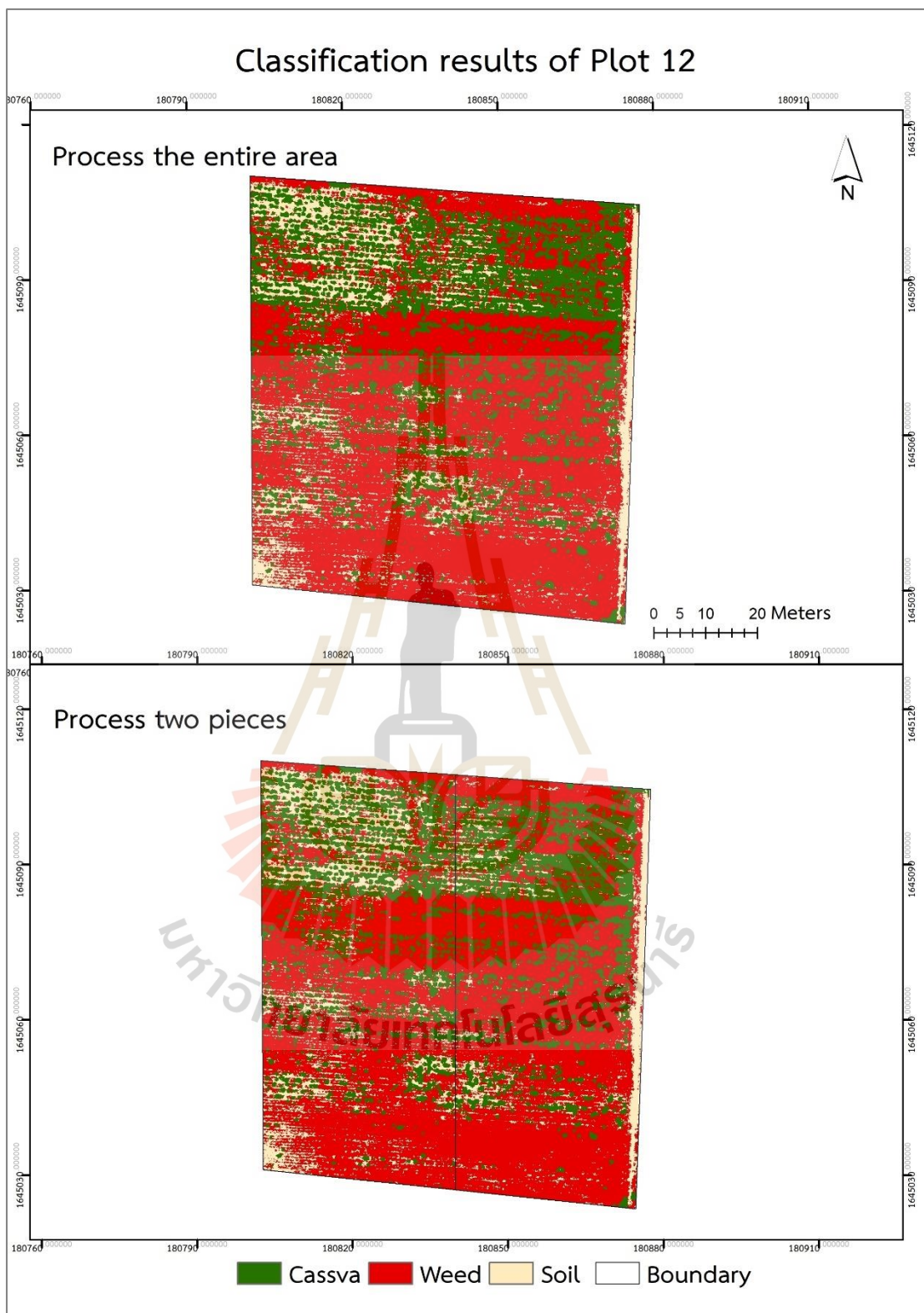
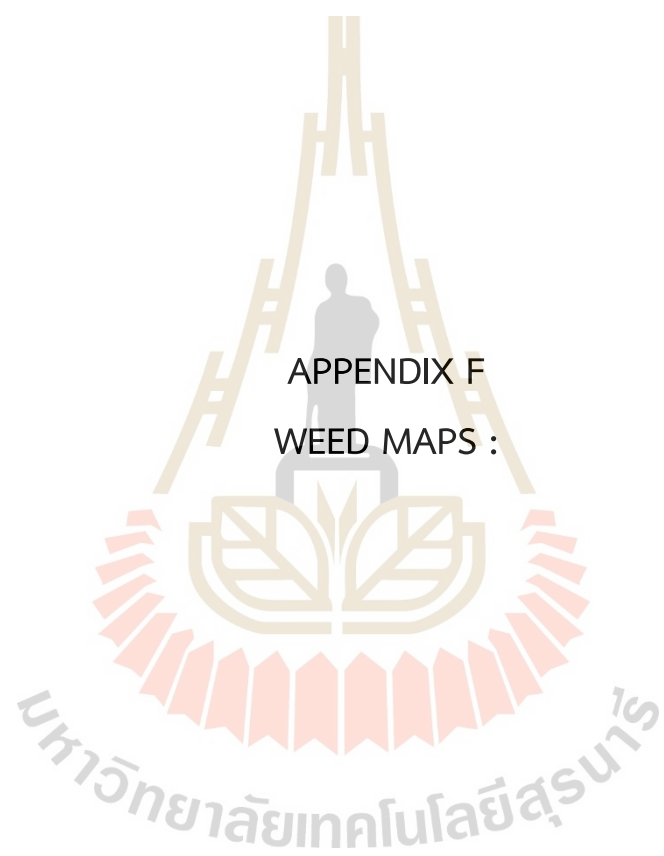


Figure E12 Classification results of plot 12.



APPENDIX F
WEED MAPS :

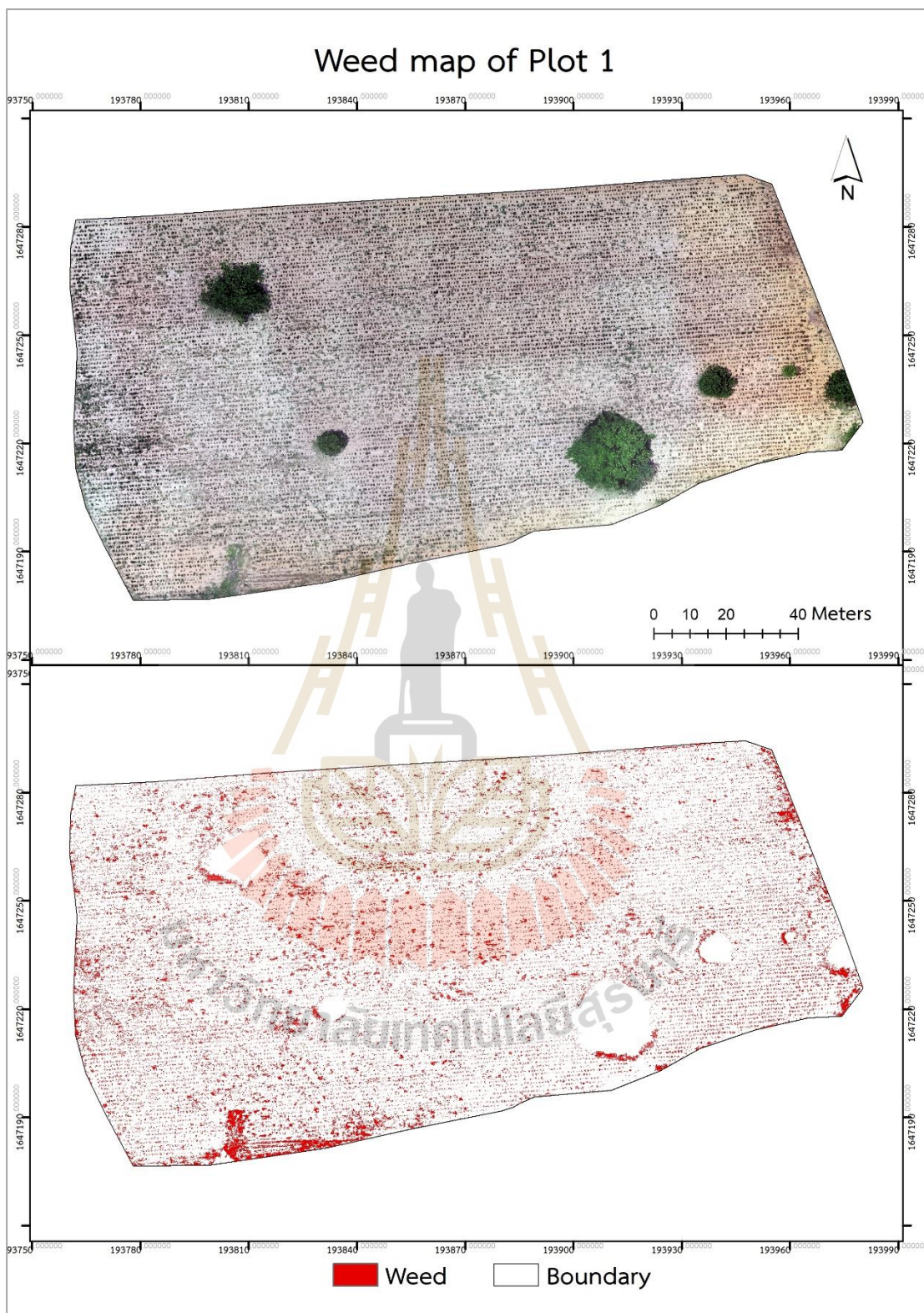


Figure F1 Weed map of plot 1.

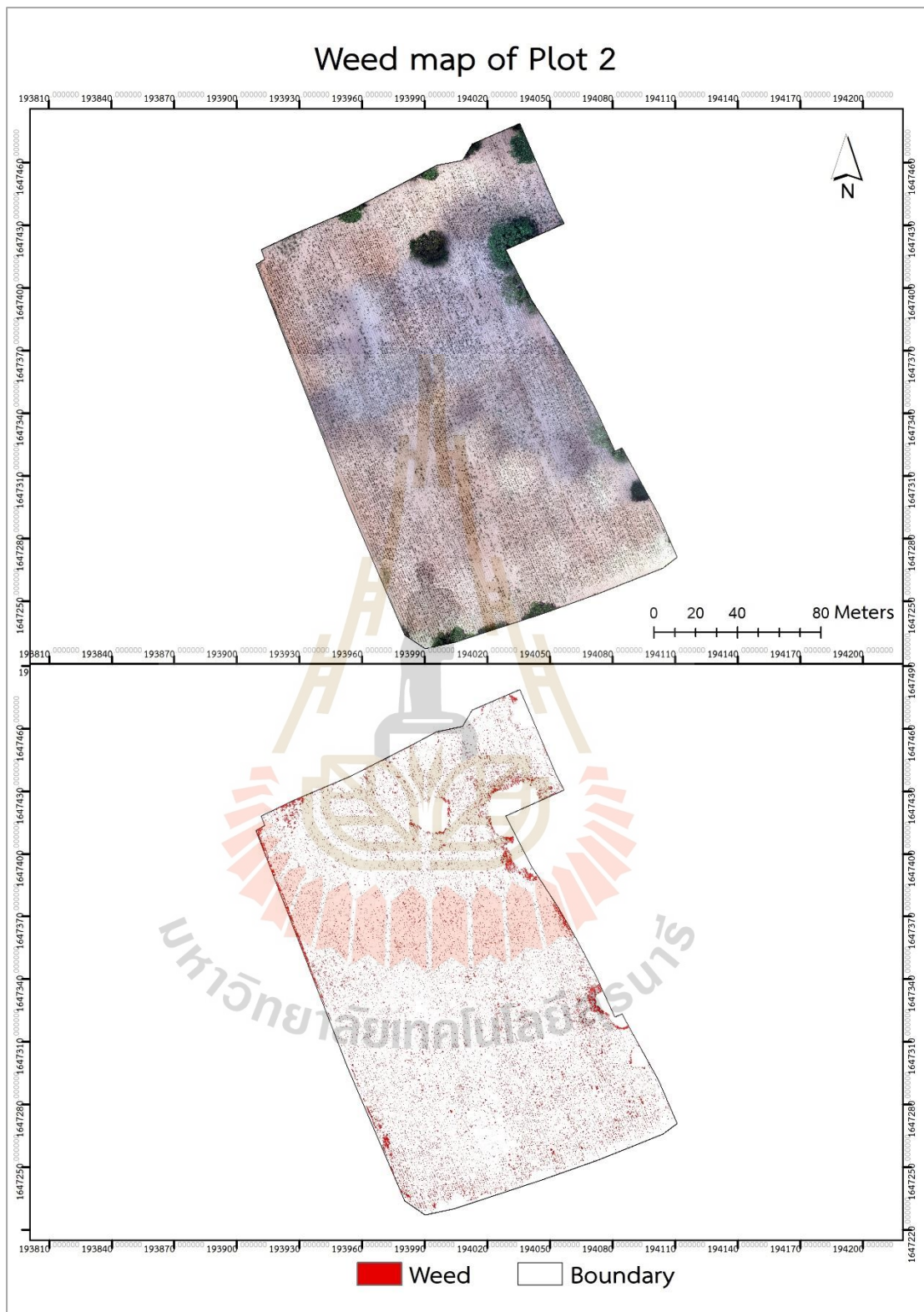


Figure F2 Weed map of plot 2.

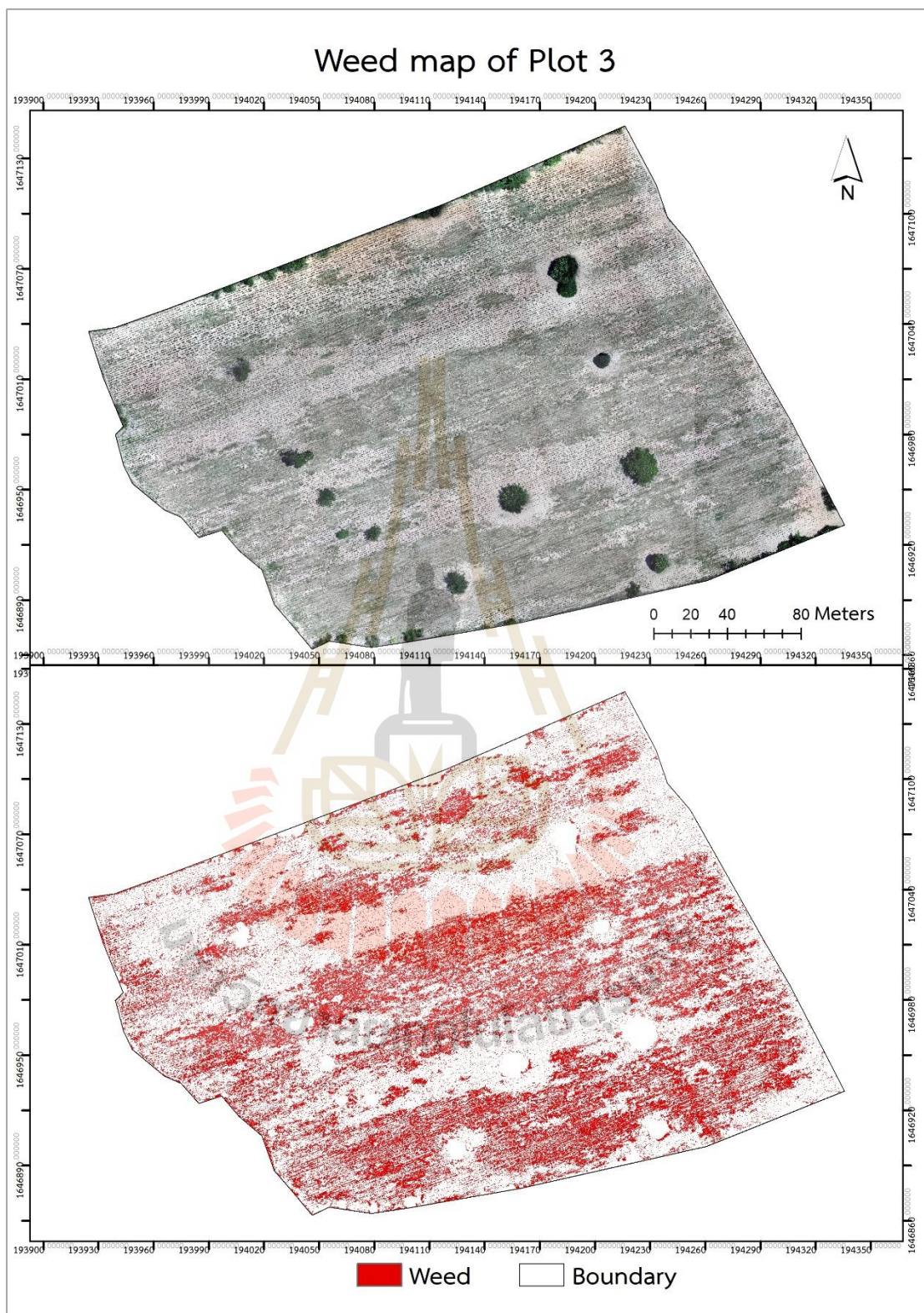


Figure F3 Weed map of plot 3.

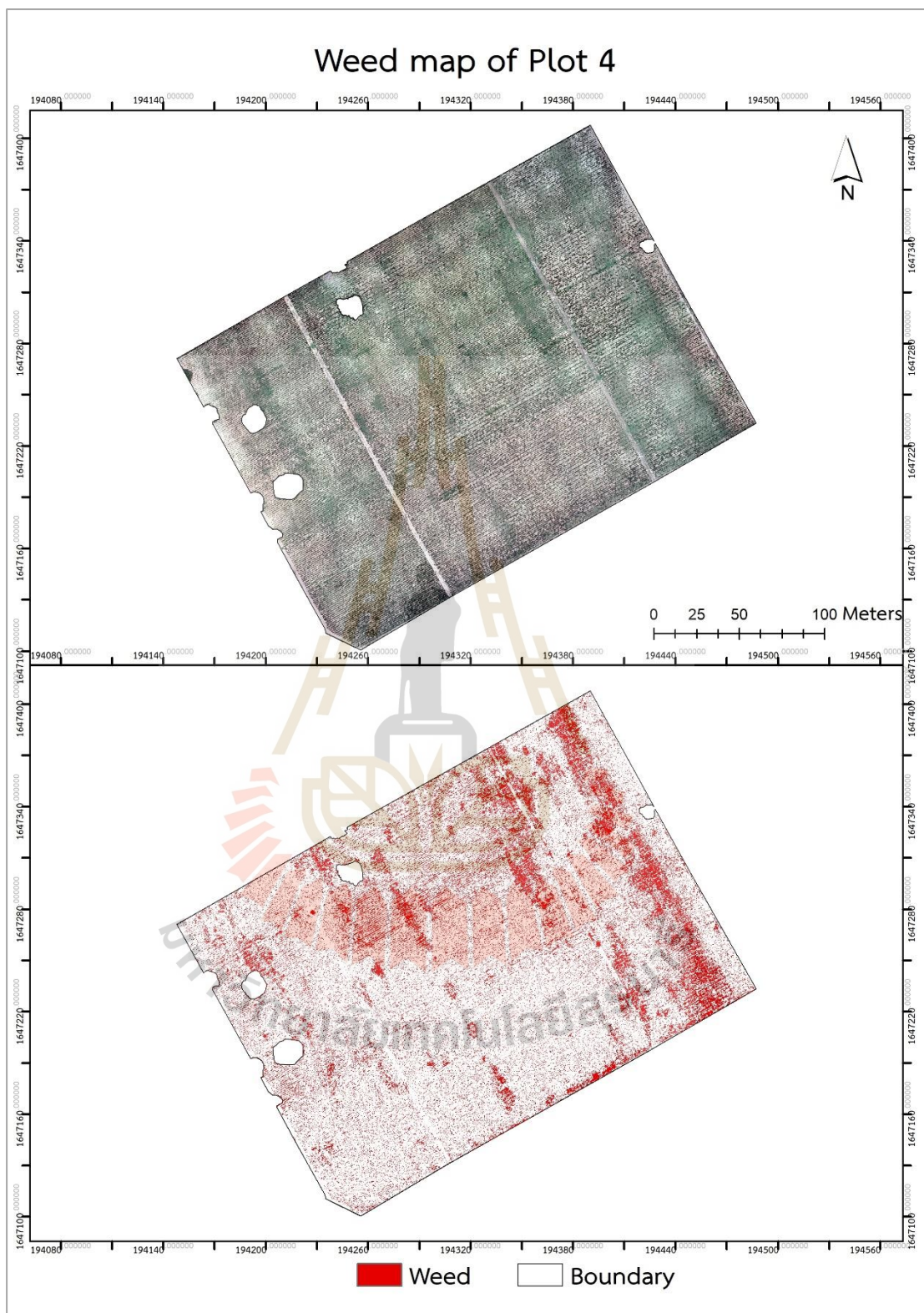


Figure F4 Weed map of plot 4.

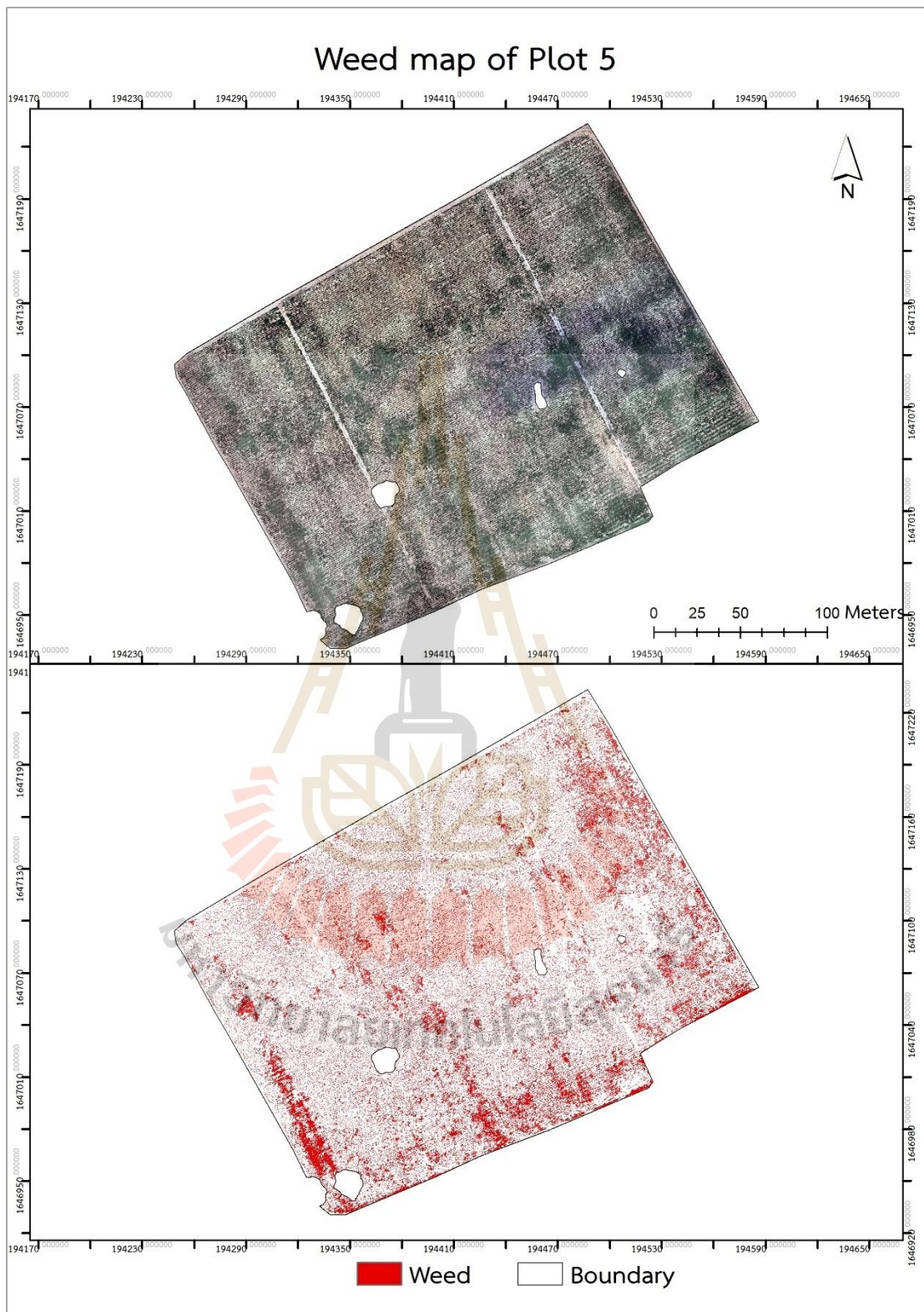


Figure F5 Weed map of plot 5.

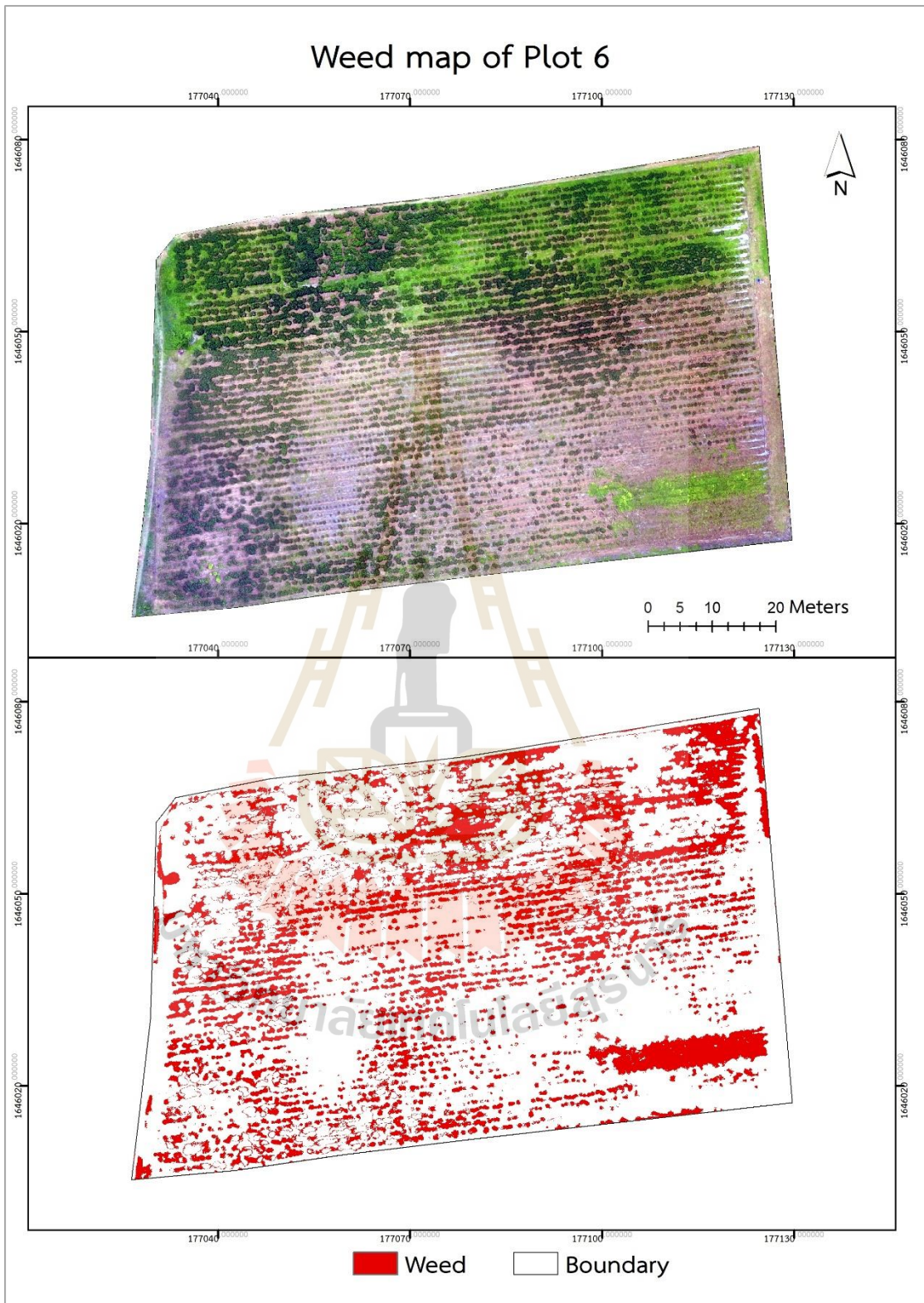


Figure F6 Weed map of plot 6.

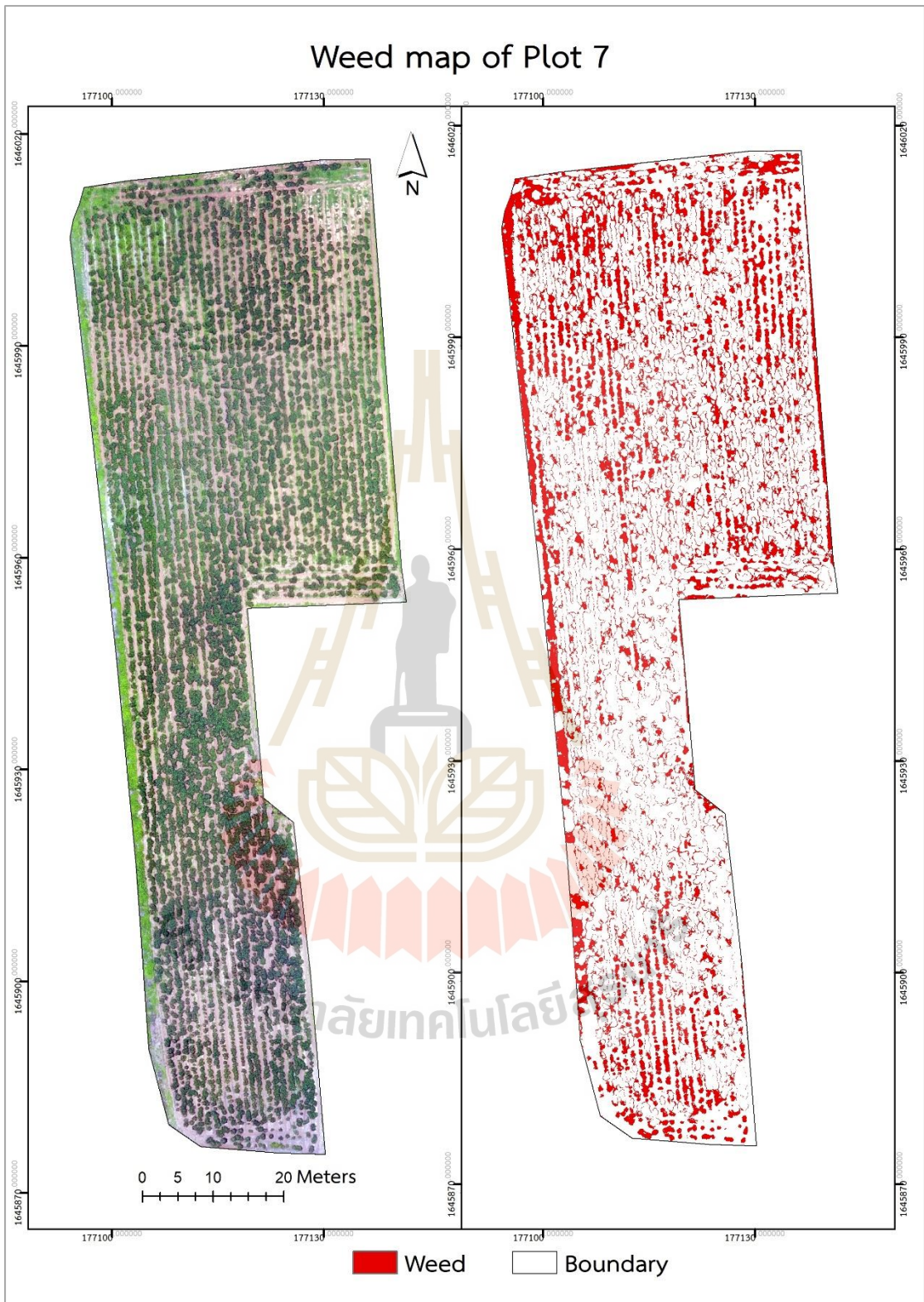


Figure F7 Weed map of plot 7.

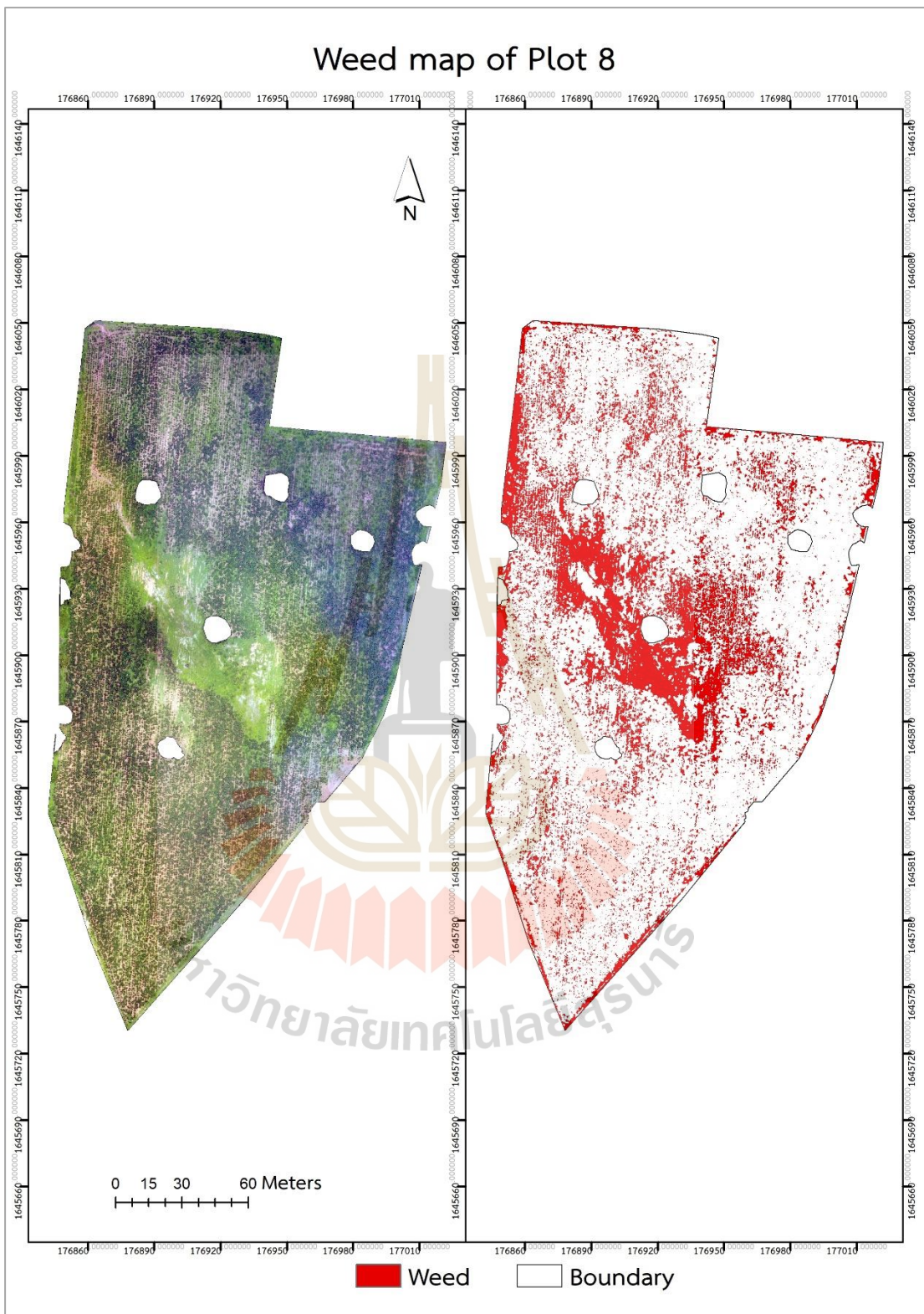


Figure F8 Weed map of plot 8.

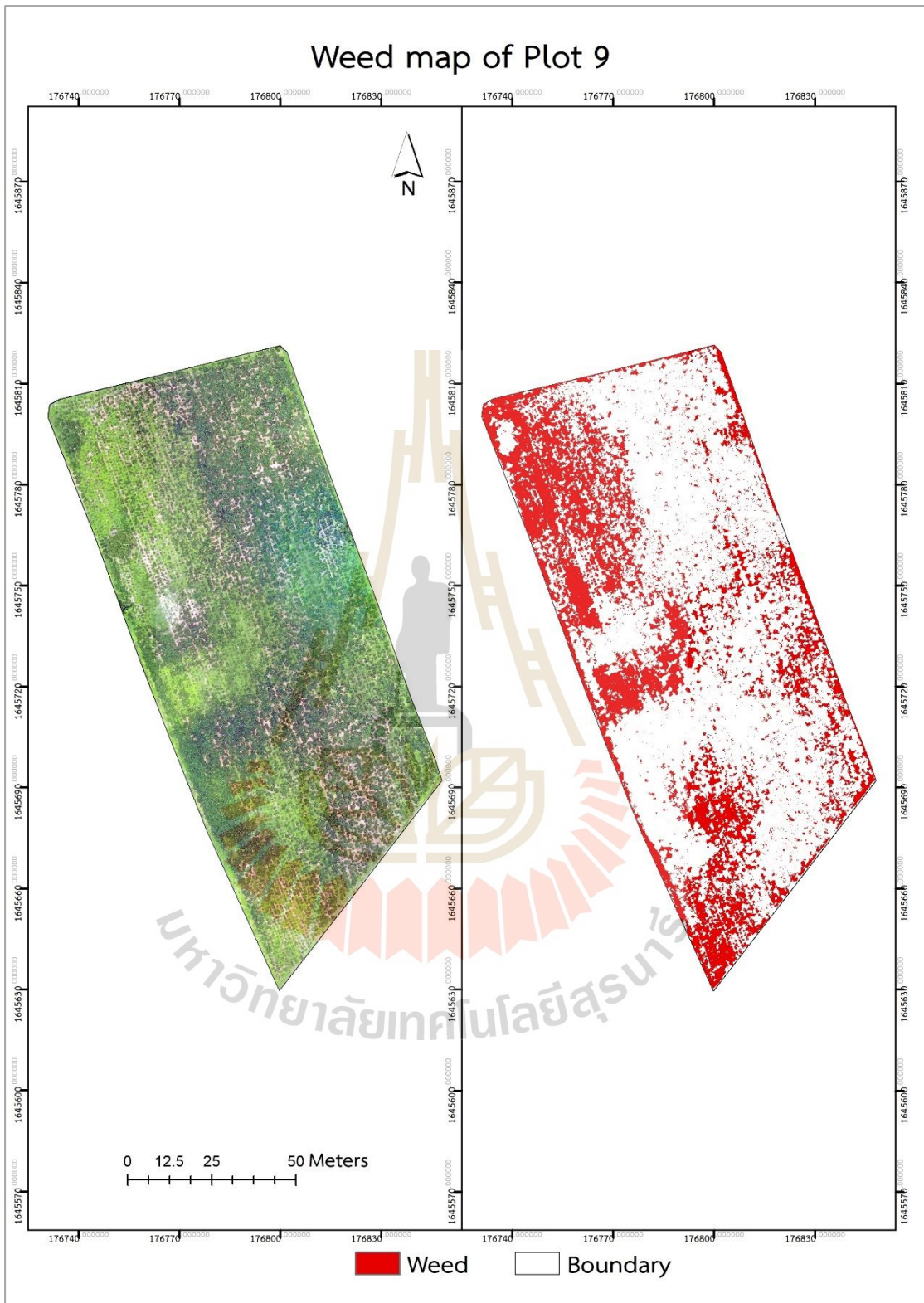


Figure F9 Weed map of plot 9.

Weed map of Plot 10

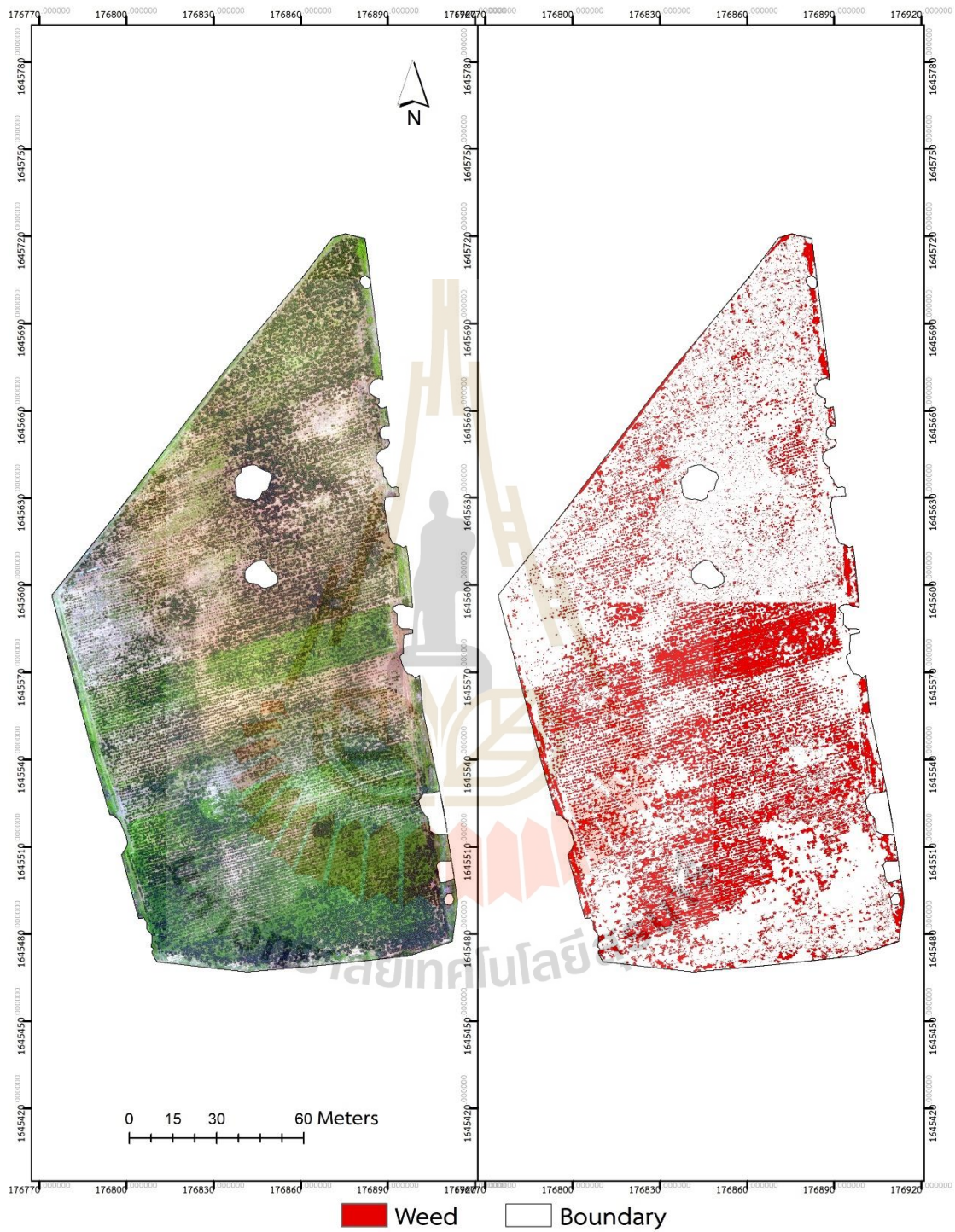


Figure F10 Weed map of plot 10.

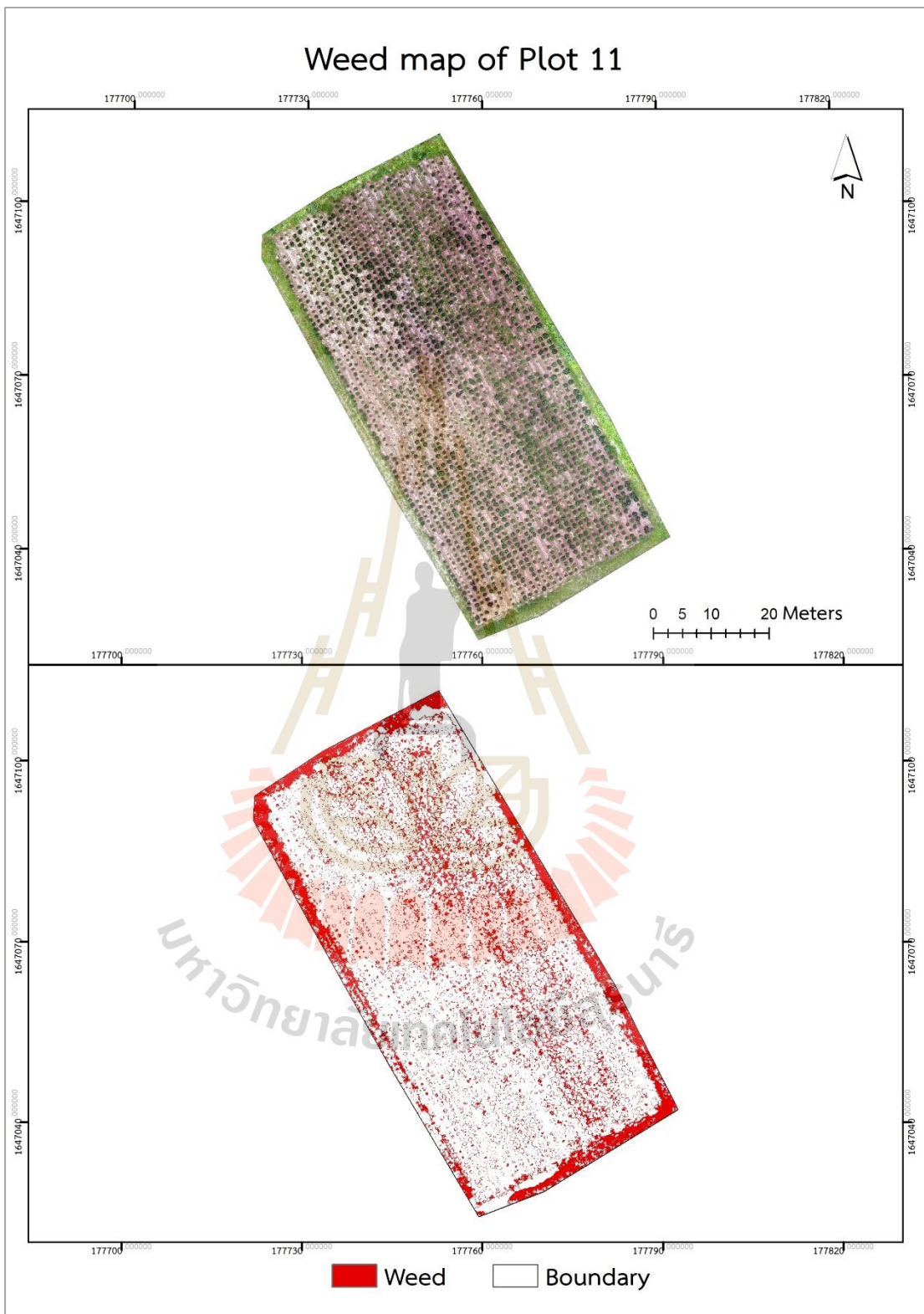


Figure F11 Weed map of plot 11.

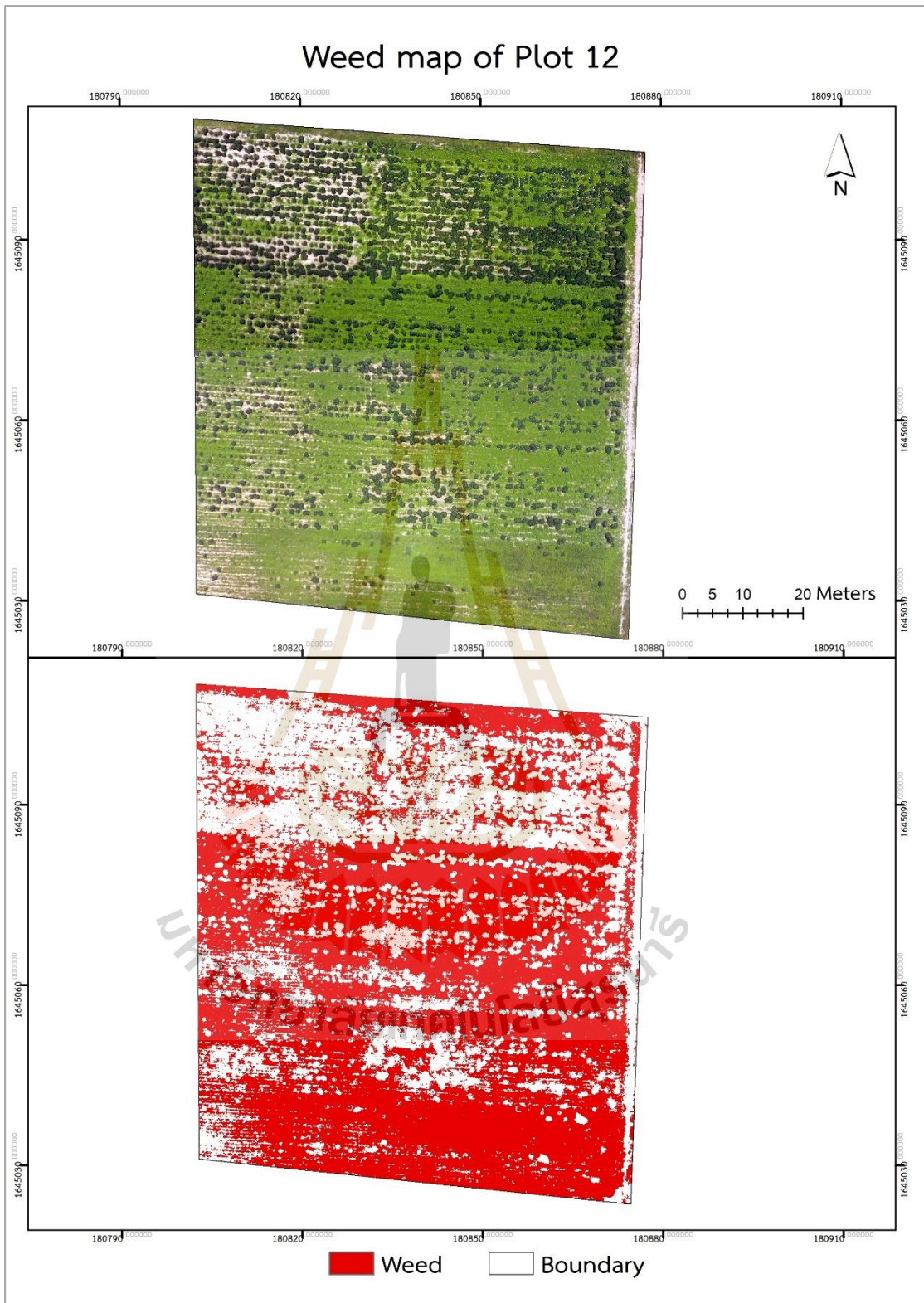


Figure F12 Weed map of plot 12.

CURRICULUM VITAE

Name Miss Apinya Boonrang
Date of Birth August 15, 1990
Place of Birth Phayao Province, Thailand

Education

2016: Master of Science in Applied Physics, Chiang Mai University, Thailand.

2013: Bachelor of Science in Physics, Chiang Mai University, Thailand.

Publications

Boonrang, A., Sritarapipat, T., and Piyatadsananon, P. (2021, November). Applicable Mean-Shift Filtering Parameters for Mapping Weed in Cassava Fields based on UAV Images. Proceeding of the 42nd Asian Conference on Remote Sensing (ACRS2021), Can Tho University, Can Tho city, Vietnam. Retrieved from https://a-a-r-s.org/proceeding/ACRS2021/2%20Algorithm%20and%20Image%20Processing/ACRS21_146.pdf.

Piyatadsananon, P., **Boonrang, A.**, Piyasilp, P., and Nuansing, W. (2021) Investigation of the moisture expansion as a deterioration factor of an ancient sandstone Buddha in Nakhon Ratchasima, Thailand. *SPECTRUM: UAS for Environmental Monitoring, ISPRS*. 14(4) April 2021.

Chaiwong, C., and **Boonrang, A.** (2020). SiO₂-like film deposited by plasma polymerization of HMDSO + O₂ using repetitive high voltage pulses. *Journal of Coatings Technology and Research*, 17 (6), pp. 1497 – 1503. DOI: 10.1007/s11998-020-00369-6.

Awards -

Grants and Fellowships 2009-2023: Science Achievement Scholarship of Thailand

Position and Place of Work -